Cirrus Cloud Properties Deduced from Zvenigorod Experiments and Theoretical Investigations, 1986-90

Eva M. Feigelson[1] and Stephen K. Cox, Editors

[1] Institute of Atmospheric Physics, Moscow

Funding Agencies:

National Aeronautics & Space Administration
Contract Number NAG 1-1146, S-01

Office of Naval Research
Contract Number N00014-91-J-1422, P00002

National Science Foundation
Contract Number ATM 9113129

Department of
Atmospheric Science

Paper No. 516

CIRRUS CLOUD PROPERTIES DEDUCED FROM ZVENIGOROD EXPERIMENTS AND THEORETICAL INVESTIGATIONS, 1986-90

Eva M. Feigelson

and

Stephen K. Cox, Editors

Department of Atmospheric Science
Colorado State University
Fort Collins, CO 80523

November 1992

Atmospheric Science Paper No. 516

PREFACE

Soviet scientists are pleased to present for publication in the Colorado State University Department of Atmospheric Science Report Series results from analyses of five years of study of cirrus clouds. These studies offer results on the cloud-radiation effects of cirrus clouds in the context of the World Climate Research Program (WCRP) and its regional experiments: in the United States (FIRE); in Europe (ICE); in the USSR (Zvenigorod).

It is in these contexts of the global scientific scope of the study of cirrus cloud systems and their effects upon climate, and the international political environment in which these studies take place, that we offer these results. The WCRP Regional Experiments have been performed in diverse locations, yielding results important to our understanding of the cirrus cloud systems. The next step is to integrate the separate results of the regional experiments into a common understanding of cirrus cloud systems. This compilation of theoretical and experimental results from the USSR is one way to encourage this integration by making the USSR results conveniently available in the English language.

We express our appreciation for supporting the USSR research on cirrus cloud systems to Academician G.S. Golytzin, Director of the Institute of Atmospheric Physics, to Professor A.A. Chernicov, Director of the Central Aerological Observatory and to Professor M.A. Petrosyanz, Head of the Climatology Department of Moscow State University. We also thank the Soviet authors for their contributions to this document.

It is the mutual desire of the editors that our goal of integration of ideas and knowledge gained from our separate studies be pursued in the future by closer collaboration with our scientific colleagues around the world.

Eva M. Feigelson
Stephen K. Cox

ACKNOWLEDGEMENTS

The editors gratefully acknowledge the support from the following agencies in the effort to develop stronger scientific cooperation among scientists from the United States and the former Soviet Union.

Institute of Atmospheric Physics

National Science Foundation

National Aeronautics and Space Administration

Office of Naval Research

Cirrus Cloud Properties Deduced from Zvenigorod Experiments and Theoretical Investigations, 1986-90

Eva M. Feigelson and Stephen K. Cox, Editors

TABLE OF CONTENTS

INTRODUCTION

Cirrus Cloud Properties Deduced from Zvenigorod Experiments and Theoretical Investigations, 1986-90

In connection with WCRP, the Soviet programme of clouds and radiation climatology (SCRCP) was organized in 1985. In this context, beginning in 1986 Soviet scientists undertook collaborative activities to study the radiative properties of cirrus clouds as well as factors which determine these properties. The Institute of Atmospheric Physics of the USSR Academy of Sciences (IAPh) assumed the organizing role and scientific leadership. Three field experiments in the month of May of 1986, 1987, and 1989 were carried out at the Zvenigorod Scientific Station (Z.S.S.) of IAPh (60 km from Moscow). Together with IAPh, the Central Aerological Observatory (CAO) of the USSR State Hydrometeorology Committee participated in the experiments and provided lidar measurements, radiosonde data (Station Dolgoprudny 80 km from Zvenigorod) and analyses of the synoptic situation. The CAO flying laboratory aircraft Il-18 took part in the experiment of 1989. The microphysics parameters, water content, scattering coefficients and integral fluxes of solar radiation were measured on board the aircraft.

Surface actinometric observation (spectral and integral fluxes of direct, diffuse and global radiation), as well as visual observations of clouds were provided by Meteorological Observatory of the Geography faculty of the Moscow State University (MSU).

The Moscow Instrument-making Institute took part in the experiments of 1986-87 and measured the cloud emissivities.

The Institute of Experimental Meteorology (IEM) together with the IAP developed the optical models of ice clouds.

The employees of the Hydrometeorological Centre analyzed the information from the satellite NOAA-II AVHRR (1989 experiment).

The IAPh provided the measurements of spectral optical thicknesses of clouds, the theoretical investigations and in 1989 the measurements of downward integral fluxes of thermal radiation.

Main results of 1986-88 experiments and theory were presented in the Abakumova, G.M., et al., 1989. The results of 1989-90 as well as summarizes of all experimental and theoretical works during the five year period (1986-90) are described in this issue.

In evaluating these results, let us note that:

We are merely beginning to effectively use the combination of surface, aircraft and satellite data and in these studies basically concentrated on the connection between different data from surface measurements and theory.

The existence of data of the directly measured main optical parameter, i.e. the optical thickness of clouds, together with data of cloud heights and thicknesses, vertical distribution of extinction coefficients of the visible light within cloud and actinometric information, allows us to produce rather complete descriptions of radiative and optical properties of ice clouds; these investigations have four main thrusts:

1. The statistics of radiative fluxes arriving at the Earth's surface.
2. The construction of optical models from measurements of the spectral transmittance, from solutions of inverse problems and from calculations of particles optical parameters.

3. The development of regression relationships between optical and meteorological parameters.

4. The evaluation of the radiation balance at the boundaries of the atmosphere and clouds.

In addition we offer in this publication as Appendices other recent papers by soviet authors concerning Ci clouds.

Chapter 1

The Synoptic Processes and Cloudiness in the Atmosphere during Cirrus Cloud Experiments (May of 1986, 1987 and 1989)

by E. V. Yarcho, and N. A. Zaytseva

1.1 The Synoptic Processes

May in Moscow differs considerably from year to year in connection with a great instability of the global circulation at this time. The high level circumpolar vortex which determines rather stable zonal westerlies in the middle atmosphere and significant cyclonic activity in the middle latitudes breaks down at this time.

Large variations of synoptic situations accompanied by frequent frontal passages were observed in 1986. On the 6th of May 1986 Moscow was in a zone of meridional invasion of the cold Arctic air in the whole troposphere accompanied by a steady northeast jet (the direction 20-40, speed 25-45 m/s) at the height about 9 km. The Ci clouds which were observed in the afternoon of the 6th of May evidently formed by upgliding associated with the secondary fronts which are typical in the cases of Arctic air invasions. On the 8th of May the low level, quick moving cyclone passed Moscow, leaving Moscow in an anticyclonic zone. The pressure maximum came into the region on the 11th, and the surface wind abated. The low level occlusion took place at a distance of about 450 km to the west and it caused the appearance of cirrus clouds.

During the period 11-15 May, the Arctic air invasion occurred practically at all levels in troposphere. On May 13th, according to the observations, Ci clouds

were within the layer 10.0-10.5 km i.e. directly under the tropopause. The occlusion passed the region on this day. On the 15th of May, the weather was influenced by a strongly occluded cyclone, however, at higher levels the pressure crest remained over Moscow. The high level clouds formed in wide temperature ranges (from -25° to -65° C) in the presence of northerly winds with speeds from 10 to 25 m/s. The largest outbreak of the high level clouds occurred on the 16th of May. Although the Moscow region was under the influence of anticyclone's periphery, the system of fronts stayed to the west-north-west and determined the cloud system's formation and development. Cu_{cg} and Cb clouds were developed in this region and their outflow increased the formation of Ci. The weather on the 21st and 22nd was associated with a slowly moving front. This situation was maintained also on the 23th of May, but later the pressure crest of the cold anticyclone located to the west moved into the Moscow region.

Thus in May of 1986, the weather was very changeable and rather cold on the whole. The Ci formation was mainly associated with frontal activity, but the fronts were rather low and mainly were occluded, therefore only limted regions of high level clouds were encountered. The only exception was the period of the 15th and 16th of May with well developed multilayer Ci.

The first half of May 1987 was characterized by the prevalence of anticyclonic systems. On the 4th of May, lidar revealed Ci clouds over Zvenigorod, but the meteorological observations in Moscow and Dolgoprudny didn't confirm their presence. On this day, Moscow was in the area of a warm stationary

anticyclone. The small thin Ci were dispersed in a layer 400-600 m below the tropopause in the southeast flow with speeds of 10-15 m/s. On the 6th of May the front lay along the latitude to the North of Moscow. The cirrus clouds observed on this day were associated with this front. The air temperatures of the Ci level were -52 to -43 C and the wind was south with speeds of 7-12 m/s.

The warm, pressure maximum came to the region on the 15th of May, but it was confirmed to the lower levels and changed to cyclonic circulation at the level of 5-6 km. The cloudiness was observed at these heights. The origin of this cloudiness was connected with systems of fronts of a developing cyclone centered over Estonia. In addition the active development of the Cb clouds over the Moscow region produced cirrus outflow. As in previous periods, on the 19th and 20th of May, the anticyclonic situation present in the region, with a complicated frontal system to the west. On these days, together with Ci clouds, clouds at low and medium levels also were observed. On the 22nd of May, Moscow was influenced by a warm sector cyclone and active development of Cu_{cg} and Cb took place over the region. Stratification was unstable. Such conditions were favorable for formation of variable and sometimes thick Ci clouds.

At the beginning of May 1989, the high level circumpolar vortex had still not dissipated, but it drifted to the western hemisphere. The European sector of the Arctic stayed under the influence of the high level anticyclones, however they were not well developed. The alternation of cyclones and anticyclones was observed in the zone of 40-60 N, therefore there was no persistent upper air transfer. At the

beginning of the month, the Moscow region was located in the pressure col. Usually this situation is associated with unstable weather, with weak winds. As a rule, the fronts were secondary or occluded which is confirmed by repeated reports of stratocumulus clouds. The anticyclonic cloudless weather settled in the region at the end of the first ten day period of May. The air temperature was rather high ±12 to ±14° C during the daytime and 6 to 7° C at night.

Formed at the beginning of the month, the synoptic situation in the upper troposphere changed insignificantly during the month, but the circumpolar vortex drifted to the east in the North Atlantic in the second ten day period. Therefore Europe was periodically influenced by this vortex circulation, but mainly the northern areas. During this period, Moscow was outside of the active baroclinic systems, either at their periphery or at the pressure col. This was confirmed by rather weak winds both near the surface and in free atmosphere. The synoptic processes became more active only on the 16th and 17th of May and strong north winds (to 25-30 m/s) were observed over Moscow on these days. These winds were caused by the intensified pressure maximum over West Europe (the extension of the Azores anticyclone). The intensification of the wind was also observed during some later periods: 18-19th, 21st and the 23-25th of May. The baroclinic situation in the upper troposphere over Europe and the European sector of the Arctic continued to be complicated over the last ten day period. In connection with the westward movement of the main circumpolar vortex the alternation of the high level pressure ridges and troughs was registered here. The Moscow region turned

out mainly to be in the peripheral zones of small cyclones which actively developed in Scandinavia and the Barents Sea region; the pressure field was characterized by small gradients.

An abrupt weather change (cooling) was registered in the period from the 20th until the 23rd of May. On the 19th of May, after the cold front passage, Moscow was under the influence of Arctic air. On the 20th of May, a second cold front passed over Moscow with additional passages of some secondary fronts later up to the 24th. A small gradient pressure field formed once again around the region at the end of the month.

The situation on days with Ci clouds will be briefly described below:

On May 14th and 15th, Moscow was in the area of surface pressure col. The frontal zone (which was the old occluded front in the north part and a stationary front with frontal waves in the south part) aligned along the direction from Scandinavia to the Volga region and Kazakhstan. The winds in the free atmosphere were moderate (10-12 m/s). The appearance of Ci clouds was caused by that frontal zone. The CAO flying laboratory IL-18 worked on the 15th of May. The flights were made in the conditions of a cold front extending a line from the northeast to the southwest. The active cyclone formed in the morning of the 15th over the Kursk region and drifted during the day to the northeast. The high level frontal zone with the stable jet on the 250 gPa level corresponded to this cold front. The jet wind speed was about 35 m/s. Moscow was on the cyclonic side of the jet.

The Ci-Cs cloudiness observed on this day is evident as a narrow zone on the NOAA-II picture (Figure 1.1, Point B). Since this cloud zone was separated from the main frontal cloudiness by a clear space and distinguished by bright exposure, one may suppose that some zone of upward vertical motion with similar contours should exist. Calculations of vertical motions on isentropic levels confirmed this assumption and a zone of upward motions up to 10 cm/s had been revealed (Figure 1.2). This zone was bordered from above by the tropopause which is a natural upper altitude limit of Ci clouds as a rule. These upward motions appear to be primarily responsible for the Ci-Cs formation on the 15th of May.

May 18: A cold front passed over Moscow. It belonged to the cyclonic system with the center over the south part of Novaya Zemlya. The Ci clouds were associated by this front.

May 20: The region was under the influence of an old, dissipating anticyclone. Moscow was located on the west and later on the north periphery of this anticyclone during almost all of the second ten day period. The Ci was associated with the cold front which passed Moscow on the 20th of May.

May 31: The Ci clouds were connected with the system of old occluded fronts and belonged to the large cyclonic system stretching from the southwest (France) to the northeast (Kola Peninsula).

June 2: The Moscow region was influenced by a high pressure ridge, but Ci clouds were originated from the same frontal system as on May 31.

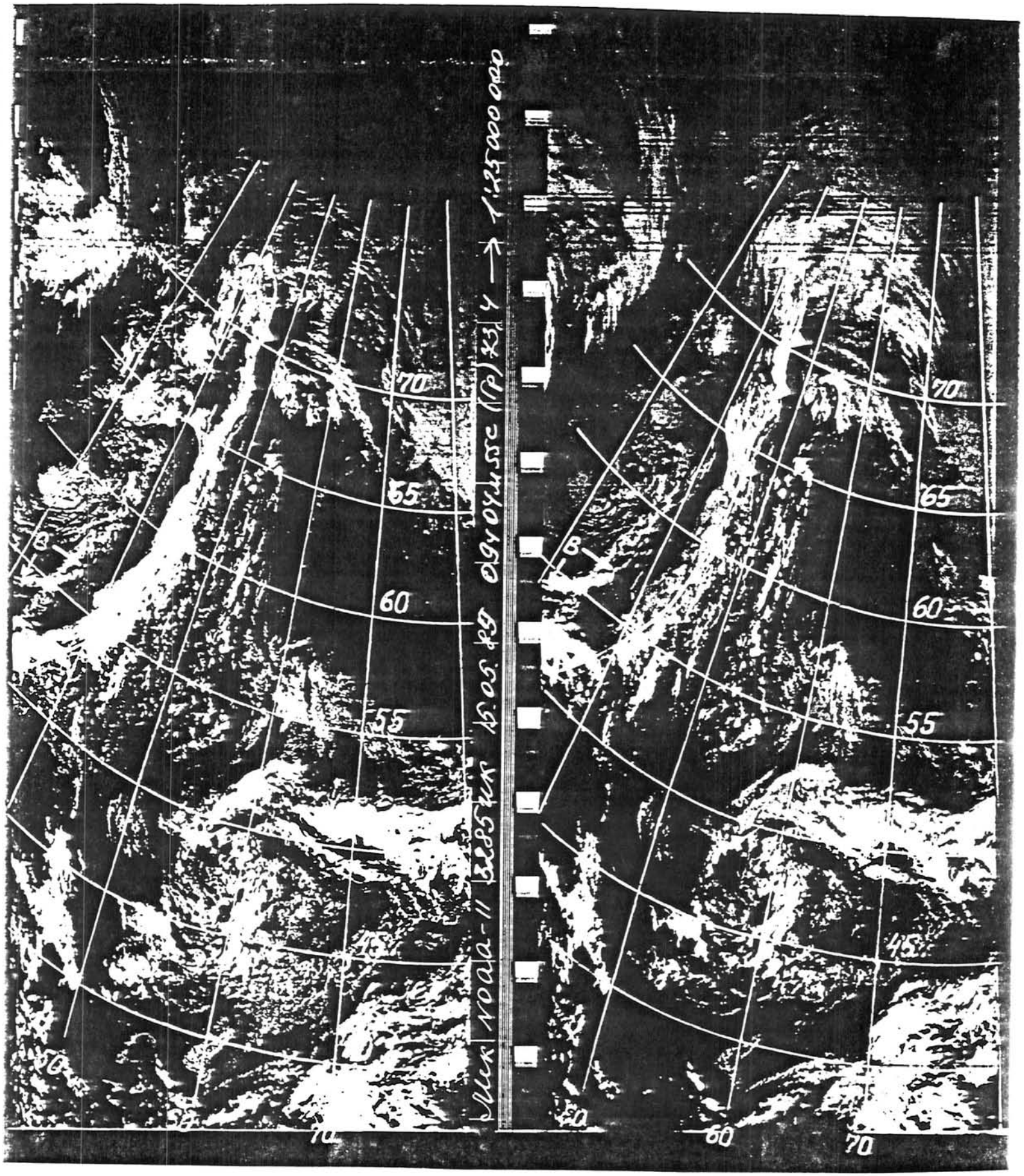

Figure 1.1 Satellite picture of the cloudiness on the 15th of May 1989. Left side is visible image and the right side is IR. Letter B shows Ci clouds investigated.

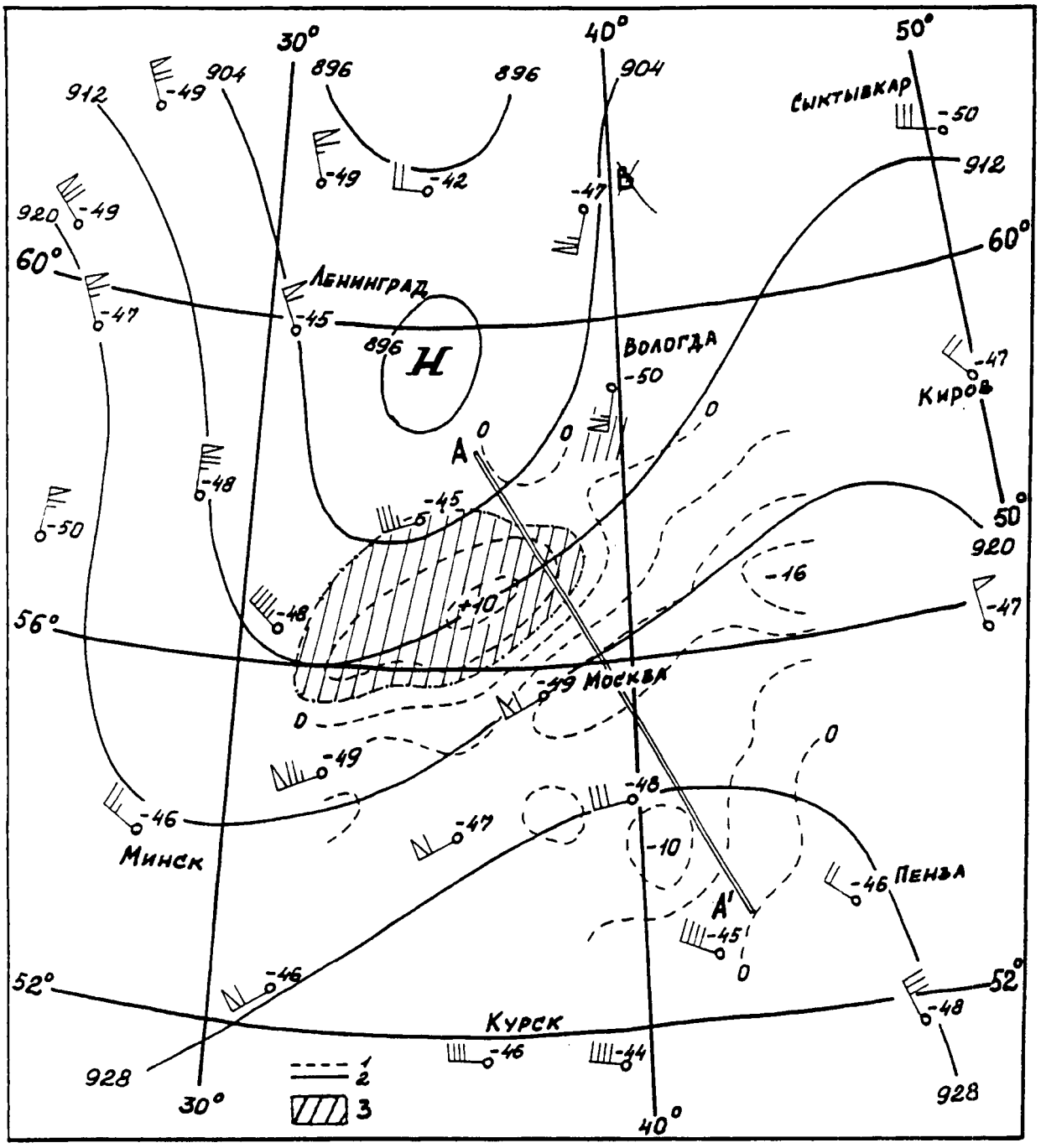

Figure 1.2 Absolute topography map of 300 hPa level.
1 - vertical velocities, $v \cdot 10^{-2}$ cm·s^{-1}
2 - isohypses, dkm
3 - area of vertical motions, $w \geq 1$ cm·s^{-1}
A A' - flight route.

June 4: The surface pressure was relatively high because of the pressure ridge. The Ci clouds were a forerunner of an approaching frontal zone from the southwest. The change to the cyclonic situation took place on the 5th of June.

June 7: Ci clouds were caused by a front which passed Moscow on the day before.

As a result, the weather and the synoptic processes of May 1989 may be characterized as slightly anticyclonic. The air temperatures were a little bit higher than normal. Baroclinic processes were not active because the Moscow region turned out to be in small gradient pressure fields.

On the whole, May 1986 was most favorable for observations of Ci clouds. The largest number of days with Ci clouds as well as the largest variability of Ci forms were found in this period. The cyclonic circulation was more active in May 1986, therefore the atmospheric fronts passed more often. In 1987 and 1989 atmospheric circulation in May over the Moscow and Zvenigorod regions was close to anticyclonic and therefore the fronts were rare and they were not well marked either in temperature or in cloudiness fields. However Ci clouds were observed at higher levels in May of 1987 and 1989. The generation and the development of the Ci were associated with the frontal activity in all three phases of the experiment. Only in the case of the 22nd of May 1987 were Ci clouds nonfrontal and generated by an air mass containing many convective Cu_{cg} and Cb clouds.

1.2 The High-Level Cloud Regimes

There were only 40 days during April-May 1986, May 1987 and May-June 1989 when high-level clouds were observed. Among these situations Ci cloud amounts of 8-10/10 were reported in 65% of the cases, cloud amounts of 3-7/10 were found 20% of the time and less than 3 in 15% of the cases. In 29% of the situations Cu were observed together with Ci. Cs was observed in 7% of the cases.

Multi layer cloudiness was observed more frequently. The low and middle clouds were recorded against the background of high-level clouds. They were Ac, Cu, Cu frac., Sc. The usual amounts of Ci in these cases were small and in only 32% of the cases were observed together with extensive Ci cover (8-10).

Table 1.1 presents the data of simultaneous visual observations of clouds in the experiments of 1989 together with some measurement data. Column 6 contains the values of measured optical thicknesses, τ, averaged for 30 minutes when Ci clouds were close to the sun's disk and were not underlayed by other forms of clouds. Column 7 contains the heights of cloud base Z of Ci. Column 8 shows their thicknesses, H, determined by lidar sounding and averaged for 30 minutes. If values of τ, Z and H are present in the table, but sun or zenith positions were was not obscured by Ci at the moment of observations, this means that during 30 minutes on the average the obscuration of sun or zenith by cirrus clouds was considerable.

Table 1.1

The observations of cloudiness during the Zvenigorod experiment in May 1989 (the days and times when Ci clouds were observed).

Date	Moscow Time	Amount total/ low						
			On the sky	On the sun	In the zenith	τ	Z_M	H_M
	1	2	3	4	5	6	7	8
May 14	14.00	8/4	Ci,Cu,Cu fr	Cu fr	Cu	0.80	8350	1650
	15.00	10/4	Ci,Cu,Cu fr	Ci	Cu fr	0.47	8500	1450
	16.00	10/4	Ci,Cc,Cu,Cu fr	Ci, Cu	Ci	0.65	8350	2200
May 15	9.00	10/1	Ci,Cu fr	Ci	Ci	0.78	7350	1000
	9.40	10/1	Ci	Ci	Ci	0.63	6700	1800
	10.00	8/2	Ci,Cu,Cu fr	Ci	Cu fr	0.90	6400	1250
	13.00	7/2	Ci,Cc,Cu fr	Ci	Ci	0.94	8700	600
	13.30	7/1	Ci,Cc,Cu,Cu fr	0/0	0/0	0.89	7950	650
	14.00	10/1	Ci,Cc,Cs,Ac, Cu,Cu fr	Ci	Ci	0.87	7500	1550
	14.30	10/1	Ci,Cc,Cs,Cu fr	Ci	Ci	0.68	7500	1850
	15.00	10/1	Ci,Cs,Ac,Cu fr	Cs	Ci,Cu	0.34	7200	1600
May 31	10.00	7/0	Ci	Ci	Ci	0.86	8550	1500
	10.30	9/0	Ci,Cc	Ci	Ci	0.76	8550	1650

Date	Moscow Time	Amount total/ low						
			On the sky	On the sun	In the zenith	τ	Z_M	H_M
	1	2	3	4	5	6	7	8
June 2	1.30	7/4	Ci,Cc,Cu,Cu fr	Ci	Cu	0.22	8200	600
	12.00	9/4	Ci,Cu,Cu fr	Ci	Ci,Cu	0.66	1.570 2.795	950 400
	16.48	5/2	Ci,Cu,Cu fr	Ci	Ci	0.20	7350	850
June 7	11.00	8/0	Ci,Cc	Ci	Ci	0.86	1020 0	500

Chapter 2

The Optical Properties of Cirrus Clouds Determined by Lidar and Spectrophotometer; Parameterization of High Cloud Optical Properties as a Function of Height, Thickness and Temperature

by Kravetz L. V., and P. P. Anikin

The vertical distribution and thickness of Ci clouds during the experiments are presented in the histograms shown in Figure 2.1. The distributions of clouds heights and thicknesses are nearly homogeneous. The mean height of the lower boundary of the clouds observed throughout the experiment is 7.7 km and the mean vertical thickness is 1.35 km. The maximum thickness was observed on May 2, 1989 and equaled 4.4 km. The mean distance between the cloud upper boundary and the tropopause was 1.5 km. We should note that lidar measurements in 1989 were much more numerous than in the two preceding stages of the experiment. In 1989 900 measurements were taken, while the total number of observations for all three years was about 1200. Therefore the averages of the values presented are more attributable to the situation of 1989.

The procedure described in the Abakumova, G.M., et al., 1989, Chapter 2 was used for the definition of vertical distribution of the visible light extinction coefficient.

To obtain the mean distributions of the retrieved profiles of the extinction coefficient all the observed clouds were classified according to their lower boundary height and thickness (see Table 2.1). A single cloud case is defined to be a continuously existing cloud with breaks not exceeding one hour in time.

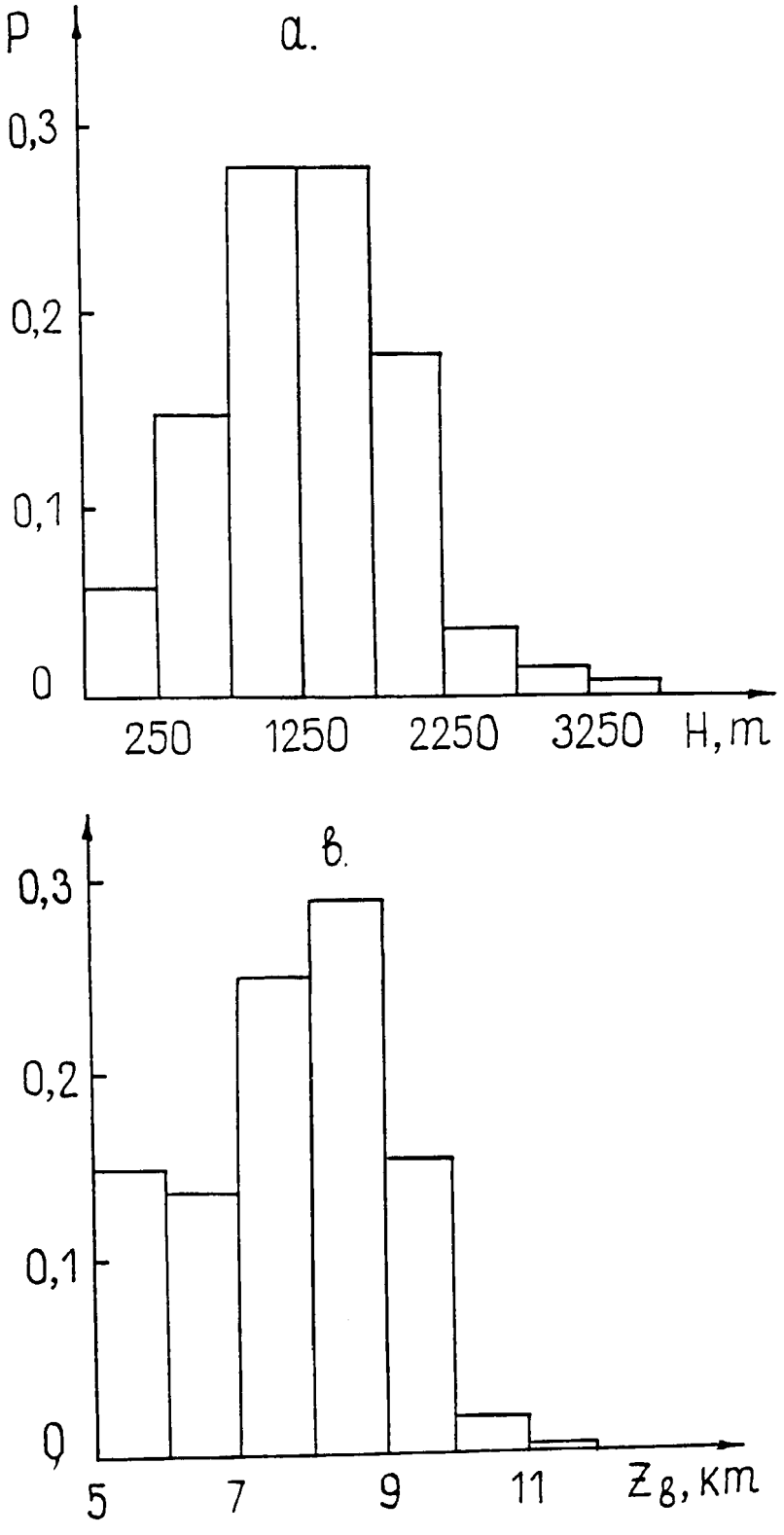

Figure 2.1 Histograms of thickness (a) and lower boundary height (b) of Ci clouds. P is the distribution density.

Table 2.1

The list of cloud classes differentiated by the thickness H and the lower boundary height Zb. Presented is the number of lidar measurements within each class. In brackets - the number of observed cloud systems.

H, km	Zb, km				
	5-6	6-7	7-8	8-9	9-10
0.5-1.2	13(1)	46(2)	88(4)	13(1)	46(4)
1.2-1.8	18(1)	106(4)	104(4)	110(5)	78(4)
>1.8	64(2)	14(1)	105(4)	118(3)	-

Profiles of the extinction coefficient for various heights (and, respectively, temperatures) and various vertical thicknesses of clouds (less than 0.5 km thicknesses were not taken into consideration) were deduced from the data file. The results are presented in Figures 2.2a,b,c. In the Figures, on the ordinate the $\frac{\beta}{<\beta>}$ value is plotted where β is the extinction coefficient, and $<\beta>$ is defined by (1):

$$<\beta> = \frac{1}{H}\int_{o}^{H} \beta\ (Z)\ dZ \qquad (1)$$

The curves of the vertical distribution and of the extinction coefficient shown in Figure 2.2a for the clouds of 0.5 - 1.2 km thickness for different intervals of their lower boundary heights, have an approximately identical form with the maximum close to H/2. Noticeable here is some shift of the maximum $\frac{\beta(z)}{<\beta>}$ for the clouds with Zb=7 to 8 km in comparison with the distribution $\frac{\beta(z)}{<\beta>}$ for the clouds with Zb=6 to 7 km.

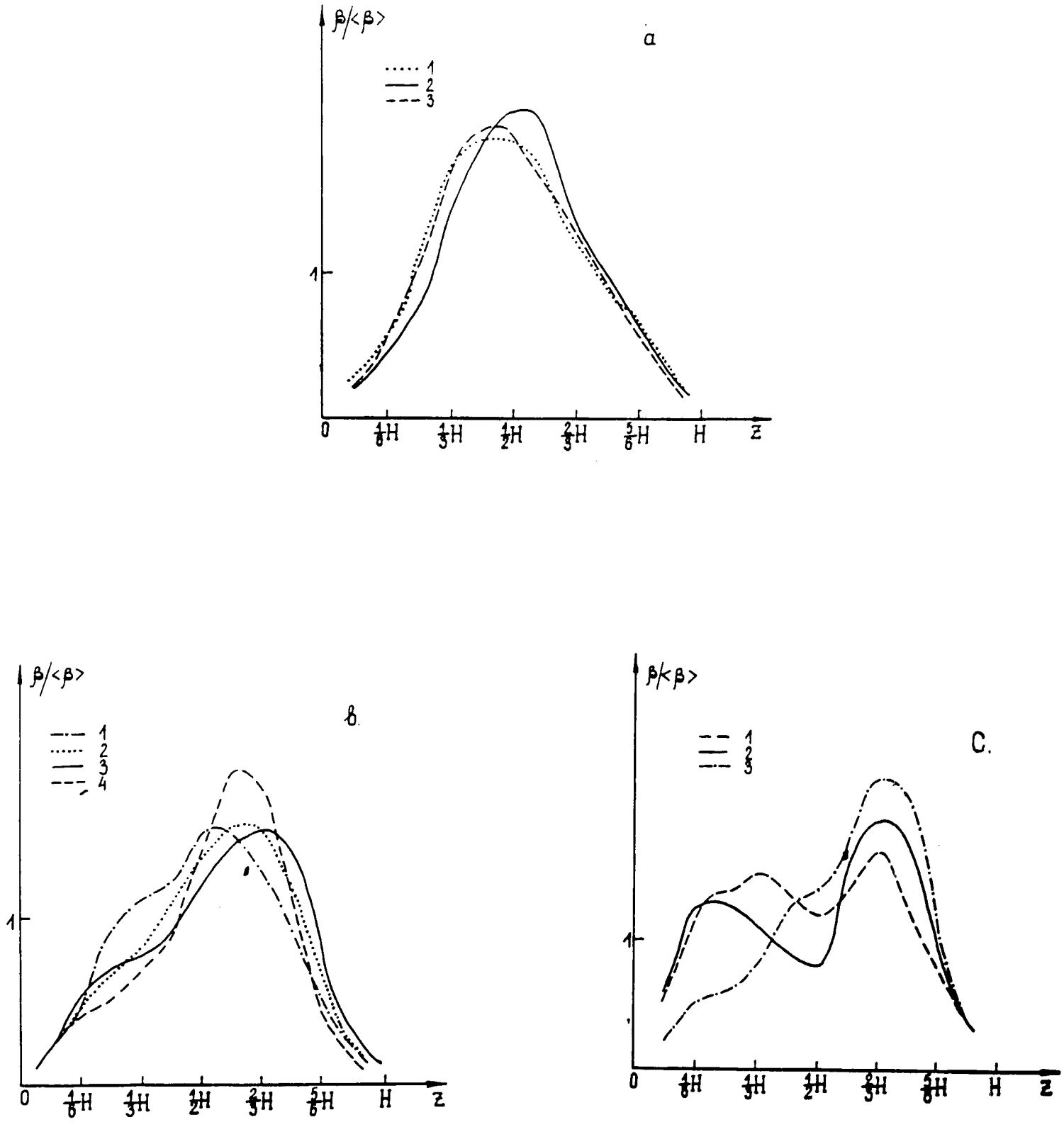

Figure 2.2 Vertical distribution of the relative extinction coefficient $\beta/<\beta>$ in Ci clouds. a - (0.5 km < H < 1.2 km); b - (1.2 km < H < 1.8 km); c - (H > 1.8 km); curve 1: Z_b = (6-7 km); 2: (16-7 km); 3: (8-9 km); 4: (9 km).

Let us consider the curves of the vertical profiles of the average extinction coefficient presented in Figure 2.2b. The range of cloud thicknesses corresponding to the curves was found most often in the experiments. The mean thickness value is found in the range 1.2 km < H < 1.8 km. Therefore we may consider the distributions $\beta(Z)$ shown in Figure 2.2b as the most typical of the observed Ci clouds. The curves presented in Figure 2.2b obviously differ from each other. Curve 1 for the clouds with the lower boundary varying within the range of 6-7 km shows the vertical distribution of the extinction coefficient with the maximum near the middle of the cloud (H/2). As the lower boundary height grows (curves 2.3) the curves become asymmetric - the maximum of the extinction coefficient distribution shifts to the cloud upper boundary. For the clouds whose lower boundary was within the interval of 9-10 km (curve 4), directly beneath the tropopause or higher, the maximum again shifts to the center of the cloud. In this case the absolute value in the maximum $\frac{\beta \cdot (z)}{<\beta>}$ is higher than in other cases. Apparently, the major scattering mass of such clouds accumulates directly beneath the tropopause in a thin layer. The mean distance from the tropopause to the maximum $\frac{\beta (z)}{<\beta>}$ for the clouds of this class was 400m.

The distribution curves $\frac{\beta (z)}{<\beta>}$ in Figure 2.2c corresponding to the thick clouds, H > 1.8 km, have a more complicated form than the ones in Figure 2.2b. Also apparent is some tendency to shift the center of the visible light coefficient distribution to the upper boundary for the clouds of low temperature. We should mention that the maximum thickness of the clouds with the lower boundary Z_b = 5 to 6 km reached 4.4 km. For this reason, within the same class of thick clouds the mean values of H differ as a function of Z_b. Characteristic of vertical distribution of the extinction coefficient for the thick clouds

is the presence of a minimum, approximately in their central part. Most of the observed thick clouds had a two-mode vertical structure.

The curves of the vertical distribution $\beta(Z)$ for some classes of clouds are not presented in Figure 2.2 for lack of observations in the corresponding ranges of heights and thicknesses.

The curves of the vertical profile $\beta(Z)$ presented in Figure 2.2 are the result of averaging over several tens of different profiles for each class. Some individual cases, may have a much more complicated form. Therefore the distributions of $\beta(Z)$ presented in Figure 2.2 were used to calculate the variation coefficients $\delta_\beta = \sigma_\beta/\beta$ for different heights z (σ_β is a rms deviation). The δ_β value near the cloud boundaries is found to reach 0.5, and in the central part δ_β reduces to 0.3-0.35. These high values of relative deviations from the average profiles $\beta(Z)$ emphasize a high variability of the extinction coefficient structure. As was discussed above, the curves of the mean profiles $\beta(Z)$ can make sense when averaged over distances of, at least, several kilometers along the cloud deck.

Computations of the mean profiles $\beta(Z)$ were performed for nine selected series of lidar observations of various clouds (1.2 km < H <1.8 km). The time interval represented by each series is 15-20 min, and the number of lidar measurements in each is 15-20.

Cloud covered areas with horizontal extent from 5 to 20 km were observed (wind speed changed from 5 m/s to 25 m/s). It was found that for the seven series the deviation of the series average profile (β_{av} (Z)) from the total average did not exceed 20% for all the Z values. For two series the deviations for different Z were 30-40%.

Next we examine the dependence of high cloud thickness, H, on temperatures at the center of the cloud (H/2). The points in figure 2.3 refer to the mean H values in the eight degree intervals of the center of the cloud temperature. The vertical segments represent the range of H values in the experimental data. The dependence in Figure 2.3a is obtained from our experimental data, the dependence in Figure 2.3b for the summer season in Australia at 38°S was obtained during the experiment described in (Heymsfield A. I., C.M.R. Platt, 1984). We should note that the averaging intervals in Figure 2.3b are equal to 10° C. As is evident from Figure 2.3 the dependencies H(Tc) differ somewhat for the two experiments. In the present case the clouds were thinner; this might be caused by the following. We assumed a cloud to be a single entity if the extent of the vertical breaks in it, i.e. the distance between the upper boundary of one layer and the lower boundary of the next one, did not exceed 0.5 km, while Heymsfield and Platt used a criterion of 1 km. Common to both plots 2.3a and 2.3b is a tendency for the Ci thickness to decrease with a lowering of temperature for $T_c < -40°$ C. The maximum of the clouds mean thickness, in accordance with the results of (Heymsfield, A. I., C.M.R. Platt, 1984) was observed at $T_c \approx -35°$ C. In our case the maximum was local at $T_c \approx -40°$ C. With the temperature increase the mean thickness decreases at $T_c \approx -35°$ C, and then again increases at $T_c \approx -24°$ C. The variation coefficient (δ_H) in the eight-degree smoothing intervals was about 0.5 at $T_c \approx -24°$ C, in the other T_c intervals - about 0.4. These values show that the thicknesses are highly variable.

The mean thickness dependence on T_c presented in Figure 2.3 can be approximated with a polynomial of the second degree:

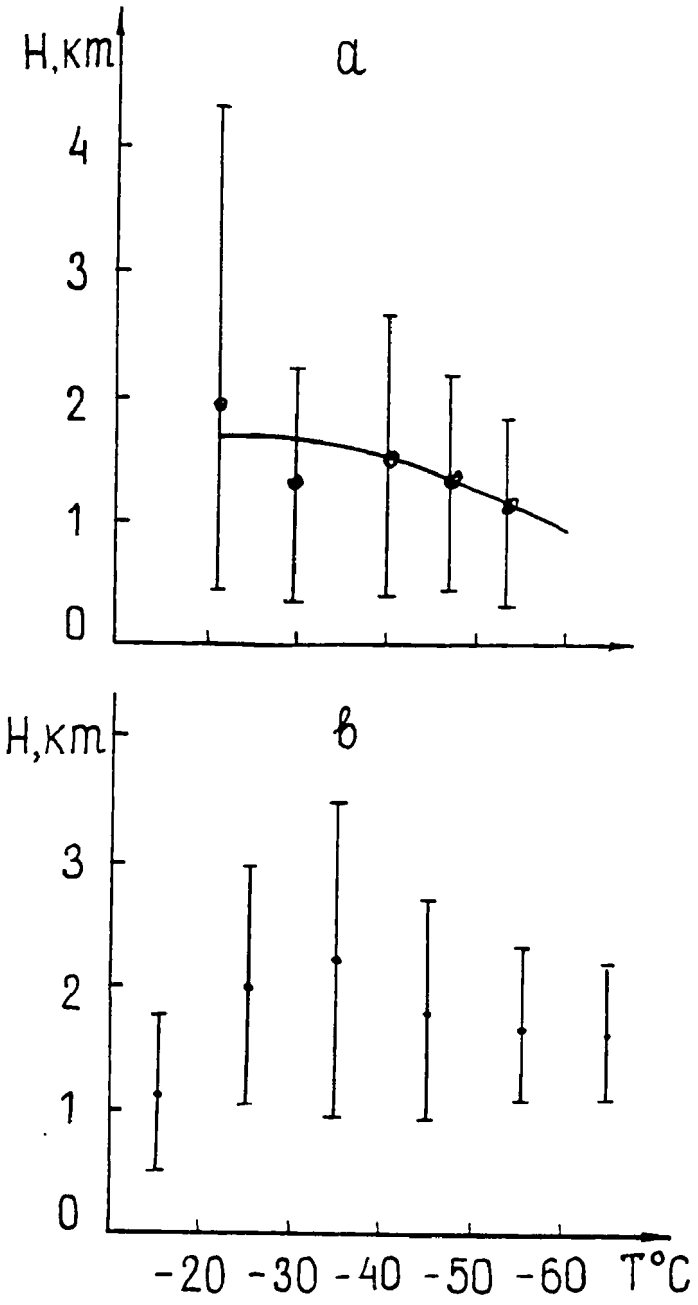

Figure 2.3 Dependence of Ci cloud thickness (H) on temperature (T_c) at H/2 level.

$$H(T_c) = 1.28\text{-}0.034\ T_c\ \text{-}0.00068\ T^2_c \qquad (2)$$

in the temperature range -60° C ≤ T_c ≤ -20° C, where H is measured in km. The curve described with formula (2) is shown in Figure 2.3.

Nevertheless, all data indicate that cloud thickness H(Tc) should decrease as the temperature decreases for Tc ≤ -35° C.

Correlations connecting Ci cloud parameters were approximated from the experimental data. The vertical profiles of the extinction coefficient for 1.2 ≤ H ≤ 1.8 km are well described by the function of the following form:

$$\beta(\xi) = [1.17<\beta>(1\text{-}\xi)^{2.56\text{-}0.125|Z_b|}] * [\exp((0.83 + 0.47\ Z_b)\xi)\ 1] \qquad (3)$$

where $\xi = \frac{Z-Z_b}{H}$ and Z, Z_b, H are measured in km. Equation (3) describes the curves presented in Figure 2.2b if the upper boundary height $Z_t < Z_{tr}$ (Z_{tr} being the tropopause height). The rms deviation of the experimental curves from the curves of (3) is about 10% of the value $<\beta>$.

For the curves presented in Figure 2.2a the function of the following from is a good approximation for curves 1, 3:

$$\beta = 0.12<\beta>[\exp(-11.6(\xi^2\text{-}\xi))\text{-}1] \qquad (4a)$$

for curve 2:

$$\beta = 0.19<\beta>[\exp(-9.6(\xi^2\text{-}\xi))\text{-}1] \qquad (4b)$$

When these functions are combined with functions (4a) and (4b) the rms deviation from the experimental curves is less than 10% in $<\beta>$ units.

The values described with formulas (3) or (4) can be transformed into the function of the atmospheric temperature. This can be done by introducing the averaged dependence of the temperature on altitude. The latter, after averaging over all the hours of measurements, can be approximated with the following function:

$$Z(T) = 0.13|T| + 3.1 \qquad (5)$$

Then expression (3) can be transformed into the following:

$$\beta(\xi) = 1.17<\beta>(1-\xi_T)^{(2.17-0.16|T_b|)} * (\exp((2.07 + 0.52|T_b|)\xi_T-1) \qquad (6)$$

where $\xi_T = (Z - Z_b) / (T_t - T_b)$; Z_b, Z_t, - the temperatures at the levels of the lower and upper boundaries, respectively. The temperature in (6) is measured in degrees Celsius.

Analyzing the results obtained from applying Eq. 6, we can draw the following conclusions. The form of the vertical distributions of the extinction coefficient in Ci clouds is different for clouds of different thickness situated at different levels. It has been found that the maximum of $\beta(Z)$ - distribution shifts to the upper boundary for colder (higher) clouds. This can be explained by the center of ice crystal generation being situated closer to the boundary of a mature cloud. As the cloud particles grow, the largest ones fall downwards. For higher clouds with smaller ice crystals and hence smaller fall velocities, there is less separation of the ice mass by differential fall velocities, therefore the maximum $\beta(Z)$ will be nearer to the level of the initial center of ice crystal generation. For clouds situated directly beneath the tropopause the bulk of the cloud mass is in a thin layer, the maximum $\beta(Z)$ occurring at the level which is 0.3 to 0.5 km lower than the tropopause.

In the case of thick Ci clouds of more than 1.8 km thickness a break in the vertical distribution of the extinction coefficient is found approximately in the middle of the clouds' thickness.

Next the dependence of the mean extinction coefficient $<\beta>$ on temperature is examined. The results are shown in Figure 2.4 in the form of four points (crosses) for eight - degree intervals of average temperature. Curve (2) can be described with the following expression:

$$< \beta\ (T) > = 3.2 * 10^{-4}\ (T\text{-}T_o)^2 \qquad (7)$$

where $T_o = 82.5^\circ$ C. This expression is a new development of the empirical formula for the infrared absorption coefficient σA obtained in (Platt, C.M.R., Harshvardhan, 1988), from the approximation $<\beta> = 2\sigma A$.

Figure 2.4 shows that the points describing our data are situated somewhat lower than curve 2. A function analogous to (7), with other factors, can be used to approximate our data:

$$< \beta\ (T) > = 2.1 * 10\text{-}4\ (T\text{-}T_o)^2 \qquad (8)$$

Thus, in our experiments we observed clouds with smaller values of the extinction coefficient in comparison with the data of Platt and Harshvardhan.

We have also carried out a comparison of the measured cirrus cloud thicknesses with $<\beta>$. In Figure 2.5 the results of comparison for clouds with a lower boundary varying between 7 and 9 km are shown. In this figure the crosses present the results of $<\overline{\beta}>$ and $\overline{H}$ measurement. The time duration of an individual series measurement is about 30 min. The solid line in Figure 2.5 is plotted using the mean values of $<\overline{\beta}>$ for the

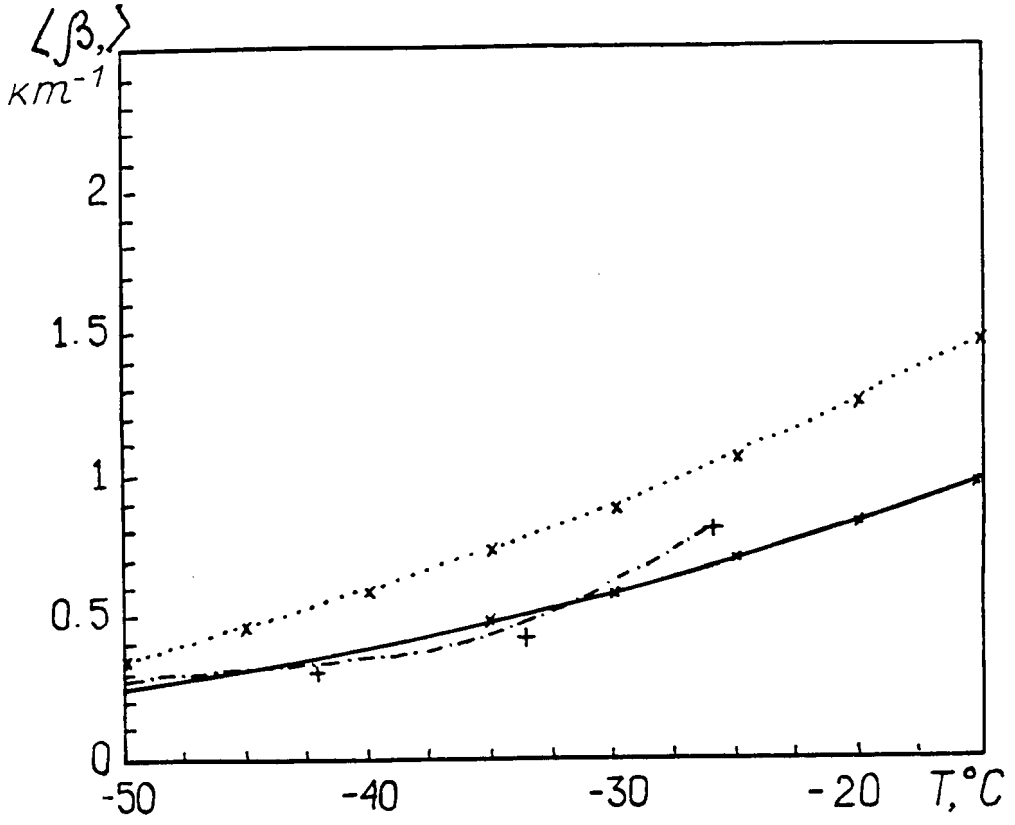

Figure 2.4 Dependence of the mean extinction coefficient $<\beta>$ on temperature (T) in Ci clouds.
1 .-.-.- from our data
2 · · · · from formula (7)
3 —— from formula (8)

respective interval $\overline{H}$ over the total number of the observed series in it. The pattern of the $(<\overline{\beta}>, \overline{H})$ points suggest a tendency of $<\beta>$ to decrease with an increase of <H>. This phenomenon can be explained as follows. For the clouds situated in a narrow height interval (and thus in a narrow temperature interval) the extinction coefficient in the cloudy medium also shows little variation - perhaps partly due to the vertical resolution of the lidar from which β is derived. The vertical structure of cirrus clouds may be typically inhomogeneous. While thin clouds may be relatively uniform, thick clouds can include voids and be composed of multiple-layers. Therefore, $<\beta>$ in thicker clouds may be smaller than in thin ones.

When considering the experimental data presented in Figure 2.5 it is necessary to emphasize the potential for the following misinterpretations. It is possible that the only thin clouds observed had large values of $<\beta>$. If a cloud is thin and its β is small, then its optical thickness may be very small, and such clouds can hardly be discerned visually in the day-time. Lidar measurements were carried out continuously only when high clouds were evident. Therefore the experimental data for the clouds of small thickness might be biased by decisions of when to collect lidar data. More exactly, only the areas of small thickness in large and well-developed cloud systems were examined.

It is interesting to note that during the lidar measurements of the profiles of the aerosol back scattering coefficients (β_π) made by CAO, the following phenomenon could be often observed at the altitudes of cirrus cloud generation. Most often near the tropopause, some time before cirrus clouds emerged, the parameter β_π increased by a factor of 2 or 3. This time between the precursor signal and cirrus onset varied from several

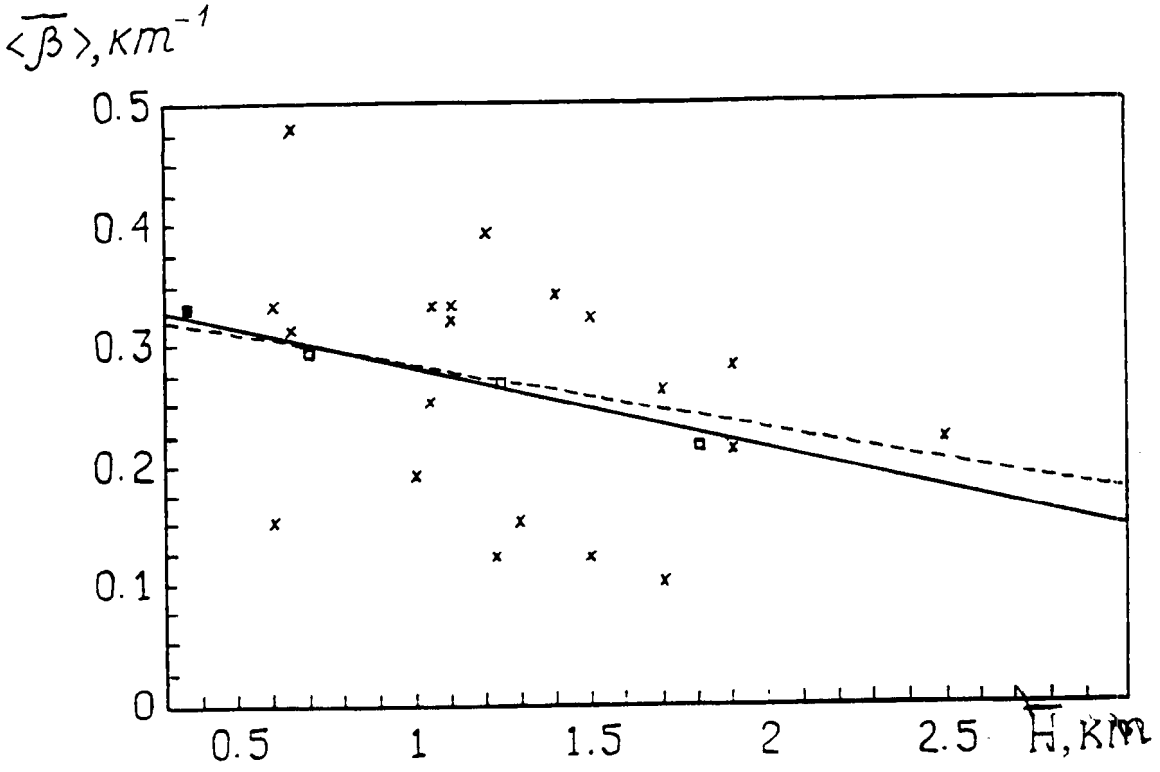

Figure 2.5 Dependence of the mean extinction coefficient (<β>) on the Ci cloud thickness (H).
- - - - mean values of <β> and H for a half hour's measurement;
—— mean values of <β> and H over the total number of half hour measurements in respective intervals of H.

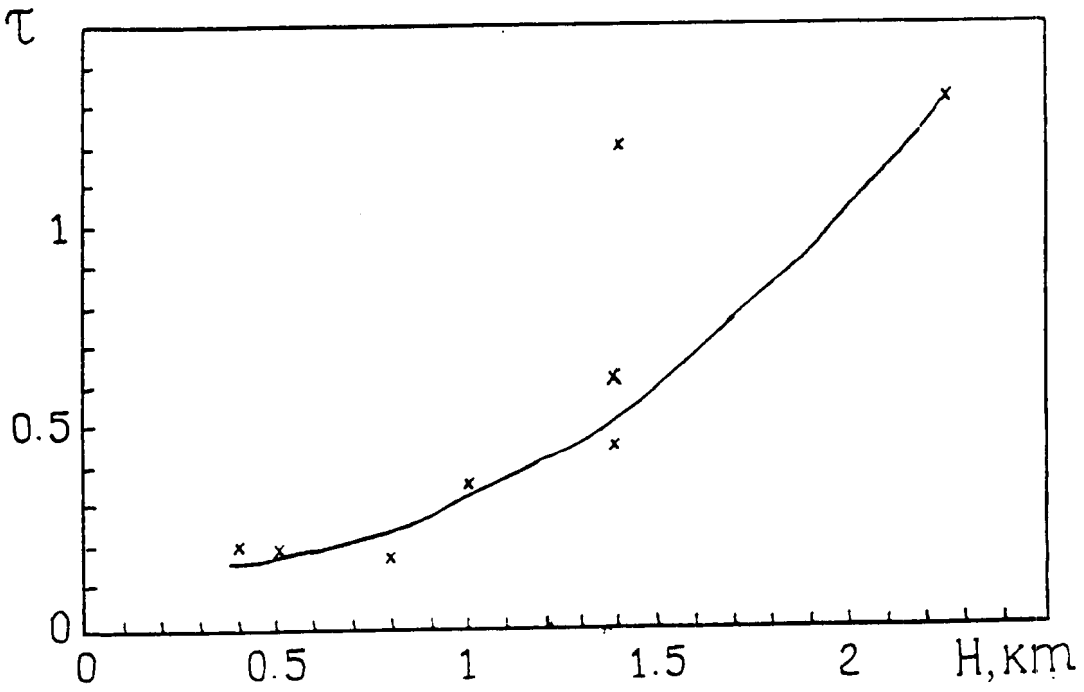

Figure 2.6 Dependence of the mean optical thickness (τ) on the cloud thickness for individual days of 1986-1989 experiment.

hours to twenty four hours and more. What is an such an increase of β_π caused by? It can be explained by aerosol injection before a front passage, or it may be some initial phase of cirrus cloud generation. One thing is clear, if these are "super thin" clouds they could not be detected with our lidar in the day time.

For the approximation of the experimental dependence of $<\beta>$ on cloud thickness shown in Figure 2.5, a linear function of the following form can be used:

$$<\overline{\beta}> = -0.06\overline{H} + 0.34 \qquad (9)$$

where β is measured in km^{-1}, and H in km. The coefficient of variation for this approximation is about 15%.

We should note that, irrespective of the decrease of $<\beta>$ with the growth of H, the integrated optical thickness (τ) grows as H increases. Figure 2.6 shows the dependency of the cirrus cloud optical thickness (τ) on the cloud thickness (H) obtained through averaging half-hour intervals during one day. Seven days have been examined in this manner (1 - 1986, 4 - 1987, 2 - 1989). Figure 2.7 presents the dependence of optical thickness on cloud temperature. The experimental data spread in figures 2.6 and 2.7 is caused by the errors of comparison between τ and H. Optical depth was measured in the direction of the solar disc and converted to an equivalent zenith value while cloud thickness was measured in the direction towards the zenith. Therefore, of all the periods of observation, only seven days, with good correlations between the lidar and spectrophotometer data, were chosen.

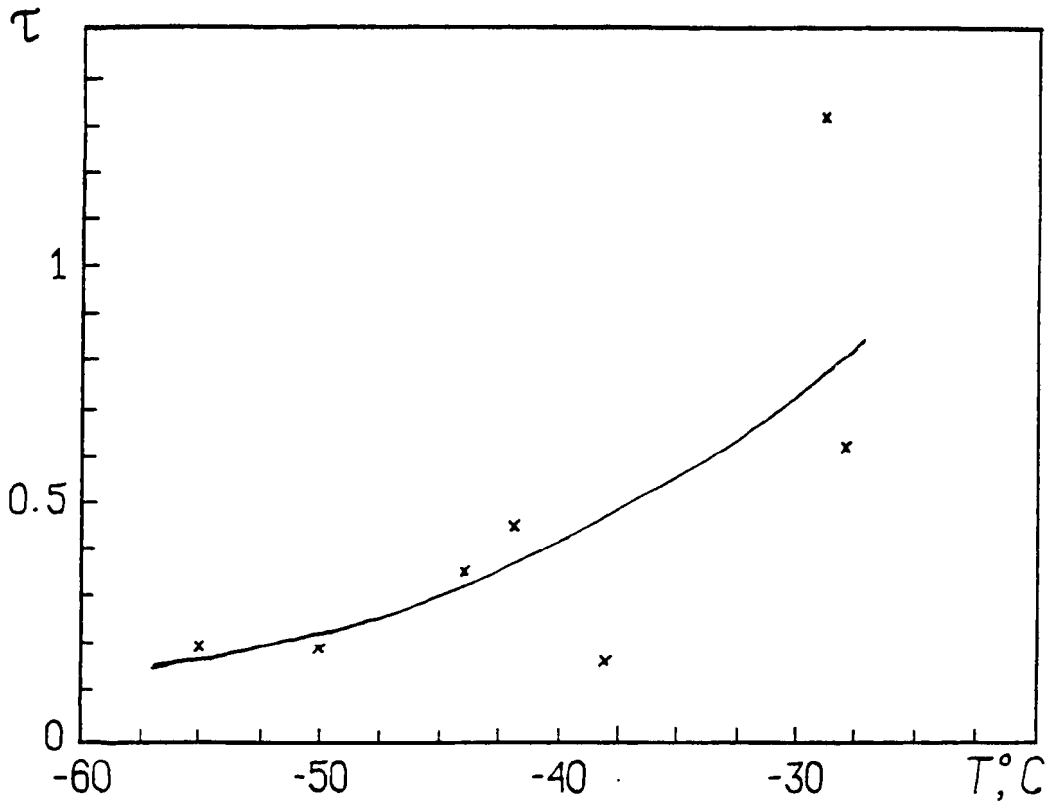

Figure 2.7 Dependence of mean optical thickness (τ) on temperature (T °C) at H/2 level for individual days of 1986-1989 experiment.

Figure 2.8 shows both the $<\beta>$ and τ dependencies on the cloud thickness H for one day of measurements - June 2, 1989. Each point is obtained by averaging 30-minute intervals. On June 2, there was an excellent case of Cs clouds of a significant optical thickness all over the sky, and that enabled us to process the experimental results with minimum errors.

In conclusion we should like to note that only few data are available to date from which to speak with confidence about any statistical regularities of the β, τ, H and T dependencies. Further investigation is necessary for verifying and improving our analysis.

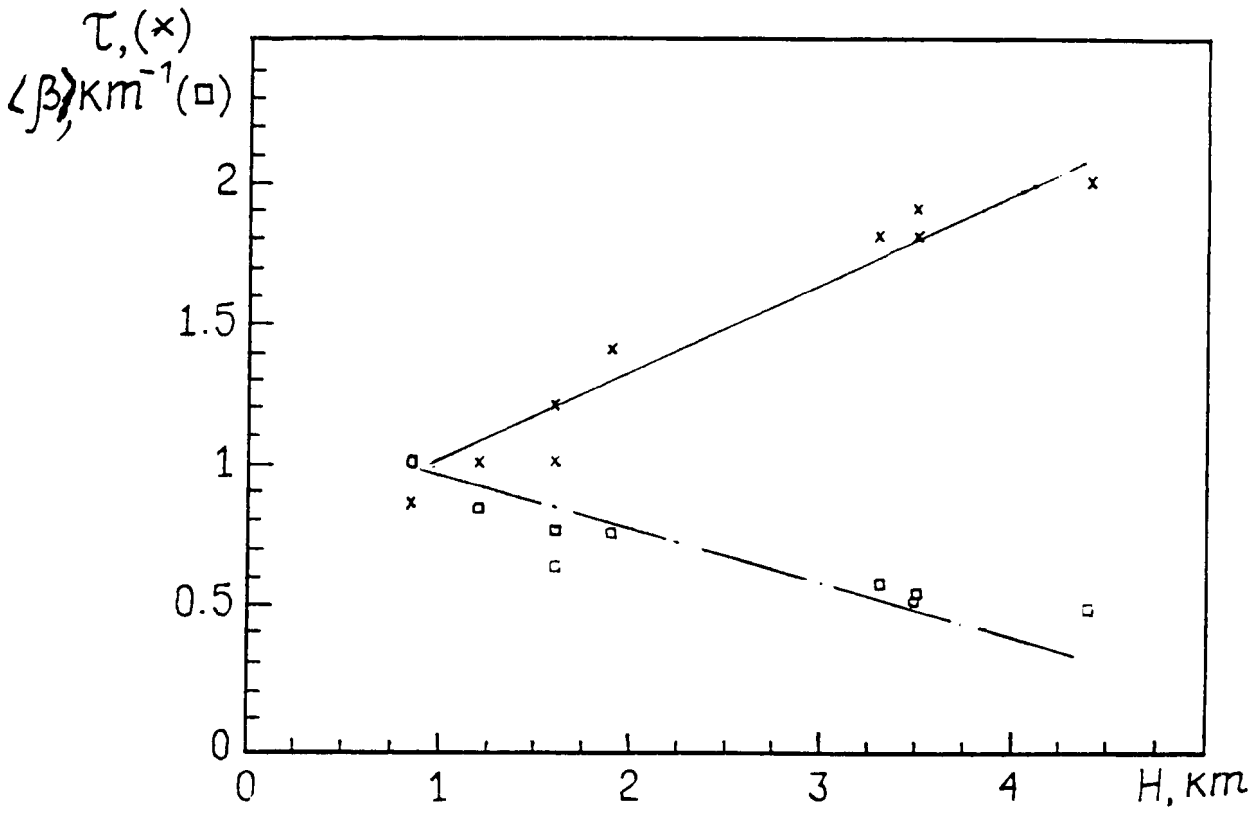

Figure 2.8 Dependence of the optical thickness (τ) and the extinction coefficient (β) for half hour's intervals on 2.06.89 on cloud thickness (H).

REFERENCES

Abakumova, G. M., et al., 1989: The Geometrical, Optical and Radiative Properties of Cirrus Clouds. Colorado State University, Atmospheric Science Report No. 456, 61 pp.

Heymsfield, A. I., and C.M.R. Platt, 1984: Parameterization on Particle Size of Ice Clouds in Terms of the Ambient Temperature and Ice Water Content. *J. Atmos. Sci.*, 41, 846-855.

Platt, C.M.R., and Harshvardhan, 1988: Temperature Dependence of Cirrus Extinction: Implication for Climate Feedback. *J. Geophys. Res.*, 93, 11,051-11,058.

Chapter 3

Determination of Optical Thicknesses and Effective Sizes of Cirrus Particles

by P. P. Anikin, G. M. Abakumova, E. V. Romashova, and A. V. Tikhonov

In Grassl, H., 1970 and Anikin, P. P., 1989 the first attempts were made to explain the observed spectral dependence of optical thicknesses of cirrus clouds. The possibility of determining the sizes of large ice particles on the basis of spectral measurements of solar radiation transmission through cirrus was shown. The present work extends the aforementioned work. For various models of log normal distributions of sizes of ice spheres, n(r), we calculated the coefficients of extinction, absorption and scattering. Simultaneously the mean effective radius r_{eff} was calculated for each model:

$$r_{eff} = \frac{\int_0^\infty r^3\, n(r)\, dr}{\int_0^\infty r^2\, n(r)\, dr} \qquad (1)$$

Having used r_{eff}, we can resolve the problem of scattering for polydisperse media as a problem for an equivalent monodisperse medium (McCartney, E. J., 1977). The major characteristic which determines extinction in clouds, is the volume coefficient of extinction:

$$K(\lambda) = \pi N \int_{r_1}^{r_2} Q_{ext}\,(r,\lambda)\, n(r)\, r\, dr \qquad (2)$$

where N is the number of cloud particles in a unit of volume; λ is the wavelength; Q_{ext} is the extinction efficiency whose values are obtained from Mie theory for spherical particles. K (λ) values were calculated for 14 wavelengths (λ = 0.6; 1.2; 2.1; 3.9; 4.7; and from 8 to 12 μm in 0.5 mcm increments) for the models of ice clouds with modal radii (r_{mod}) from 1 μm to 30 μm and dispersions σ^2 from 0.1 to 0.5. The optical thickness is defined as $\tau(\lambda) = K(\lambda)H$, where H is the thickness of a cloud. Coefficients of the refractive index of ice were taken from (Irvine W.M., Pollack J.B.,1968). Figure 3.1 presents the results of calculations of the ratio $\frac{K(\lambda)}{K(\lambda - 2.1\ \mu m)}$ as a function of λ for $\sigma^2 = 0.1$ and various values of r_{mod}. This representation is most suitable for comparison with the experimental data, since the measurements of transmission of radiation determine only a relative value of the extinction coefficient. For particles with $r_{mod} < 10$ μm the minimum of the ratio $\frac{K(\lambda)}{K(\lambda - 2.1\ \mu m)}$ is located in the region $\lambda = 10$ μm. The figure shows smoothed curved lines of relative spectral extinction of radiation from one calculated point to another. This behavior is possible for these wavelengths where imaginary and real parts of complex index of refraction are strongly changeable. Figure 3.2 shows the dependence of the ratio $\frac{K(\lambda)}{K(\lambda - 2.1\ \mu m)}$ for particles with size $r_{eff} > 4$ μm at $\lambda = 0.6$ μm and 10 μm. Note that $\frac{K(\lambda-0.6\ \mu m)}{K(\lambda-2.1\ \mu m)} \sim 1$ for $r_{eff} \geq 20$ μm and $\frac{K(\lambda-10\ \mu m)}{K(\lambda-2.1\ \mu m)} \sim 1$ for $r_{eff} \geq 60$ μm. At the same time for particles with $r_{eff} < 16$ μm a clear dependence

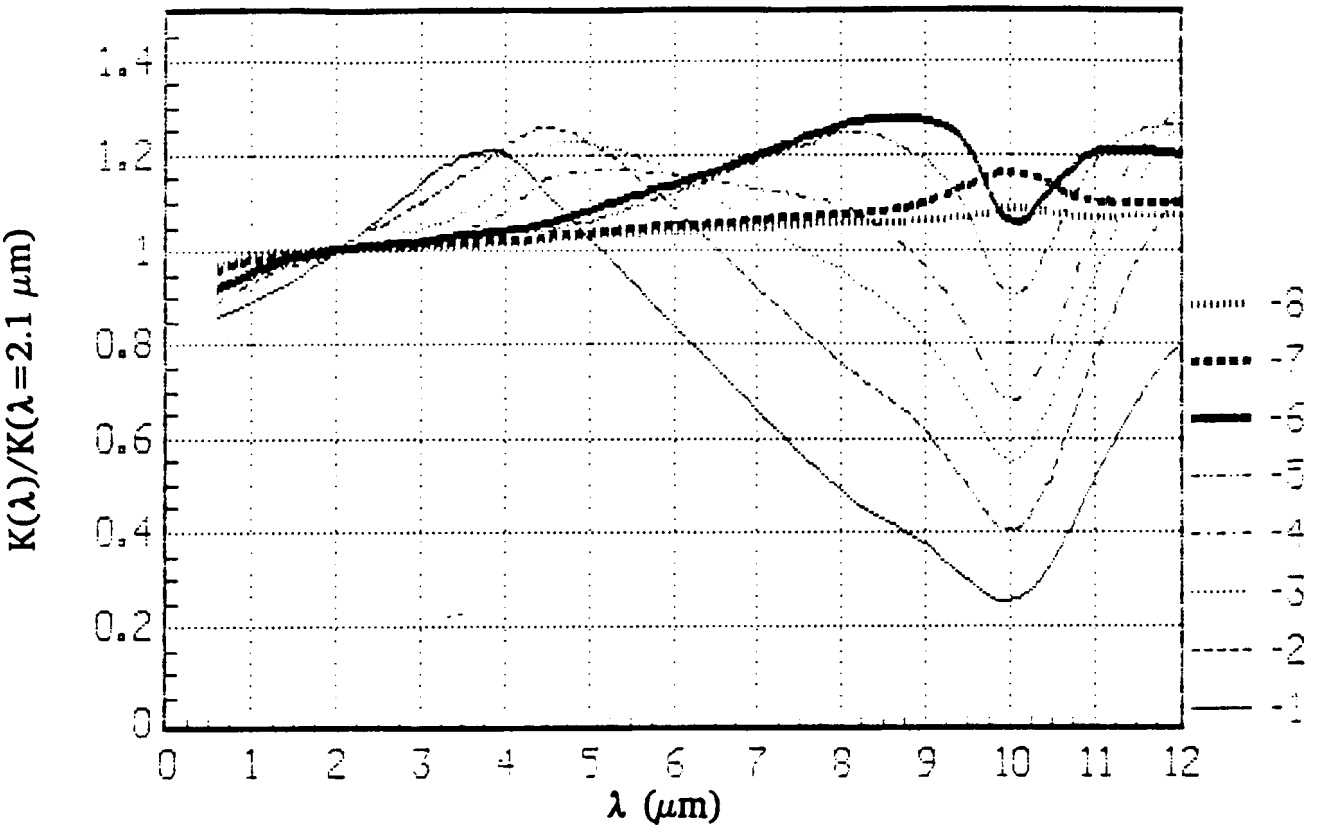

Figure 3.1 Dependence of relative coefficient of extinction $K(\lambda)/K(\lambda=2.1\ \mu m)$ upon wavelength λ for dispersion $\sigma^2 = 0.1$ and modal radius: 1 to 3 μm; 2 to 4 μm; 3 to 5 μm; 4 to 6 μm; 5 to 8 μm; 6 to 10 μm; 7 to 20 μm; 8 to 30 μm.

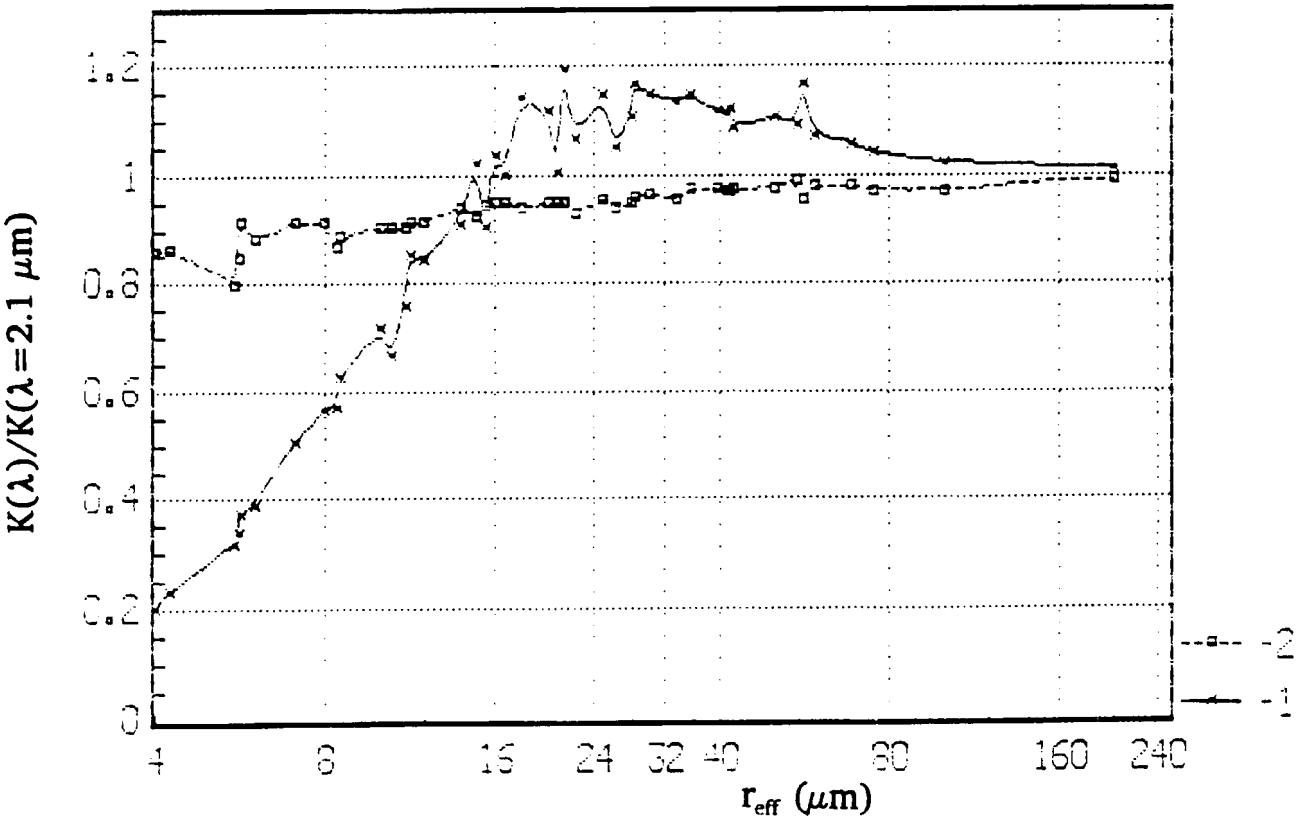

Figure 3.2 Dependence of $K(\lambda)/K(\lambda=2.1\ \mu m)$ upon effective radius of spherical ice particles; 1 - $\lambda=10\ \mu$m; 2 - $\lambda=0.6\ \mu$m.

on r_{eff} exists for the ratio $\frac{K(\lambda\text{-}10\ \mu m)}{K(\lambda\text{-}2.1\ \mu m)}$, which suggests that one may determine the effective size of particles within ice clouds - on the basis of measurements of the transmitted radiation through clouds at two wavelengths. Calculations of $K(\lambda)$ have been made assuming that only direct solar radiation comes to a measuring device. Yet, in reality a certain part of forward scattered radiation is always present in a measured signal. Therefore, the measured optical thickness of a cloud $\bar{\tau}_\lambda$ will be smaller than the actual τ_λ:

$$\tau_\lambda = \bar{\tau}_\lambda + \Delta\tau^{sc} \tag{3}$$

where $\Delta\tau_\lambda^{sc}$ is the incremental optical thickness, obtained as a result of scattered light coming into the receiver. To determine $\Delta\tau_\lambda^{sc}$ the scattering functions were calculated for spherical ice particles at λ = 0.6 μm; 2.1 μm; 4.7 μm; 10 μm with a small step: in 0.1° increments from 0° to 5° and in 1° increments from 5° to 180°. Special attention was paid to the normalized flux of radiation which comes to the receiving aperture Δ of the measuring device by single scattering:

$$D = \frac{\int_0^{\Delta} \frac{P(\Theta)}{4\Pi} \sin\Theta d\Theta}{\int_0^{\Pi} \frac{P(\Theta)}{4\Pi} \sin\Theta d\Theta} \tag{4}$$

where Δ = 15'; 1°; 2°; 3°; 4°; 10°; $P(\Theta)/4\pi$ is the scattering indicatrix normalized in accordance with the section of scattering. Θ is the angle of scattering. For clouds with large optical thicknesses, the influence of higher order scattering becomes significant. In these cases, we used the Monte Carlo method to calculate transmitted radiance.

In Anikin, P.P., 1989 and Abakumova, G.M., et al., 1989 the results of calculations of the ratio $\frac{\bar{\tau}(\lambda)}{\tau(\lambda)}$ for different r_{eff} and angles of view α taking only scattering into account were presented. In the present work we also took into consideration absorption and calculated the single scattering albedo, $\omega(\lambda)$, for various models of ice clouds. Figure 3.3 (a, b, c, d), shows the ratios $\frac{\bar{\tau}(\lambda)}{\tau(\lambda)}$ for various λ, visual angles α, and sizes - r_{eff}. Accounting for absorption makes the behavior of the curves $\frac{\bar{\tau}(\lambda)}{\tau(\lambda)}$ for $\lambda > 2.1$ μm significantly different from the analogous curves in (Anikin, P. P., 1989 and Abakumova, G. M., Anikin, P. P., et al., 1989) where $\omega(\lambda) = 1$. Nevertheless, the conclusion reached by the previous authors is still valid: with $\lambda = 4.7$ and $\lambda = 10$ μm the diffused light does not practically come to the entrance of the receiver with α = 15', i.e. the measured $\tau(\lambda = 10$ μm) is the real one, and at $\lambda = 2.1$ μm the above is true for $r_{eff} \leq 60$ μm.

In the experiments conducted in 1986-1989, measurements of transmission of solar radiation by cirrus clouds were made with the use of devices with angles of view α_1 = 15' and α_2 = 10°, therefore calculations of the ratio $\frac{\tau(\alpha_2)}{\tau(\alpha_1)}$ from r_{eff} for various λ are of special interest. Figure 3.4 shows (for $\lambda = 0.6$ μm) dependencies of ratios $\frac{\bar{\tau}(\alpha-10°)}{\bar{\tau}(\alpha-0°)}$

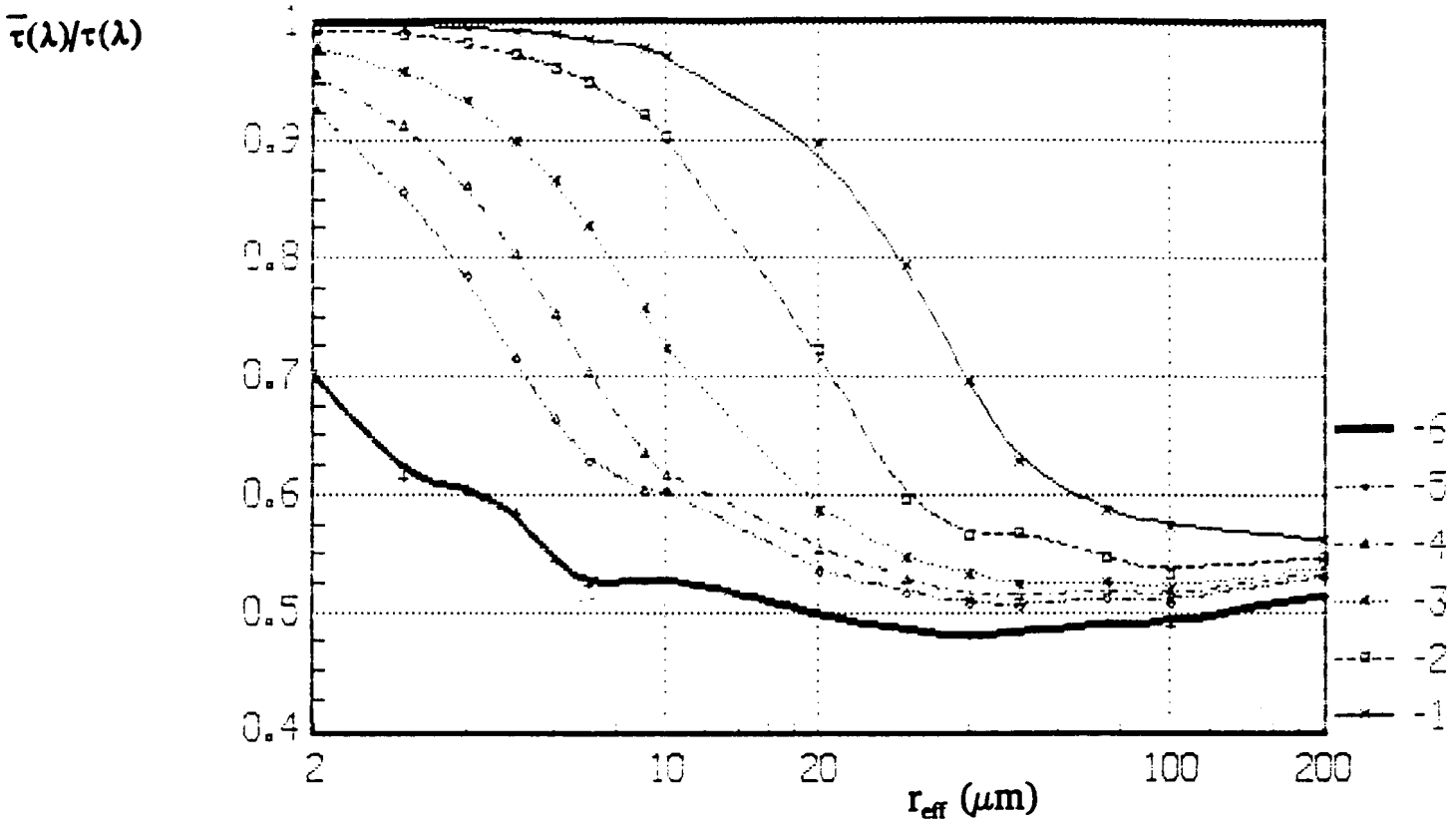

a) λ=0.6 μm;

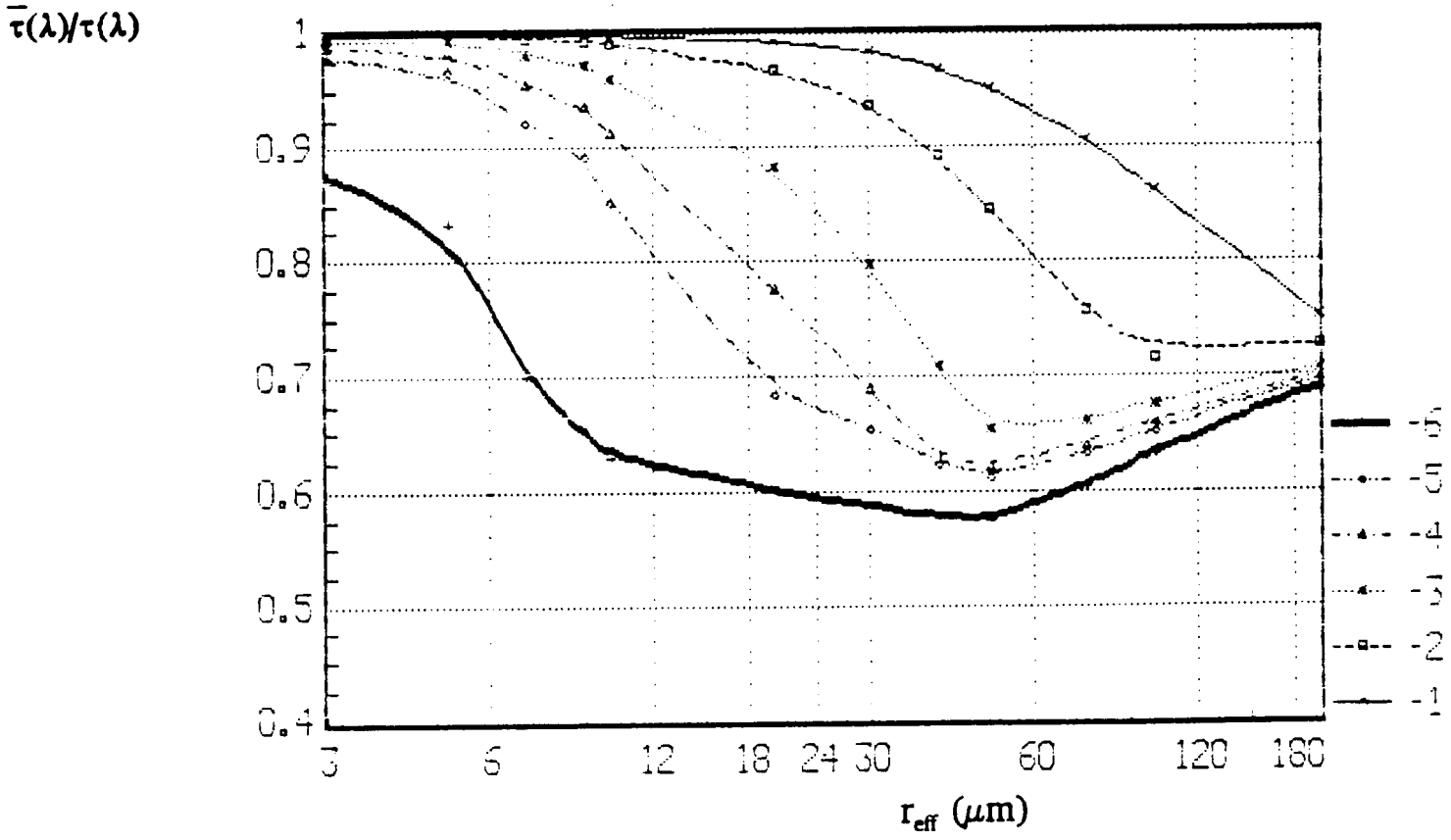

Figure 3.3 Dependence of ratio $\frac{\bar{\tau}(\lambda)}{\tau(\lambda)}$ on effective radius of particles r_{eff} for various angles of view. 1α = 15'; 2 - 1° ; 3 - 2°; 4 - 3°; 5 - 4°; 6 - 10°.

b) λ=2.1 μm;

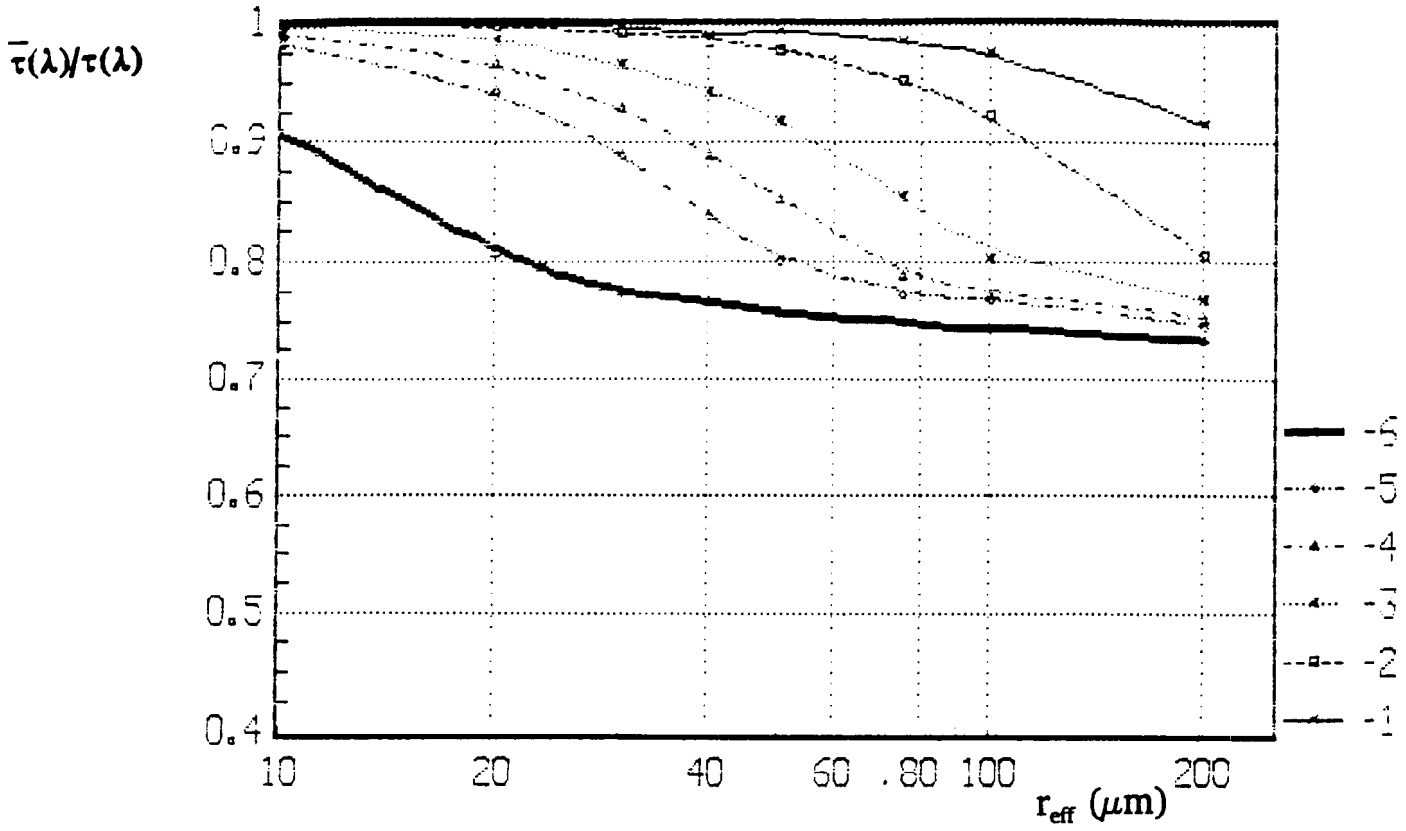

c) λ=4.7 μm

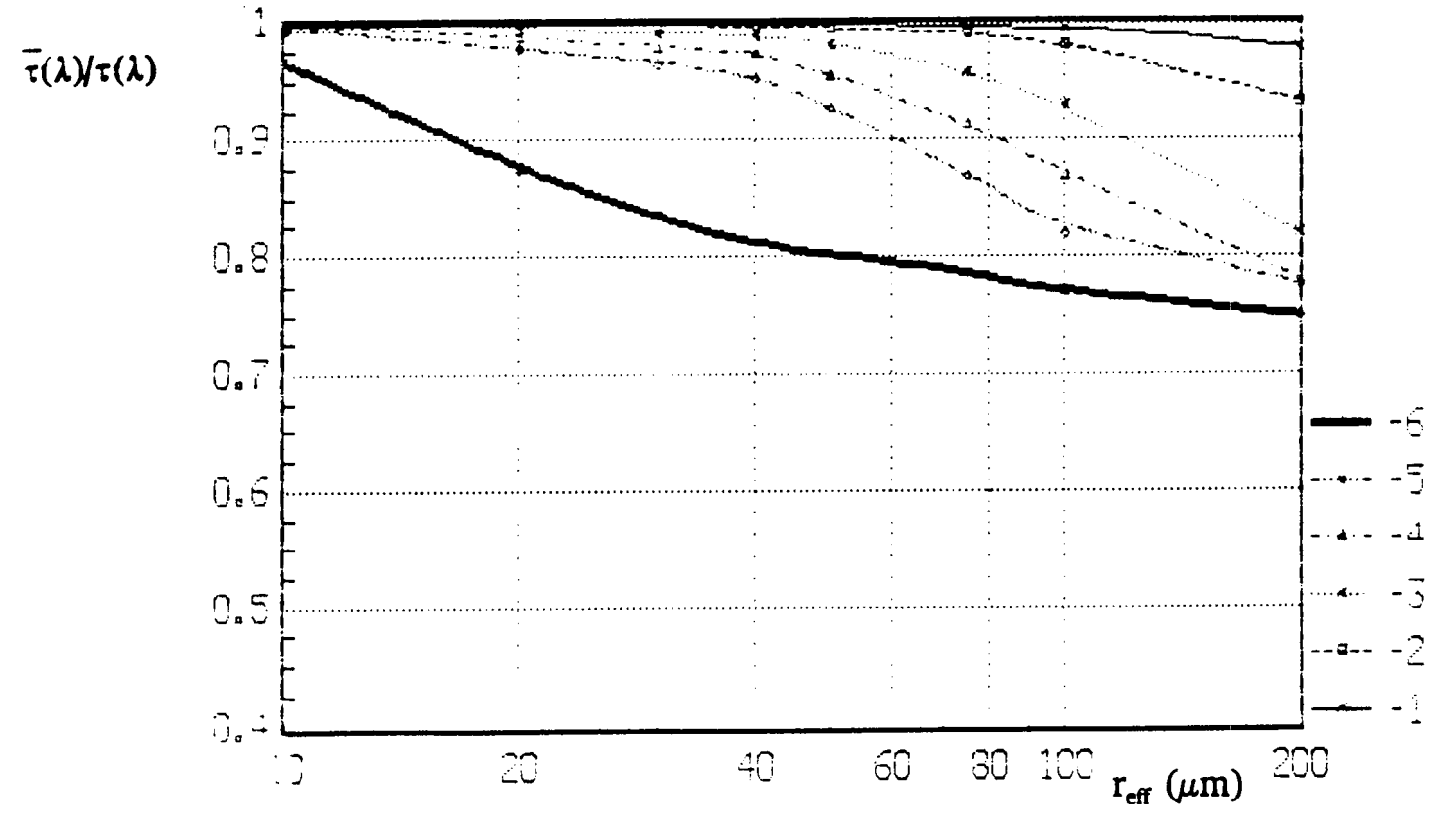

Figure 3.3 Dependence of ratio $\frac{\bar{\tau}(\lambda)}{\tau(\lambda)}$ on effective radius of particles r_{eff} for various angles of view. 1α = 15'; 2 - 1° ; 3 - 2°; 4 - 3°; 5 - 4°; 6 - 10°.

d) λ=10 μm.

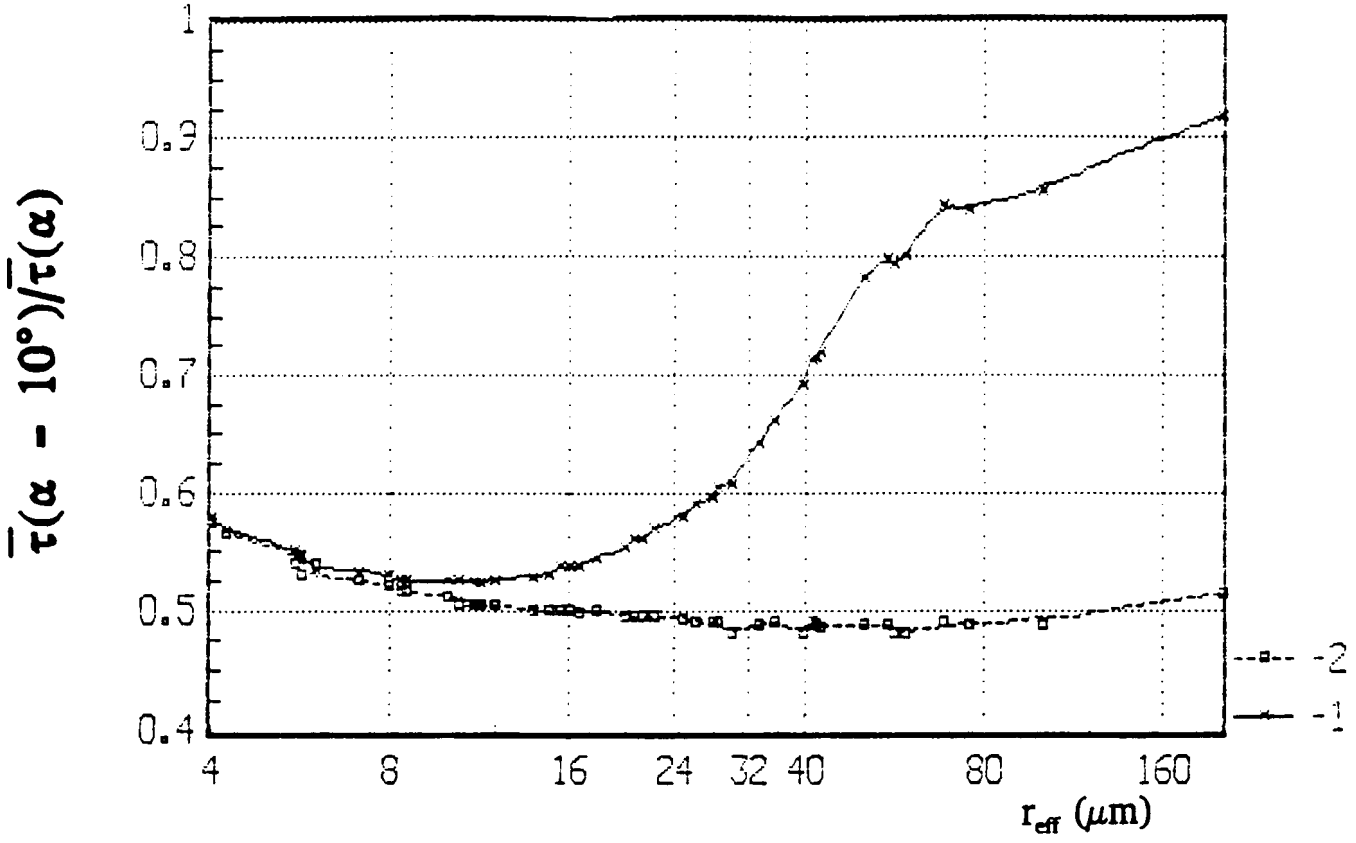

Figure 3.4 Dependence of the ratio of calculated optical thicknesses $\frac{\bar{\tau}(\alpha - 10°)}{\bar{\tau}(\alpha)}$ at wavelength λ=0.6 μm (curve lines 1-2) as a function of effective particle radius 1: - α = 15'; 2: - α = 0°.

and $\frac{\bar{\tau}(\alpha-10°)}{\bar{\tau}(\alpha-15')}$ upon r_{eff}. The figure shows that (at least from $r_{eff} = 20\ \mu m$ to $r_{eff} = 200\mu m$) there is a simple dependence between $\frac{\bar{\tau}(\alpha-10°)}{\bar{\tau}(\alpha-15')}$ and r_{eff} which may be used for determining r_{eff}. At the same time, the ratio $\frac{\bar{\tau}(\alpha-10°)}{\bar{\tau}(\alpha-0°)} \neq 0.5$ for $r_{eff} > 10\ \mu m$. Therefore, the optical thickness of clouds, $\bar{\tau}(\lambda)$, consisting of particles with $r_{eff} > 10\ \mu m$ can be surely measured by a device with an angle of view $\alpha = 10°$ in the visual range of wavelengths. Actual values of $\tau(\lambda)$ (without accounting for forward scattered radiation) can be found in accordance with formula $\tau(\lambda)-2\bar{\tau}(\lambda)$. The same conclusion was obtained in experimental work of Abakumova, G. M., Anikin, P. P., et al., 1989.

To confirm the above calculations, let us consider the results of experiments on determining optical thicknesses of cirrus clouds. Using the data obtained during the three years 1986, 1987, and 1989, further verification was made of the conclusion about the feasibility of determining τ, and its time variability from measurements of the integral direct solar radiation (thermoelectric actinometer model AT-50 with angle of view $\alpha = 10°$). Two methods were used: method one was used in the analyses conducted by researchers from the Institute of Atmospheric Physics; and method two was applied by researchers from Moscow State University.

To determine $\bar{\tau}$ using method 1, synchronous measurements were made of transmission of solar radiation through cirrus by actinometer and by a five wavelength spectral radiometer (SR) (Anikin, P.P., Chavro, A.I., et al., 1981). The angle of view of

the SR was approximately 15'. Measurements were made synchronously during a day with the data recorded every 5 seconds by an IBM PC/AT; therefore, any number of points (usually from 20 to 1000 points) could be chosen for processing.

Transmission (P_λ) and optical thickness $\bar{\tau}_\lambda$ of cirrus for wavelength λ were determined from the SR data using the following relationships:

$$P_\lambda = \left(\frac{S_\lambda}{S_{0,\lambda}}\right)^{1/m} ; \bar{\tau}_\lambda = -lnP_\lambda \qquad (5)$$

where S_o, λ is the relative value of spectral flux of solar radiation measured in clear spaces between clouds (100% line); S_λ is the relative value of spectral flux of solar radiation passed through a cloud; and m is the optical mass of the atmosphere.

Similar ratios were used to determine P_A and $\bar{\tau}_A$ in accordance with relative values of integral direct solar radiation (S) measured by the actinometer. The 100% line was chosen in most clear spaces between clouds.

Values of $\bar{\tau}_\lambda$ for wavelengths λ = 2.1 μm and λ = 10.2 μm, $\bar{\tau}_{2.1}$ and $\bar{\tau}_{10.2}$, were considered close to actual values because the scattered radiation in the near and far infrared regions of spectrum coming to the device within the visual angle 15', is small and can be neglected.

To evaluate the ratio $\frac{\bar{\tau}_\lambda}{\bar{\tau}_A}$ we used the method of least squares, assuming that

the relation between $\bar{\tau}_\lambda$ and $\bar{\tau}_A$ is linear one, i.e.

$$\bar{\tau}_\lambda = a\bar{\tau}_A + b \qquad (6)$$

where a and b are constant parameters (see Table 3.1).

Figure 3.5a shows the dependence of $\bar{\tau}_{2.1}$ and $\bar{\tau}_A$ on time obtained with measurements when cirrus covered the sun's disk during ~27 min (317 points), and Figure 3.5b shows dependence of $\bar{\tau}_{2.1}$ on $\bar{\tau}_A$ for the same points. Small deviations of points from the straight line can be explained by different time constants of two devices. The analysis of the data have shown that $\bar{\tau}_{2.1}$ and $\bar{\tau}_{10.2}$ are always larger than $\bar{\tau}_A$, and ratio $\frac{\bar{\tau}_{2.1}}{\bar{\tau}_A}$ and $\frac{\bar{\tau}_{10.2}}{\bar{\tau}_A}$ are constant, at least up to $\tau = 3$.

The second method of processing experimental date (that of Moscow State University) differs from the first one because the direct radiation passing through a cloud (S) and radiation from the sun's disc, not covered by clouds (S_o), were obtained with the same height of the sun, h_o, and transmission of the atmosphere. S_o was taken from a graph of S_o versus h_o which was constructed for each specific day using measurements in clear spaces between clouds (0^2). The results were plotted with one minute resolution.

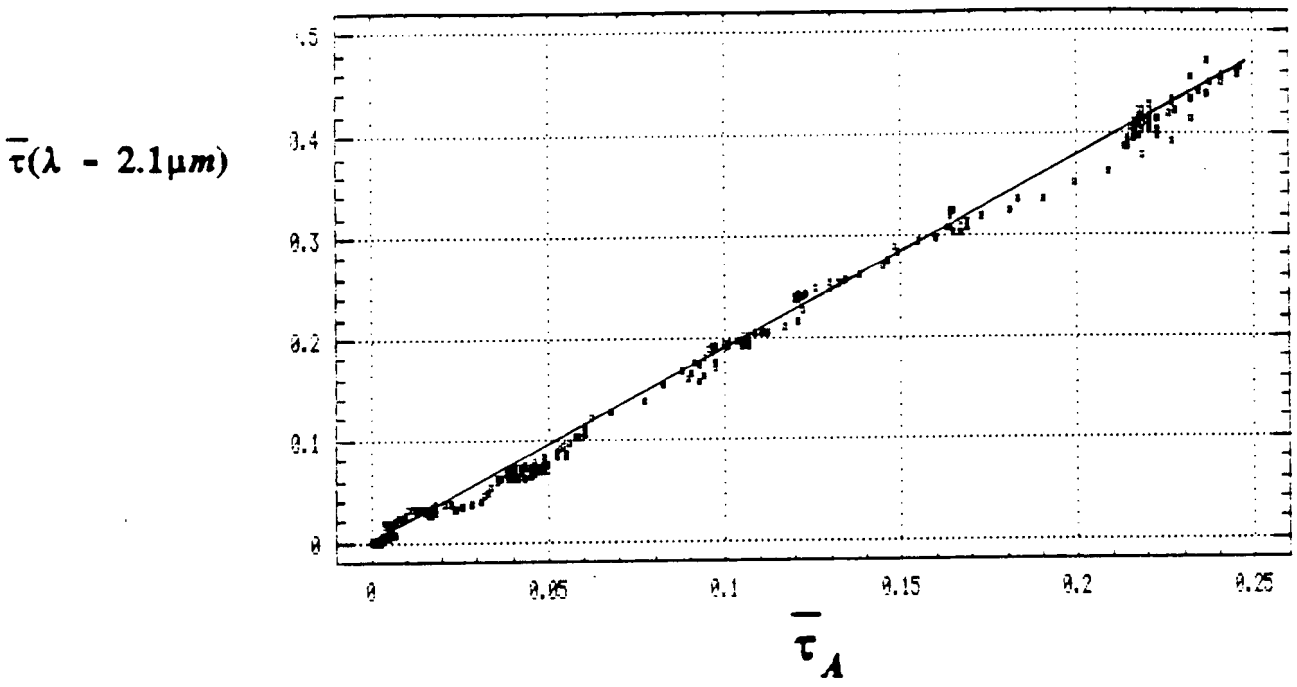

Figure 3.5a Dependence of $\bar{\tau}_{2.1}$ and $\bar{\tau}_a$ upon time.

(a) relation between $\bar{\tau}_{2.1}$ and $\bar{\tau}_a$

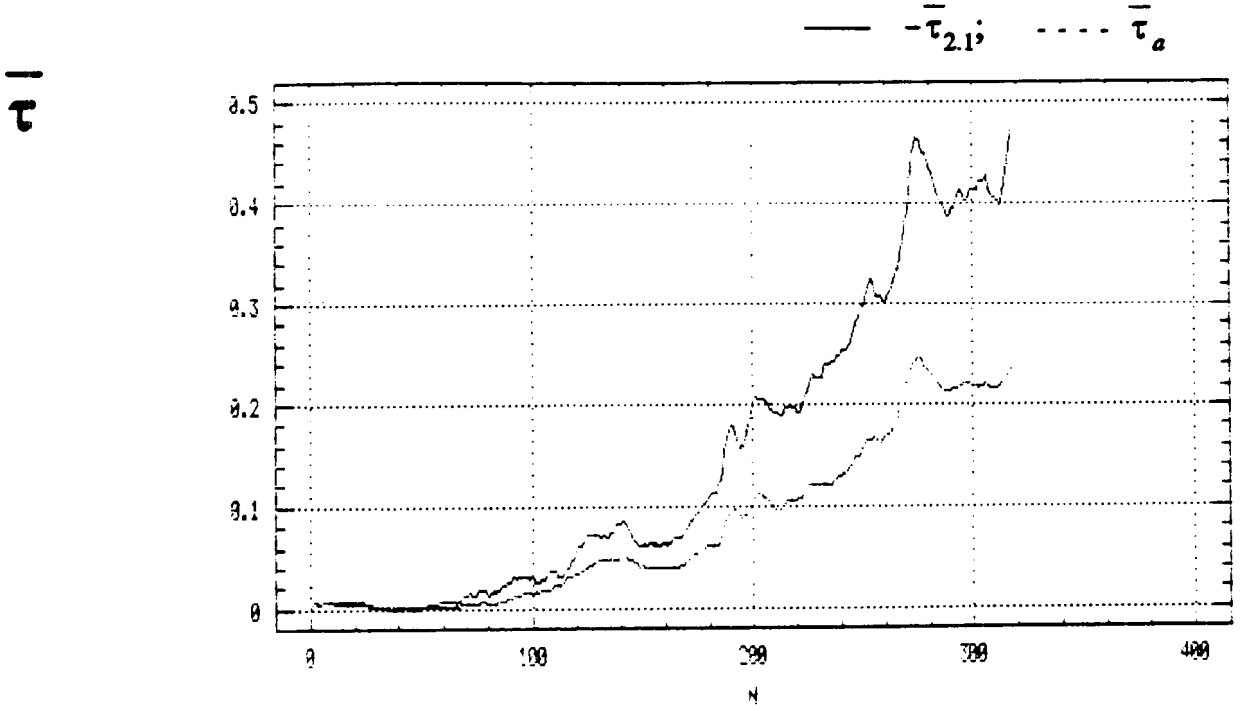

Figure 3.5b Dependence of $\bar{\tau}_{2.1}$ and $\bar{\tau}_a$ upon time.

(b) —— $-\bar{\tau}_{2.1}$; - - - - $\bar{\tau}_a$

Instantaneous values of $\tau_{2.1}$ corresponding to τ_A were found by averaging 12 values, (in accordance with the SR data) since $\bar{\tau}_{2.1}$ was measured every 5 seconds. Averaging was performed so that the one minute corresponding to $\bar{\tau}_A$, was in the middle of the series of 12 measurements for $\bar{\tau}_{2.1}$.

To study the relation between $\bar{\tau}_{2.1}$ and $\bar{\tau}_A$ using the data from the 1989 measurements, five days (May 14, 15, 18 and 31, June 5) were selected when measurements were performed both with and without cirrus on the sun's disk. These days were selected with the aim of a more correct determination of S by excluding the influence of aerosol upon the value of S. On these days fibrous cirrus (Ci fib) were observed across the sun's disk.

The coefficient of correlation between $\bar{\tau}_{2.1}$ and $\bar{\tau}_A$ is high (Table 3.1). Among the various days the parameter σ in equation $\bar{\tau}_{2.1} = \alpha\bar{\tau}_A + b$ changes slightly. The value of parameter b, as a rule, is small and can be neglected. As we see in Table 3.1, some days are characterized by a number of different cases. To exclude this inhomogeneity of the data, values of $\bar{\tau}_{2.1}$ and $\bar{\tau}_A$ for each day under consideration were selected in accordance with intervals $\bar{\tau}_{2.1}$ (0-0.10; 0.10-0.20, etc.) and were averaged. The ratio between averaged values of $\bar{\tau}_{2.1}$ and $\bar{\tau}_A$ is shown in Figure 3.6. This ratio can be approximated by equation $\bar{\tau}_{2.1} = 1.90\bar{\tau}_A$ which is very close to the equation

obtained for the entire data sample (n = 569), and values a are close for both methods. Therefore, the conclusion about constancy of the ratio $\frac{\bar{\tau}_{2.1}}{\bar{\tau}_A}$ is confirmed.

TABLE 3.1

Values of parameters a and b in equation $\bar{\tau}_{2.1} = a\bar{\tau}_A + b$ of correlation coefficients r and number of kinds n.

date	a	b	r	n	a(IAPh)
11.05.86	1.89	0.06	0.955	60	1.91
24.05.86	1.88	-0.01	0.975	23	1.89
19.05.87	2.04	-0.06	0.984	110	1.99
14.05.89	1.89	0.02	0.967	52	1.82
15.05.89	1.84	0.02	0.995	107	1.89
18.05.89	1.79	0.00	0.961	56	1.92
31.05.89	1.82	0.00	0.993	121	1.85
05.06.89	1.76	0.01	0.983	31	1.79
All day	1.86	0.00	0.986	560	1.88
All day (after means for intervals $\bar{\tau}_{2.1}$)	1.92	0.00	0.994	65	1.94

During the cirrus experiments, conducted from 1986 through 1989, synchronous data of transmitted solar radiation through clouds were collected at five wavelengths λ = 0.31 μm; 0.63 μm (0.55 μm); 1.2 μm; 2.1 μm; 10.2 μm with α = 15' using the spectrophometric device shown in Figure 3.7. The range of measurements by the spectrometers are: DMR-4 -0.25-0.5 μm; MDR-2 - 0.32-0.8 μm; SPM-1 - 0.4 μm-2.2 μm; SPM-2 - 0.5-2.2 μm; MDR-3 - 8-14 μm; UR-20 - 2-25 μm. The solar light was received using an automatic tracking system located on an 18 meter tower and recorded every 5 seconds. Figure 3.8 shows that the ratios $\frac{\bar{\tau}(\lambda)}{\bar{\tau}(\lambda - 2.1\ \mu m)}$ varies significantly for different types of clouds. Comparison of results of Figure 3.8 with calculations of Figures 3.1 and 3.2 shows that cirrus clouds have effective particle sizes of more than $20\ \mu m; \left(\frac{\bar{\tau}(\lambda - 10\ \mu m)}{\bar{\tau}(\lambda - 2.1\ \mu m}\right) > 1.0.$ At the same time, cloud types of Cc and Ac have particles of effective size smaller than $10\ \mu m; \left(\frac{\bar{\tau}(\lambda - 10\ \mu m)}{\bar{\tau}(\lambda - 2.1\ \mu m}\right) < 1.0.$ Having the advantage of a spectrometer in every channel, we decided to record the continuous spectrum of transmitted radiation through clouds in the range λ = 8 to 14μm. For example, Figure 3.9 shows the dependencies on wavelength of the ratio $\frac{\bar{\tau}(\lambda)}{\bar{\tau}(\lambda - 2.1\ \mu m)}$ for three cases. When processing, in the range 9 to 14 μm, we used only the points free from water vapor and other gas absorption lines. The minimum value of the ratio at the point λ = 10 μm in the case of Cc shows that there are particles smaller than 10 μm in the cloud. At the same time, there is no minimum for either of the cirrus cases in this region of spectrum; this fact allows us to conclude that significant numbers of large particles with r_{eff} > 20 μm are present in this cloud.

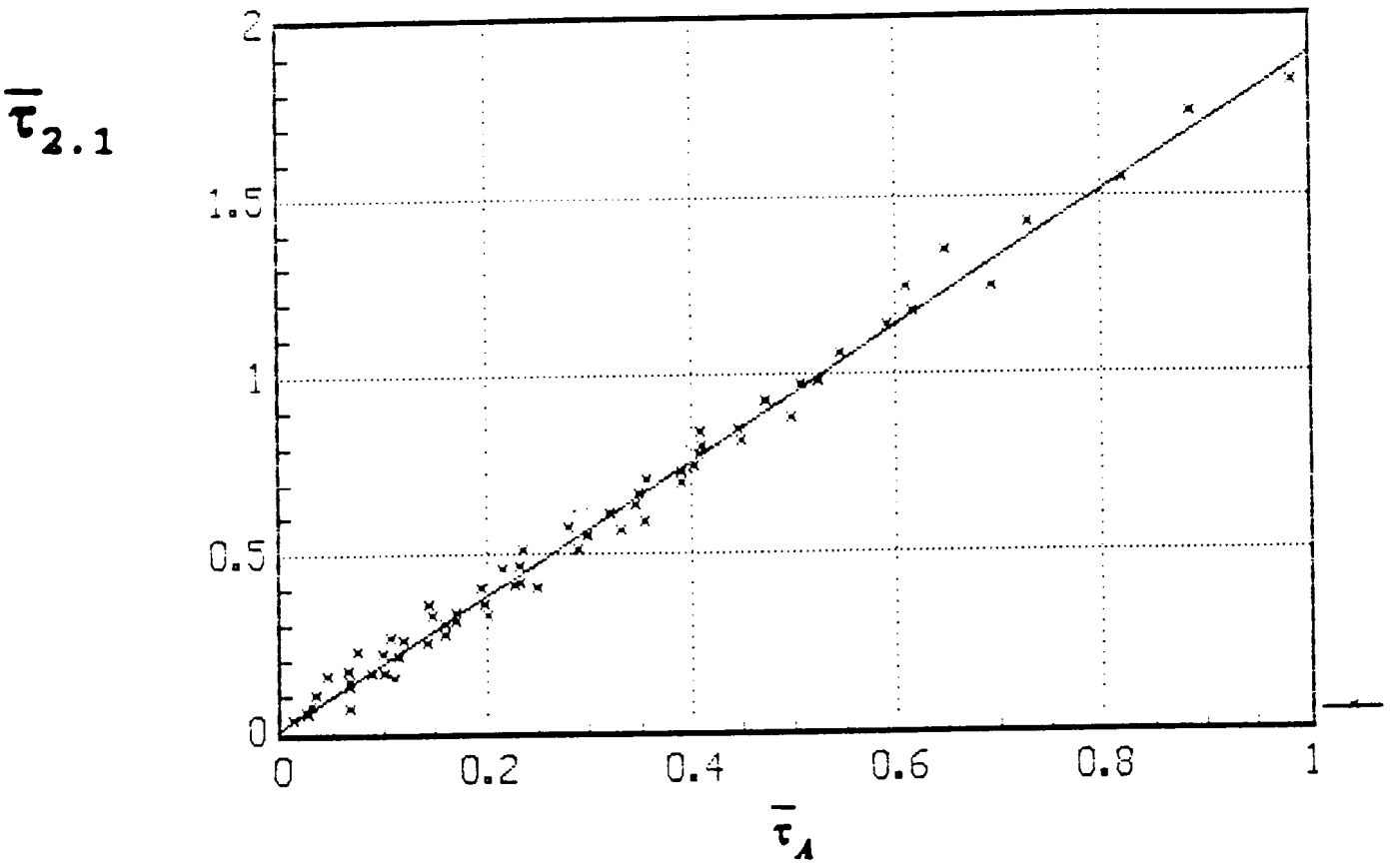

Figure 3.6 Relation between $\overline{\tau}_{2.1}$ and $\overline{\tau}_A$.

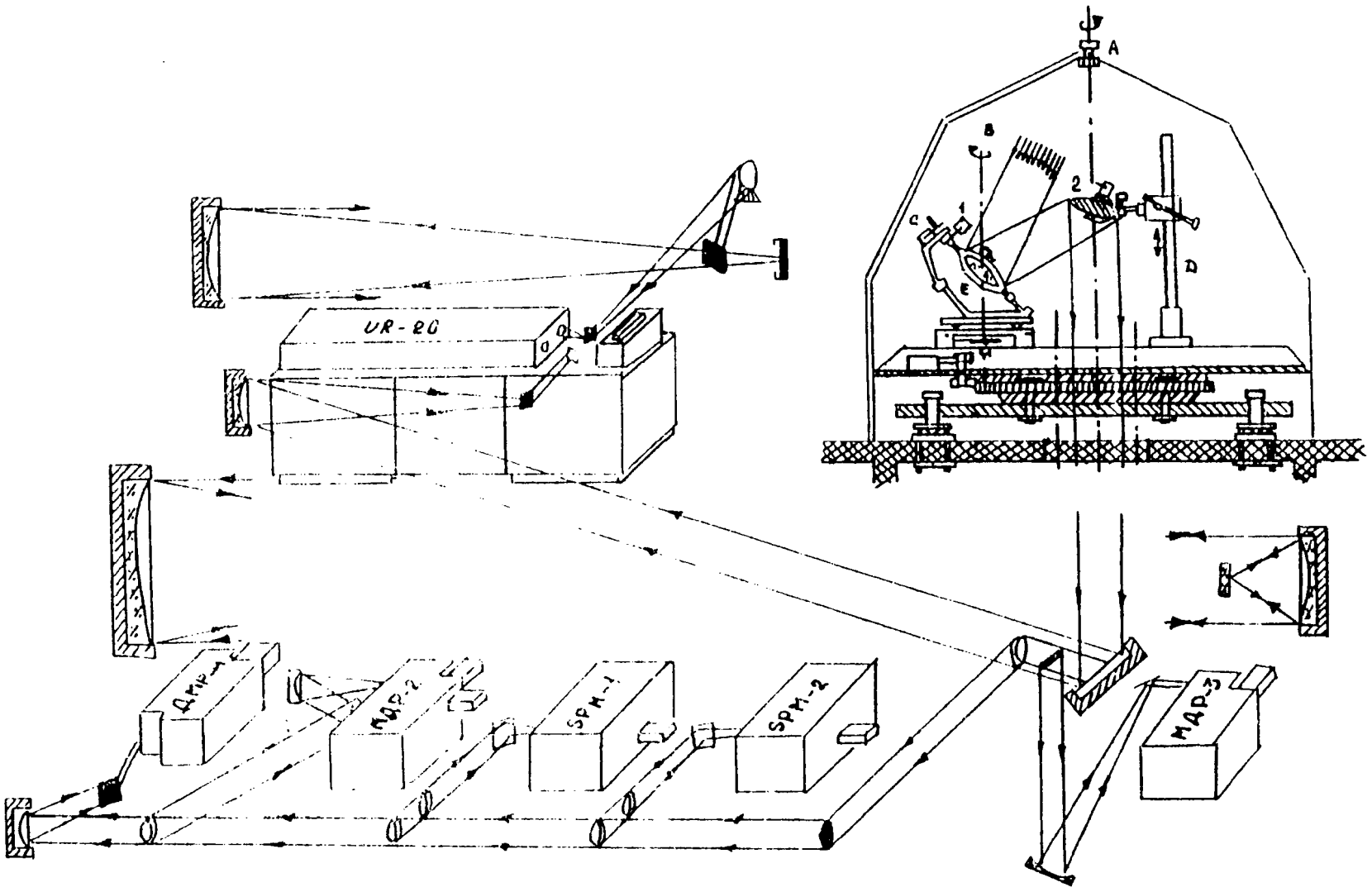

Figure 3.7 Sketch of the instrumentation used for studying the spectral radiation of the atmosphere in the range of wavelengths $\lambda = 0.25$ to 25 μm.

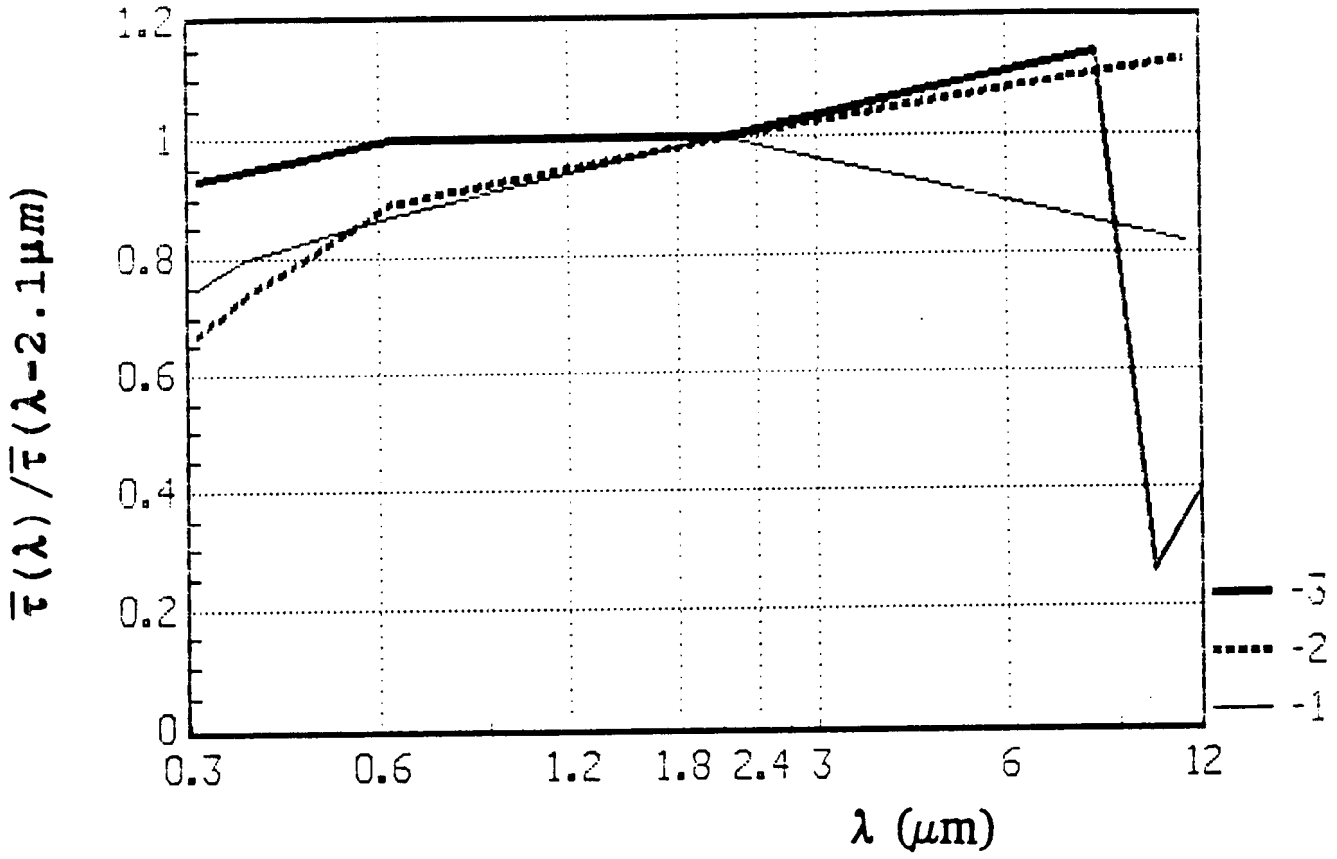

Figure 3.8 Dependence of the ratio of optical thicknesses $\frac{\bar{\tau}(\lambda)}{\bar{\tau}(\lambda - 2.1\ \mu m)}$ wavelength upon λ:

1 - cirrocumulus, February 20, 1981;
2 - dense cirrus, February 28, 1981;
3 - high-cumulus, September 5, 1985.

During the 1989 experiment, we processed continuous spectra in the range 8 to 14 μm with resolution $\delta\lambda$ = 0.04 μm. Such spectra are shown in Figure 3.10a (May 27, 1989 - cirrocumulus Cc) and Figure 3.10b (June 2, 1989 - cirrostratus Cs). From the values of the ratio $\frac{\bar{\tau}(\lambda - 10.2\ \mu m)}{\bar{\tau}(\lambda - 2.1\ \mu m)}$, we can again say that Cc consist of particles with $r_{eff} < 10\ \mu$m, and Cs with $r_{eff} > 20\ \mu$m. Obviously, continuous spectral measurements of the transmission in any region of spectrum are difficult because of the variability of the clouds. Therefore, only a few spectra were recorded. The evaluation of effective particle size in cirrus during 1986-1989 experiment shows that generally r_{eff} 20 μm except May 6, 1989 and June 7, 1989. As the measurements of spectral transmission in 1978 - 1989 show, r_{eff} smaller than 10 μm is more frequently seen in cirrocumulus. All in all, during the three years of measurements, small particles were found in nearly 15% of cases.

To make the comparison with other works easier, the experimental results of transmitted radiation through cirrus P_λ are transformed to the value of transmission in the direction of zenith P_λ^0

$$P_\lambda^0 = P_\lambda^{1/m} \tag{7}$$

where m is the optical mass of the atmosphere.

The results are presented in Table 3.2 and of Figure 3.11 for 1989 year. The use of the observing system developed at the Inst. of App. Physics allowed us to avoid errors when determining P_λ arising from inaccuracy aiming the instrument at the sun. The errors in determining P_λ arising in S_o from unseen particles between clouds and

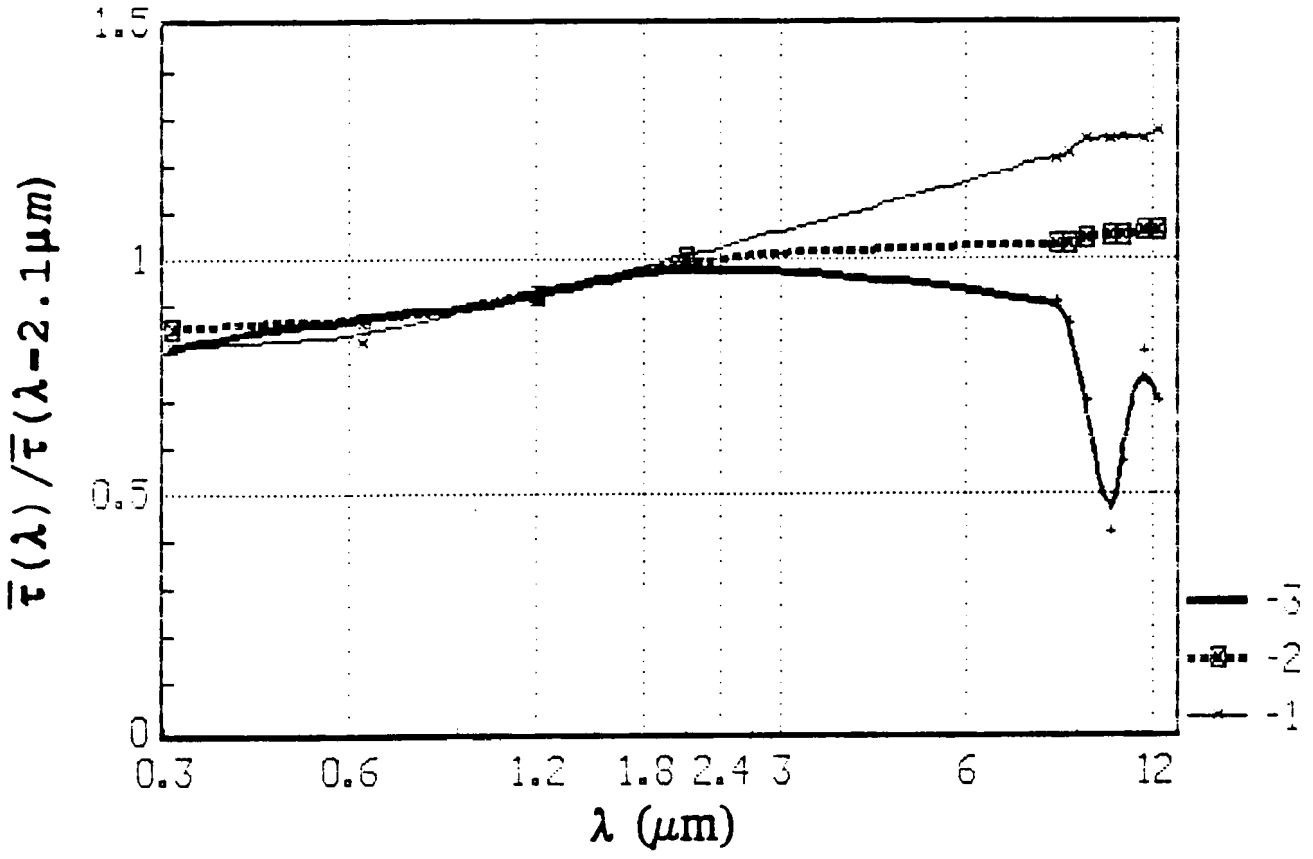

Figure 3.9 Dependence of the ratio of optical thicknesses $\frac{\bar{\tau}(\lambda)}{\bar{\tau}(\lambda - 2.1\ \mu m)}$ upon wavelength λ:

1 - cirrus May, 11, 1986;
2 - cirrus May, 24, 1986;
3 - cirrocumulus, May 6, 1987.

instability of instruments are not more than 5%. The days selected for analysis contained mainly cirrus clouds (the whole time of observations was 32 hours). The densest cirrus were observed on June 2, 1989 -Cs. Mainly the observed cirrus were half-transparent and thin. Figure 3.11 shows the histogram of distribution of $P^{\bullet}_{\lambda\text{-}2.1\,\mu m}$ for 1989 data.

During the experiment, we tried to select the cases with only cirrus but frequently (up to 70% cases) there were other clouds in either or both lower and middle layers. Figure 3.12 shows, as an example, a time cross section plot of the transmission of cirrus where the smooth line of $P^{\bullet}_{\lambda\text{-}2.1\,\mu m}$ was interrupted by discarding measurements, because altocumulus type clouds were present in the foreground of the Ci clouds. In Table 3.2 attention should be paid to minimum values of $P^{\bullet}_{\lambda\text{-}2.1\,\mu m}$ which sharply differ from the mean values in 30 minutes. This indicates that at this time there were lower level clouds layers in the sky. We believe that further investigations of cirrus in relation with other types of clouds should be done.

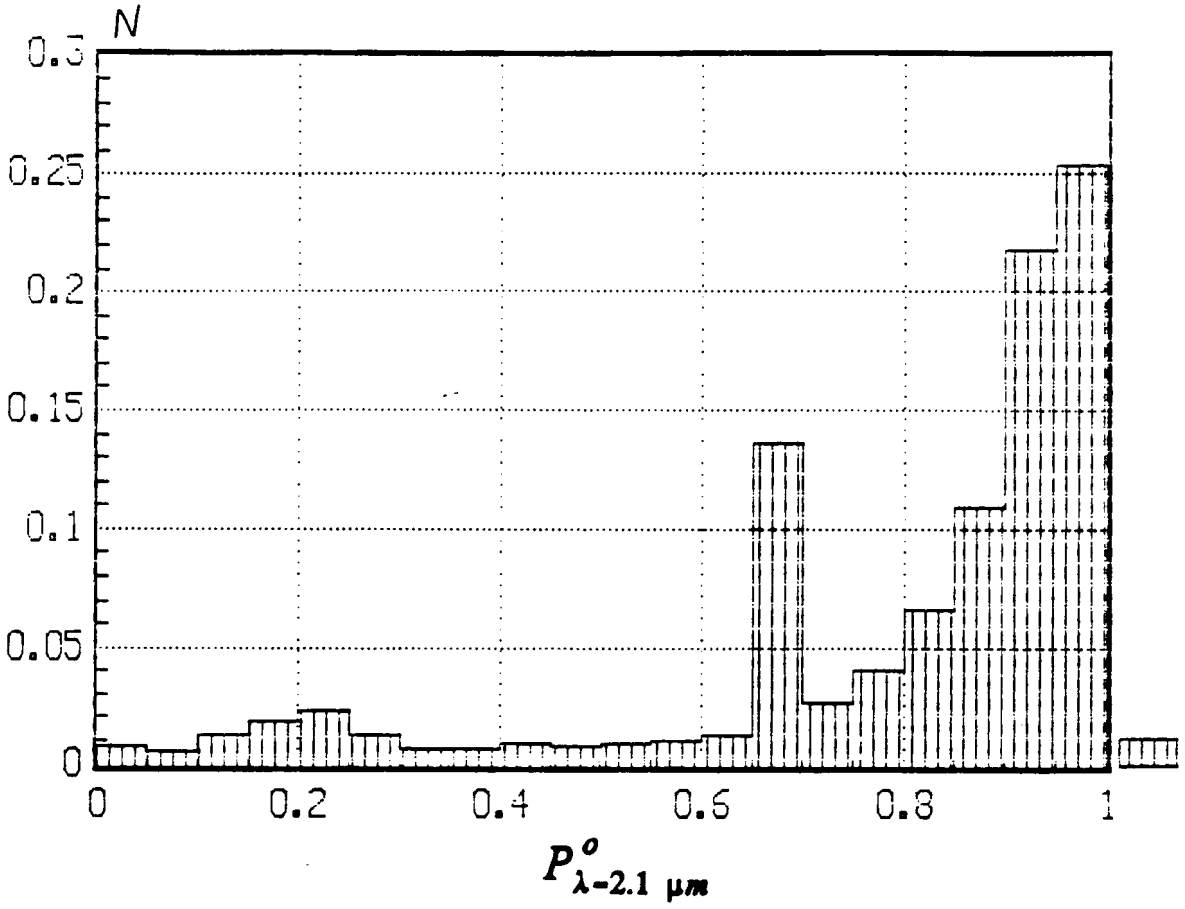

Figure 3.11 Distribution of probabilities of transmission of radiation - $P^o_{\lambda-2.1\ \mu m}$ by cirrus clouds in the 1989 experiment.

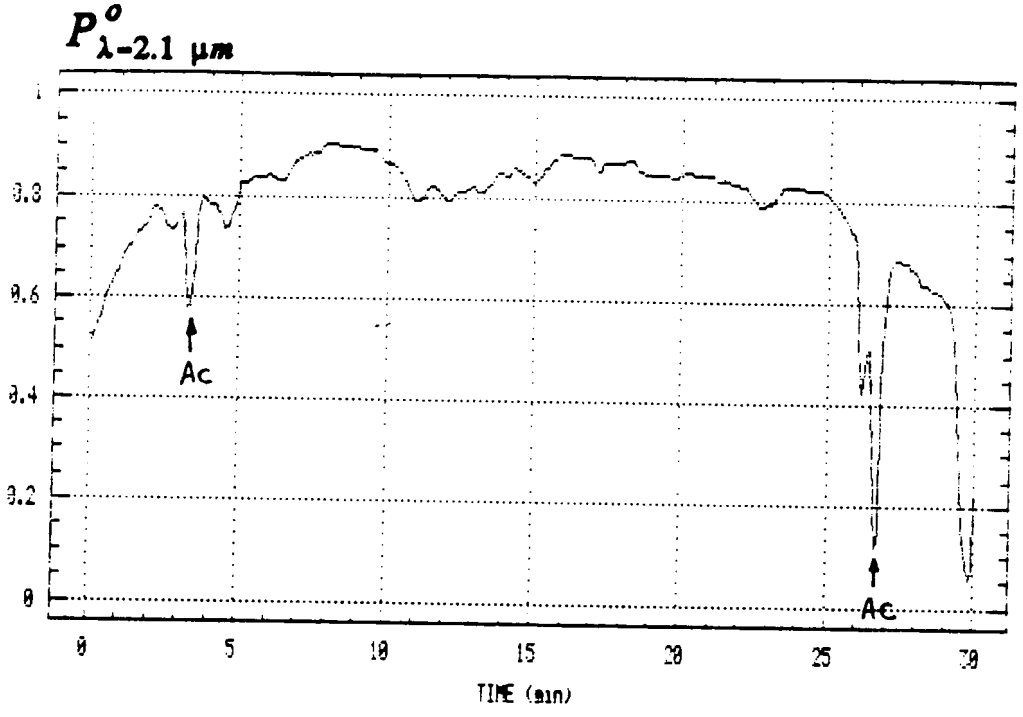

Figure 3.12 Typical dependence of transmission of radiation by clouds, when cirrus and high-cumulus were present simultaneously.

TABLE 3.2

Means - $\overline{P}^{0}$, maximum - P^{0}_{max} and minimum - P^{0}_{min} values of P_0 mean-square deviations - S of the transmission of radiation by cirrus clouds in the direction toward the zenith.

	27.05.89				31.05.89			
Time	$\overline{P}^{0}$	P^{0}_{max}	P^{0}_{min}	S	$\overline{P}^{0}$	P^{0}_{max}	P^{0}_{min}	S
8-8:30	0.951	1.006	0.405	0.126	0.944	0.977	0.919	0.012
8:30-9	0.840	0.966	0.361	0.162	0.985	0.985	0.901	0.015
9-9:30	0.924	0.939	0.907	0.007	0.967	1.000	0.837	0.036
9:30-10	0.713	0.927	0.096	0.288	0.929	0.973	0.874	0.025
10-10:30	0.461	0.916	0.067	0.297	0.845	0.934	0.632	0.069
10:30-11	0.655	0.847	0.078	0.234	0.748	0.843	0.643	0.063
11-11:30	0.723	0.833	0.141	0.127	0.634	0.815	0.005	0.252

Table 3.2, Continued

15.05.89					7.06.89			
Time	$\overline{P}^{0}$	P^{0}_{max}	P^{0}_{min}	S	$\overline{P}^{0}$	P^{0}_{max}	P^{0}_{min}	S
8-8:30					0.962	0.988	0.776	0.037
8:30-9								
9-9:30	0.776	0.902	0.058	0.146				
9:30-10	0.627	0.857	0.213	0.134	0.937	0.990	0.828	0.046
10-10:30	0.895	0.984	0.355	0.110				
10:30-11								
11-11:30					0.861	0.967	0.786	0.035
11:30-12					0.912	0.950	0.625	0.035
12-12:30								
12:30-13	0.900	0.946	0.300	0.047				
13-13:30	0.941	0.984	0.759	0.038				
13:30-14	0.892	0.995	0.570	0.102				
14-14:30	0.868	0.963	0.621	0.055				
14:30-15	0.683	0.896	0.200	0.154				
15-15:30	0.340	0.811	0.077	0.184				

Table 3.2, Continued

14.05.89					5.06.89			
Time	$\overline{P}^{0}$	P^{0}_{max}	P^{0}_{min}	S	$\overline{P}^{0}$	P^{0}_{max}	P^{0}_{min}	S
7-7:30	0.958	0.996	0.831	0.035	0.814	0.937	0.723	0.061
7:30-8	0.979	0.990	0.949	0.007				
8-8:30	0.902	0.997	0.566	0.122	0.916	0.985	0.744	0.057
8:30-9	0.984	0.998	0.928	0.011	0.930	0.956	0.892	0.016
9-9:30	0.958	0.973	0.947	0.007	0.907	0.948	0.846	0.028
9:30-10	0.972	0.989	0.931	0.012	0.908	0.942	0.879	0.014
10-10:30	0.960	0.976	0.936	0.010				
10:30-11	0.932	0.987	0.888	0.019				
11-11:30	0.912	0.949	0.872	0.019				
16-16:30	0.650	0.860	0.393	0.138				

Table 3.2, Continued

18.05.89					2.06.89			
9:30-10					0.963	0.981	0.936	0.013
10-10:30					0.963	0.980	0.942	0.012
10:30-11					0.956	0.988	0.911	0.017
11-11:30	0.604	0.701	0.398	0.081				
11:30-12	0.570	0.674	0.368	0.085				
12-12:30	0.676	0.860	0.453	0.126	0.660	0.897	0.211	0.225
12:30-13	0.844	0.896	0.753	0.025				
13-13:30	0.909	0.973	0.881	0.019				
13:30-14	0.966	0.990	0.911	0.011				
14-14:30	0.953	1.000	0.896	0.023				
14:30-15	0.974	0.995	0.945	0.013				
15-15:30	0.953	1.000	0.927	0.017	0.216	0.296	0.138	0.041
15:30-16	0.958	0.981	0.924	0.017	0.137	0.286	0.013	0.095
16-16:30	0.964	0.977	0.951	0.005				
16:30-17	0.977	0.990	0.963	0.006	0.200	0.378	0.002	0.080
17-17:30	0.964	0.978	0.940	0.007	0.796	0.993	0.104	0.302

In summary, the combination of the above calculations and measurements allows one to determine the optical thickness of Ci clouds and the dependence of relative optical thickness $\frac{\bar{\tau}(\lambda)}{\bar{\tau}(\lambda_{const})}$ $\bar{\tau}_{const}$ = 2.1 μm or 10 μm) on wavelength, the size of cloud particles, and angle of view of the detector. The use of our spectral device made it possible to distinguish the cases of small (r_{eff} < 10 μm) particles. It was also shown that the optical thickness of cirrus clouds can be found using a standard actinometer with angle field of view 10°.

REFERENCES

Abakumova, G. M., Anikin, P. P., Glushenko, Yu. V. Comparison optical thickness of cirrus determined in accordance with the measurements by devices with various angles of view. Moscow: Nauka Publ., 1989. p 162-168.

Abakumova, G. M., Anikin, P. P., et al. The geometrical, optical and radiative properties of cirrus. Colorado State University, Atmospheric Science Report No. 456.

Anikin, P. P. The input of scattered light in the spectral transmission of half-transparent clouds. In collection: Radiative properties of cirrus clouds. Moscow: Nauka Publ., 1989, p. 156-161.

Anikin, P. P., Chavro, A. I., Shukurov, A. Kh. Complex optical device for researches of spectral transmission of the atmosphere on oblique and horizontal routes in ultraviolet, visible and infrared spectral (0.3:25 μm). Physic Aspects of the Remote Sensing of the Ocean-Atmosphere System, Moscow, Nauka Publ., 1989, p.200-211.

Grassl, H. Determination of clouds drop size distribution from spectral transmission measurement. Beitr Phys. Atmos. 1970. p. 225-284.

Irvine, W. M., Pollack, J. B. Infrared optical properties of water and ice spheres. Icarus, 1968. V.8. p. 324-366.

McCartney, E. J. Optics of the atmosphere. 1977.

Chapter 4

Influence of Upper Level Clouds Upon the Atmospheric Long-Wave Radiation Deduced from Surface Measurements and Calculations

by I. A. Gorchakova and I. N. Plakhina

1. Experimental Data

Continuously recorded values of thermal radiation flux near the Earth's surface $-F\downarrow$ both in the presence of clear sky and clouds were obtained in April-June 1989 at the Zvenigorod Scientific Station. The flux was measured with a pyrgeometer [Plakhina I.N., Yu. A. Volkov, et al., 1989]; the general error in measurements with this type of instrument is 5-10%. The pyrgeometer was placed on a mast at a height of 10-12 m above the earth's surface. Records were transferred to magnetic tape for selected half-hour intervals with a resolution of 180 points in 30 min. All in all, we have analyzed 15-20 half-hour, daylight periods, of which five represent clear sky conditions, and the remainder upper level clouds.

Table 4.1 presents the characteristic values of thermal fluxes for a number of half-hour time intervals: mean values $F\downarrow$ for a given time interval; standard deviations $\sigma_{F\downarrow}$; and maximum values of $F\downarrow$.

The table shows that: 1) influence of the cirrus cloudiness upon the value of $\overline{F}\downarrow$ (mean for 30 min) is insignificant; 2) maximum effect of cirrus is nearly 10 W/m^2 for two cases on May 18, 1989, with clear sky and solid cirrus mean values for a day agreeing with similar evaluations by Whitlock, C. H., et al., 1986, ; 3) the influence of high cumuli (Ac) upon the downward radiation at the surface is ~50 W/m^2; 4) more clearly seen is also the

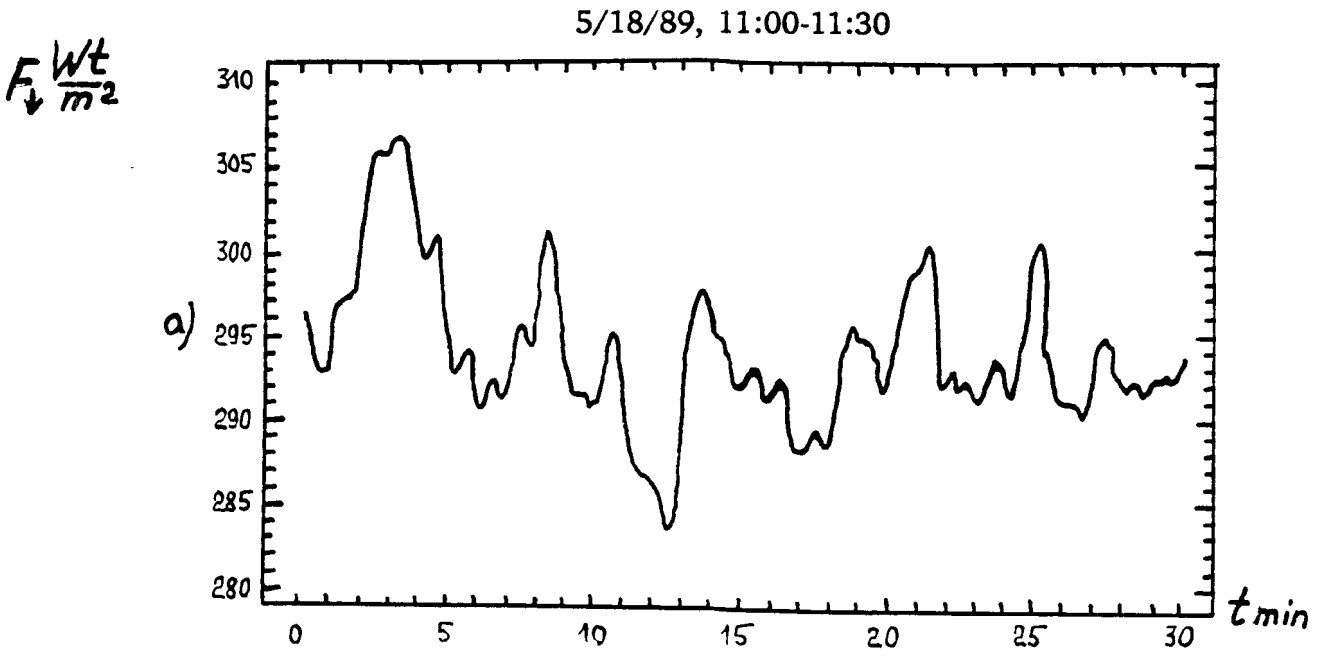

a) 5/18/89, 11:00-11:30, $\overline{F}_o\downarrow$ = 294 W/m², $F_o\downarrow$min = 273 W/m², $F_o\downarrow$max = 292 W/m², σ=5 W/m², T=17°C, cloudiness 10/0 Ci.

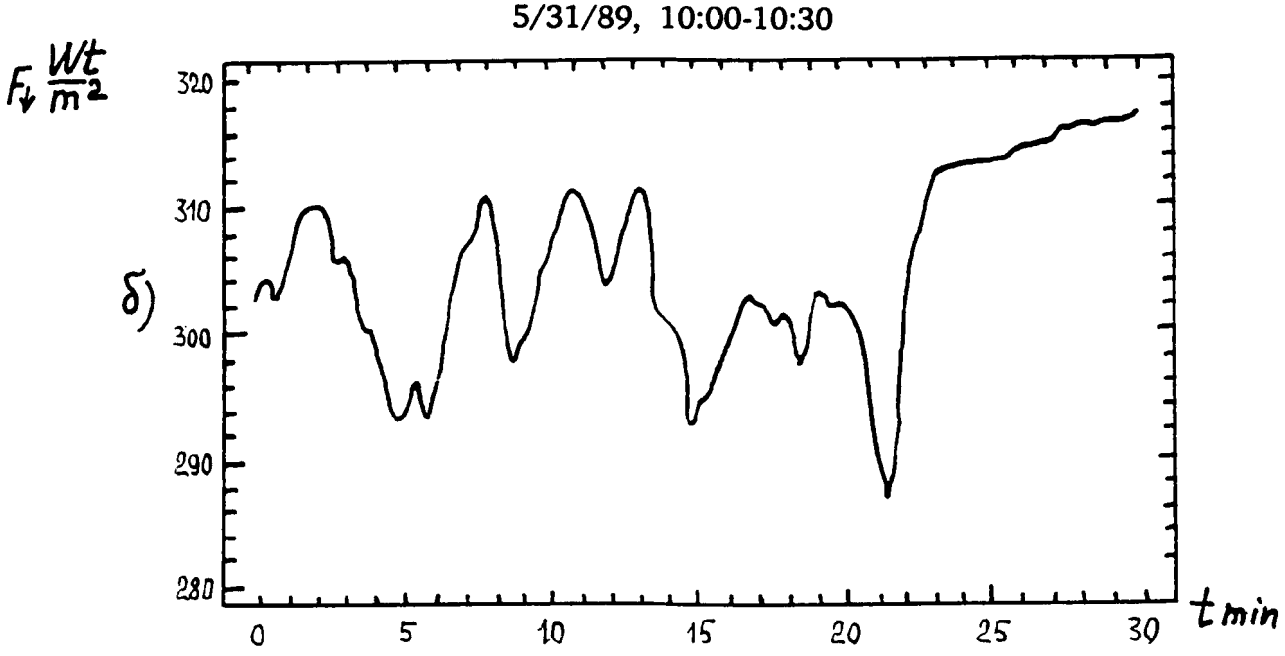

b) 5/31/89, 10:00-10:30, $F_o\downarrow$ = 305 W/m², $F_o\downarrow$min = 287 W/m², $F_o\downarrow$max = 317 W/m², σ = 7 W/m², T - 19-20°C, cloudiness 9/10 Ci, Cc.

Figure 4.1 The variability of the thermal radiation fluxes $F_o\downarrow$ at the earth's surface for solid cirrus clouds:

influence of cloudiness upon the standard deviation. In conditions of cloudiness the mean $\sigma_{F\downarrow}$ grows by 1.3-1.7 times; $\Delta F\downarrow = F\downarrow_{max} - F\downarrow_{min}$ also significantly grows, while this effect is larger for lower temperatures.

Table 4.1

Characteristic value of thermal radiation fluxes for clear sky and for cloud conditions.

N	Date	Time	Temperature °C	Cloudiness	τ	$F\downarrow$ W/m$_2$	Standard deviation $\sigma_{F\downarrow}$ W/m^2	$F\downarrow$ max-$F\downarrow$min=ΔF W/m^2
1.	6/3/89	9:30-10:00	19-20	0/0	-	337	9	359-321=38
2.	6/2/89	9:00-9:30	19-20	3/0, Ci, Cc	-	339	12	364-322=42
3.	5/19/89	8:00-8:30	13	0/0	-	248	4	358-241=17
4.	5/18/89	8:00-8:30	14	10/0, Ci, Cc, Ac	-	304	7	318-284=34
5.	5/18/89	11:00-11:30	~17	10/0 Ci	0.48	294	5	292-273=19
6.	5/18/89	16:00-16:30	~18	0/0	-	283	4	306-283=24

In summary, the cirrus influence upon the flux of the thermal radiation coming to the surface is small, about 10 W/m^2, but it is necessary to note that the cirrus observed during the experiment, were optically thin: mostly $\tau \leq 0.5$.

A more detailed picture of the time variability of $F\downarrow$ (in half-hour intervals) is shown in Figures 4.1 and 4.2 (with clear sky and solid cirrus). Standard deviation $\sigma_{F\downarrow}$ from the mean value in half-an-hour intervals is 1-3 per cent with clear sky and 2-4% with solid

5/18/89, 11:00-11:30

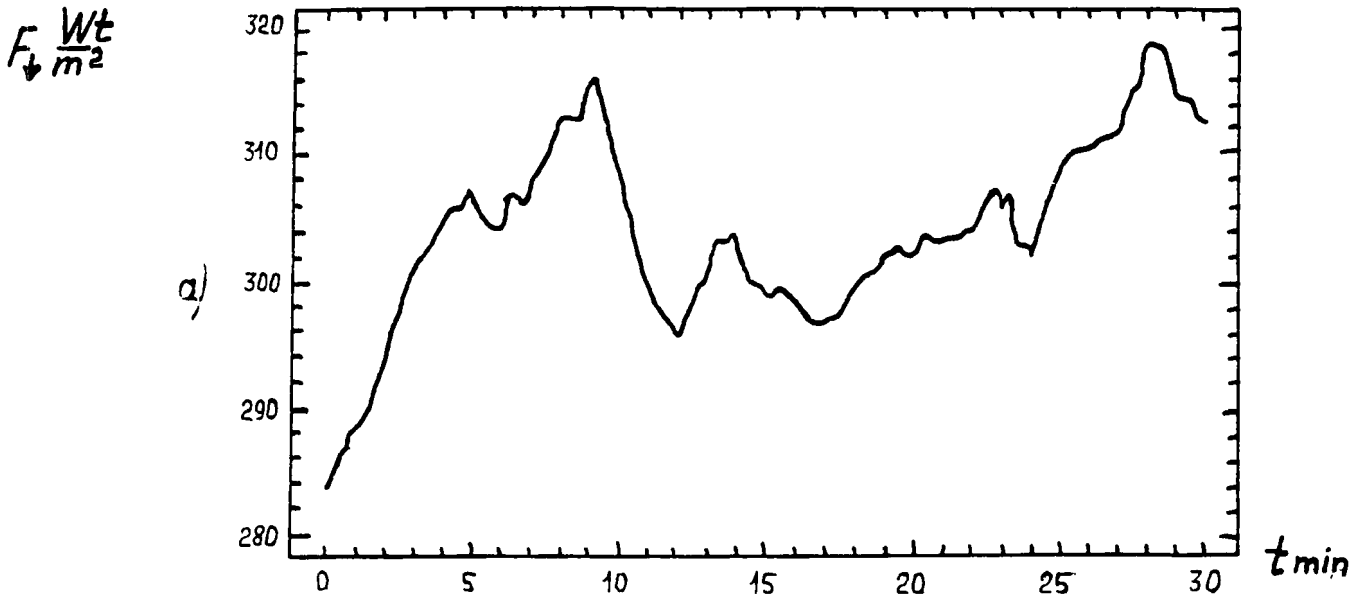

a) 5/18/89, 11:00-11:30, $\overline{F}_o\downarrow$ = 294 W/m², $F_o\downarrow$min = 273 W/m², $F_o\downarrow$max = 292 W/m², σ=5 W/m², T=17°C, cloudiness 10/10 Ci.

5/31/89, 10:00-10:30

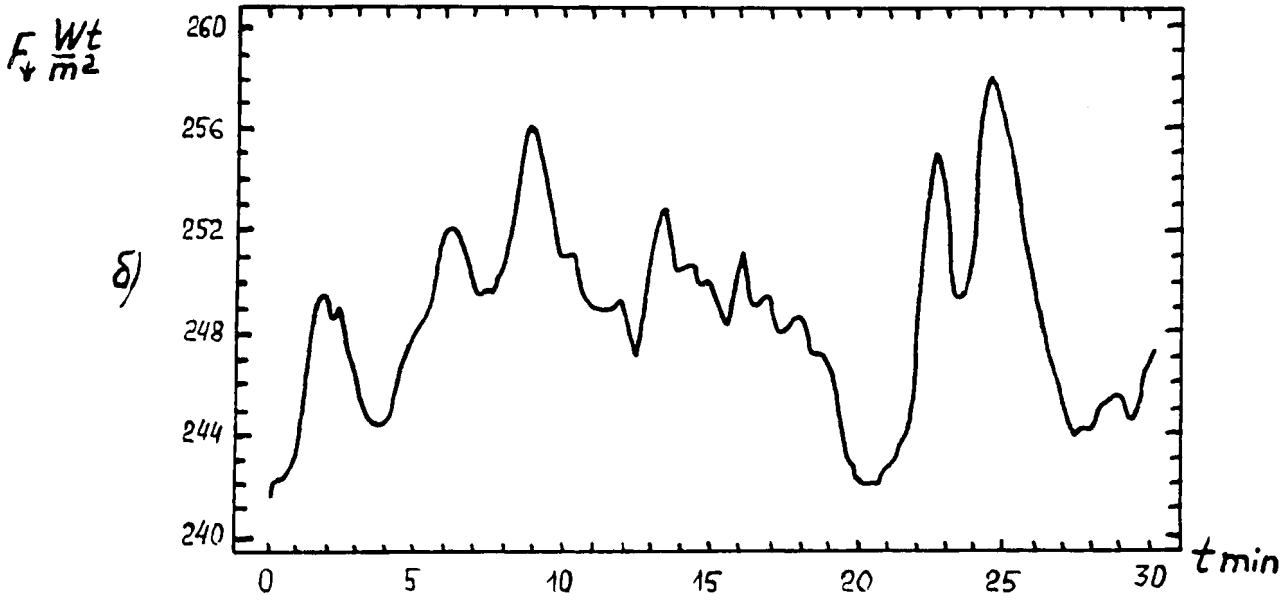

b) 5/31/89, 10:00-10:30, $F_o\downarrow$ = 305 W/m², $F_o\downarrow$min = 287 W/m², $F_o\downarrow$max = 317 W/m², σ = 7 W/m², T - 19-20°C, cloudiness 9/10 Ci, Cc.

Figure 4.2 Comparison of variability of the thermal radiation fluxes $F_o\downarrow$ at the earth's surface:

cirrus. Possible reasons of $\overline{F}\downarrow$ variations under cloudless conditions include fluctuations of wind velocity and temperature in the boundary layer as well as the effects of subvisible cloudiness or aerosol layers.

2. Comparison of measurements and calculation of integral thermal downward radiative fluxes near the surface.

Data representing the independent variables in the radiative transfer equation are needed to calculate integral thermal radiation fluxes. These data and the methods used to obtain them are presented below and in Abakumova, G. M., et al. 1989, Chapter 5. To evaluate the degree of mutual coincidence of experimental and calculated values of thermal radiation we compared its values with clear sky and in solid high cloud conditions. Such comparison was done to verify the reliability of calculation of fluxes in accordance with chosen methods and additional evaluation of experimental errors.

It is necessary to know the following variables to calculate integral fluxes of thermal radiation: the distributions of temperature and moisture as a function of height, values of the temperature and moisture at the earth's surface, the levels of cirrus boundaries, the optical thickness of the cloud and the vertical profile of the liquid/ice water content inside the cloud, Abakumova, G. M., et al. 1989, Chapter 5. Values of temperature T_o° C and relative humidity f_o% at the earth's surface were measured at ZNS thrice a day: at 0900; 1200; 1500 LST. The aerological sounding data in Dolgoprudny (80 km from Zvenigorod), as a rule, were taken at 0900 and 1400.

Temperature, moisture and pressure were measured at heights $Z \geq 200$ m. Therefore it was necessary to bind the temperature and moisture at the earth surface to

the aerological profile. Let us notice that the upper air relative humidity data had great fluctuations. The upper air relative humidity and values of earth-surface moisture ρ_o were used only for determination of the total moisture content in accordance with formula:

$$m^* = \int_0^\infty \rho\ (Z)\, e^{-\alpha z} \qquad (1)$$

where ρ (Z) is absolute moisture at Z height. It is suggested that r (Z) can be described by:

$$\rho\,(Z) = \rho_o e^{-\alpha z} \qquad (2)$$

Since ρ_o and m^* are both known, we can determine parameter α from (2) and (1).

Table 4.2 presents the results of comparison of measured $F \pm \Delta F$ and calculated - $F\downarrow c$ integral thermal radiation fluxes coming to the Earth surface (with clear sky). Experimental values of the above fluxes were averaged over 10-minute intervals. $F\downarrow$ systematically is larger than $F\downarrow c$ but not by more than 3%. It is close to the mean value of the experimental error of $F\downarrow$, reported by [Plakhina, I. N., Yu. A. Volkov, et al., 1989]. The error in the calculation $F\downarrow c$, is no greater than 3% and one would generally expect $F\downarrow c$ to be lower.

Table 4.3 presents the comparison of measurements and calculations for cases of solid or almost solid cirrus clouds. Because in a number of cases the optical thickness changed significantly during the given intervals of measurements, the calculations were

Table 4.2

Comparison of the measured and calculated integral influxes of thermal downward radiation at the earth surface for clear sky

Date	Time	Meteorological data at the earth's surface and total moisture content	$\overline{F}\downarrow \pm \Delta F$ W/m^2	$F\downarrow C$ W/m^2	$\frac{F\downarrow - F\downarrow C}{\overline{F}\downarrow}$ %
5/18/89	15h.±5m	t°C = 18.6 f_o = 36% m^* = 1.6 cm	293 ± 6	284	3
5/19/89	9h.± 5m	t°C = 12.7 f_o = 61% m^* = 0.8 cm	252 ± 3	250	1
5/21/89	9h.± 5m	t°C = 18.0 f_o = 58% m^* = 2.4 cm	316 ± 5	307	3
6/3/89	9h.± 5m	t°C = 21.0 f_o = 74% m^* = 2.2 cm	327 ± 5	328	0

Note: "Time" is the time of measurements of $F\downarrow$. The time of aerological soundings is almost the same.

done only for edge and intermediate values. The agreement between $\overline{F}\downarrow$ and $F\downarrow c$ degrades from that of clear sky case. The reasons are obvious: first, the aerological and lidar probing of the atmosphere (shown in Table 4.3) were nonsynchronous. The second factor was the variability of optical thicknesses in time (also shown in Table 4.3); because of this variability, the agreement of the half-hour mean values of calculated and measured integral fluxes of thermal radiation and optical thickness of clouds is better (see Table 4.3,

May 31, 1989, 10:00-10:30 a.m.). To better understand the reasons for differences between calculations and measurements, a numerical experiment was performed to evaluate the sensitivity of the fluxes coming to the Earth's surface to the following factors:

1. Addition of the surface relative humidity measured at the Zvenigorod station to the radiosonde data from Dolgoprudny station for $Z \leq 200$ m; the effect was (according to our evaluation) nearly 3% even in the case of a strong inversion in the near earth-surface layer.
2. Changing the cloud layer's height: this effect accounted for less than 10 W/m^2 when the height changed from H = 6-7.5 km to 8-9.5 km (see Table 4.4).
3. Changing the optical thickness of a cloud in the interval $0 \leq \tau \leq 0.5$: the relative estimates of this effect on $\Delta F\downarrow$o (compared to cloudless conditions) are given in Table 4.4; they are, on the average, for $\tau = 0.47$ - ~ 30 W/m^2, and for $\tau = 0.28$ - ~ 20 W/m^2.

Table 4.3

The same as Table 4.2 but for solid cirrus clouds (W/m^2)

Data and time of measurement	Cloud Condition			$\overline{F}\downarrow \pm \Delta F$		The condition of calculation			$\overline{F}\downarrow$	$\frac{\overline{F}\downarrow - \overline{F}\downarrow_c}{\overline{F}\downarrow}$
	Type	Amount	Optical thickness τ	$\frac{Wt}{M^2}$	surface meteorological data	time of aerological sounding	time and results of sounding	τ	$\frac{Wt}{M^2}$	%
15.V. 14h-14:30 15h ± 5min	Cu, Cc Ac, Ci, Cs, Ci	10/1 10/1	$0.04 \le \tau \le 0.47$ $\overline{\tau} = 0.14$	43 308 ± 15 310 ± 10	t°C = 18.6 f_o = 54%	14h	14h. 30m H=7.5-9km	τ=0.47 $\overline{\tau}$ =0.14 τ=0	312 297 384	-1 +4 +8
31.V. 9h±5min 10h±5min 10-10:30	Ci Ci Ci,Cc	8/0 7/0 9/0	$0.05 \le \tau \le 0.43$ $\overline{\tau}$ =0.15	288±22 320±10 305±19	t°=18.8 f_o=59% m*=1.5cm	8h30m- 10h5m	10h H=8.5-10km	τ=0.15	301	-5 +6 +1
7.V. 9h±5min	Ci,Cc	4/0	$0 \le \tau \le 0.15$	304±2	t°C=19.9 f_o=79%	8h30m- 9h30m	17h H=10-10.5km	τ=0.15 τ=0	319 311	+4
11:00-11:30	Ci,Cc	8/0	$0 \le \tau \le 0.24$ τ=0.15	29 339±20	t°C=24.2 f_o=60%	8h30m- 9h30m	17h H=10-10.5km	τ=0.15 τ=0	326 318	+6

4. Distribution of τ (Z) inside a cloud according to height: the calculations presented in Table 4.4 have shown, it is practical to replace the ice water profile W (Z) by the profile of the scattering coefficient in a cloud, β (Z) (see section 3), and, that the even distribution of τ(Z) inside a cloud can be considered: $\tau(Z) = \text{const} = \Sigma_{\tau_i}/N = \tau/N$, where N is the number of intervals in the calculations.

The agreement obtained between measured and calculated integral thermal radiation fluxes coming to the surface is quite satisfactory. In practice, in all the cases the disagreement is not much above the limits of the expected errors of measurements and calculations. Evidently, the reason is that the decisive contributions to the flux under consideration comes from the temperature and moisture of the lower atmospheric layers. These parameters were measured directly at the location of the radiation observations.

5. Calculations of integral thermal radiative fluxes in the atmosphere.

Calculations of the integral fluxes of heat radiation are based upon the measurements of the parameters of cirrus and atmosphere obtained in May 1986, 1987 and 1989. The methods of calculations are described in Abakumova, G. M., et al., 1989, Chapter 5. The results of calculations for three years of the experiment AT ZSS. are given in Table 4.5.

The dependencies of the fluxes coming to the Earth's surface $F\downarrow_o$, the fluxes radiated at clouds boundaries $F\uparrow$ (Z_t), $F\downarrow(Z_b)$ and the fluxes leaving the upper boundary of the atmosphere $F\uparrow$ (∞) upon the optical thicknesses τ of the clouds are examined below. Here Z_t and Z_b are the levels of the upper (top) and lower (base) boundaries of the cloud, respectively. Naturally, the values of these fluxes depend on the temperature and moisture

Table 4.4

Calculated fluxes with given conditions (W/m^2)

Date and time	Surface Meteorological Data		τ	Cloud boundaries level in km	$F\downarrow c$	$\Delta F\downarrow c$
	t°C	f_o%				
5/18 0900 h	14.2	70	0.47 0.28 0.14 0	6-7.5 - " - - " -	308 298 288 275	33 23 13 0
0900 h	- " -	- " -	0.47 0.28 0	8-9.5 - " -	300 292 275	25 17 0
1200 h	17.8	48	0.47 0.28 0	6-7.5 - " -	315 305 282	33 23 0
1200 h	- " -	- " -	0.47 0.28 0	8-9.5 - " -	307 300 282	25 18 0

Table 4.5

Integral fluxes of thermal radiation (W/m^2); $T(Z)\cdot K$ temperature on the levels Z, M^* - water vapor content of the whole thickness of the atmosphere

	1986						1987					
Date	11 May		24 May				19 May		20 May		22 May	
fluxes	clear sky	τ=0.12 9.7-10km	clear sky	τ=0.21 6-8km	τ=0.53 6-8km	τ=1.2 6-8km	clear sky	τ=0.33 8.4-10	clear sky	τ=0.17	clear sky	τ=0.46 8-10.5km
$F\uparrow(0)$	370.6	370.6	422.1	422.1	422.1	422.1	404.0	404.0	443.2	443.2	448.6	448.6
$F\downarrow(0)$	236.4	245.3	307.0	321.4	335.0	356.1	309.2	321.4	343.8	350.1	372.1	383.1
$F\uparrow(Z_b)$	252.5	252.5	306.5	306.5	306.5	306.5	255.4	255.4	264.3	264.3	264.7	264.7
$F\downarrow(Z_b)$	70.3	86.0	131.7	184.2	184.2	210.5	93.1	123.7	94.6	111.4	116.8	156.2
$F\uparrow(Z_t)$	248.4	231.6	276.7	233.4	233.4	211.0	239.9	205.5	241.3	218.0	254.4	216.9
$F\downarrow(Z_t)$	64.2	64.2	93.9	93.9	93.9	93.9	75.7	75.7	69.8	69.8	104.2	104.2
$F\uparrow(\infty)$	220.2	204.8	235.0	215.5	195.8	175.8	216.0	186.2	222.8	202.6	207.9	178.5
$T\cdot K$	284.1		293.5				290.0				299.6	
$T(L_{bo})\cdot K$	230.2		254.2				235.4				237.8	
$T(L_t)\cdot K$	223.4		240.0				221.1				217.8	
m^*_{cant}	0.6		1.8				1.3				1.9	

Table 4.5, Continued

1986							1987			
Date	15 May 9h. -10h.		18 May 11h. -11h30m		31 May 10h- 10h30m		2 June 16h30m -17h		7 June 11h- 11h30m	
fluxes	clear sky	τ=0.47 63-8km	clear sky	τ=0.47 8-10km	clear sky	τ=0.15 8-10km	clear sky	τ=1.6 6.5-8km	clear sky	τ=0.15 10-10.5km
$F\uparrow(0)$	378.5	378.5	405.7	405.7	441.4	441.4	449.8	449.8	442.7	442.7
$F\downarrow(0)$	263.7	295.5	282.9	307.0	292.4	301.3	312.6	358.3	318.0	325.0
$F\uparrow(Z_b)$	298.4	298.4	285.5	285.5	279.1	279.1	292.9	292.9	287.9	287.9
$F\downarrow(Z_b)$	63.2	138.1	56.3	117.7	47.2	69.8	86.5	181.8	31.0	55.7
$F\uparrow(Z_t)$	286.7	235.1	274.8	210.5	268.5	240.1	281.0	185.8	285.1	252.0
$F\downarrow(Z_t)$	33.1	33.1	37.2	37.2	30.7	30.7	69.1	69.1	27.4	27.4
$F\uparrow(\infty)$	275.0	225.0	264.1	202.4	264.0	236.5	257.4	167.2	279.5	247.2
T°K	285.8		290.8				298.4		297.2	
$T(L_{bo})$°K	247.0		236.9				240.2		223.0	
$T(L_t)$°K	233.5		224.5				234.0		219.0	
m^*_{cant}	1.9		1.6				2.0		1.9	

$\tau \neq 0$ - the cloudy case; the levels of the cloud boundaries are given: Z_b - the altitude of the clouds bottom; Z_t - the same for the cloud tops.

of the atmosphere and underlying surface. To minimize the effects of these variables on the differences (F_{cld} - F_{clr}), F_{cld} and F_{clr}, were calculated with the same surface and atmospheric parameters.

The coefficient of regression is obtained by regressive correlations in the shape of linear dependence Y = a + bx. Table 4.6 presents values a, b and coefficients of regression k for corresponding fluxes.

The regression equations allow one to make approximate estimates of the change of the integral fluxes of heat radiation as a function of the optical thickness of the cirrus clouds.

Using Table 4.5, we can calculate cooling rates of thermal radiation for the layers over, inside and under clouds, as well as for the whole atmosphere.

It is worthwhile to consider detailed profiles of the cooling rate R (Z) inside a cloud. Figure 4.3 shows R(Z) for the case of May 15, 1989, 9 a.m. The clouds were in the layer 6.3 to 7.6 km; the average optical thickness was 0.47. To calculate the cooling rate profile, optical thickness was distributed in proportion to the scattering coefficient $\beta(Z)$ (see chapter 2). It was assumed that distributions of $\beta(Z)$ and $\tau(Z)$ by height are analogous. The values Z_b, Z_t, $\tau(Z)$, $\beta(Z)$ were measured at the same time. It is seen, that heat radiation cools the cloud layer, compared to the case of the clear sky. The cooling sharply decreases near the boundaries of the cloud, and we can observe heating at its lower boundary (as compared to clear sky). The data show the significant influence of cirrus clouds upon heat radiation. We can certainly say that even an optically thin cloud diminishes the flux of outgoing heat radiation $F\uparrow(\infty)$ by nearly 10 W/m^2.

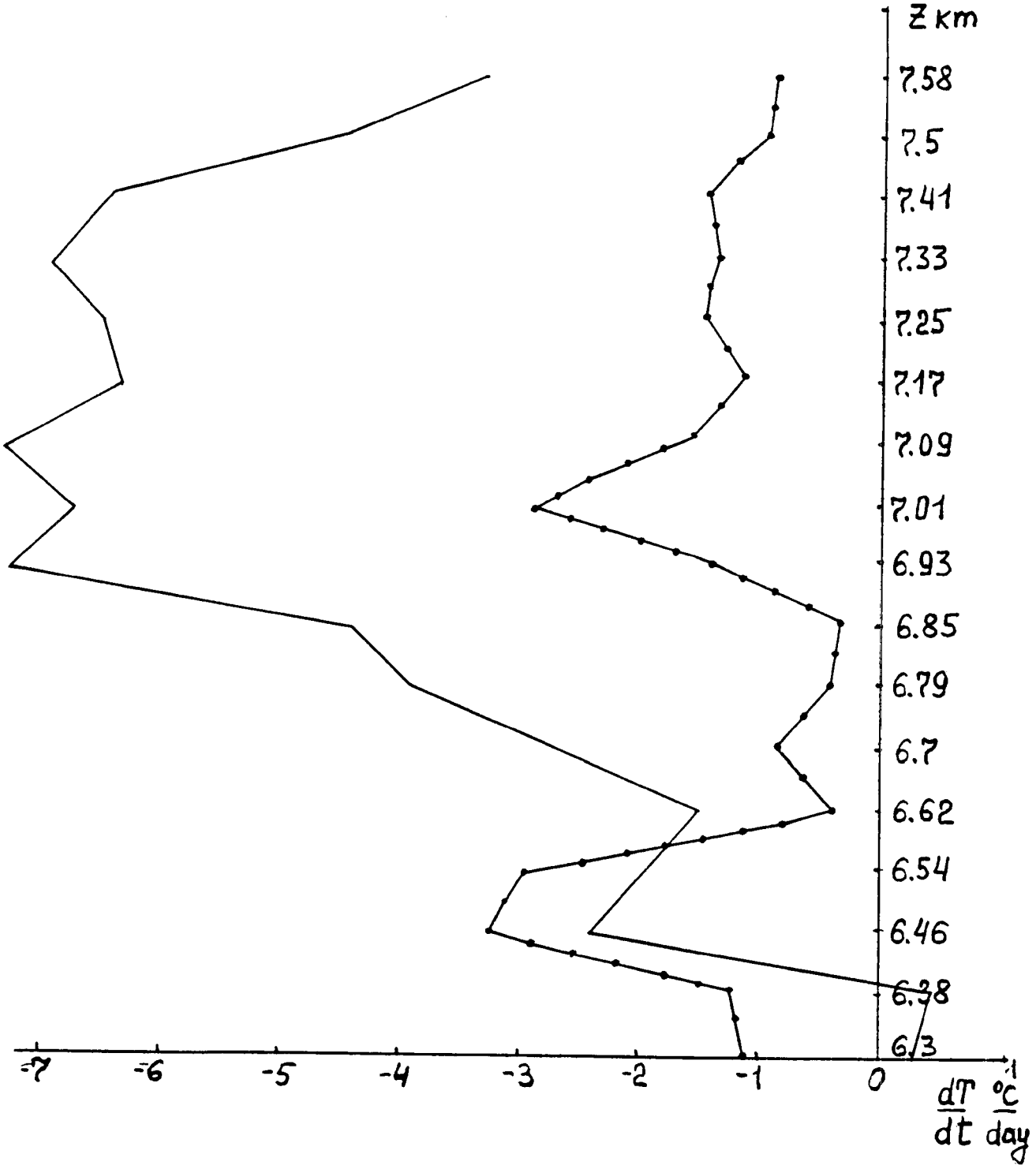

Figure 4.3 Profile of the cooling rate in °C/day May 15, 1989, 9 a.m.
(——) - with cirrus
(.____.) - with clear sky

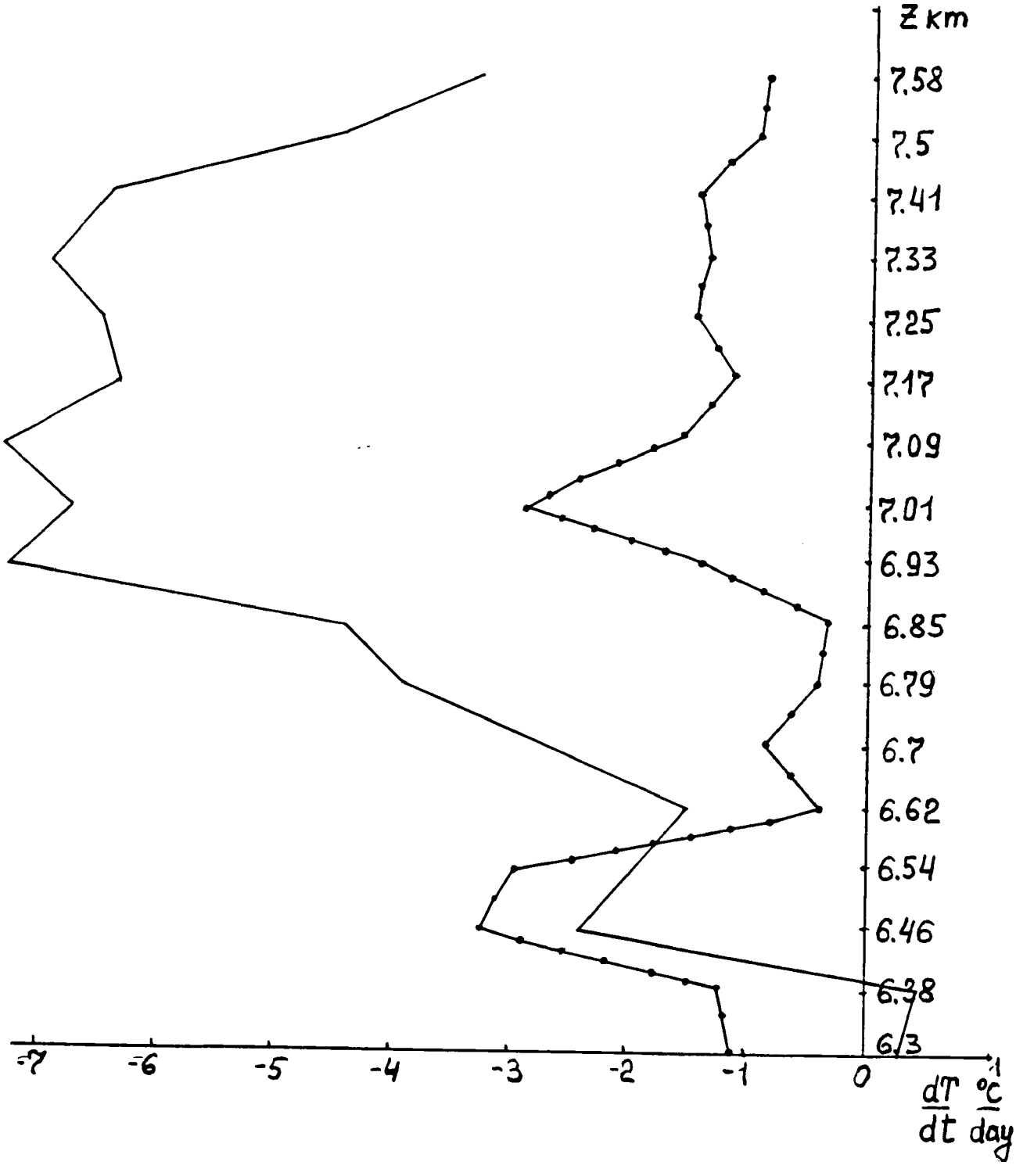

Figure 4.3 Profile of the cooling rate in °C/day May 15, 1989, 9 a.m.
(——) - with cirrus
(.____.) - with clear sky

Table 4.6

Coefficients a, b and correlation coefficient k of the regression relations

$$F\downarrow\uparrow_{cld}(Z) - F\downarrow\uparrow_{clr}(Z) = a + b\tau$$

Fluxes	$F\downarrow_{cld}(0) - F\downarrow_{clr}(0)$	$F\downarrow_{cld}(Z_b) - F\downarrow_{clr}(Z_b)$	$F\uparrow_{cld}(Z_t) - F\uparrow_{clr}(Z_t)$	$F\uparrow_{cld}(\infty) - F\uparrow_{clr}(\infty)$
a	5.28	16.77	19.52	16.63
b	29.56	52.13	45.70	43.51
k	0.929	0.950	0.922	0.905

REFERENCES

Abakumova, G. M., et al., 1989: The Geometrical, Optical and Radiative Properties of Cirrus Clouds. Colorado State University, Atmospheric Science Report No. 456, 61 pages.

Plakhina, I. N., Yu. A. Volkov, A. S. Ginzburg, V. N. Gulcov. The estimation of the longwave radiation of the atmosphere at the ocean surface from calculations and measurements. IZV. A. S. USSR. PhAO.

Whitlock, C. H., L. R. Poole, S. R. Le Croy, D. A. Robinson, 1988: Surface radiation observations for October 27-28, 1986. During the Wisconsin FIRE/SRB Experiment. In: First of SCCP Regional Experiment; FIRE Sciences Team Workshop, July 11-15, 1988, Vail, Colorado, 167-170.

Chapter 5

Upper Level Cloud Influence upon Direct, Diffuse and Global Radiation in Different Regions of the Spectrum

by G. M. Abakumova, T. V. Evnevich, E. I. Nezval,
N. E. Chubarova, O. A. Shilovzeva and E. V. Yarcho

The present chapter deals with the influence of cirrus cloudiness upon direct, diffuse and global radiation in various parts of the solar spectrum (UVR, PAR, NIRR, INTR) according to observations taken at the ZSS in the 1986, 1987, and 1989 spring experiments. This publication is the continuation of investigations represented in Abakumova, G. M., et al. 1989, Chapter 4, and the synthesis of the analyses of the multi-year experiment. The results obtained are compared with the data from many years of measurements made by the Moscow State University meteorological observatory.

5.1 Direct Solar Radiation

To investigate high level cloud effects upon direct solar radiation in various parts of the spectrum, ground-based measurements using thermoelectric actinometer AT-50 with light filters BC-8 and KC-19 were made. Application of the specified filters made it possible to determine integral (INTR, $\lambda < 4000$ nm), photosynthetically active (PAR, $\lambda = 380$ to 710 nm) and near infra-red (NIRR, $\lambda > 710$ nm) radiation. Observations were performed every half an hour, both with clouds being present and absent at the sun's disk. Measurement accuracy is typically 4 per cent.

The data analysis revealed that direct solar radiation S varies within large limits in various parts of the spectrum when high level clouds are present (see Fig. 5.1). The mean value of coefficient variation of INTR and NIRR stratified into groups according to five

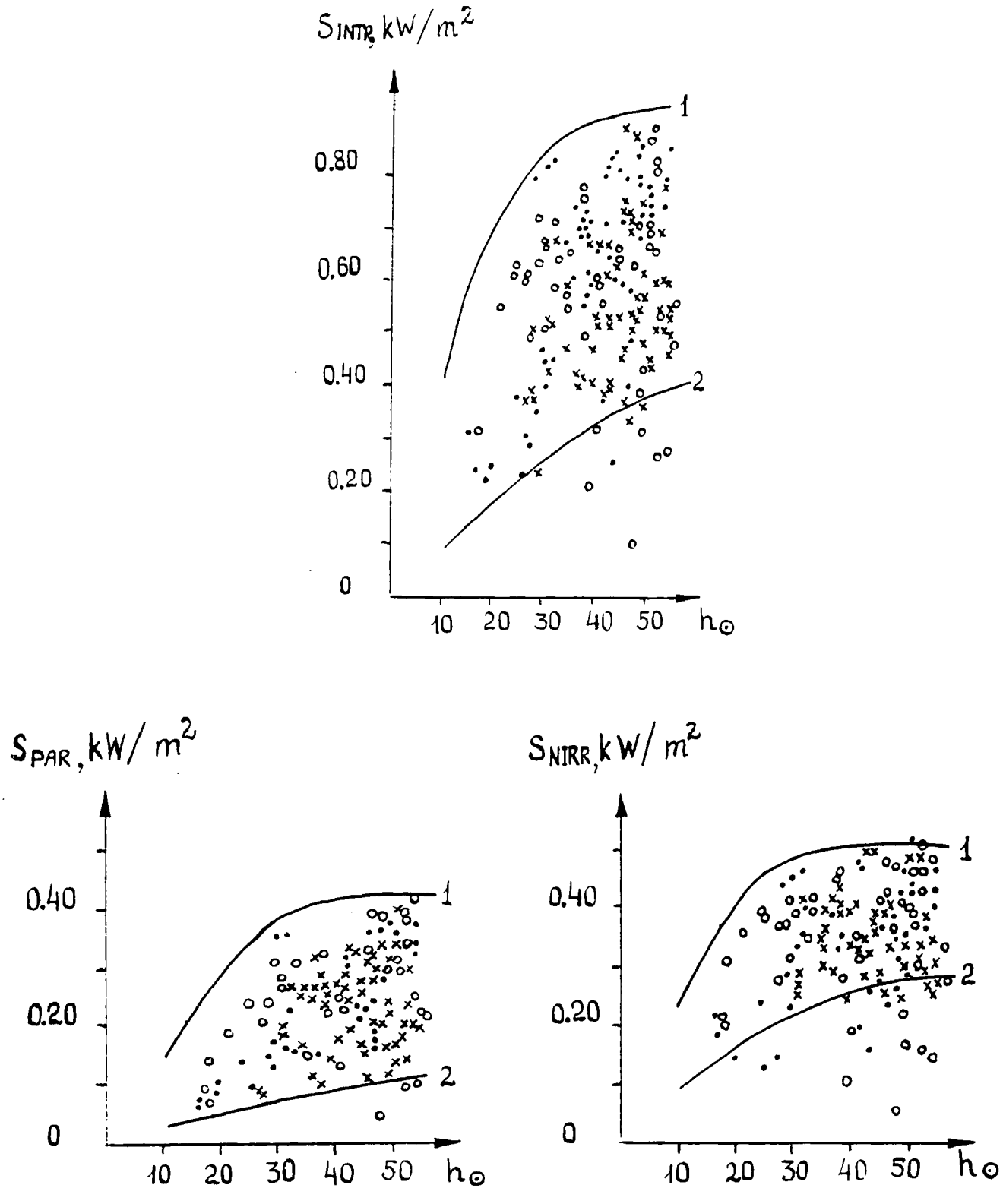

Figure 5.1 The dependence of direct radiation in various regions of the spectrum upon the sun's height (h_o) when the sun was clear (1,2) and when there were upper layer clouds at the sun disk.
1 - high atmosphere transparency, $\tau_{a,\lambda,o} = 0.10$
2 - low atmosphere transparency, $\tau_{a,\lambda,o} = 0.89$
(· - 1986, x - 1987, o - 1989)

intervals of the sun's height h_0 (15 to 20°, 20 to 25°, etc.) is equal to 25%, while PAR > 30%. As seen from Figure 5.1, the range of variation of S, with cirrus clouds (Ci) being present, is comparable, and in some cases exceeds the variations caused by the variations of an optical aerosol atmosphere thickness $\tau_{a,}(\lambda_0)$ for wavelength of λ_0 = 550 nm. However, it should be borne in mind that the S values represented in Figure 5.1 are over estimated in comparison with the real direct solar radiation, because of Ci presence. For a very assymetric phase function of Ci clouds, a significant amount of scattered light finds its way into the actinometer with an angle of view of 10° (see Chapter 3). Estimates of the scattered light contribution to the direct integral radiation measured by an actinometer will be made below.

The spread in points in Figure 5.1 is caused by a combination of the effects of the clouds and aerosols upon the radiation. To exclude aerosol effects calculations were made for transmission coefficient P_A and optical thickness τ_A of Ci clouds as follows:

$$P_A = (S/S_o)^{1/m};\ \tau^A = -\ell n\ P_A; \qquad (1)$$

where S is the direct radiation having passed through a cloud;

S_o is direct radiation, with the sun's disk not being covered with clouds;

m is the atmospheric air mass corresponding to the sun's height at the time of observation.

The quantity S_o was determined either according to measurements in gaps between clouds or on the day neighboring a cloudy one with the similar synoptic situation and atmosphere transparency, according to the procedure described in Abakumova, G. M., et al. 1989, Chapter 4.

Average values of P_A and τ_A, were determined from simultaneous measurements made in various parts of the spectrum both in separate years and, as a whole, for three years, are listed in Table 5.1.

These observations make it possible to conclude that the attenuation of direct radiation by high level clouds is approximately neutral.

As mentioned above, when measuring the direct radiation passing through Ci, some diffuse radiation finds its way into the actinometer due to light diffraction on ice crystals. This leads to an apparent increase of the transmission coefficient and an apparent decrease of the optical thickness of high level clouds, (see equation 1). The actual values of Ci optical thickness τ are approximately twice those tabulated in Table 5.1. On the basis of the 1986 and 1987 data the regression equation between τ and τ_A has been calculated. Here τ is determined from the measurements made by the IFA spectral radiometer at a wavelength of λ = 2.1 μm (see Chapter 3)

$$\tau_{2.1} = 1.88\ \tau_A. \qquad (2)$$

Values of $\tau_{2.1}$ are close to actual ones, because diffuse radiation in the NIR spectrum region finding its way into the device within an angle of view of 15' is negligible.

Table 5.1

Average values of transmission coefficients P_A and optical thicknesses τ_A of upper layer clouds.

Year	Number of Cases	P_A			τ_A		
		INTR	PAR	NIRR	INTR	PAR	NIRR
1986	67	0.84	0.84	0.84	0.18	0.18	0.18
1987	36	0.87	0.86	0.87	0.14	0.16	0.14
1989	45	0.83	0.83	0.84	0.21	0.22	0.21
1986, 1987, 1989	148	0.85	0.84	0.85	0.18	0.19	0.20

Table 5.2

Statistical characteristics of real optical thickness of upper layer clouds

Year	mean	min	max	±6	M_e	M_o	A	E	Number of cases
1986	0.31	0.02	1.12	0.25	0.26	0.07	1.33	1.76	82
1987	0.23	0.02	0.95	0.20	0.15	0.13	1.55	2.56	64
1989	0.35	0.02	2.83	0.52	0.17	0.02	2.85	9.73	52
1986, 1987, 1989	0.29	0.02	2.83	0.33	0.22	0.02	3.36	18.08	198

Using equation (2) and value for τ_A, the real values of optical thickness of high level clouds $\tau_{2.1}$ were determined. This allowed us to estimate the contribution of the diffuse radiation of the near-solar zone of radius of 5° (ΔS) to the direct solar radiation measured by the actinometer. The quantity ΔS is determined from the following equation:

$$\Delta S = S\text{-}S_r/S_r \cdot 100\%;$$

S_r represents the real values of direct radiation, having passed through a cloud, determined on the basis of $\tau_{2.1}$ from equation 2 and ratio given in equation 1.

According to the data of the Zvenigorod experiment (185 events) for $\tau_{2.1} \leq 1.6$ the quantity ΔS changes from 30 to 150%. It does not depend on the sun's height but does depend greatly on optical Ci thickness (see Figure 5.2).

The correlation coefficient between ΔS and $\tau_{2.1}$ is high: $\gamma = 0.98$ and the regression relationship may be expressed as follows:

$$\Delta S = 90.7 \cdot \tau_{2.1} = 2.7 \quad \%. \tag{4}$$

The statistical characteristics of the actual optical thickness of high level clouds (standard deviation δ, median M_e, mode M_o, skewness A and kurtosis E) determined with regard to equation (2), are listed in table 5.2 for separate years of the experiment and for the three year average.

The variation of the magnitudes of the extreme values of $\tau_{2.1}$ is large. This suggests considerable differences in the vertical thickness and cloud microstructure for different days and periods of observation; consequently, this leads to a large radiation variability.

The $\tau_{2.1}$ distribution is characterized by large positive asymmetry exhibiting a sharp apex (see Figure 5.3). The occurrence maximum (about 50%) is related to the interval of values from 0.01 to 0.20, which points out the fact that during the experiment thin clouds were mainly dominant. Occurrence of $\tau_{2.1}$ values > 1 comprises 4% of the sample.

As one would expect, cirro-stratus clouds have characteristically large values of $\tau_{2.1}$, cirro-cumulus typically have smaller values of $\tau_{2.1}$ (see Table 5.3), however one should be cautious in making generalizations based upon the data in Table 5.3 because of the small sample sizes for C_s and C_c.

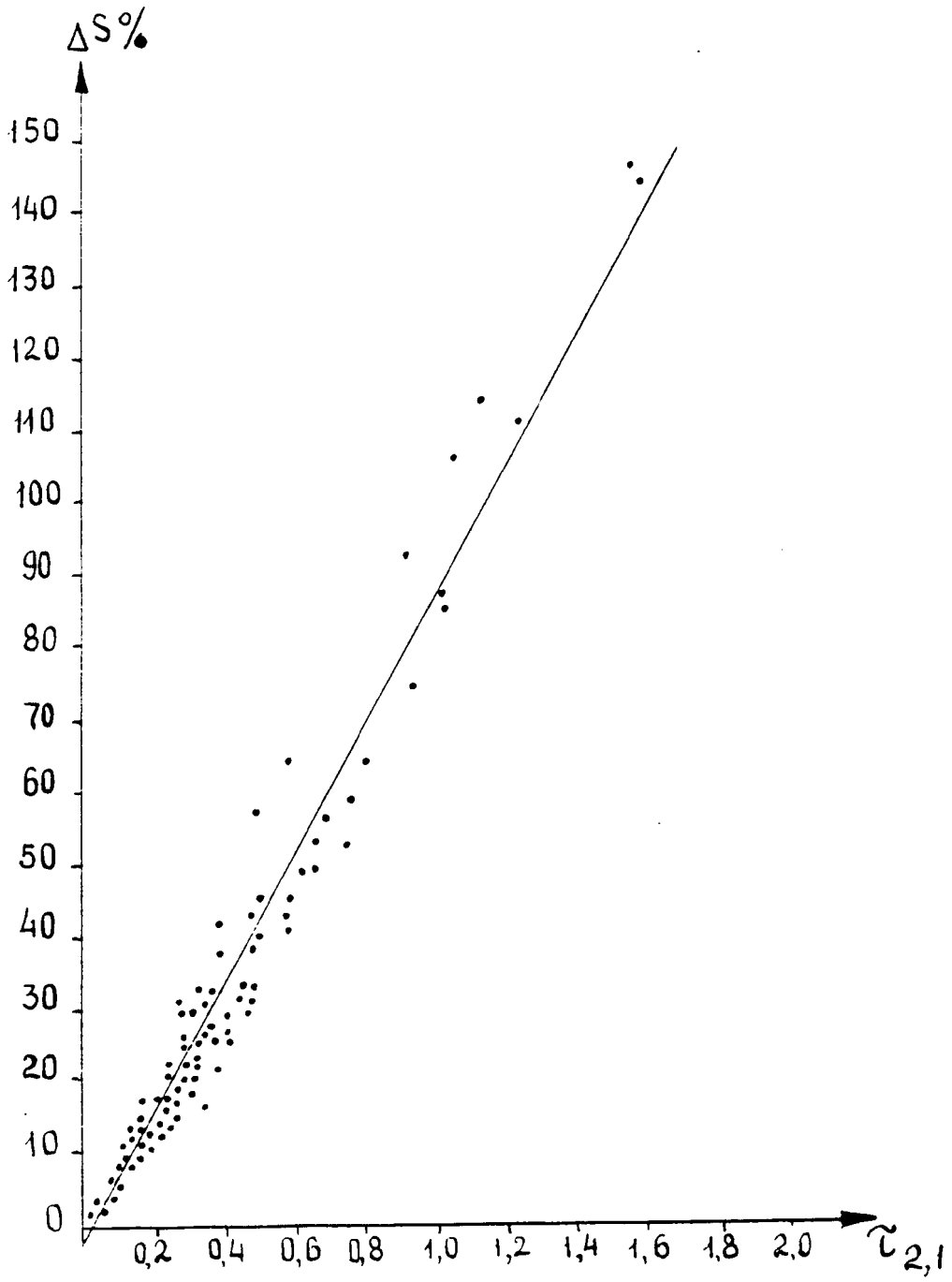

Figure 5.2 Deviations ΔS% of direct radiation values measured by actinometer from actual values as a function of optical thickness of clouds, $\tau_{2.1}$, in the presence of Ci.

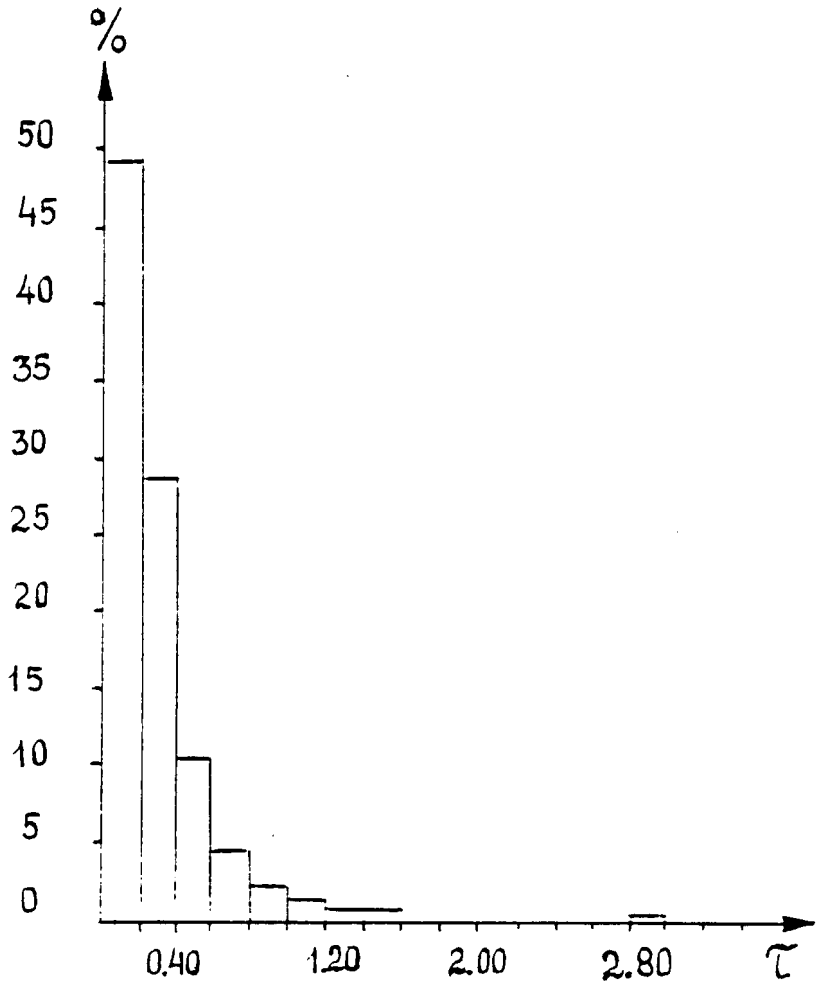

Figure 5.3 Frequency of optical thickness of upper layer clouds, in per cent.

Table 5.3

Optical thickness of different types of upper layer clouds for three years.

Clouds form	Ci	C_c	C_s	Ci,C_c	Ci,C_s
Mean	0.28	0.16	0.50	0.29	0.58
min	0.02	0.02	0.17	0.04	0.17
max	2.83	0.49	1.05	1.01	1.12
	0.35	0.15	0.28	0.30	0.35
Number of cases	149.00	21.00	12.00	9.00	7.00

Table 5.4

Values of optical thickness of upper layer clouds, τ, and aerosol optical thickness of atmosphere τ_a,λ_o averaged for a day.

Year date	τ	τ_a,λ_o	Year date	τ	τ_a,λ_o	Year date	τ	τ_a,λ_o
1986			1987			1989		
25.04	0.50	0.59	4.05	0.15	0.29	14.05	0.24	0.23
6.05	0.26	0.20	6.05	0.34	0.47	15.05	0.20	0.14
8.05	0.16	0.34	7.05	0.39	0.47	18.05	0.25	0.18
11.05	0.10	0.23	19.05	0.23	0.61	19.05	0.10	0.08
15.05	0.23	0.31	20.05	0.17	0.23	31.05	0.29	0.30
16.05	0.38	0.31	22.05	0.18	0.52	2.06	1.13	0.28
18.05	0.47	0.14				5.06	0.02	0.16
20.05	0.39	0.12						
23.05	0.04	0.19						
24.05	0.48	0.19						
28.05	0.02	0.11						

Comparing average daily values of $\tau_{2.1}$ with the optical aerosol thickness of the atmosphere τ_a,λ_o for wavelength of λ_o = 550 nm, (determined according to the measurements of a direct photosynthetic active radiation (PAR), with the sun's disk not being covered with clouds) Abakumova, G. M., et al., 1989), revealed that $\tau_{2.1}$ of high level clouds is often close to τ_a,λ_o, and in a number of cases exceeds it (see Table 5.4).

5.2 Diffuse Radiation

To investigate the influence of the continuous cover of high level clouds upon the diffuse radiation (D), fixed observations over an interval of 30 minutes were analyzed.

Diffuse integral radiation (INTR, $\lambda < 4000$ nm) was measured using a thermoelectric pyranometer M-80, ultra violet radiation (UVR, $\lambda < 380$ nm) - by means of an ultraviolet meter from the Moscow State University meteorological observatory, photosynthetically active radiation (PAR, $380 < \lambda < 710$ nm) - with the red-white thermoelectric pyranometer from the Main Geophysical observatory; near infra-red radiation (NIRR, $\lambda > 710$ nm) was determined as the difference between INTR and (UVR + PAR). When measuring diffuse radiation, a standard actinometric shade with diameter of 10° was used to exclude the radiation from the sun's disk and the near solar zone. Measurement of accuracy was 10 to 15 per cent.

Specifically, in the presence of high level clouds D_{NIRR} shows the largest variability while D_{UVR} shows the smallest variability. Within the interval of the sun's heights $h_o = 45$ to 50°, the coefficient of variation for diffuse UVR, PAR, NIRR and INTR are 10, 23, 61 and 34 per cent, respectively. As illustrated in Figure 5.4, the data show that the Ci influence upon diffuse radiation outside the near-solar zone of diameter of 10° is comparable with the influence of aerosol turbidity in various spectral regions.

For estimation of cloud effects upon diffuse radiation, the following ratio has been considered: $C_D = D/D_o$, where D and D_o is diffuse radiation when there is continuous cover of high level clouds and for clear skies respectively, with the sun's heights and aerosol atmosphere turbidity being the same.

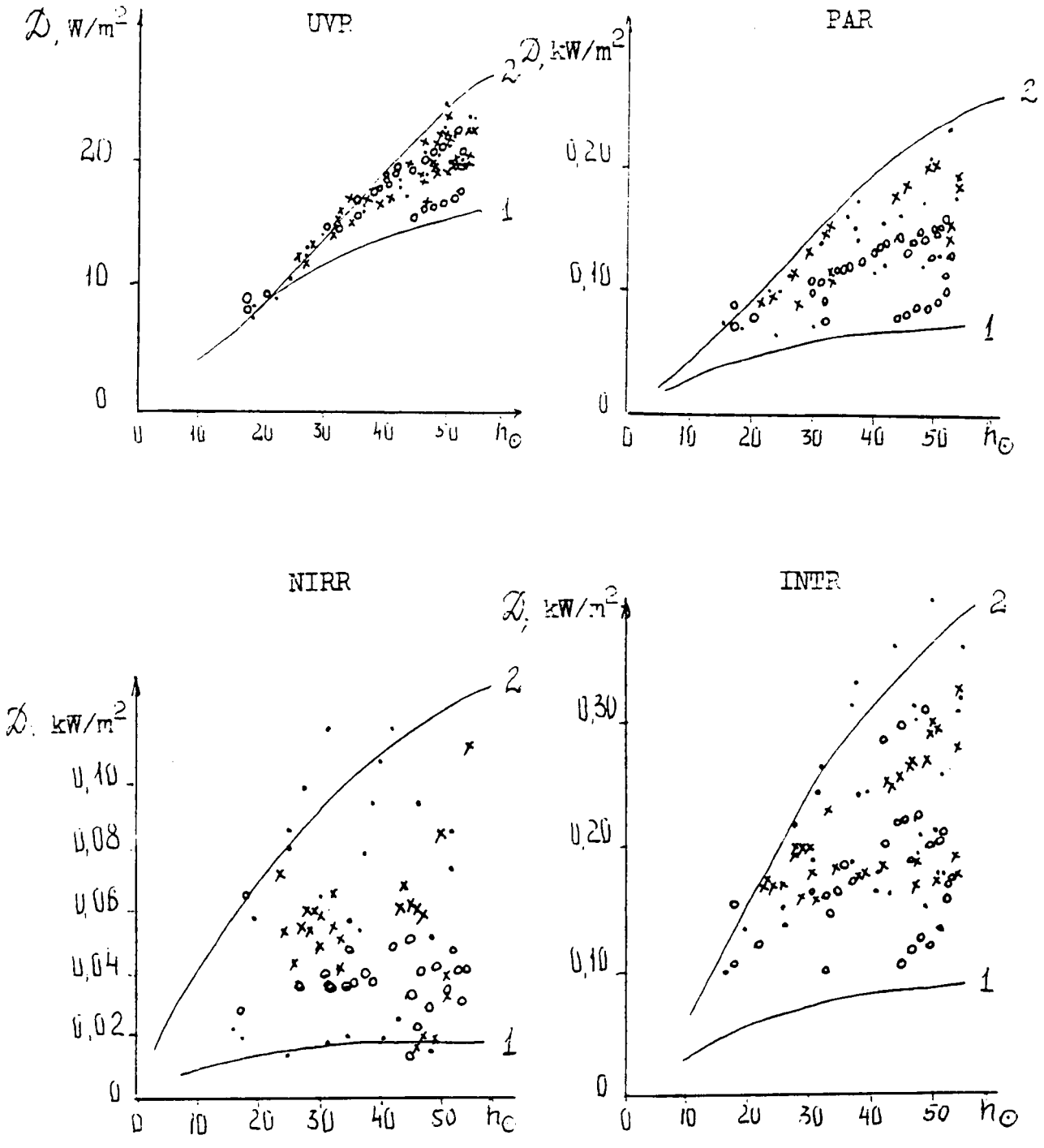

Figure 5.4 Diffuse radiation in different regions of the spectrum as a function of the sun's height (h_o): cloudless sky (curves land 2); continuous high cloud cover (1).
(· - 1986, x - 1987, o - 1989)
curve 1: $P_2 = 0.79$; curve 2: $P_2 < 0.50$
where P_2 = coefficient of atmosphere transparency for cosec $h_o = 2$.

For $h_o > 10°$ there appears to be no relationship between C_D and h_o (see Figure 5.5). This permits calculating statistical characteristics for the entire data set of C_D, including average quantity M, mode, M_o, median, M_e, variation coefficient V, per cent, standardized skewness A/σ_A and standardized kurtosis E/σ_E (σ_A and σ_E are standard deviations for A and E) (see Table 5.5). Tabulated in Table 5.5 for comparison are the values of the above parameters, obtained by analyzing many years of data observations carried out by the Moscow State University meteorological observatory.

On the average, Ci clouds increase diffuse radiation in all the spectral intervals considered: most of all, NIRR, least of all, UVR. This is explained by the different asymmetry of total phase function: the largest for NIRR and the smallest for UVR. In this context, values of $C_D < 1$ may be observed for UVR frequently in the presence of cirrus cloudiness.

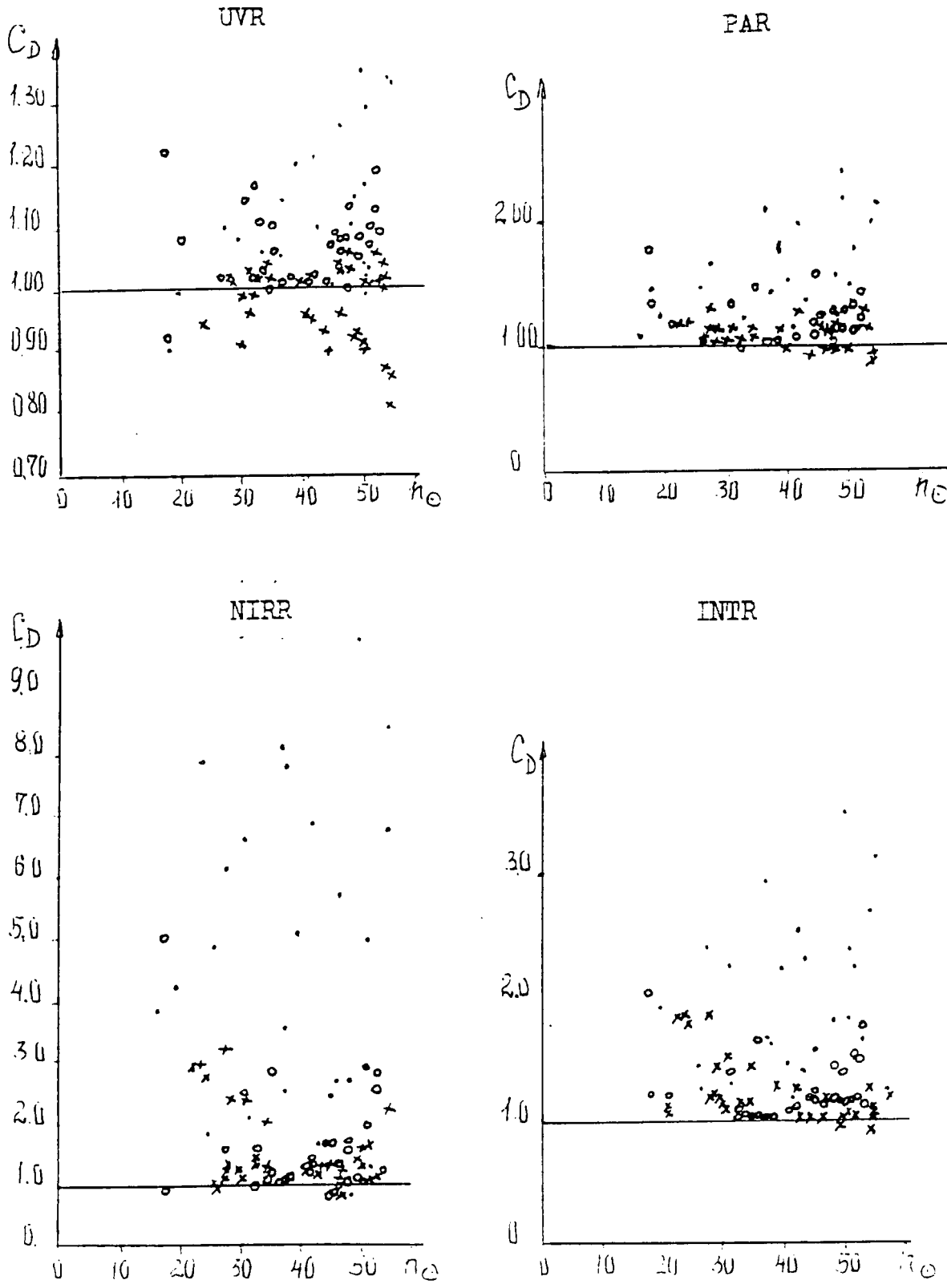

Figure 5.5 C_D values for UVR, PAR, NIRR, INTR as a function of the sun's height (h_o).

Table 5.5

C_D values and its statistics

Year	M Mean	M_o Mode	M_e Median	max	min	V%	A/σ_A	E/σ_E	n
				$C_{D,VFR}$					
1986	1.12	1.10	1.10	1.35	0.90	11	0.92	-0.66	24
1987	0.98	1.02	1.01	1.06	0.81	6	-2.43	0.31	39
1989	1.07	1.08	1.07	1.22	0.92	6	0.60	0.64	32
mean MSU, May	1.05	1.02	1.03	1.35	0.81	10	3.24	2.97	95
1968-85	1.02	1.00	1.03	1.36	0.51	14	-2.71	1.16	336
				$C_{D,PAR}$					
1986	1.49	1.14	1.44	2.40	1.00	25	1.78	-0.03	26
1987	1.10	0.98	1.13	1.31	0.87	11	0.41	-1.03	31
1989	1.20	1.07	1.14	1.79	0.99	15	3.50	2.89	30
mean, MSU, May	1.25	1.14	1.16	2.40	0.87	23	6.85	6.80	87
1980-85	1.32	1.14	1.31	2.18	0.55	20	1.74	0.85	114
				$C_{D,NIRR}$					
1986	5.42	1.32	5.92	9.88	1.133	49	-0.53	-0.84	18
1987	1.84	1.23	1.47	3.25	1.00	42	1.34	-1.04	19
1989	1.47	1.06	1.99	5.00	0.82	58	6.68	12.18	28
mean, MSU, May	2.67	1.06	1.47	9.88	0.82	87	5.10	2.16	65
1980-85	2.16	3.18	1.73	9.82	0.60	44	8.34	11.30	106
				$C_{D,INTR}$					
1986	1.91	1.82	1.82	3.51	1.01	38	1.29	-0.50	23
1987	1.25	1.04	1.17	1.87	0.93	22	3.36	0.98	37
1989	1.27	1.05	1.18	2.04	1.03	20	3.35	2.26	31
mean, MSU, May	1.43	1.04	1.22	3.51	0.93	36	7.85	8.31	91
1980-85	1.48	1.11	1.40	3.76	0.56	30	10.45	11.56	477

n - number of cases

The distributions of various C_D values for PAR, NIR and IR for three years of measurements have sharp peaks and are characterized by large positive asymmetries (see Figure 5.6). The distribution of C_D for UVR is close to normal. In separate years, because of differences in the nature of cloud cover as well as because of small numbers of samples, the slopes of the distribution of C_D values differ from the distribution for the whole period of observations.

Average values of C_D for UVR, PAR, NIRR and INTR according to the observations taken in Zvenigorod turned out to be close to the values deduced from the MSU data. However, very low minimum values of C_D were detected from the multi-year analysis. This may, to some extent, arise from the fact that the calculations of C_D for the Moscow measurements used the mean of mullti-year values of D_o as well as from the severe pollution of the city atmosphere.

As mentioned above, the near-solar zone with a diameter of 10° is being screened during measurements of D. Due to light diffraction by large Ci ice crystals, a significant amount of diffuse radiation gets into this zone and may be estimated as an integral flux on the basis of the actual values of direct solar radiation S_r. So, the real values of diffuse radiation (D_r), including also the quantity of the diffuse radiation of the near-solar zone in an angle of 10°, were determined from the following expression:

$$D_r = Q - S_r \sinh_\odot \tag{5}$$

where Q is the global radiation.

The contribution of the diffuse radiation to the near-solar zone within an angle of 10° is given from the following ratio:

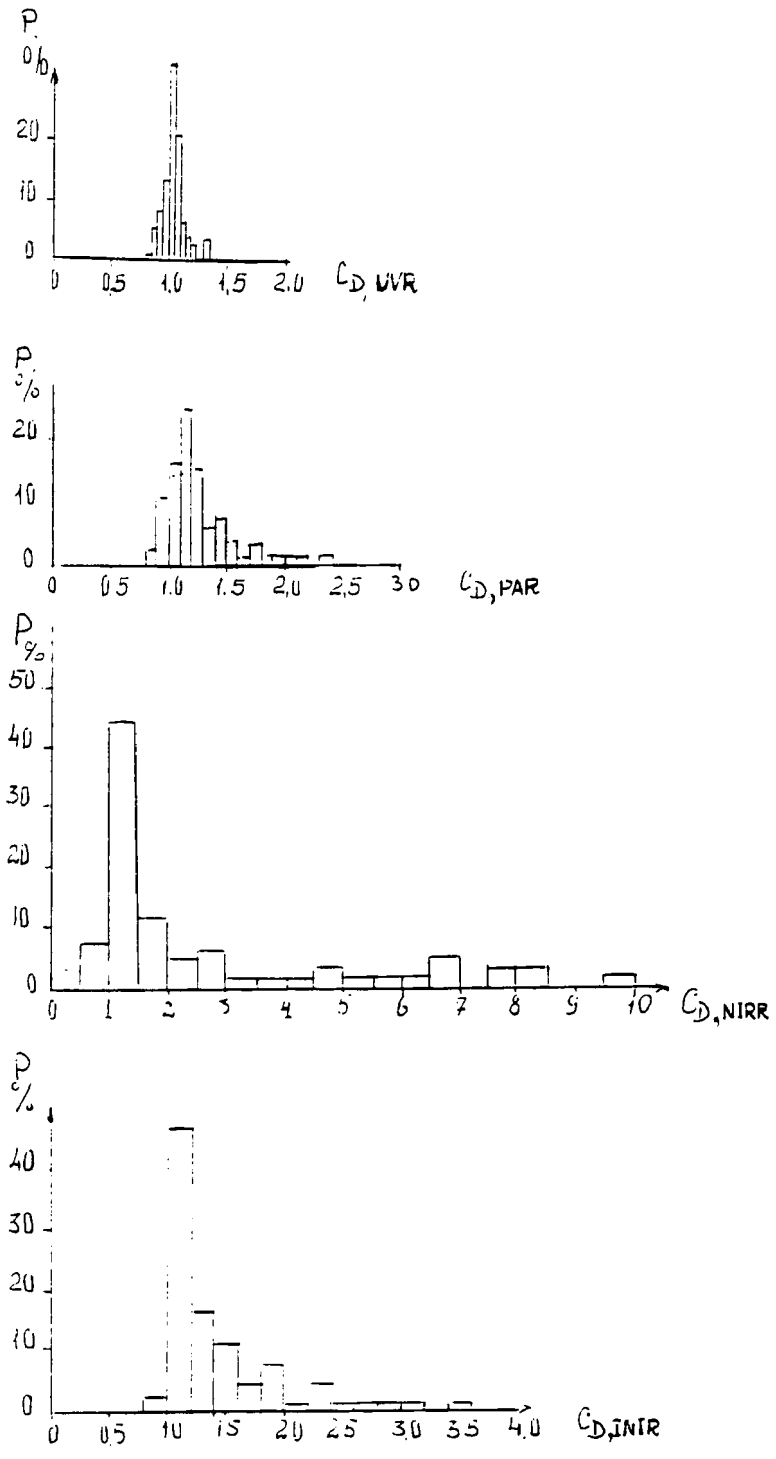

Figure 5.6 Recurrence of the different C_D values.

$$\Delta D, \% = (1 - D/D_r) \cdot 100\% \quad (6)$$

From the analysis of the Zvenigorod experiment data for $\tau_{2.1} \leq 0.5$, ΔD varied from 2.5 to 47 percent; a noticeable coupling of ΔD with optical thickness is evident (see Figure 5.7).

The coupling of C_D values for UVR, PAR, NIRR and INTR with optical thickness τ for $\lambda = 2.1$ μm ($\tau_{2.1}$), depicted by equation (2), is represented in Figure 5.8. The closest tie between C_D and $\tau_{2.1}$ is observed for NIRR and INTR (see Table 5.6).

From the real values of integral diffuse radiation D_r, values of $C_{D,r}$ have been calculated; these may exceed non-corrected values of C_D by more than 30 per cent. Differences between C_D and $C_{D,r}$ depend upon on $\tau_{2.1}$. The correlation coefficient between $C_{D,r}$ and $\tau_{2.1}$ is somewhat higher than between C_D and $\tau_{2.1}$ (see Table 5.6) and the parameter a (is 1.8 times larger in the equation for $C_{D,r} = a \cdot \tau_{2.1} + b$.

5.3 Global radiation

Global (INTR, UVR, PAR) radiation was continuously recorded during the experiment; using the same instruments that were used for measuring diffuse radiation. Global NIRR was also determined as the difference between fluxes INTR, UVR, PAR. The greatest variation of global radiation takes place up for solar heights $h_o \leq 25°$, then it decreases and for $h_o > 45°$, for all the spectral regions, the variation coefficient is within the limits of 7 to 11 per cent.

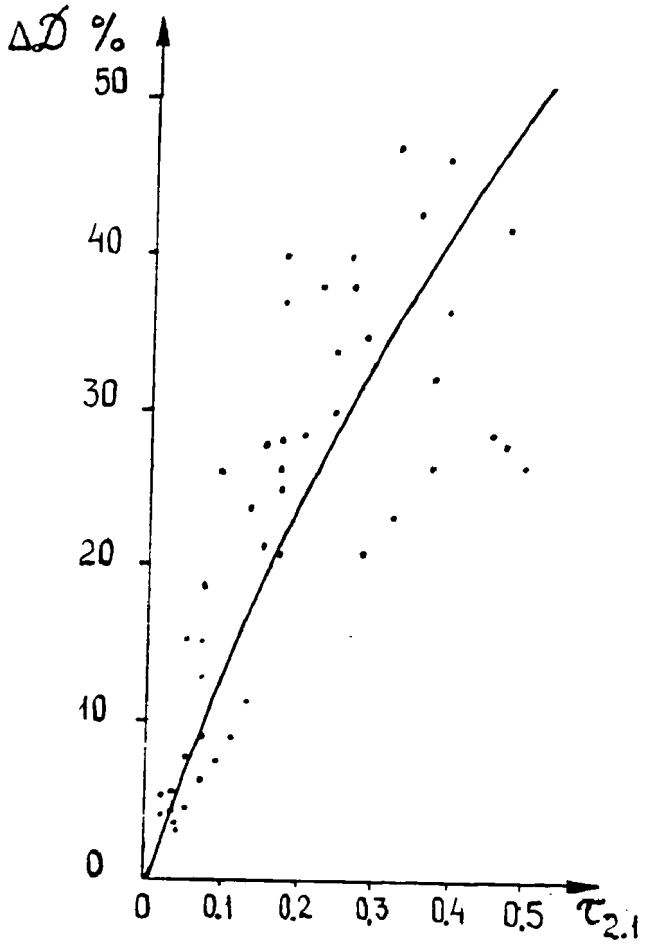

Figure 5.7 The correlation between ΔD_{INTR} and $\tau_{2.1}$.

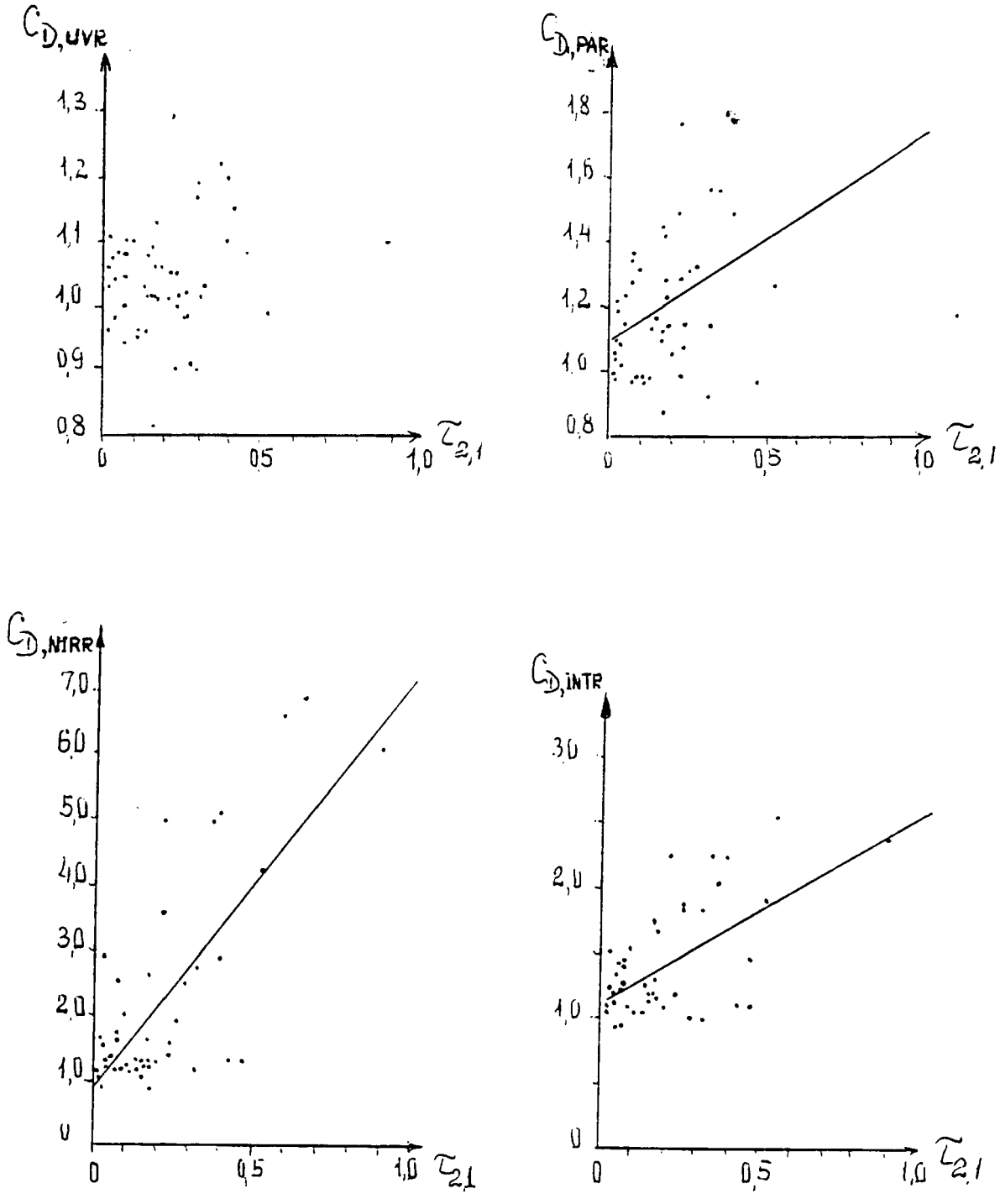

Figure 5.8 The correlation between C_D and $\tau_{2.1}$.

Table 5.6

The parameters a and b in the regression equation $C_D = a\tau_{2.1} + b$, correlation coefficients r and its standard deviation - δ_μ.

C_D	a	b	τ	δ_μ	n
$C_{D,UVR}$	0.04	1.04	0.08	0.14	49
$C_{D,PAR}$	0.64	1.09	0.45	0.11	50
$C_{D,NIRR}$	6.22	0.90	0.74	0.07	48
$C_{D\ INTR}$	1.44	1.12	0.62	0.09	50
$C_{D,r\ INTR}$	2.57	1.24	0.70	0.07	50

Table 5.7

$C_{Q\ UVR}$	$C_{Q\ PAR}$	$C_{Q\ NIRR}$	$C_{Q\ INTR}$
0.21	0.10	0.31	0.34

Table 5.8

C_Q values and its statistics

years	M	M_o	M_e	Max	Min	V%	A/σ_A	E/σ_E	n
$C_{Q\ UVR}$									
1986	0.93	0.94	0.94	1.11	0.68	7	-3.21	1.73	328
1987	0.93	0.98	0.95	1.02	0.71	7	-6.11	2.76	163
1989	0.95	0.98	0.97	1.11	0.64	9	-7.55	7.85	126
mean MSU, May	0.94	0.98	0.95	1.11	0.64	8	-9.11	7.35	617
1968-85	0.93	0.92	0.94	1.33	0.45	15	-4.97	4.59	336
$C_{Q\ PAR}$									
1986	0.93	1.00	0.96	1.14	0.57	12	-6.55	0.42	328
1987	0.93	0.96	0.96	1.09	0.44	10	-9.05	13.29	163
1989	0.92	0.98	0.97	1.15	0.41	14	-9.53	10.79	126
mean, MSU, May	0.93	1.00	0.96	1.15	0.41	12	-14.61	13.81	617
1980-85	0.95	1.03	0.97	1.46	0.49	15	-2.31	4.22	115
$C_{Q.NIRR}$									
1986	0.97	0.93	0.89	1.17	0.46	15	-2.95	-0.46	328
1987	0.95	1.02	0.98	1.16	0.47	12	-9.06	10.41	163
1989	0.86	0.94	0.93	1.15	0.11	26	-7.77	5.47	126
mean, MSU, May	0.89	0.94	0.92	1.17	0.11	17	-15.47	18.79	617
1980-85	0.93	0.91	0.92	1.33	0.61	15	1.70	1.10	117
$C_{Q\ INTR}$									
1986	0.90	0.96	0.92	1.15	0.53	13	-4.61	-0.29	328
1987	0.94	0.99	0.97	1.08	0.51	10	-9.87	11.96	163
1989	0.89	0.94	0.95	1.11	0.25	20	-8.71	7.12	126
mean, MSU, May	0.91	0.98	0.95	1.15	0.25	14	-16.70	19.69	617
1965-85	0.91	0.98	0.93	1.30	0.38	15	-5.09	4.64	477

High level cloud effects upon global radiation in various spectral regions as well as upon diffuse components are comparable with atmospheric turbidity effects (see Figure 5.9). These results confirm those reported earlier Abakumova, G. M., et al. 1989, Chapter 4, Figure 4.2).

To investigate Ci effects upon global radiation, the ratio $C_Q = Q/Q_o$ was used, where Q and Q_o represent global radiation, with a high level cloud cover being continuous and the sky being clear, respectively. The quantity C_Q for various spectral regions varies significantly depending on the sun's height; this is pointed out by the small values of correlation coefficients, *r*, between C_Q and $h_\odot$ (see Table 5.7). This makes it possible to derive statistical characteristics of C_Q for each year separately and for three years on the average (see Table 5.8). Average quantities of C_Q vary slightly year by year and, for all the spectral regions, are sufficiently close that on the average, may be considered as neutral. In separate cases, a selective radiation reduction takes place. The quantity C_Q may vary within a large range that is specified by a different Ci density and microstructure. An increase of global radiation in all the spectral regions in comparison with a cloudless sky is noted in the presence of continuous Ci cover of a different density: thin clouds at the sun's disk slightly reduce solar radiation and dense clouds in other parts of the sky greatly increase diffuse radiation.

The closeness of the average values C_Q, obtained in Zvenigorod and in Moscow, engages our attention (see Table 5.8). Maximum values of C_Q deduced from multi-year, Moscow observations taken by the MSU meteorological observatory are 30 to 40 per cent higher than those derived from the data of the Zvenigorod experiment; this may, to some

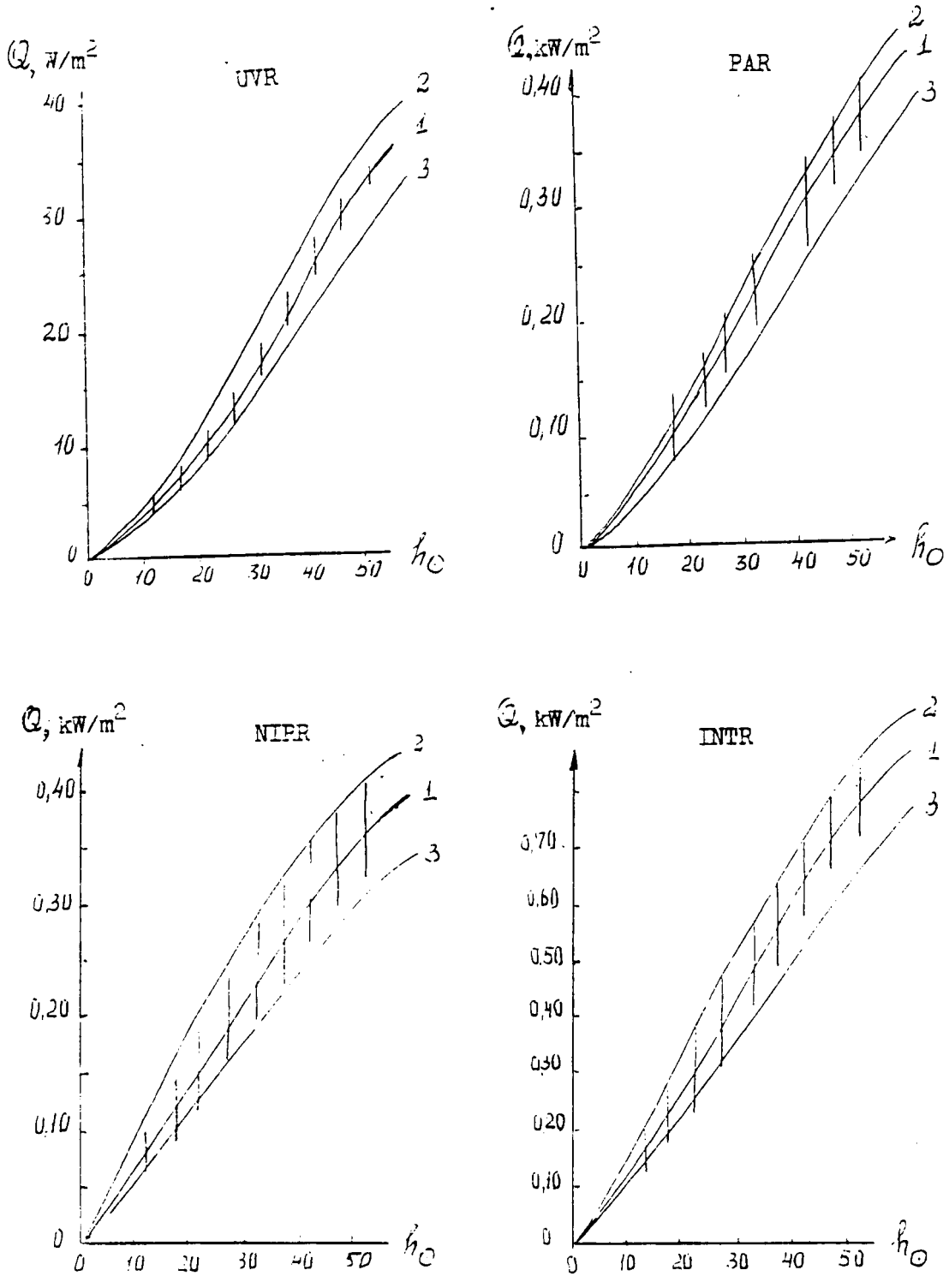

Figure 5.9 Global radiation in different regions of the spectrum as a function of the sun's height (h_o): cloudless sky (curves 2 and 3); continuous high cloud cover (1).
Curve 2: $P_2 = 0.79$; Curve 3: $P_2 < 0.50$
where P_2 = coefficient of atmosphere transparency for cosec $h_o = 2$.

extent, be a result of the usage of average multi-year values of Q_o, when calculating C_Q for the measurements made in Moscow, as well as by larger scale optical cloud property variations.

The distributions of occurrence of C_Q difference values for all spectral regions for the three year sample are characterized by a left-hand asymmetry and positive kurtosis (see Figure 5.10), however, each spectral region has its own pecularities. These are explained by a different Ci effect on the diffuse radiation and by the change of the direct to diffuse radiation ratio, for sky which does depend on wave length (Collection, 1989). When determining the correlation between C_Q and $\tau_{2.1}$, values of C_Q determined in steps of 1 minute and $\tau_{2.1}$, averaged within one minute were used. There is an inverse dependence between C_Q and $\tau_{2.1}$ for all the spectral intervals (see Figure 5.11).

In order to exclude the influence of dissimilar numbers of observing days in the three years, values of C_Q were averaged for increments of $\Delta \tau_{2.1} = 0.1$ for every observation day (Table 5.9, Figure 5.11).

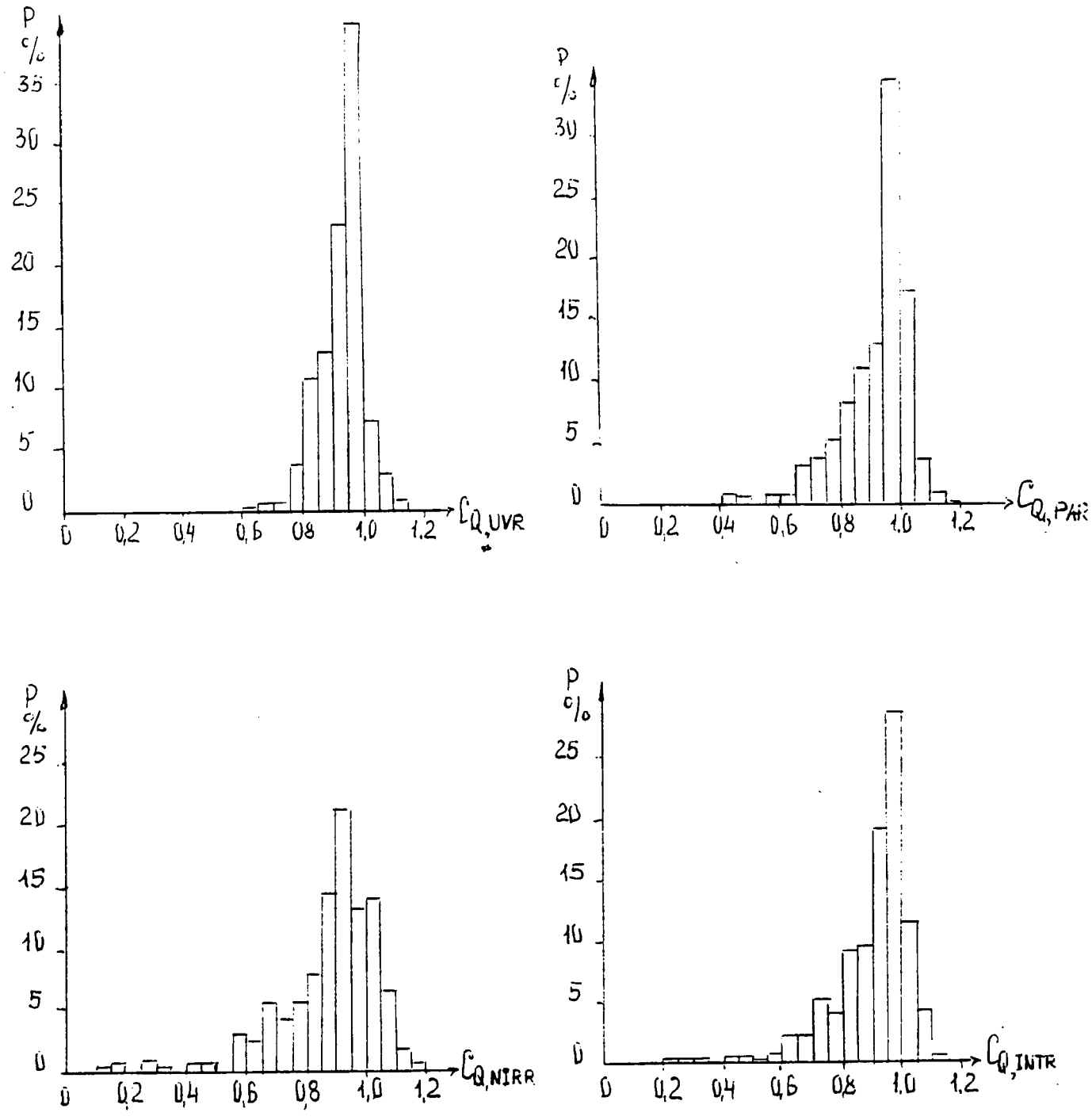

Figure 5.10 The frequency of the different C_Q values.

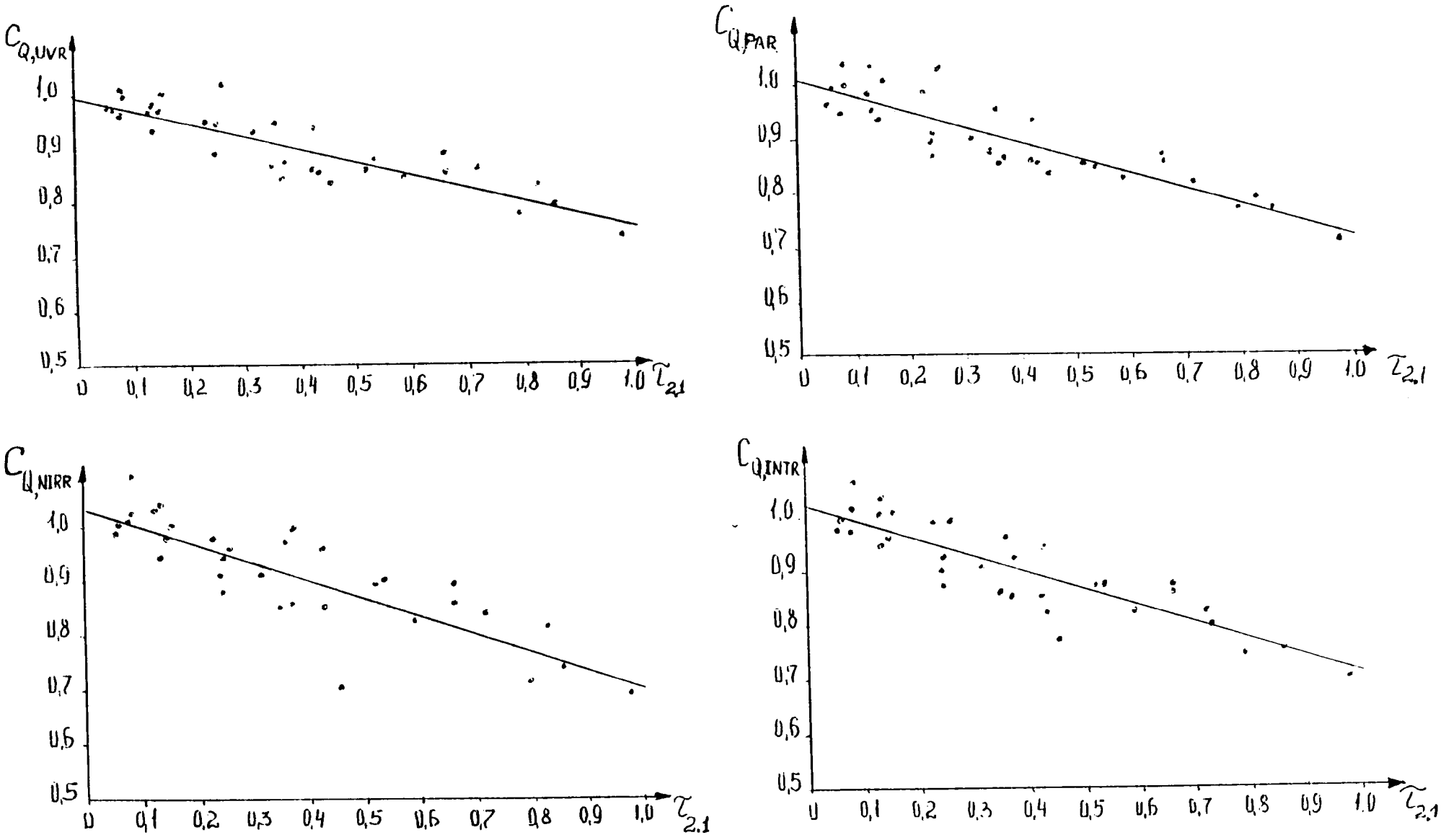

Figure 5.11 The correlation between $C_{Q\ UVR}$, $C_{Q\ PAR}$, $C_{Q\ NIRR}$, $C_{Q\ INTR}$ and $\tau_{2.1}$.

TABLE 5.9

The parameters a and b in regression equations $C_Q = a\ \tau_{2.1} + b$, and correlation coefficients r.

coefficients	$C_{Q\ INTR}$	$C_{Q\ UVR}$	$C_{Q\ PAR}$	$C_{Q\ NIRR}$	*n*
a	-0.31	-0.24	-0.29	-0.34	
b	1.02	1.00	1.01	1.04	34
τ	-0.88	-0.88	-0.88	-0.83	

Analysis of the data obtained revealed that the $\tau_{2.1} < 0.3$, Q_{UVR} is reduced most of all, while Q_{NIRR} least of all. The direct radiation component of Q_{NIRR} is considerably larger than the direct component of Q_{UVR} while the diffuse radiation in near IR region increases considerably more than in UV spectral region.

A reverse picture is observed for $\tau_{2.1} > 0.5$: the greatest reduction of global UVR and the smallest reduction of global NIRR. This is caused by a decrease of direct solar radiation by the more dense clouds, which is not compensated by the increase of diffuse radiation in the near IR spectral region and thus leads to a net reduction in Q_{NIRR}. For $\tau_{2.1}$ = 0.3 to 0.5 global radiation transmission is practically neutral.

Global and diffuse near IR radiation exhibit the most sensitivity to the variations of the optical properties of high level clouds, while global and diffuse ultra-violet components

show the least sensitivity. The large scale variation of C_Q and C_D in all spectral regions points arise from the different density, microstructure and inhomogeneity of high level clouds. On the average, according to the three-year observations taken in Zvenigorod as well as according to multi-year data obtained in Moscow, the reduction of global radiation in various spectral regions by Ci clouds may be considered to be nearly spectrally neutral.

The higher correlation between the global radiation transmission and Ci optical thickness in comparison with diffuse components for all the spectral intervals suggests the possibility of using the global transmission as the basis of an indirect method to estimate a Ci optical thickness.

REFERENCES

Abakumova, G. M., I. N. Plakhina, and T. A. Tarasova, 1989. The estimate of the aerosol optical thickness of the atmosphere from the data of ground-based and ship-based actinometry (comparison of different techniques). Meteorologiya i Gidrologiya, No. 10.

Abakumova, G. M., et al., 1989. The geometrical, optical and radiative properties of cirrus clouds. Atmospheric Science Paper No. 456.

Collection, 1989. "*Radiative properties of cirrus clouds.*" Nauka Publishers, 130 pgs. (in Russian).

Chapter 6

Radiative Properties of Upper Level Clouds in UV Spectral Regions

by Ye. I. Nezval' and N. Ye. Chubarova

6.1 Radiative properties of upper level clouds according to the data of spectral measurements and calculations.

6.11 Spectral Measurements

During the 1989 Zvenigorod experiment UV spectral radiative measurements were made using a recording spectrometer which has double monochromator DMR-4 with quartz optics; this instrument was developed at the Meteorological Observatory of Moscow State University (Visotsky, et al., 1982). A photo-multiplier with a cesium-antimonic cathode is used as a detector for measurements within the spectral region from 300 to 575 nm. During scanning (1.5 min) within the range of 300 to 560 nm signal averaging is carried out in 70 narrow spectral parts, 44 of which are related to the UV spectral region. The width of spectral intervals varies from 2 nm near λ = 300 nm to 10 nm for 575 nm. A singular type of integrating sphere with an angle of view of 180° is located in front of the monochromator entrance slit. Special collimator tubes with angles of view of 5° and 10° are slipped over the monochromator to measure direct solar radiation. When measuring diffuse radiation an actinometric screen is used to exclude radiation from the sun's disk and the near-solar zone in the angle of 10°.

The influence of continuous cover of high level clouds upon direct 10° field of view, diffuse and global radiation of different wavelengths is illustrated in Figure

6.1 which contains data collected on May 31, 1989. The values are represented as follows:

$$P_\lambda = (S/S_o)^{1/m};\ C_{D,\lambda} = D_\lambda/D_{o\lambda};\ C_{Q,\lambda} = Q_\lambda/Q/_{o\lambda} \quad (1)$$

where P_λ is the cloud transmission coefficient; m = cosec h_o, h_o - is the solar elevation angle; S_λ, D_λ, Q_λ are direct, diffuse and global radiation at the wavelength λ, respectively, with the continuous cirrus cloud cover and $S_{o\lambda}$, $D_{o\lambda}$, $Q_{o\lambda}$ are the same variables for the cloudless sky case.

In order to determine the denominators in Eq. 1 the dependencies $S_{o\lambda}$,$D_{o\lambda}$ and $Q_{o\lambda}$ upon the sun's height were considered for various conditions of atmosphere turbidity. In order to exclude ozone influence in the short wavelength part of the UV spectrum, the radiation values are normalized to the quantity of the general content of ozone X = 0.30 atm. cm (M. P. Garadzha and Ye. I. Nezval, 1984).

On May 31st cirrus fibratus (Ci fib) clouds were observed with optical thickness of $\tau_{2.1}$ = 0.35, Figure 6.1. The values of $\tau_{2.1}$ were determined expression (see Chapter 5) Eq. 2:

$$\tau_{2.1} = 1.88\ \tau_A,\ r = 0.96 \quad (2)$$

where $\tau_{2.1}$ and τ_A are the optical thickness of Ci obtained by the IAP spectral radiometer with the angle of view of 15' at λ = 2.1 μm, and from the actinometer with the angle of view of 10°, respectively; r is the correlation coefficient.

Since the direct radiation measured at an angle of 10° under ci cloudiness is considerably influenced by the contribution from scattered radiation of the near-solar zone, which is wavelength dependent P_λ values are larger for longer

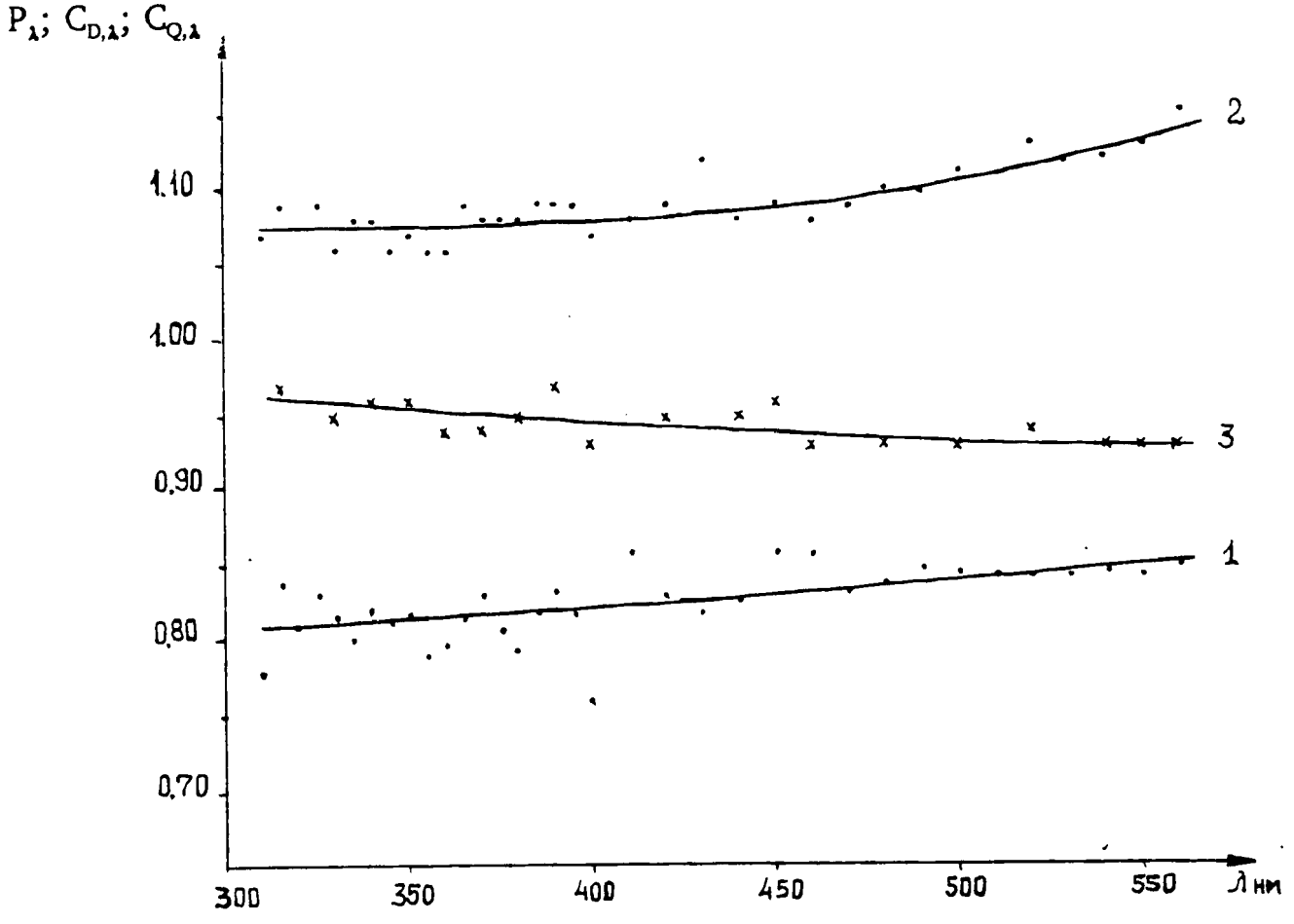

Figure 6.1 The transmission of the radiation at different wavelengths by Ci fib May 31, 1989 $\tau_{2.1} = 0.53$, $h_o = 45°$.
Curves: 1: $_\lambda$; 2: $C_{D,\lambda}$; 3: $C_{Q,\lambda}$.

wavelengths. A weaker growth of diffuse radiation in the UV spectral region ($C_{D\lambda} < 1$) is a result a less anisotropic phase function for large optical thicknesses of Rayleigh scattering or by additional absorption in the UV spectral region in the presence of cirrus clouds. There is a tendency of $C_{Q\lambda}$ to decrease with increasing wavelength; this decrease in $C_{Q\lambda}$ as a function of wavelength arises both from effects of cirrus clouds and the cloud free atmosphere on the direct and diffuse radiation.

Additional reduction of global radiation in the visible spectral region (see Figure 6.1) is explained by the fact that the losses of direct radiation, which increases in importance with wavelength, are not compensated by the growth of diffuse radiation.

In the case of very thin cloudiness at sun's disk, when direct radiation transmission is close to one and the growth of diffuse radiation is greater in the visible spectral region than in the UV, the dependence of $C_{Q\lambda}$ upon λ should be reversed. This was illustrated in an example of measurements made on May 22nd, 1987 for large spectral intervals, Abakumova, G. M., et al. 1989. It is unfortunate that spectral data of diffuse and global radiation with the continuous cover of very thin and dense Ci clouds are not available.

6.12 Model Calculations

Radiative atmospheric models provide a mechanism for coupling optical cloud characteristics and radiative properties of the cloudy atmosphere and may also serve as one of the methods to make up for deficiencies of experimental data. In this

publication the results of analyses performed for a 5-level model of the atmosphere are represented. Calculations of the diffuse and global solar radiation were made using a two-stream method with δ-Eddington (E. P. Shettle and J. A. Weinmann, 1970 and J. A. Joseph, et al., 1976).

The choice of altitudes was carried out in a way to take into account more precisely the peculiarities of ozone and aerosol vertical distributions and geometric thickness and heights of clouds, (see Table 6.1). All the calculations were done using the general content of ozone of X = 0.3 atm.cm.

The coefficients of ozone absorption were taken from data provided by the Global Ozone Research and Monitoring Project, 1985, at T = 203° K. For the lowest level a temperature of T = 273° K was used.

The distribution of aerosol with respect to height and its optical properties were specified for a continental model (11 CONT-1) up to a height of h = 12 km; for the higher levels a stratospheric model was used (WMO/TD, N 24, 1986). Spectral distribution of the optical aerosol thickness was calculated from Eq. 3:

$$\tau_{\lambda aer} = \tau_{\lambda oaer} (\lambda/\lambda_o)^{-1.3}, \quad (\lambda_o = 0.55\mu m) \tag{3}$$

The spectral distribution of solar radiation on the upper boundary of the atmosphere for the wavelength range of 280 to 400 nm in 5 nm increments and for λ = 550 nm was adopted from WMO/TD, N149, 1986. A smoothing was carried out over 5 nm intervals. The spectral change of Rayleigh optical thickness $\tau_{ray,\lambda}$ for each level was calculated from Eq. 4.

$$\tau_{ray,\lambda,i} = 0.0002008\ K_i/\lambda^{4+c} \tag{4}$$

where $c = 0.398\,\lambda + \frac{0.09426}{\lambda} - 0.3223$ and K_i is the coefficient of the distribution of $\tau_{ray,\lambda}$ i'th level (see Table 6.1).

The spectral values of grass albedo were approximated by the following dependence (Dirmhirn, 1957):

$$A_\lambda = 0.368\,\lambda - 0.0916 \qquad (5)$$

The optical characteristics of high level clouds in the UV spectral region have not been studied yet. That is why the values of $\mu = 0.7$ and $\omega = 1$ for $\lambda = 550$ nm were chosen (See Chapter 9), where μ is the average cosine of the phase function and ω is the albedo of single scattering of large ice crystals.

Table 6.1

The distribution of model's parameters at each layer (Δz = 10 - 12.5 km - Ci layer, δX is the distribution of ozone amount in the layers in per cent)

Height of layers Δz, km	$\tau_{aer,\lambda/o}$	δX, %	K, %
0-2.0	0.2	1.2	20.2
2-10.5	0.02125	4.9	55.9
10.5-12	0.00375	1.4	1.8
12-30	0.005	65.4	19.9
30-100	0.00002	27.1	2.2

Polluted ice has larger absorption coefficients than pure ice (Grinberg, 1979) and, hence, it can lead to the decreasing of ω values.

Since the $C_{Q\lambda}$ parameter, (introduced earlier), is convenient for characterizing clouds, let us take into account the influence of different factors upon $C_{Q\lambda}$ in the UV spectral region.

For submicron particles, varying the following optical properties through the specified ranges ($\omega_{aer,\lambda}$ = 0.89-0.99, $\mu_{aer,\lambda}$ = 0.55 to 0.65, Abakumova, G. M., et al. 1989, and τ_{aer} from 0.18 up 0.6) introduced uncertainties of 0.2-0.8 per cent in $C_{Q\lambda}$ for clouds with $\tau < 2$.

The $C_{Q\lambda}$ quantity is relatively unsensitive to cloud layer height for practically the whole spectral region, except for $\lambda < 300$ nm (see Table 6.2).

For the shortwave part of the UV spectral region, there is a tendency toward larger transmission as cloud height decreases. A similar situation for droplet clouds was reported by (M. S. Nack and A. E. S. Green, 1974), however, solar radiation with wavelengths shorter than 300 nm does not practically reach the earth's surface; therefore this effect will not be taken into account.

Perhaps the most important factor which influences the solar radiation input at the earth's surface is the sun's height h_o. We will examine the influence of h_o upon the quantity of $C_{Q\lambda}$. In Figure 6.2 values of $C_{Q\lambda}$ for various optical parameters of clouds at different solar heights are given. A distinct dependence of $C_{Q\lambda}$ upon h_o is noted in the visible region of spectrum; in the UV there is a slight dependence for ω = 0.9 but virtually none for ω = 1.0; i.e. the h_o influence upon

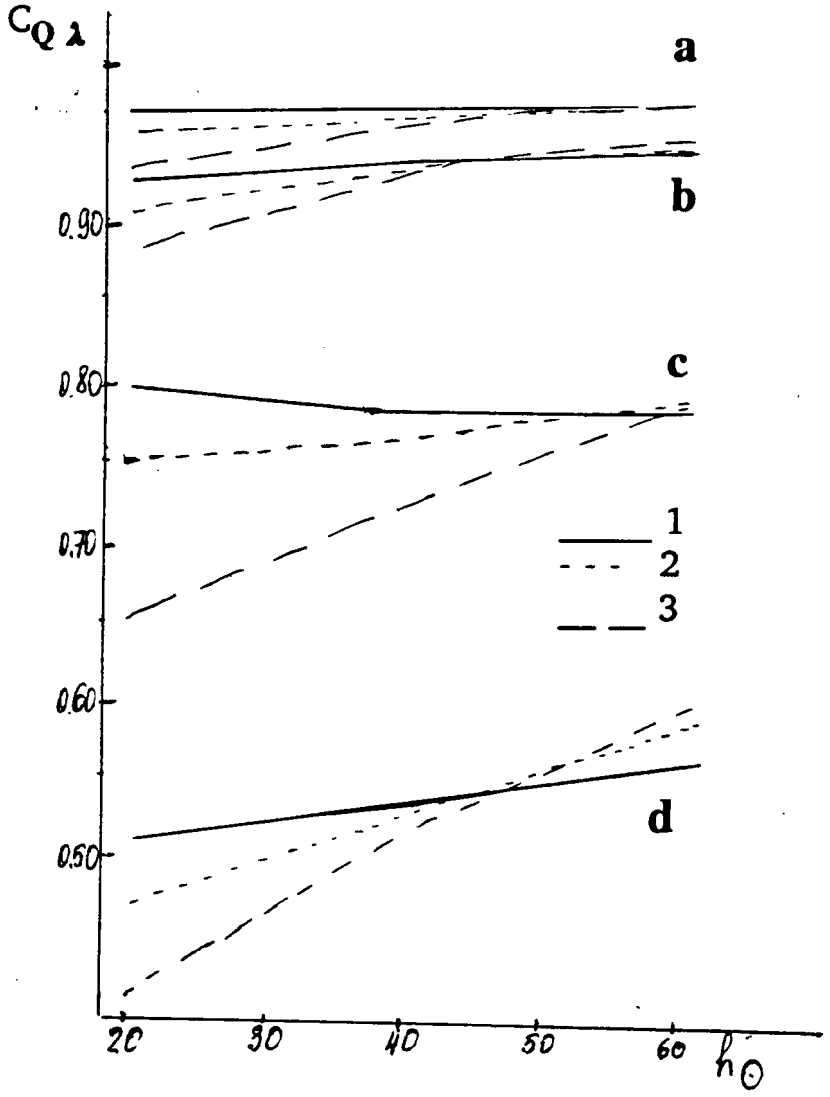

Figure 6.2 The influence of sun's height upon global radiation transmission.

a: - ω=1	μ=0.7	τ=0.2;	1-310 nm;
b: - ω=0.9	μ=0.7	τ=0.2	2-380 nm;
c: - ω=1	μ=0.7	τ=2;	3-550 nm;
d: - ω=0.9	μ=0.7	τ=2.	

$C_{Q\lambda}$ is virtually negligible in the UV spectral region. Therefore, the optical properties of Ci are the only basic factors determining $C_{Q\lambda}$ values in the UV portion of spectrum.

Table 6.2

The influence of cloud layer height upon the $C_{Q,\lambda}$.

$h_o = 40°$, X = 0.3 atm. cm

	$C_{Q,\lambda}$			
Cloud layer height	$\omega = 1.0$	$\mu = 0.7$	$\omega = 0.9$	$\mu = 0.7$
	$\lambda = 290$ nm	$\lambda = 380$ nm	$\lambda = 290$ nm	$\lambda = 380$ nm
H = 10.5 - 12.0 km	0.800	0.865	0.689	0.726
H = 0.5 - 2.0 km	0.859	0.864	0.721	0.724

The spectral consistency of the diffuse and global transmission with different optical parameters of Ci are shown in Figure 6.3. The diffuse radiation transmission $C_{D\lambda}$ is illustrated in Figure 6.3a. The increase of diffuse radiation in the presence of Ci relative to the clear sky case is seen for $\lambda > 300$ nm, however, possible pollution of ice crystals ($\omega < 1$) leads to decreased scattered radiation, even when the clouds are thin, and especially in the shorter wave length part of the ultraviolet spectral region. Analysis of the change in $C_{Q\lambda}$ (see Figure 6.3b) as a function of wavelength reveals that for all specified parameter values within the range of 300

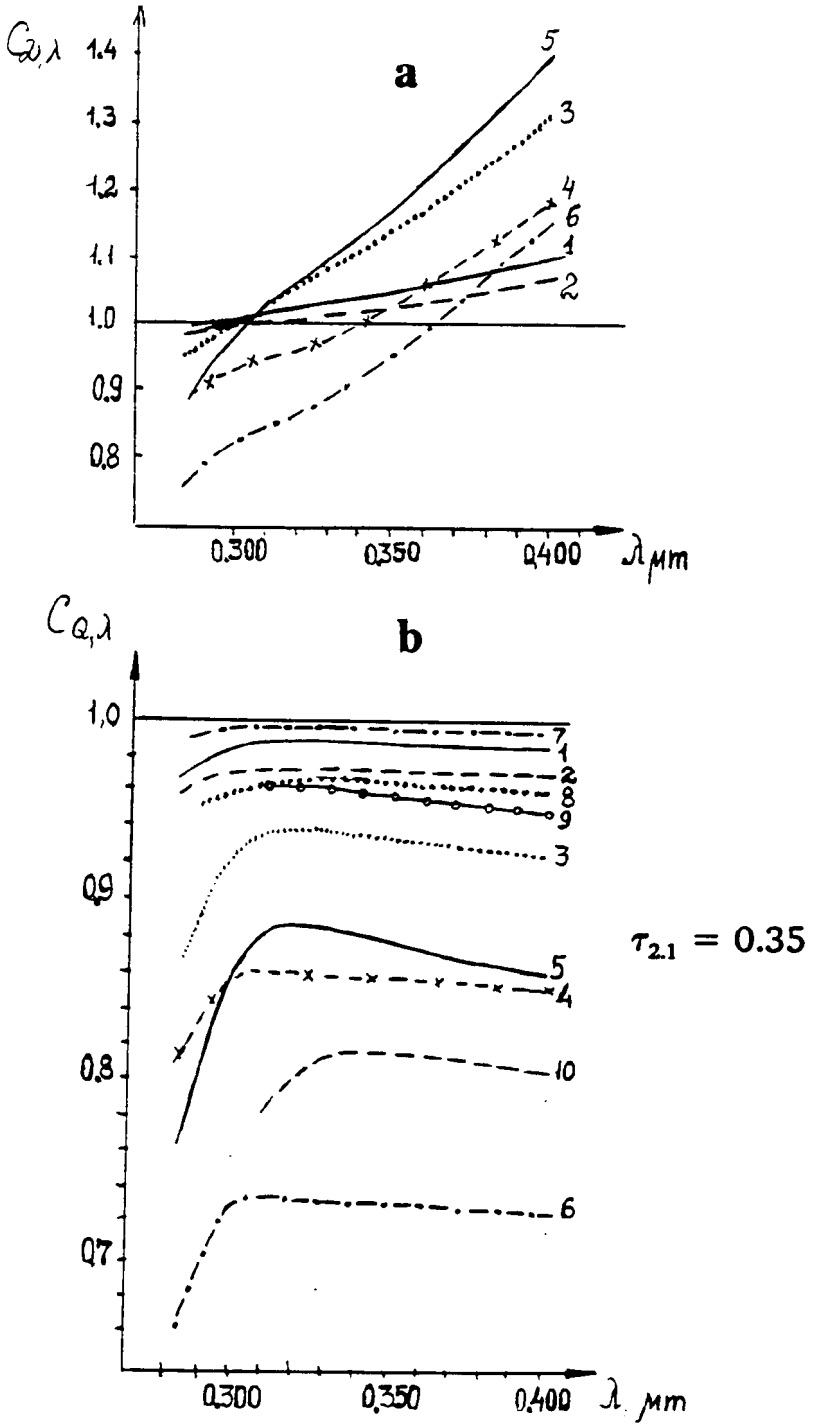

Figure 6.3 The $C_{D,\lambda}$ (Panel a) and $C_{Q,\lambda}$ (Panel b) dependencies upon wavelength influenced by different optical cloud characteristics.
h=40°, X=0.3 atm.cm
1a,b: τ=0.1, ω=1, μ=0.7; 2a,b: τ=0.1, ω=0.9, μ=0.7;
3a,b: τ=0.5, ω=1, μ=0.7; 4a,b: τ=0.5, ω=0.9, μ=0.7;
5a,b: τ=1, ω=1, μ=0.7; 6a,b: τ=1, ω=0.9, μ=0.7;
7b: τ=0.1, ω=1, μ=0.84; 8b: τ=0.5, ω=1, μ=0.7;
9b, 10b - measurement results.

to 330 nm, there is a maximum in global radiation transmission which shifts toward shorter wavelengths as ω is decreased. Figure 6.3b clearly shows the spectral differences in $C_{Q\lambda}$ for thin droplet clouds (curve 7) and crystalline clouds (curve 1), where $\omega = 1$, $\mu = 0.84$ (for drops with r = 4-5μm (A. Slingo, 1989) and $\omega = 1$, $\mu = 0.7$ respectively. The selective nature of global radiation transmission is determined by reduction of diffuse radiation in the shortwave part of the UV spectral region and, on the other hand, by a greater share of direct radiation in the long-wave part of UV spectral band. Measurements demonstrate a similar picture (curves 9,10).

During the Zvenigorod experiment we were able to relate the global radiation transmission in the whole UV spectral region, $C_{Q,290 < \lambda < 380\,nm}$ to the cloud optical thickness.

Comparison of measurements with calculations showed that both for individual days and, as a whole for the experiment period, the best correspondence is observed with the results of model calculations with optical cloud parameters $\mu = 0.7$, $\omega = 0.9$ (Figure 6.4). The lower value of ω played a vital role in obtaining agreement between calculations and observations. This may be caused by "dirty" ice crystals in the clouds and/or by some influence of a heterogeneous cloudiness structure upon the slopes of the regression lines derived from the observational results. The similar ratio of experimental and calculated quantities of C_Q have been obtained for integral radiation as well as for the regions of near infra-red and photosynthetically active radiation (Chapter 6).

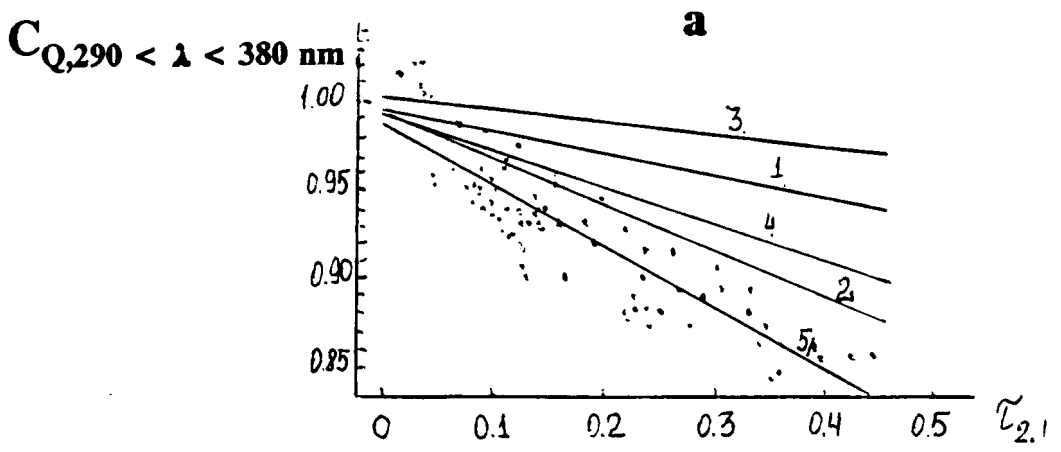

a) May 20, 1987. 1: ω=1, μ=0.7; 3: ω=1 μ=0.84;

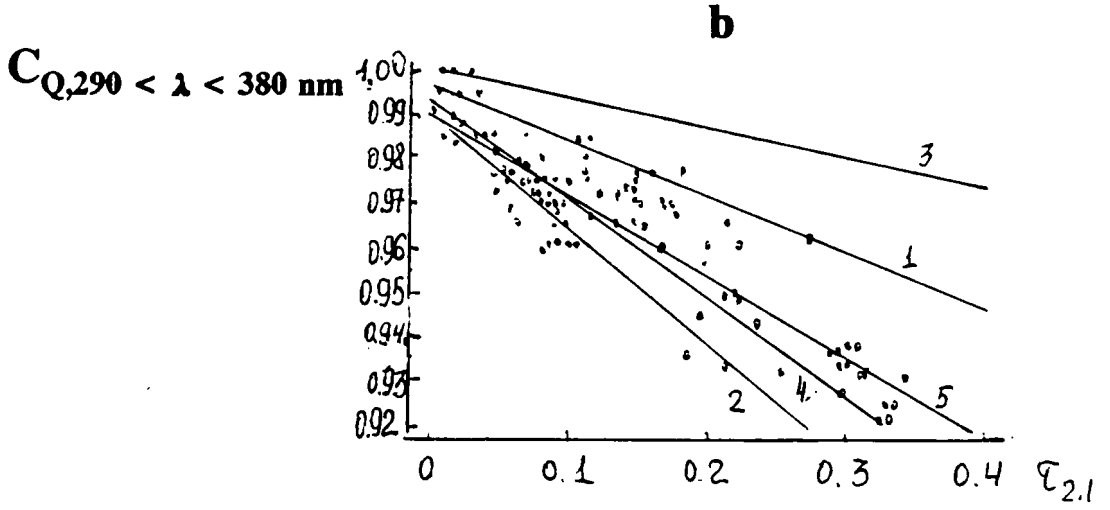

b) May 31, 1989. 2: ω=0.9, μ=0.7; 4: ω=0.9, μ=0.84;
5: regression line based upon measurements;

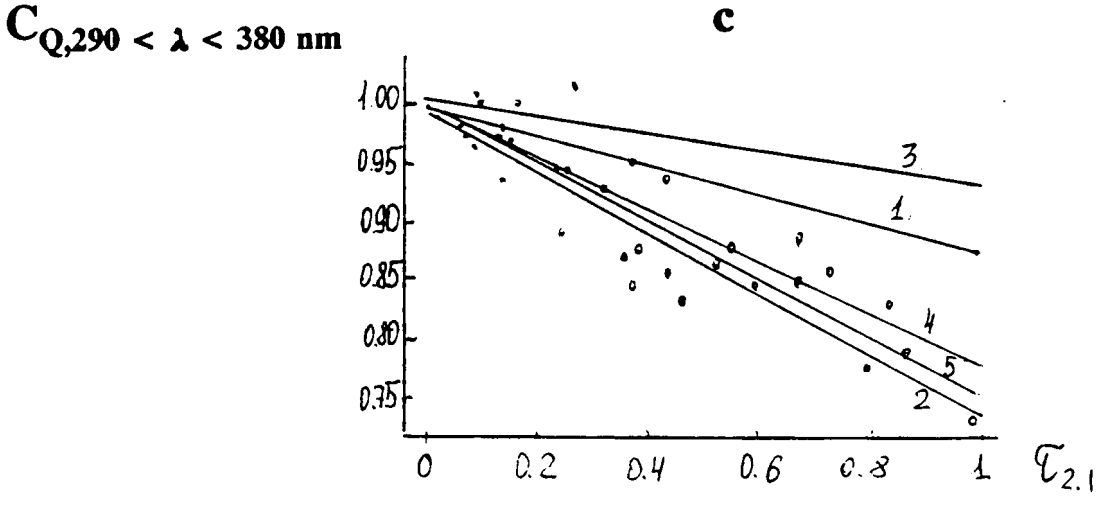

c) for the whole period of observations.

Figure 6.4 The dependence of transmission $C_{Q,290 < \lambda < 380\ nm}$ upon cloud optical thickness according to the results of measurements and calculations (h_o = 40°).

Approximate formula relating C_Q to atmospheric optical parameters have been suggested for transmitted integral global radiation C_Q by Ci, Abakumova, G. M., et al. 1989, as follows:

$$C_Q = 1 - 0.19 \cdot (1 - \mu^{-2}\omega) \cdot \tau/\sinh_o \qquad (6)$$

In the UV spectral region the calculations lead to other values of coefficients for a large range of optical characteristics of Ci and the various solar heights (μ = 0.6 - 0.84, ω = 0.8 - 1.0, τ = 0.1 - 2.0, h_o = 20-60°):

$$C_{Q,290 < \lambda < 380\ nm} = 1 - 0.395\ (1-\mu^{-0.72}\omega^{4.5})\tau^{0.79}/(\sinh_o)^{0.32} \qquad (7)$$

Equation 6 demonstrates less influence of the sun's height and a considerably greater role of ω.

6.13 Influence of the near-solar zone scattered radiation upon the quantities of optical Ci cloud thicknesses

In publication (Abakumova, G. M., et al. 1989, page 162) the error in determination of optical thicknesses of Ci from an actinometer with a field of view of 10° arising from the contribution of the scattered radiation of the near-solar zone was estimated. With the help of spectrometer measurements made by the meteorological observatory of Moscow State University (MSU) it was possible to analyze the dependence of this error upon wavelength in the UV and visible spectral regions. For this purpose, the spectral measurements of direct radiation for the field of view of 10° (6 series) and of 5° (18 series) with Ci clouds were used. Values of $\tau_{2.1}$ derived from Eq. 2 were considered to be the actual values of optical thicknesses of Ci.

The presence of a high correlation between $\tau_{2.1}$ and τ_A made it possible to use measurements made by actinometer as the control over changes of the optical thickness of a cloudy layer during recording of the direct radiation spectrum.

An optical thickness of Ci may be obtained from the following expression:

$$\tau_{ci,\lambda} = \tau_{\lambda} - \tau_{o,\lambda} \tag{8}$$

where τ_{λ} and $\tau_{o,\lambda}$ are atmospheric optical thicknesses obtained from the direct radiation measurements made by MSU spectrometer with Ci being present and with the clouds being absent at the sun's disk and in the near-solar zone, respectively. The values of $\tau_{o,\lambda}$ were determined before and after Ci when the solar disk was unobserved.

The data represented in Table 6.3 is testimony to the fact that real optical thicknesses are considerably larger (approximately twice) than those obtained by the MSU spectrometer. In Figure 6.5a normalized values of $\tau_{n,ci,\lambda} = \tau_{ci,\lambda}/\tau_{1.2}$ are given for the case of thin clouds ($\tau_{2.1} < 0.5$) and in Fig. 6.5b for the case of dense Ci clouds with $\tau_{2.1} > 0.9$. One can see the definite tendency of a decreasing of $\tau_{n,ci,\lambda}$ with increasing wavelength when there are thin clouds with the opposite tendency for dense Ci clouds.

In the last column of Table 6.3 the K coefficient values which were obtained from the equation of regression below are given:

$$\tau_{n,ci,\lambda} = K \cdot \lambda + b \tag{9}$$

The K values were validated using the Student T statistical test.

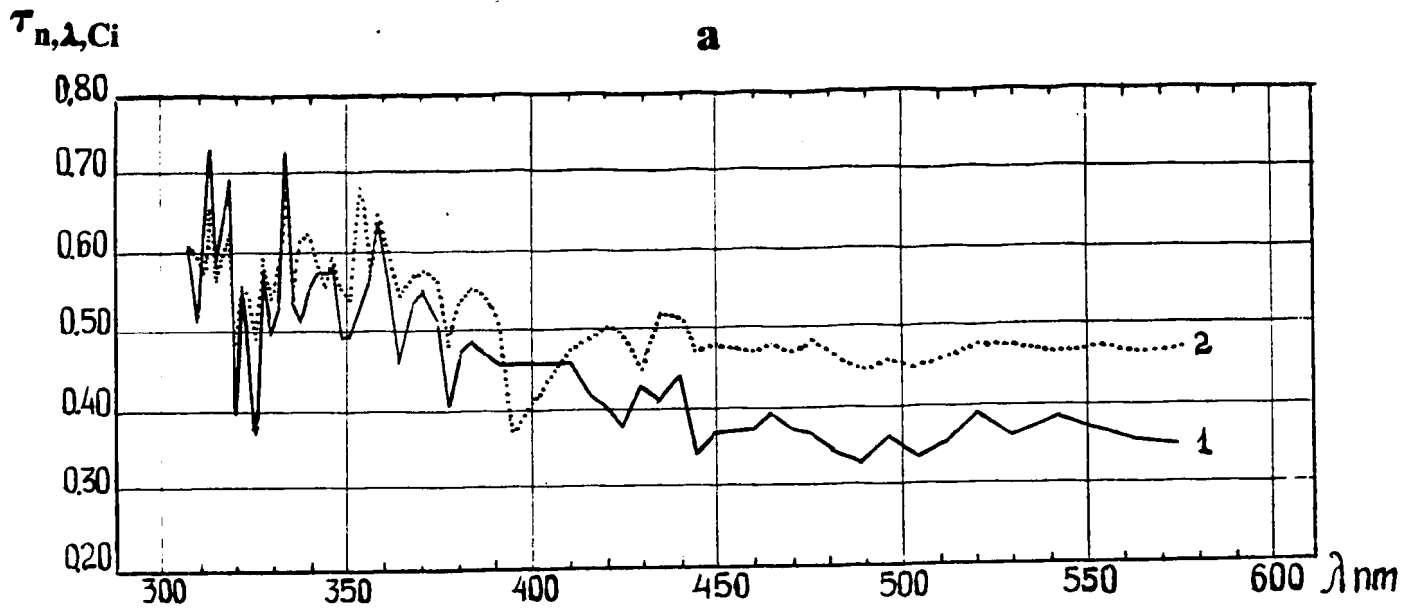

a) thin clouds Ci fib May 31
Curve 1: $\tau_{2.1}$=0.22; Curve 2: $\tau_{2.1}$=0.38;

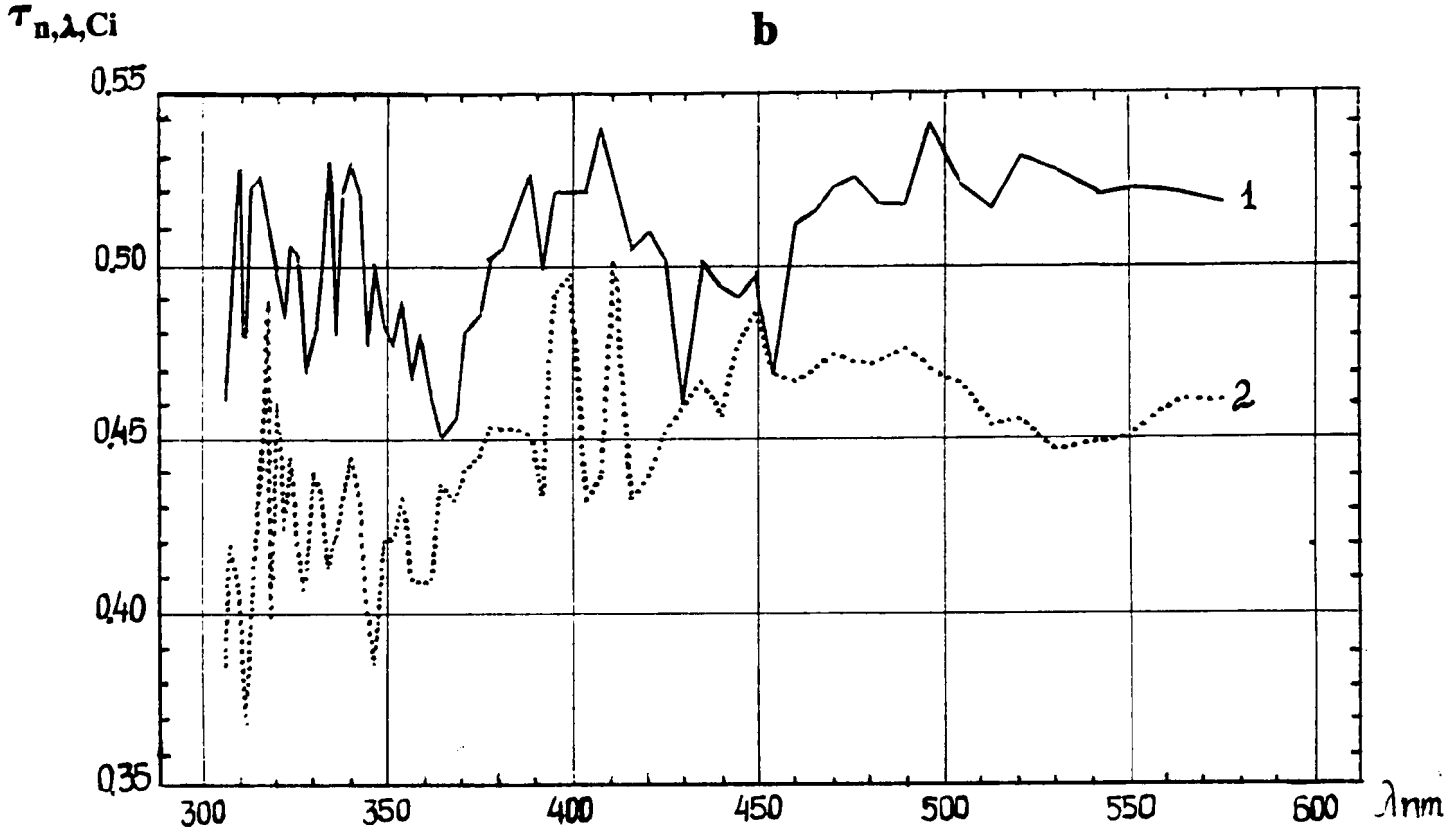

b) dense clouds June 2;
Curve 1: Ci fib, $\tau_{2.1}$=1.57; Curve 2: Ci sp, $\tau_{2.1}$=1.50

Figure 6.5 Normalized optical thickness of high level clouds of different densities obtained by spectrometer (in one angle of 10°) within UV and visible regions of the spectrum.

The variations in $\tau_{n,Ci}$ relate to the negative (for thin Ci) and positive (for dense Ci) values of K in Table 6.3. These variations may be understood by recognizing that the direct radiation in the fields of view of 5° or 10° is a sum of direct radiation proper and scattered radiation from the near-solar zone within the same field of view. Thus, the increase of P_λ with wavelength in Figure 6.1 under the influence of thin clouds becomes clear enough. In cases when ($0.5 < \tau_{2.1} < 0.9$) were observed no dependencies were noted. Various dependencies, obtained by J. Lerfard, 1981; G. Guschin, et al. 1980 may be explained by different optical thicknesses of Ci: by very thin ones as mentioned in G. Guschin, et al., 1980 and relatively dense clouds considered in J. Lerfard, 1981.

For thin cirrus clouds the scattered radiation contribution of the near-solar zone into the direct radiation flux leads to a large reduction of the derived optical thicknesses in the visible spectral region in comparison with the UV and, vice versa, for dense clouds where the derived optical thickness are reduced most of all in the region of short wavelengths.

6.2 Influence of cirrus clouds upon ultraviolet radiation fluxes, by Yu. V. Glushchenko

Fluxes of global - Q, diffuse - D and direct solar (FOV 2.3°) - S ultra-violet radiation falling on a horizontal surface were measured within the wavelength range of 0.315 to 0.400 μm at ZSS with the aid of UFimeter UF-IIAU. Data were recorded every 3.7 min. The absolute accuracy of the measurements was 15 per cent, with a precision of 3 per cent. Cirrus optical thickness - $\tau_{2.1}$ was estimated for each

Table 6.3

The optical thicknesses of the high level clouds, Zvenigorod, 1989.

Date	Moscow Time	Cloud Form	The optical λ = 0.552 μm	cloud thickness λ = 2.1 μm	angle of view	K
1	2	3	4	5	6	7
5/18	11 12	ci fib	0.26	0.43	5	-0.0021
	11 47	ci fib	0.23	0.47	5	-0.0029
	12 54	ci fib	0.00	0.15	5	-
5/19	11 00	cc tr	0.04	0.14	5	-0.0013
	11 10	cc tr	0.04	0.13	5	-0.00082
	11 40	cc tr	0.04	0.21	5	-
5/20	10 31	ci fib	0.00	0.07	5	-
	10 35	ci fib	0.00	0.09	10	-
5/31	10 07	ci fib	0.04	0.13	10	-0.0049
	10 10	ci fib	0.07	0.19	5	-0.0050
	10 33	ci fib	0.08	0.22	10	-0.0020
	10 37	ci fib	0.06	0.22	5	-0.0030
	10 56	ci fib	0.18	0.38	10	-0.0012
	10 58	ci fib	0.22	0.43	5	-0.0012
	13 32	ci fib	0.27	0.58	5	-0.0035
6/2	12 18	ci fib	0.77	1.31	5	0.00064
	12 21	ci fib	0.78	1.57	10	0.00041
	12 27	ci fib	0.97	1.78	5	0.00064
	12 35	ci fib	0.60	1.04	5	0.00037
	14 42	ci fib	0.32	0.76	5	0.00047
	14 57	ci sp	0.52	0.99	5	-
	15 01	ci sp	0.73	1.50	10	0.00042
	15 36	ci sp	0.70	1.38	5	-
	15 39	ci sp	0.73	1.38	5	-
6/7	11 11	cc tr	0.15	0.29	5	-

The comments:

Ci fib - Cirrus Fibratus
Cc tr - Cirrucumulus tractus
Ci sp. - Cirrus spissatus

observation period according to the procedure described in Abakumova, G. M., et al. 1989, pg. 162.

Illustrated in Figure 6.6 are the flux values of global and diffuse ultraviolet radiation recorded on 05/15/89 at ZSS, as functions of cirrus optical thickness, with h_o being fixed (air mass m = 1.25-1.30). When $\tau_{2.1}$ increases, D increases and Q decreases. Analogous results were obtained from the observations at ZSS under similar conditions on 04/14/87, 06/10/87. Analysis of data collected at ZSS in April-August 1987-89, shows that this tendency is preserved, at least, up to $\tau_{2.1} \leq 1.5$. In this analysis, for m = 1.30 and $\tau_{2.1}$ increasing from 0 to 0.8, Q decreases approximately 25 per cent. Variations in D and S are evidently of a non-linear nature and with the same changes of $\tau_{2.1}$ the value of D increases almost 1.5 times while S decreases by approximately a factor of three. Within the wavelength range of 0.315 to 0.400 μm in the presence of cloudiness the absorption of radiation is relatively small; therefore one may conclude that as $\tau_{2.1}$ increases, so does the albedo and this is why the decrease of Q is observed.

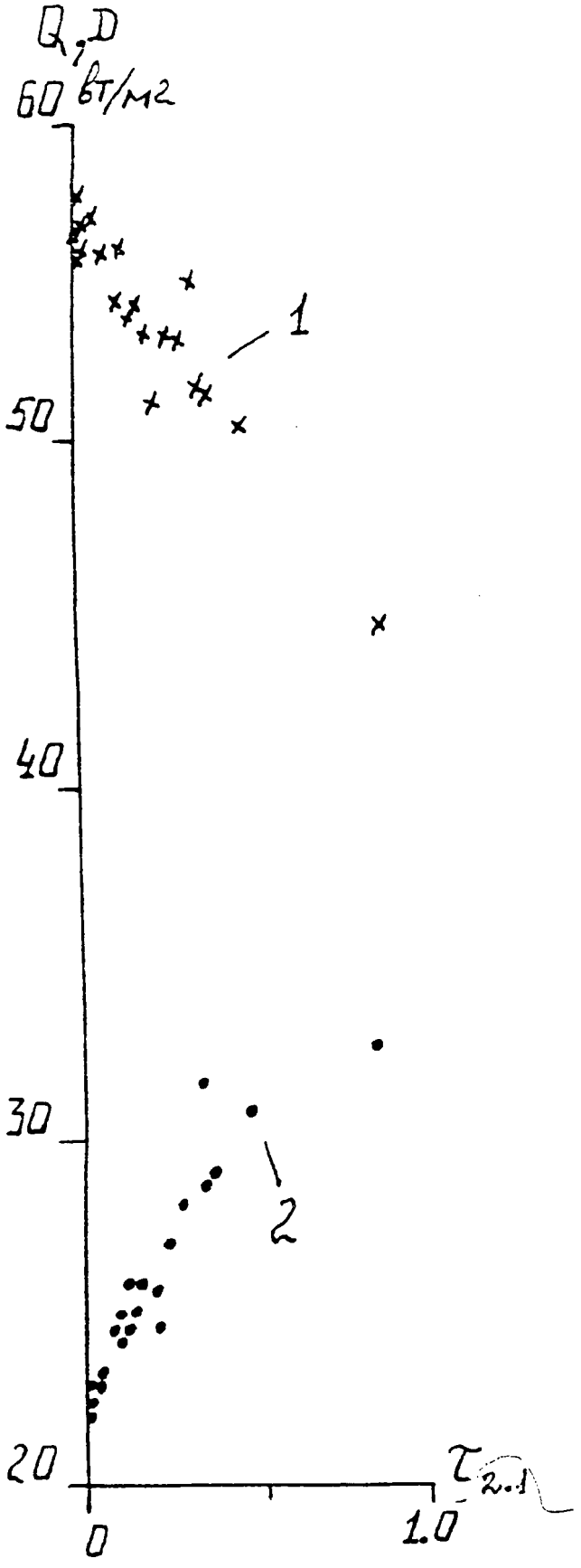

Figure 6.6 Variability of global Q (1) and diffuse D (2) ultraviolet radiation as a function of optical thickness of Ci clouds $\tau_{2.1}$ according to observations from ZSS (m = 1.3).

References

Abakumova, G. M., et al., 1989: The Geometrical, Optical and Radiative Properties of Cirrus Clouds. Colorado State University, Atmospheric Science Report No. 456, 61 pages.

Chapter 7

Aircraft Investigation of the Microstructure of Cirrus Clouds: Case Study of 15/05/89

by S. N. Burkovskaya, A. L. Kosarev, and A. Ya. Naumov

Abstract

Direct measurements of concentrations of different sizes of crystals, total water content and coefficient of visible light attenuation in a multi-layer Ci-Cs cloud, are reported. The cloud under investigation was formed in the vicinity of a jet stream within a region of upward motion. Measurements show that mean crystal concentrations vary as a function of height; concentration of crystal sizes over 50 μm (N_{50}) vary in the range 100-450 l^{-1} and N_{200} ($\ell > 200\ \mu$m) vary in the range 0.4-5 l^{-1}. Mean values of total water content were in the range 2 10^{-3} to 1.5 10^{-2} gm, while the coefficient of visible light attenuation was generally greater than 2.5 km^{-1}. The results presented may be used both for calculations of cloud optical characteristics and for comparison of analogous characteristics inferred from ground (remote) measurements.

7.1 Introduction

In May-June 1989, seven research flights of the instrumented II-18D aircraft of the Central Aerological Observatory (CAO) were performed in the area of Zvenigorod, Moscow Region. The flights were made from the airport of Sheremetievo from Ivanovskoe to Gagarin (Figure 7.1). Most interesting was the flight of 15 May 1989, when the aircraft could penetrate under, within and into the upper boundary of multi-layer Ci-Cs clouds. This paper presents an analysis of this case.

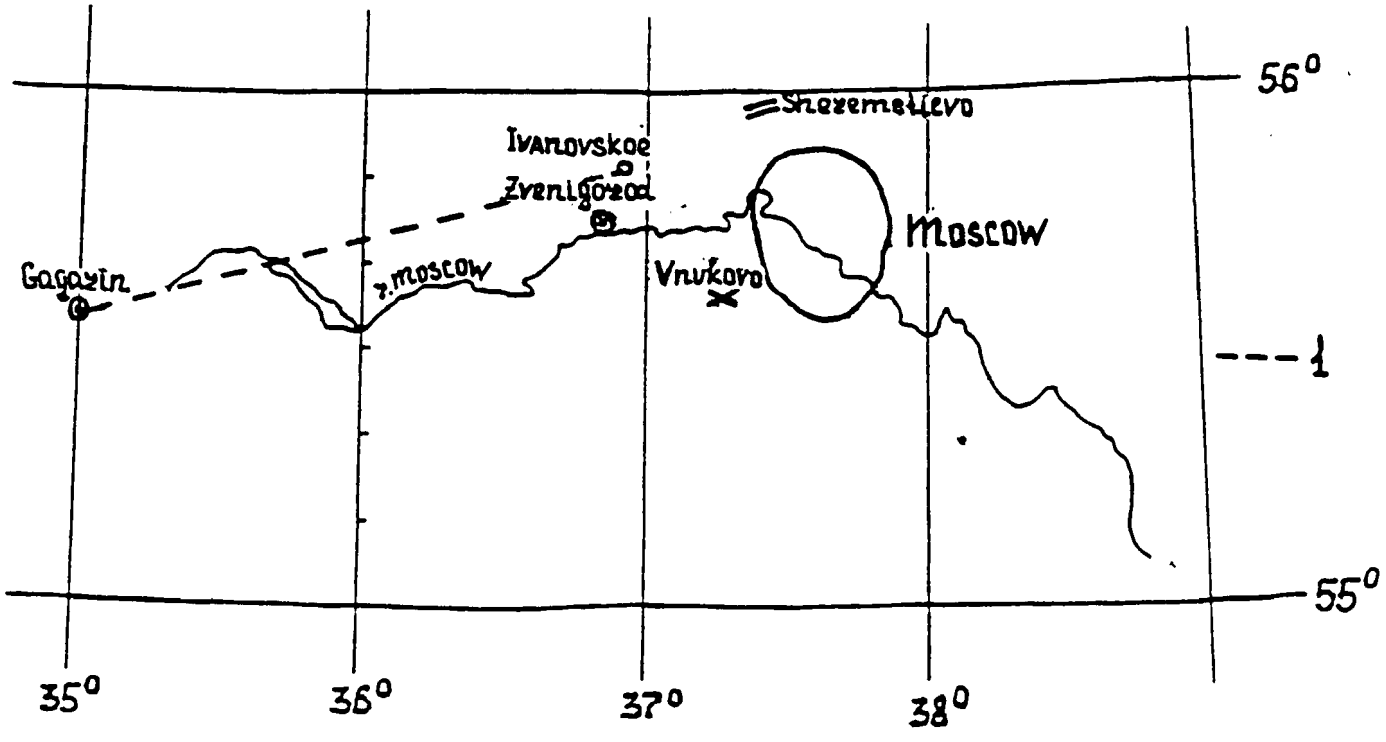

Figure 7.1 Area of flight. 1 - flight path

7.11 Aircraft equipment

The research aircraft was instrumented with standard navigation, thermodynamic, actinometric and radar equipment (Dmitriev and Strunin, 1985; Belyakov et al., 1984; Kostyanoy and Stanevskaya, Chapter 8). The aircraft mounted microphysical instrumentation included the following: cloud phase structure analyzer (CPSA), large particle size counter (LPSC), cloud total water (w) content meter (CTWCM), cloud transparency meter (CTM), Kosarev, et al., 1984, 1986. In addition, the aircraft was equipped with two spectrometers FSSP-100 and OAP-2D-C (Particle Measuring Systems, (PMS) (Heymsfield, 1976; Baumgardner, 1987). Table 7.1 presents the characteristics and operation principles.

7.12 Aircraft investigation

The microstructure of cirrus clouds was investigated using vertical and horizontal soundings of the atmosphere. The diagram of the flight in the area of Zvenigorod is shown in Figure 7.2.

7.2 Results of measurements and observations

7.21 Visual observations

The Ci-Cs cloud under investigation was inhomogeneous both vertically and horizontally (Figure 7.3). Separate layers inside it were identified as Ci fib, Ci sp and even Cc_{und}. The cloud base was at the height of 7,200 m, the top of the main layer - at the height of 9,500 m. Some very thin layers of Ci fib were found above the main layer.

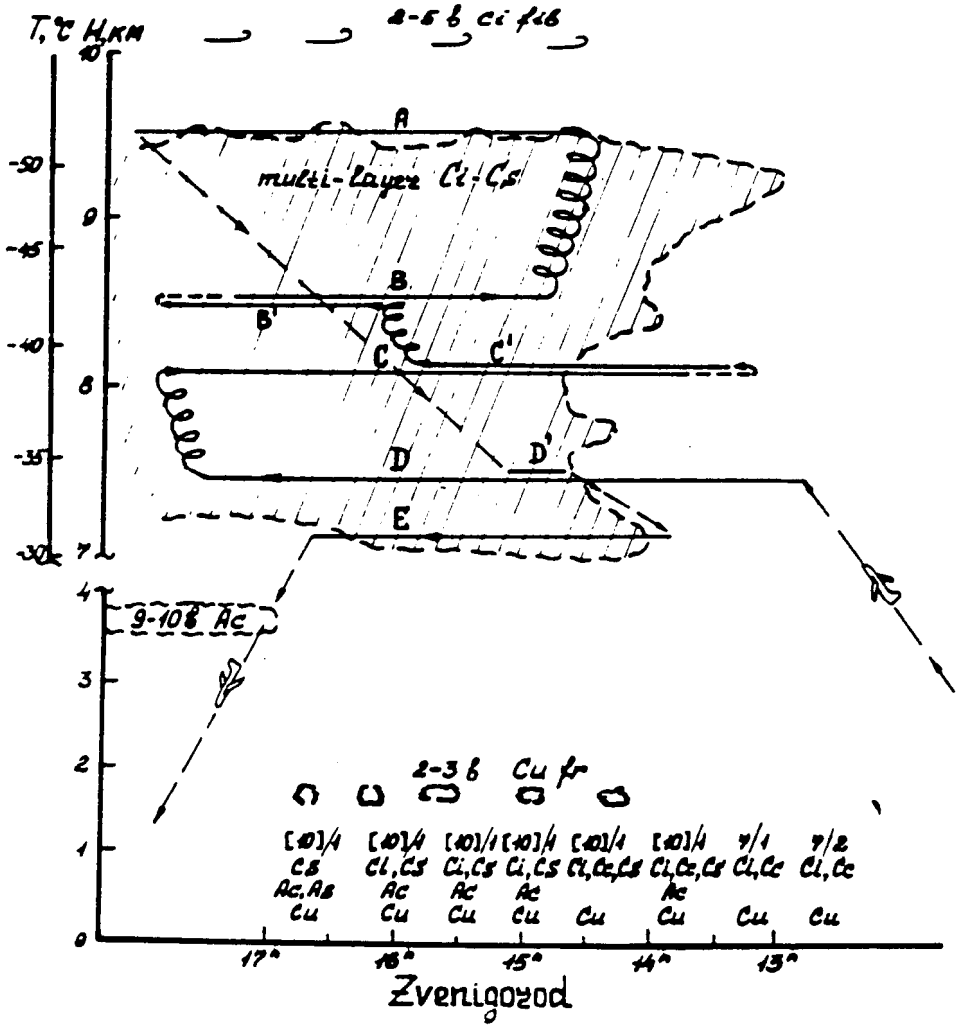

Figure 7.2 Cross-sections of Ci-Cs clouds investigated near Zvenigorod. Ground observations of cloudiness are presented in the lower part. Cloud profile is shown with account for its movement in latitude direction with the speed of 30 km/hr. Shown in Table 7.2 is time of working legs A-E.

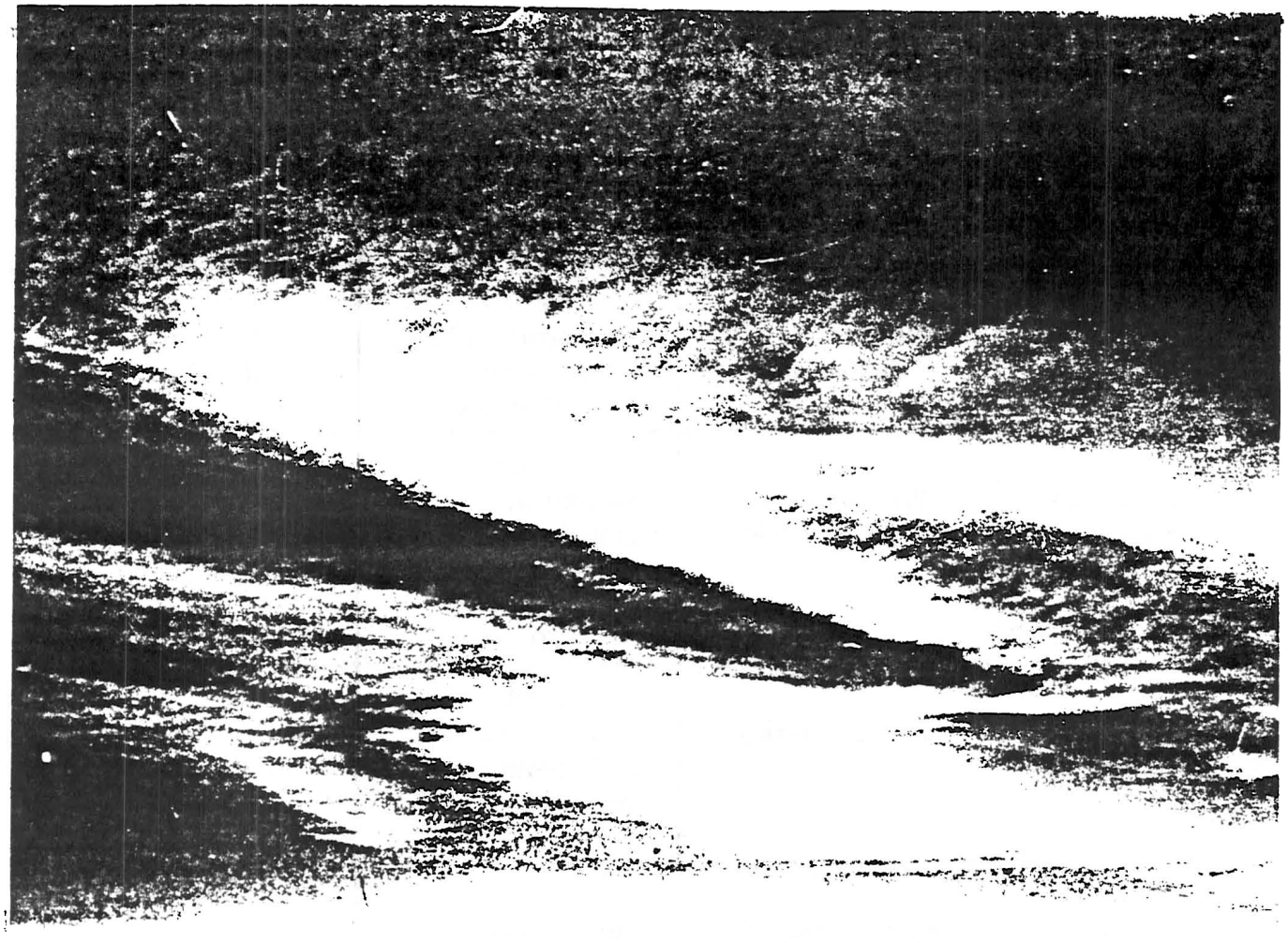

Figure 7.3 Photograph of clouds (by N.S.Ryabtsev, CAO). The photography height is 3,900 m. The surface is seen in the lower part of the photograph. The time of the photograph is 15 hr 02 min.

Table 7.1

Devices of Microphysical Complex

Device	Operation	Measured parameters	Measurement limits	Error
LPSC (large particle size counter)	Photoelectric shadow (analogous)	Particle concentration in 12 channels from 200 to 6000 μm	from 1 m^{-3} to 2 10^4 m^{-3}	30%
CPSA (cloud phase structure analyzer)	Photoelectric nephelometric	Particle concentration in 4 channels in the range of effective sizes from 20 to 120 μm*)	from 10^3 to $10^7 m^{-3}$	30%
FSSP-100 (forward scattering probe)	Laser Scattering	Particle concentration in 16 channels in the range 0.5-47 μm**)	from 0.1 cm^{-3} to 800 cm^{-3}	size-8% conc.-14%
OAP-2D-C (optical array probe)	Shadow (discrete)	Cloud particle shapes and sizes	size from ~100 μm to 1600 μm	
CTWCM (cloud total water content meter)	Electrocalorymetric	Total water content	from 3 10^{-3} to 2 10° gm^{-3}	(3 10^{-3} + 0.1w) gm
CTM (cloud transparency meter)	Transmissiometric	Visible light attenuation coefficient	from 2.5 km^{-1} to 250 km^{-1}	not over 20%

* Measurements were made with the CPSA only in two ranges (50-80 and 80-120μm) because of faults.

** In this experiment measurements were made in the range 2-32 μm

7.22 Particle concentration and size spectrum

Particle concentration and size spectrum were measured by four spectrometers with different principles of operation, working in different size ranges (see Table 7.1). All the devices are designated (conditioned by calibration) to measure droplet sizes (except OAP-2D-C), i.e., spherical particles. When crystals are present, problems of the measurement accuracy and data compatibility arise as well as ambiguities of interpretation arising from non-spherical particles. These problems are considered in detail by Kosarev, et al. (1986). To a first approximation, measurements made by CPSA and LPSC, may be represented as distributions of effective size **a**, where **a** is a mean sectional area of a crystal. Below we describe the data obtained with the CPSA and LPSC, but using the data from the FSSP-100[1] to estimate the concentration of particles less than 30-50 μm in diameter. Since there is a significant uncertainty in determining minimum particle size with the OAP-2D-C, Baumgardner, 1987, data from this device are used only to demonstrate crystal shapes.

First of all, let us note that measurements made by the FSSP-100, have shown an almost complete absence of particles of the sizes less than 10-12 μm, or alternately an absence of particles with the response equal to that of a corresponding spherical particle whose size is smaller 10-12 μm. Particles in the range 6-10 μm were registered only twice at the height of 9.5 km during several seconds of data. According to the records of the aircraft observer one of these cases

[1] The data of the FSSP-100 and OAP-2D-C are present by Yu. E. Makarow.

could be associated with crossing the contrail from the aircraft flying above. Optical measurements made with the ground spectrometer did not show small particles.

Shown in Figure 7.4 is the spatial course of accumulated concentrations N_{10} (FSSP-100), N_{50} (CPSA), N_{200} (LPSA) at different altitudes within the cloud; mean, values of the maximum and standard deviations[2] are presented in Table 7.2. For the FSSP-100, concentration N_{10} is the particle concentration for the range from 10 to 32 μm. It is seen from the figure, that this Ci-Cs cloud was horizontally inhomogeneous with most inhomogeneity being observed closer to the cloud edges. The values under consideration changed by more than one order of magnitude over a distance of ten to twenty kilometers (2-3 minutes of flying). Averaged crystal size spectra are shown in Figure 7.5. For the size range larger than 50 μm these spectra are plotted with the CPSA and LPSA data, while for the range 10 to 32 μm, the FSSP -100 data are displayed. Following Kosarev et al. (1986), the represented size spectra of particles n(a) may be described by the superposition of two distributions.

$$n(a) = \left(\frac{N_1}{\lambda_1^2}\right) a \exp\left(\frac{-a}{\lambda_1}\right) + \left(\frac{N_2}{\lambda_2}\right) \exp\left(\frac{-a}{\lambda_2}\right) \qquad (1)$$

The first term on the right hand side of (1) describes particle density in the range of a = 20-100 μm, and the second term represents the range of a > 200 μm. Table

[2]Figure 7.4 is plotted with 5-sec smoothing means; maximum values for Table 7.2 were also chosen from 5-s means. Calculations for mean values and root mean-square deviations, δ, were made throughout the whole data set.

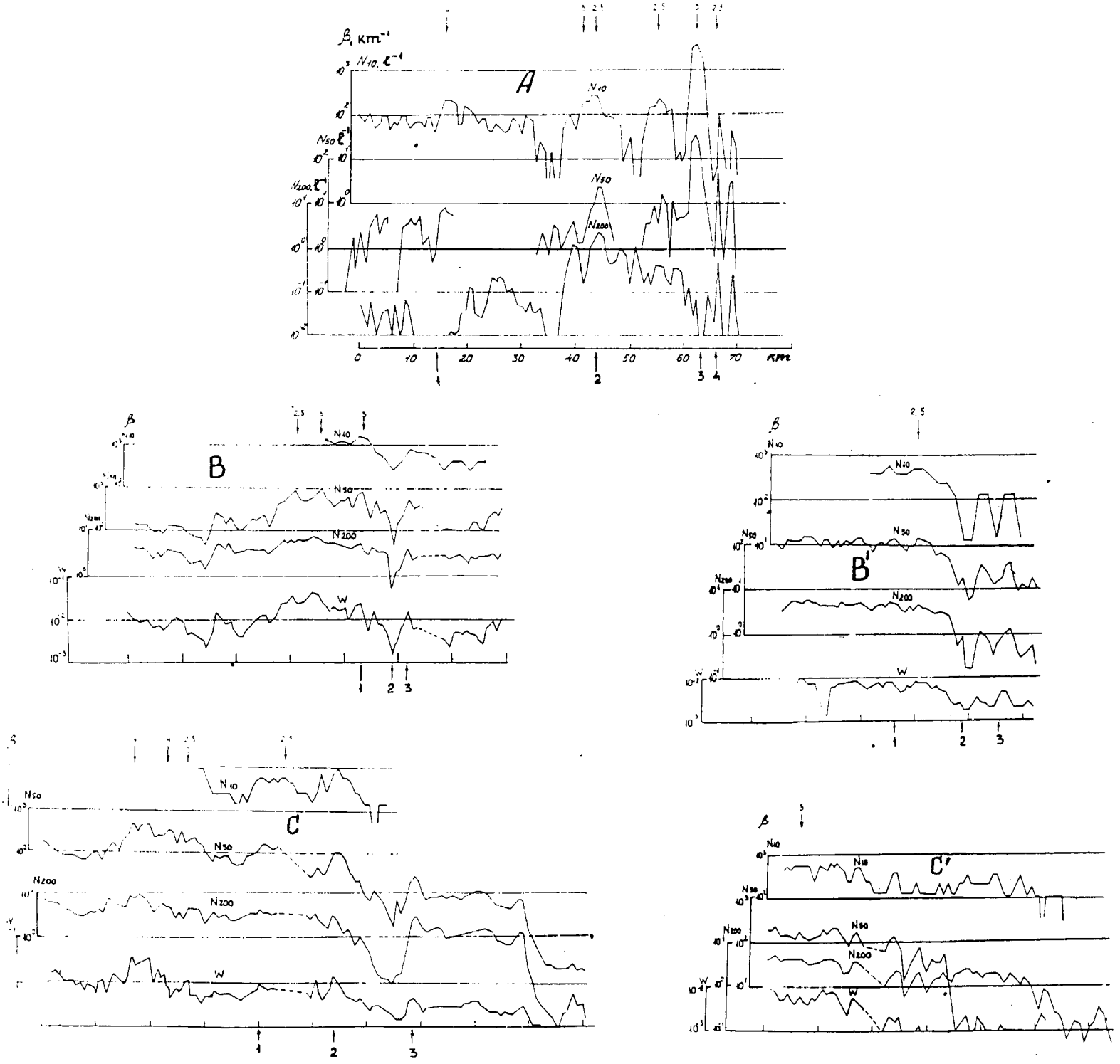

Figure 7.4 Spatial distribution of concentrations N_{10} (FSSP-100), N_{50} (CPSA), N_{200} (LPSC) and the w (CTWCM). Letters A-E correspond to legs A-E of Figure 7.2. Arrows in the upper part of each picture show the places, where the values of visible light attenuation coefficients $\beta > 2.5$ km^{-1}. Numbers and arrows in the lower part correspond to the numbers in Figure 7.7 (crystal shapes).

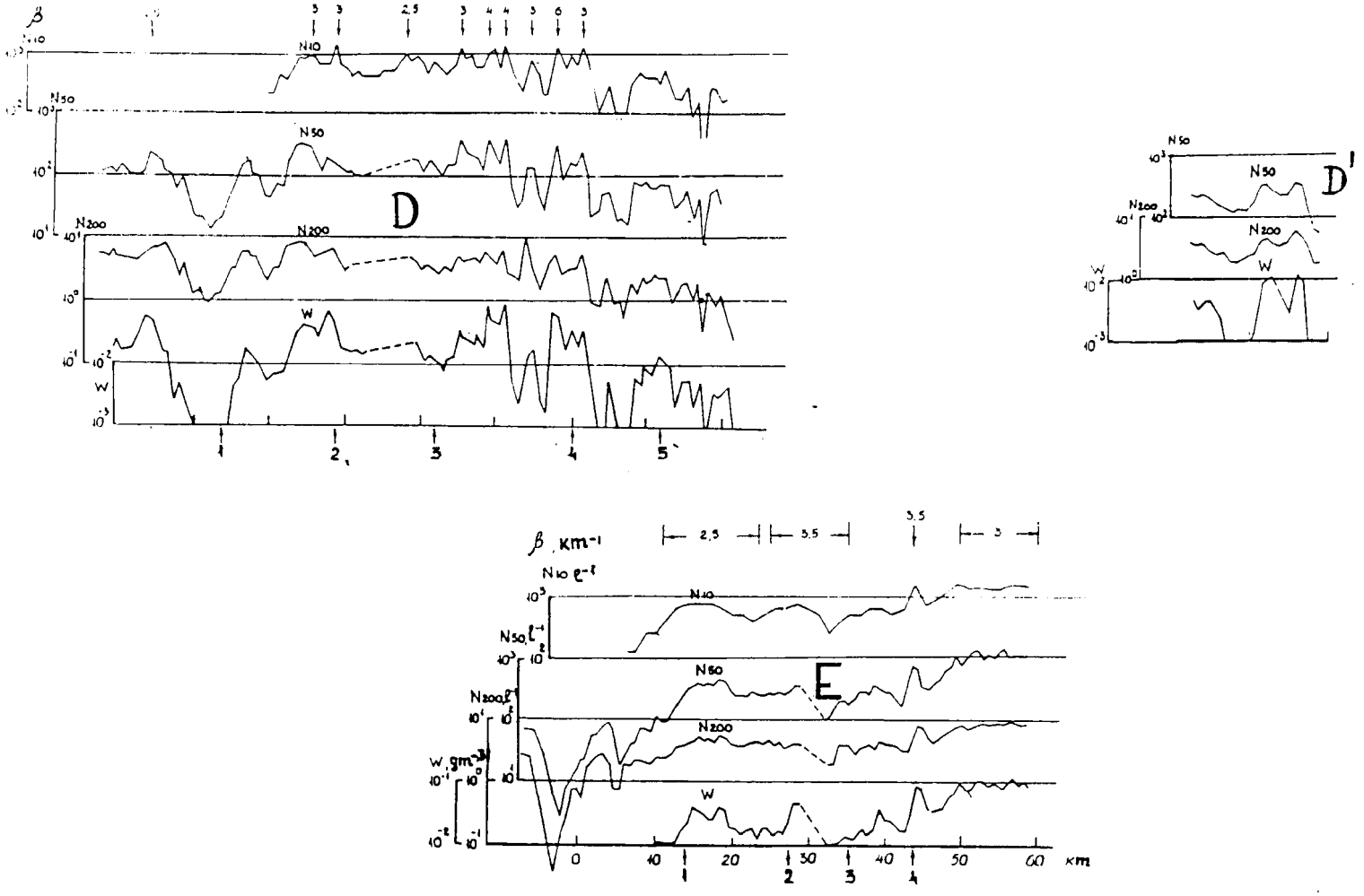

Figure 7.4 Spatial distribution of concentrations N_{10} (FSSP-100), N_{50} (CPSA), N_{200} (LPSC) and the w (CTWCM). Letters A-E correspond to legs A-E of Figure 7.2. Arrows in the upper part of each picture show the places, where the values of visible light attenuation coefficients $\beta > 2.5$ km^{-1}. Numbers and arrows in the lower part correspond to the numbers in Figure 7.7 (crystal shapes).

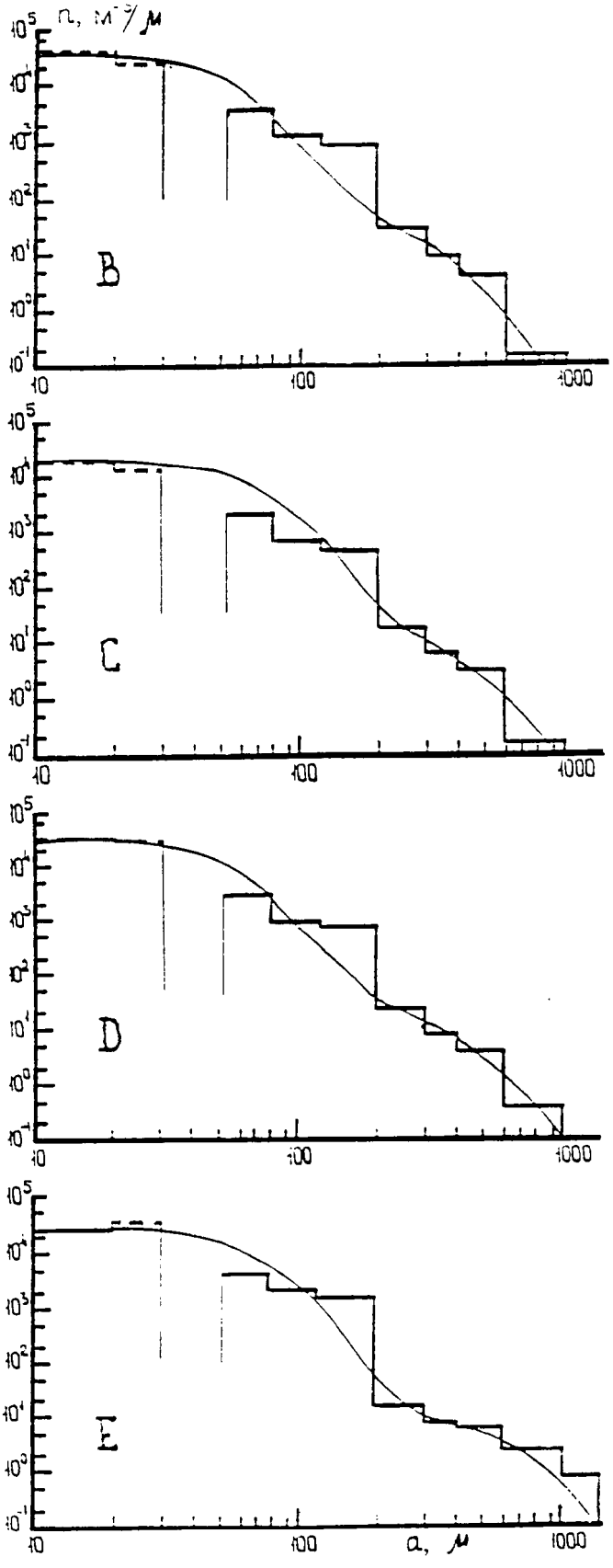

Figure 7.5 Averaged particle size spectra in cirrus cloud. Letters B-E correspond to legs B-E of Figure 7.2. Data from the FSSP-100 are marked with the dashed line.

values of $\beta > 2.5$ km^{-1} [3]; in most of the rest of the cases $\beta < 1$-1.5km^{-1}. Following Kosarev et al. (1986), in cirrus clouds $\beta < 2.5$ km^{-1} occurs approximately in 80% of the cases at temperatures below -30° C.

7.25 Dependence of microphysical parameters on height

Figure 7.6 is plotted from the data of Table 7.2, where the vertical profile of mean concentrations of N_{10}, N_{50}, N_{200} and LWC are shown. On the whole, an increase in values of the parameters from cloud top to cloud base, is seen.

7.26 Crystal shapes

The OAP-2D-C on board the aircraft presented projections of crystal shapes on a horizontal plane. Figure 7.7 shows representative crystal shapes observed when crossing a cloud at different levels. In the upper part of a cloud, single crystals of compact shapes occur more frequently; in the middle and lower parts of a cloud, crystal shapes become more diverse, sizes enlarge and occasionally aggregates may be observed.

7.27 Wind speed variability and radar reflectivity

Measurements of vertical and horizontal wind speed using instrumentation described by (Belyakov, 1984) have shown, that variations of more than 0.2 m/s were not registered during the whole flight in the cloud.

Radar reflectivity measurements at wavelength $\lambda = 3.2$ cm from the ground (Krylatskoe, Moscow) and from aircraft have failed to show echoes from the cirrus

---

[3] 2.5 km^{-1} is the lower measurement limit of β using the CTM, error being less than 20%. When β is less than 2.5 km^{-1}, error sharply increases, reaching the values of the order of 125%, when $\beta = 0.5$ km^{-1}.

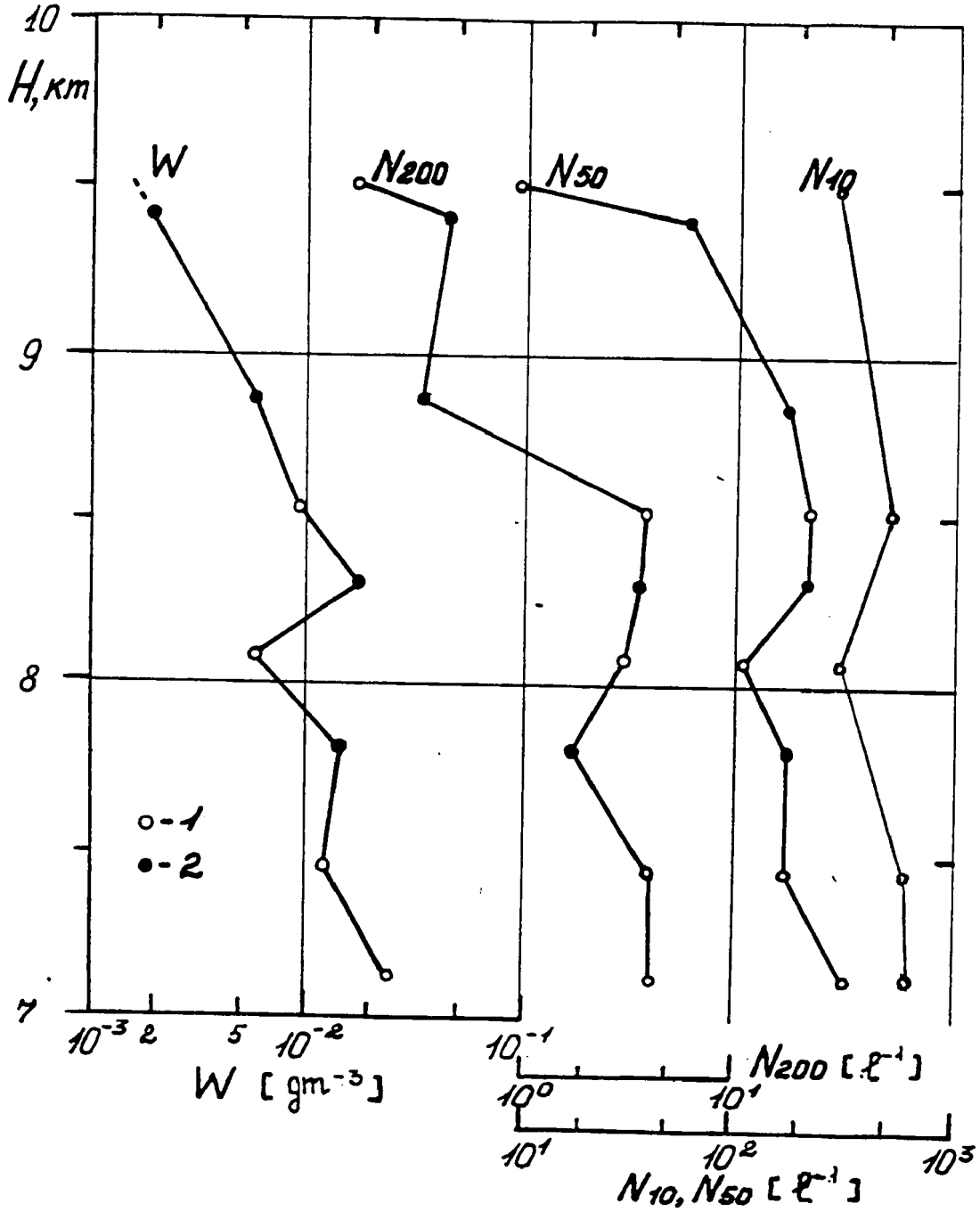

Figure 7.6 Vertical distribution of concentrations N_{10}, N_{50}, N_{200} and w.
1 - mean parameters for the horizontal leg,
2 - mean parameters from the climbing portion of the flight leg.

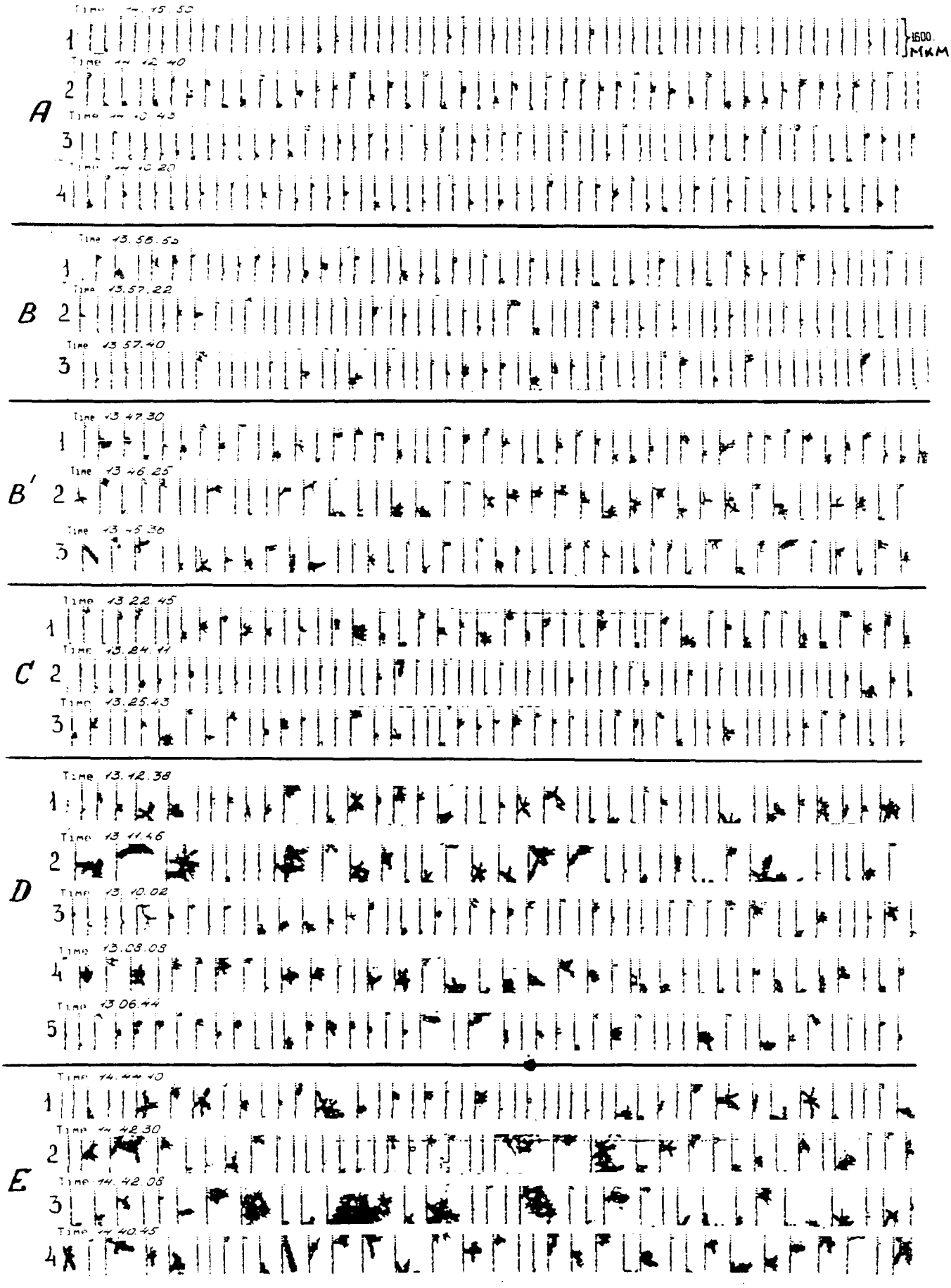

Figure 7.7. Crystal shapes of cirrus cloud.
Letters A-E correspond to legs A-E of Figure 7.2. Numbers on the left show discrete places in cloud (Figure 7.4), to which the given crystal shapes refer. The scale is shown in the upper right corner.

layer. The limit of the sensitive radar in Krylatskoe was -10 dbZ at the distance of 100 km, that of the airborne radar was -15 dbZ at 1 km. Note, that radar measurements of reflectivity in cirrus clouds in Colorado (USA) have shown that reflectivity was not larger than from -15 to -20 dbZ, Sassen et al., 1989.

7.3 On the feasibility of calculating integral characteristics of the cloud microstructure using particle size spectra

Integral characteristics of the microstructure, liquid water content and visible light attenuation coefficient may be simply calculated if the size spectrum for a droplet cloud is known. For the cases of a crystal or mixed phase cloud, such a calculation may be generally made if sufficient data on particle shape and density in the whole range of sizes are available.

Crystal size measured with the CPSA and LPSA allows one to calculate different optical characteristics. When we may assume that the size spectrum in the whole range of sizes is described by equation (1), the visible light attenuation coefficient β is simply described by the second moment of distribution (1) (Kosarev et al., 1986).

$$\beta = C_1 S \qquad (2)$$

$$S = N \pi \frac{\overline{a^2}}{4}; \qquad N \overline{a^2} = 6 N_1 \lambda_1^2 + 2 N_2 \lambda_2^2,$$

where S is a summed particle optical cross-section and C_1, is an attenuation efficiency factor, is approximately 2.

Using the data of Table 7.3, we obtain theoretical values of $\beta \approx 2\text{-}3\text{km}^{-1}$. Note, that relation (2) suggests the presence of particles in the whole range of sizes. In our case, particles of the sizes of less than 10 μm were not found, and hence β must be less than 2-3 km^{-1}.

We have not made attempts to calculate LWC in the same way as the third moment of distribution (1), because in the relation

$$w = c_2 \frac{1}{6} \pi N \overline{a^3} \qquad (3)$$

we do not know the factor C_2 which characterizes the mean volumetric density of crystals and is strongly dependent on the shapes of crystals. Note, that Kinne et al. (1990) made calculations of LWC with corrections for crystal shapes, but these corrections may be used only for sizes over 100-200 μm. At the same time, in many cases the main mass of cloud water is contained in the particles whose sizes are less than 100 μm. In our opinion at present, the most acceptable methods of determining integral characteristics of cloud microstructure are direct measurements with devices of the type of the CTM and CTWCM, not calculations of these characteristics using particle size spectra.

When evaluating characteristics of the microstructure of a multi-layer cirrus cloud, one should take into consideration that the characteristics shown in Table 7.2 were obtained using one aircraft at different levels in the cloud; these levels were chosen at random. It is very possible that separate cloud layers and cloudless spaces went undetected.

7.31 Comparison of the observed data with those of other authors

A comparison of the particle size spectra obtained in various experiments studying the microstructure of cirrus clouds is shown in Figure 7.8. Curve 1 characterizes a continuous cirrus cloud with 7-minute spiral descent from the height of 8 km to a cloud base at 6 km using a 2D-C probe, Kinne et al., 1990; curves 2 and 3 characterize data obtained in 1973-1975, each curve corresponding to ≈ 400 km of flight in a cloud using 1D and 2D devices, Heymsfield and Platt, 1984; curves 4-7 characterize cirrus clouds at different temperatures measured with a 2D probe Sassen et al., 1989. Curves 8_a, 8_b represents model particle size distributions, from Kosarev and Mazin, 1991. Curves I and II are plotted from measurements of particle concentration with the help of the FSSP-100, CPSA and LPSC[4].

One may see in Figure 7.8, that in the region of $a > 200$ μm, there is a good agreement of data obtained from the devices developed in the CAO and the PMS cloud probes; in the region of $a < 200$ μm the number density of particle size distribution from the CAO instruments is 1-2 orders of magnitude higher than from the PMS probe. Most probably, this discrepancy relates to particle underestimation with the 2D-C in the range 50-200 μm. Baumgardner (1987) considers the mechanism of particle underestimation and shows that the introduction of appropriate errors into the data from the 2D-C probe contributes to an increase of concentrations by an order of magnitude, on the average, with the maximal

[4]Curves 1-7 characterize the particle size distribution by maximal sizes, curves I, II, 8 - by effective ones.

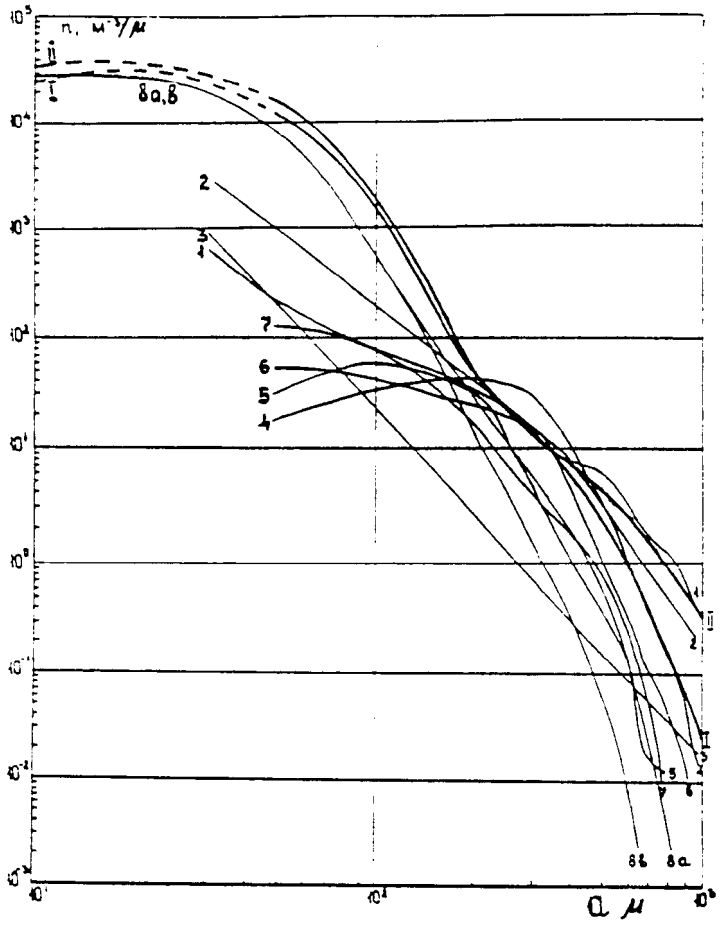

Figure 7.8 Particle size distributions in cirrus clouds based on the data of different authors.

TABLE TO FIGURE 7.8

Curve	Article	Date	Temperature, °C
1	Kinne, et al.	28.10.86	
2	Heymsfield and Platt	1973-1975	-30...-40
3	Heymsfield and Platt	1973-1975	-40...-50
4	Sassen, Starr, Uttal	17.10.83	-30...-40
5	Sassen, Starr, Uttal	17.10.83	-40...-50
6	Sassen, Starr, Uttal	08.03.85	-30...-40
7	Sassen, Starr, Uttal	08.03.85	-40...-50
8a	Kosarev and Mazin	1976-1984	-30...-40
8b	Kosarev and Mazin	1976-1984	-40...-50
I	This article	15.05.89	-40...-43
II	This article	15.05.89	-32...-35

discrepancy up to 1.5 orders of magnitude in the range 50-100 μm. A comparison of the data with the model of physical structure of cirrus clouds suggested by Kosarev and Mazin (1990) shows, that in our case the values of LWC and attenuation coefficient are somewhat lower than mean values and they are in the range of 50 - 75 percentile of accumulated frequencies of these values.

The parameters of distribution in Equation (1) (Table 7.3) for $a < 100$ μm, are, in general, close to the values given by the 75% percentile of the accumulated frequencies of the values of λ_1 and N_1 (Kosarev and Mazin, 1991). For values of $a > 100$ μm, particle concentration is 2-3 times higher than the mean values and the parameter of distribution N_2 is closer to the 90% percentile. For the parameter λ_2, which characterizes the spectrum slope, the observations showed a greater slope than suggested in the model.

7.4 Conclusion

The investigated multi-layer Ci-Cs cloud was formed within updrafts on the cyclone side of a jet stream. Particle concentration for particle size > 50 μm in cloud layers was 100-400 l^{-1} being larger than mean values presented in a model of the physical structure of cirrus clouds; this excess is 2-3 times larger in the range of $a > 200$ μm.

Particles < 10 μm were not found in the cloud. The shape of the particle size spectrum and parameters of distribution (eq. 1), in general, do not exceed the limits of values presented by Kosarev and Mazin (1991). Modal sizes of particles are in the range 15-20 μm.

Mean values of LWC were in the range from $2 \cdot 10^{-3}$ to $3 \cdot 10^{-2}$ gm^{-3}, on the whole, they were somewhat lower than the modal values. In most cases, the values of the visible light attenuation coefficient β are smaller than 2.5 km^{-1}.

REFERENCES

Baumgardner, D., 1987: Corrections for the response times of particle measuring probes. 6th Symposium Met. Observ. Inst., Amer. Met. Soc., New Orleans, 148-151.

Belyakov, I. E., Bezrukova, N. A., Burkovskaya, S. N., Postnov, A. A., Silaeva, V. I., Trutko, T. V. and Vostrenkov, V. M., 1984: Mesoscale structure of atmospheric fronts and associated cloud and precipitation systems over the European USSR. Proc. 9th Intern. Cloud Phys. Confer., 2, 339-342.

Dmitriev, V. K. and Strunin, M. A., 1985: The system of introducing mutual corrections for airborne meters for air flow velocities and temperatures (in Russian). Trudi CAO, issue 158, 104-112.

Heymsfield, A. J., 1976: Particle size distribution measurements: an evaluation of the Knollenberg optical array probes. J. Atmos. Technol., N8, 17-24.

Heymsfield, A. J. and Platt, C.T.R., 1984: A parameterization of the particle size spectrum of ice clouds in terms of the ambient temperature and the ice water content. J. Atmos. Sci., 41, 5, 846-855.

Kinne, S., Ackerman, T., Heymsfield, A. J. and Miller, K., 1990: Radiative transfer in cirrus clouds from airborne flux and microphysical measurements during FIRE-86. 7th Conf. on Atmos. Radiation, San Francisco, USA, 9-15.

Kosarev, A. L. and Mazin, I. P., 1991: An empirical model of the physical structure of upper layer clouds. Atmos. Research (in printing).

Kosarev, A. L., Mazin, I. P. and Nevzorov, A. N., 1988: The structure of cirrus clouds in middle latitudes - an empirical model: Proc. of the 10th Intern. Cloud Phys. Confer., Bad Homburg, 2, 482-484.

Kosarev, A. L., Mazin, I. P., Nevzorov, A. N. and Shugaev, V. F., 1986: The microstructure of cirrus clouds (in Russian). In: Handbook "Some problems of cloud physics", Leningrad, Hydrometeoizdat, 160-186.

Kosarev, A. L., Nevzorov, A. N. and Shugaev, V. F., 1984: On the microstructure and ice water content of high clouds. Proc. of the 9th Intern. Cloud Phys. Confer., Tallinn, 1, 73-76.

Sassen, K., Starr, D. and Uttal, T., 1989: Mesoscale and microscale structure of cirrus clouds: three case studies. J. of Atmos. Sci., 46, N 3, 371-396.

Chapter 8

Aircraft Measurements of the Radiative Characteristics of Cirrus Clouds

by G. N. Kostyanoy and Yu. F. Stanevskaya

Within the complex experiment on studying of cirrus clouds at ZSS in May 1989, measurements were made of integral upwelling ($Q\uparrow$) and downwelling ($Q\downarrow$) fluxes of shortwave radiation (SWR) using the IL-18 aircraft of Central Aerological Observatory.

Measurements of the fluxes were made using two Yanishevsky pyranometers (M-80) with the receiving surfaces directed upwards and downwards. The time and height of the flight were known and recorded, as well as headings of the aircraft, the approximate height of the sun $h_\odot$ and its location in relation to the flight path, state of the sun's disk and the amounts and forms of the cloudiness above and beneath the aircraft.

To obtain correct results, the measurements were made only during horizontal parts of the aircraft's flight with constant heading. The durations of the data legs were typically up to 15 minutes and they were performed at heights from 500 to 9600 m at 100-500 m increments.

The flights were made in the vicinity of Zvenigorod on May 12, 15, 16, 18 and 24, June 1 and 7, 1989. Cirrus clouds were not observed in all cases.

The upward and downward fluxes of shortwave radiation were measured, and the albedo of surface, together with the under-lying layer of clouds [Equation (2)], and clouds' transmittance - [Equation (3)]. The value of the albedo of clouds was strongly influenced by the flux coming through a cloud from below, therefore the albedo of the clouds was also

calculated taking transmittance into consideration [Equation (4)], where the flux of radiation coming from below was excluded.

$$As = \frac{Q\uparrow b}{Q\downarrow b} \tag{1}$$

$$Ac = \frac{Q\uparrow t}{Q\downarrow t} \tag{2}$$

$$P = \frac{Q\downarrow b}{Q\downarrow t} \tag{3}$$

$$A\ cloud = \frac{Q\uparrow t - Q\uparrow b * P}{Q\downarrow t} \tag{4}$$

There Q↑b, and Q↓b are the upward and downward fluxes at the base of the cloud respectively, Q↑t, Q↓t are upward and downward fluxes at cloud top.

The best case of Cirrus - Cs - was encountered on May 15, 1989. Cloud boundaries were located at 7 and 9.5 km. Horizontal flights were made under the layer of clouds at 6000 m and over the layer at 9600 m, as well as in the cloud at the heights of 7000, 7900, 8100, and 8600 m. The flights were performed around noon with solar elevation $h_\odot$ = 50° - 53°. Average values of the observed fluxes above and beneath the Cs layer are given in Table 8.1. The center of the cloud was less dense than at its edges, therefore the flux Q↓ was larger under the center of the cloud. A layer of Ac clouds appeared during the time of observation and passed between the flight legs below the Cs cloud and above it. The layer had a larger albedo and the flux Q↑ sharply increased.

Table 8.1

Average values of the downwelling and upwelling fluxes

(W/m^2)

	Under the cloud H = 6000 m		Above the cloud H = 9600 m	
	dense part	thin part	dense part	thin part
Q↓	909	935	948	
Q↑	138 - 179		664	328

Figure 8.1 shows that the field of radiation which passed through Cs and was reflected from Cs, is rather homogeneous and changes slightly in space and time, as compared with other types of clouds. A larger change of fluxes occurs at the beginning and at the end of the measurement path, where the Cs layer becomes more dense and some Ci clouds can be seen above it. The transmittance of radiation becomes smaller in these places, and the reflected component increases. A decrease of the transmitted radiation is also clearly seen down to 828 W/m^2 under the contrail condensation track.

From the measurements at 6000 m, the albedos of underlying surface and the layer of atmosphere above it were calculated. Values of A vary from 15 to 23% and decrease from the beginning of the measurement path (above a forest and a field with some Cu clouds nearby) to its end (above a forest). The average albedo of the Cs cloud only, calculated from [Equation (4)] was 24%; it ranged from 16 to 35%.

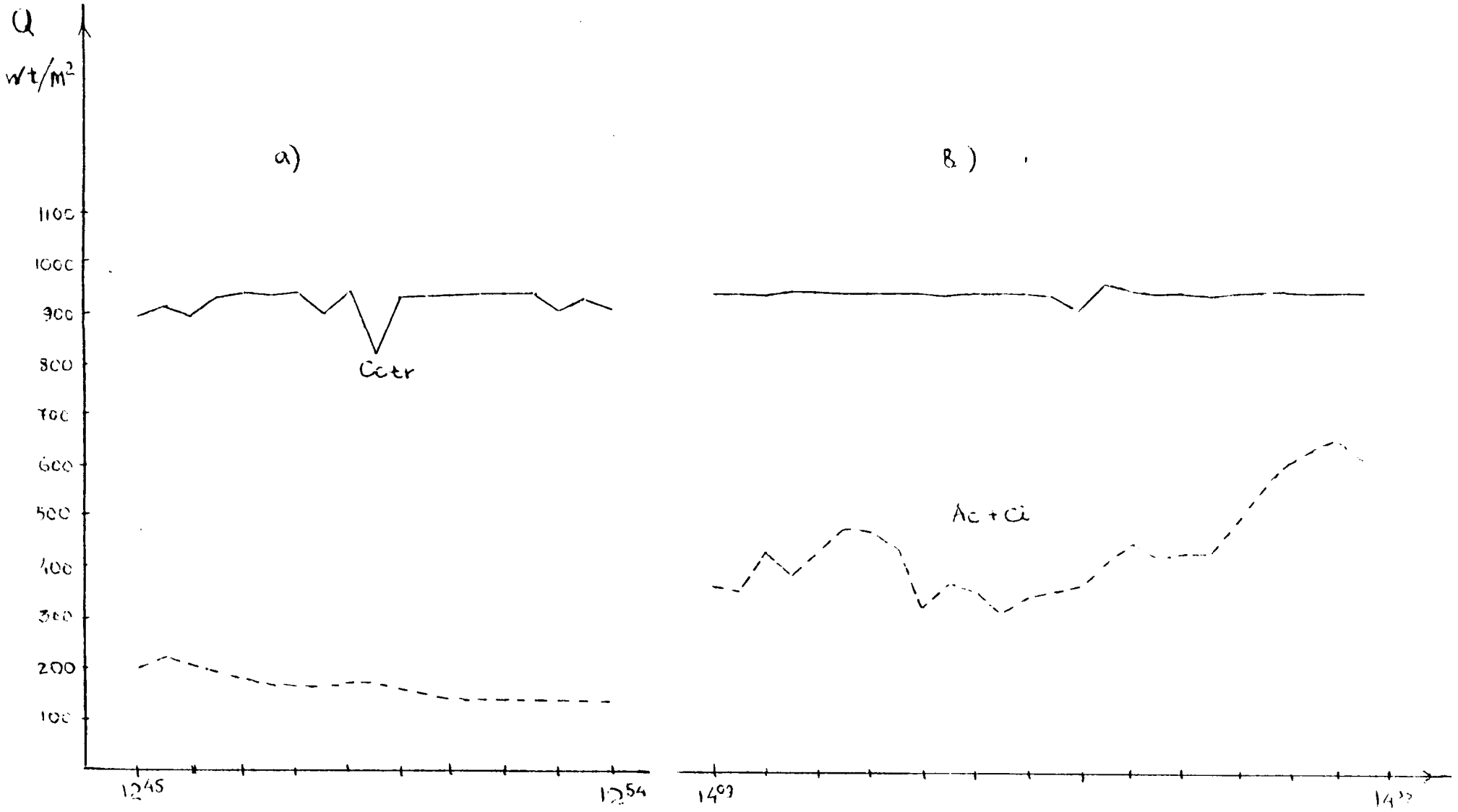

Figure 8.1 Upwelling (Q↑)-- and downwelling (Q↓)-- fluxes of SWR (Zvenigorod, 5/15/89)

a) Under the Cs cloud at 6000 m

b) Above the Cs cloud at 9600 m

Transmittances of the cloud as a whole and of its separate layers were also calculated. Before considering the calculated values of P, the transmittance, we have to point out some difficulties.

First, there is a time difference between lower and upper measurement paths. During this time interval, the cloudiness may change and, strictly speaking the upper and lower measurements do not correspond to one state of a cloud. Clear spaces may appear in the cloud layer and its thickness or the amount of cloudiness may also change. In addition, the zenith angle of the sun changes from one aircraft path to another. For example if the beginning of the flight is over the cloud, and then the solar zenith angle decreases when the aircraft begins the lower level flight leg, the observed flux under a thin cloud can be higher than that observed above the cloud. The transmittance will be overestimated and, sometimes, can even appear to be greater than 100%. Conversely if we begin with the lower level path, and then come to the upper one, while the solar zenith angle decreases, the P value will be underestimated.

Second, when we calculated the transmittance, each point over the layer must correspond to a point under the layer which is located directly under the first one. The transmittance is calculated as the ratio of downwards fluxes in these points - one under another. Since the two flight paths have opposite headings, the first point of the upper path corresponds to the last point of the lower one, etc. When the directions are the same, on the contrary, the ordering of points in the regimes coincide. It is obvious that this coincidence is rather conditional. For instance, when the upper point is located over the dense part of the cloud, and the corresponding lower point might be located under a clear

space, then, at the lower level the flux can even exceed the same one at the upper level and the transmittance will appear to be more than 100%. This case is frequently seen. The more homogeneous a cloud is, the more accurate the correspondence of points at various levels.

Third, the value of transmittance also can be significantly distorted when direct solar light is incident upon the pyranometer during the flight under a cloud. This can occur for large solar zenith angles, when the aircraft approaches the edges of a cloud, and when the device is not shaded by a cloud.

The aforementioned reasons make it difficult to calculate correctly the transmittance of the cloud as a whole and especially of its separate layers. The error arising from the change of the sun's elevation was small as the flights were performed around solar noon. When changes of the cloud themselves were also small, data were selected to give us the data of Table 8.2. It is seen that the transmittance of the layers 7900-9600 m and 7000-9600 m were significantly smaller than in other cases. Observations were collected for these two layers later than on the other ones and the cloud became thicker with time.

In Chapter 9 the dependence of the transmittance upon the optical thickness of a cloud and on the sun's elevation has been described. From the values of transmittance measured from the aircraft, the optical thicknesses of the clouds were calculated. The values vary from 0.1 to 2.5. Unfortunately, there were not simultaneous measurements of optical thickness on the surface, but we can notice that the values correspond to those obtained at Zvenigorod station during this day.

Table 8.2

The transmittance of Cs cloud as a whole and of its separate layers.

(%)

H bottom m. H top m	6000	7000	7500	7900
9600	93 - 99	72		73
8600			92	
7900			88	

In conclusion, we point out that there are currently very few data available from which to determine the albedo and the transmittance of cirrus clouds from direct aircraft measurements. It is necessary to make more flights, following very strict methods. In this case the data obtained should be compared with the surface measurements and calculation.

Chapter 9

Calculations of Solar Radiation and Comparison with Measurements

by T. A. Tarasova

9.1 Optical models

In order to calculate the integral fluxes of solar radiation in the atmosphere in the presence of cirrus clouds it is necessary to know the optical properties of these clouds: an optical thickness τ, an asymmetry factor of phase function $g = 0.5 \int_{-1}^{1} \gamma(\mu)\,\mu\,d\mu$ and a single scattering albedo $\omega_o = \sigma/\epsilon$ in the range of the wavelengths from 0.3 to 4 μm. Here $\gamma(\mu)$ is a phase function, σ is a scattering coefficient, μ = cos (scattering angle) and ϵ is an extinction coefficient. The parameter τ is derived in our experiments from the measurements of direct solar radiation.

It has not been possible to use in situ observed distributions of particles to determine the lengths (ℓ) for calculations of g, because this parameter depends strongly on the habit of particles (see Table 9.1). Table 9.1 also shows the variability of the results of the calculations of $g_{\lambda o}$ for hexagonal prisms, made by various authors. The value of g changes weakly in the range of the solar spectrum. An increase of g when $2.5 \leq \ell \leq 4$ μm due to the strong absorption of the ice substance does not significantly influence the integral fluxes of solar radiation and thus can be neglected in the calculations.

The parameter ω_o has a strong spectral dependence. There are three spectral intervals where the average values of ω_o differ significantly, Abakumova, G. M., et al., 1989, Chapter 4. The first interval is from the wavelength 0.3 μm to 1.2 μm where the

single scattering albedo is equal to one due to the small value of imaginary part of the index of refraction of ice (Warren, 1984). In the second interval from 1.2 μm to 2.5 μm there is a strong dependence of the value of $\omega_{o,2}$ on the effective particle size. The effective size is equal to the ratio of particle volume to the square of its geometrical cross section. In this spectral interval, the value of $\omega_{o,2}$ can change from 0.9 to 0.6 for the crystals in cirrus clouds. In the wavelength interval from 2.5 μm to 4 μm the value of $\omega_{o,3}$ is equal to 0.5 and is determined by the strong absorption by ice and by scattering by particles whose sizes are large compared with the wavelength. Therefore, to calculate the single scattering albedo with high accuracy for the total solar spectrum, we need detailed information about the particle habits and sizes. To date we have been unable to derive this information from in situ microphysical measurements.

Cirrus clouds may also contain aerosol particles, for instance Fe, absorbing in the visible spectrum, as is shown in Rosinski, et al., 1970. Therefore, the single scattering albedo $\omega_{o,1}$ will differ from 1.0. Models 4 and 5 (Table 9.2) correspond to this case.

Five models of the optical parameters $\omega_{o,1}$ and g for cirrus clouds are given in Table 9.2 and can be used for calculations of the integral fluxes of solar radiation in the wide spectral intervals. Comparison of calculated fluxes and those measured in the experiment allow one to choose the correct parameters.

Table 9.1

The asymmetry factor of the phase function $g_{\lambda o}$, calculated by various authors for particles with the length l μm and the diameter d μm, when the wavelength λ_o = 0.55 μm.

Shape	Size	$g_{\lambda o}$	Authors
Spheres	d >> λ	0.88	Hulst, 1957
Cylinders	1/d = 200/60	0.7	Liou, 1973
Irregular shape	1 = 5-200	0.73	Volkovitsky et al., 1984
Hexagonal	1/d = 300/60	0.99	Liou, 1986
Prisms	1/d = 20/20 1/d = 750/160 1/d = 200/50	0.77 0.86 0.74	Takano, Liou, 1989 Abakumova, G. M., et al., 1989

Γ-distribution in sizes with μ.

Table 9.2

Five models of the optical parameters $\omega_{o,l}$ and g of large spherical particles and non-spherical particles for three spectral intervals $\Delta\lambda$.

Model		$\Delta\lambda$, μm		
		0.3-1.2	1.2-2.5	2.5-4.0
1	$g_{spherical}$	0.9	0.9	0.9
	ω_o	1.0	0.9	0.5
2	$g_{non\text{-}spherical}$	0.7	0.7	0.7
	ω_o	1.0	0.9	0.5
3	$g_{non\text{-}spherical}$	0.7	0.7	0.7
	ω_o	1.0	0.6	0.5
4	$g_{non\text{-}spherical}$	0.7	0.7	0.7
	ω_o	0.95	0.9	0.5
5	$g_{non\text{-}spherical}$	0.7	0.7	0.7
	ω_o	0.9	0.6	0.5

9.2 Comparison of the model calculations with the ground-based measurements of the global solar radiation in the presence of cirrus clouds.

To separate the influences of clouds and the cloudless atmosphere on the radiation fluxes, the parameter C was used for comparison. This parameter is the ratio of the global solar flux at the surface in the presence of cirrus clouds (total amount is equal n=8-10), to the flux when the sky is clear.

Integral fluxes across the total solar spectrum were calculated (INTR) as were the fluxes in the wavelength range of the photosynthetically-active radiation (PAR) - from 0.38 μm to 0.71 μm, and in the range of near infra-red radiation (NIRR) - from 0.71 μm to 4 μm. The model of cloud-aerosol atmosphere used for the calculation and the method of calculation are described in Abakumova, G. M., et al., 1989 Chapter 4). The only distinction of the present method of calculation is more detailed spectral resolution- 23 intervals in the spectral range from 0.3 to 4 μm. In (Abakumova, G. M., et al., 1989, Chapter 4) it was shown that parameter C does not depend on the parameters of the cloudless atmosphere or on the albedo of the underlying surface.

The least square fits have been made using the results of calculations of C for the INTR, PAR and NIRR ranges of solar spectrum. The linear functions $C_Q = a + b\tau'$ were obtained, where a=const, b=const are parameters and $\tau' = \tau/\mu_o$ is the cloud effective optical thickness. The cosine of the solar zenith angle μ_o changed during the course of the measurements from 0.5 to 0.8. A linear dependence of C_Q

upon $1/\mu_o$ was obtained for $\tau \leq 1$. The value of the correlation coefficient between C_Q and τ' for various cases ranged from -0.997 to -0.994.

The parameters a and b are given in Table 9.3 for various models of the cloud optical characteristics g, $\omega_{1,o}$ and $\omega_{2,o}$. The parameter a is approximately equal to 1, because C_Q must be equal to 1 when $\tau' = 0$. The ratio of the linear regression coefficient b in the NIRR and PAR ranges of solar spectrum characterizes the absorption by ice in the NIRR range, i.e. $\omega_{2,o}$, for the cases with the same g and $\omega_{1,o}$.

Linear regression parameters, a and b, obtained for the six days of measurements of cirrus clouds in May 1986, 1987, 1989 at ZSS are also given in Table 9.3. Correlation coefficients of C_Q and τ' are range from 0.8 to 0.84.

In all cases the regression coefficients obtained using the experimental data are larger than the theoretically calculated ones. This is clearly seen Figure 9.1 from the slopes of the curves. Especially large differences were obtained using the model of large spherical particles in calculations ($g = 0.9$, $\omega_{1,o} = 1.0$, $\omega_{2,o} = 0.9$). We can use optical parameters $g < 0.7$, or $\omega_{2,o} < 0.9$ for calculations of the solar radiation fluxes to better fit the measurements. The decrease of g to the value 0.5, which is unrealistic for the large particles of cirrus clouds, provides only a small increase of the linear regression coefficient b. The decrease of $\omega_{2,o}$ to the value 0.6 also gives a small increase of coefficient b, but it greatly increases the ratio of the values of b in the NIRR and PAR ranges. This does not agree well with the average experimental data.

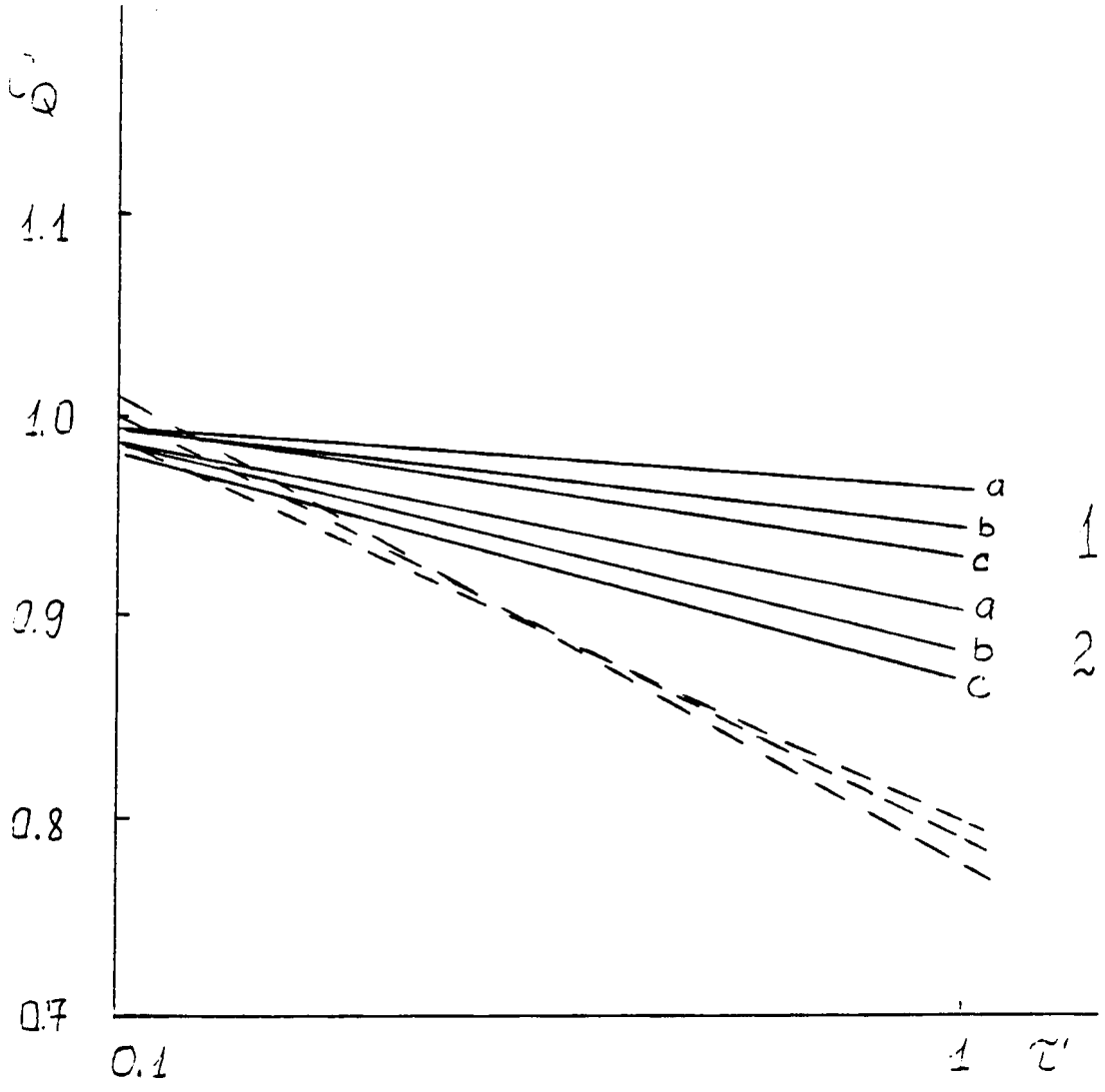

a - PAR

b - INTR

c - NIRR

Figure 9.1. Solid curves are the least square fits for parameter C_Q, which was calculated for three spectral intervals: a-PAR, b-INTR, c- NIRR and two models: No 1 and No 2 from the table 9.2. Dashed curves are least square fits of measured values of C_Q during May 1986, 87, 89.

An increase of absorption in the visible spectrum (models 4 and 5) creates better agreement of the slopes of the experimentally and theoretically based linear regression coefficients in the three spectral intervals. The points in Figure 9.2 show the direct measurements of the values of C_Q. Some measurements agree also with the model 2 results. The values $C_Q > 1$ when $\tau' < 0.3$ can be explained by the horizontal inhomogeneity of cirrus clouds optical thickness. This effect could not be simulated by our solar radiative flux calculations, which were carried out for a homogeneous cloud layer.

There may be other reasons for the disagreement between the experimental data and theoretical calculations. There are the errors of the existing methods of calculation and measurements and horizontal and vertical inhomogeneity of the cloud layers. A similar attempt to compare calculations and measurements of the downward solar fluxes was made by (Stackhouse and Stephens, 1990). They suggested a value of $g = 0.7$ in calculations of solar fluxes. This is smaller than the value $g = 0.88$ for the large spherical particles, which were used in their calculations.

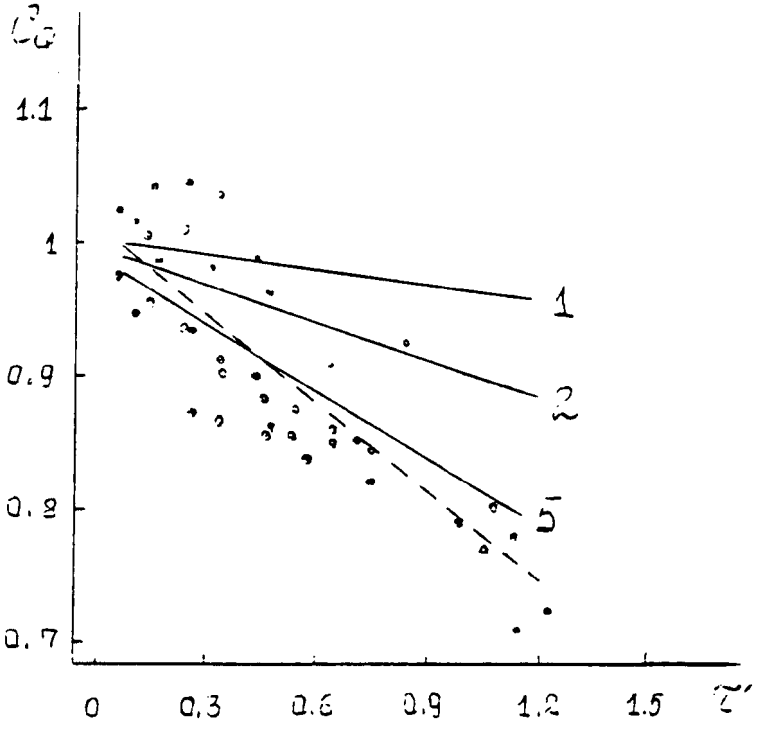

Figure 9.2a - PAR

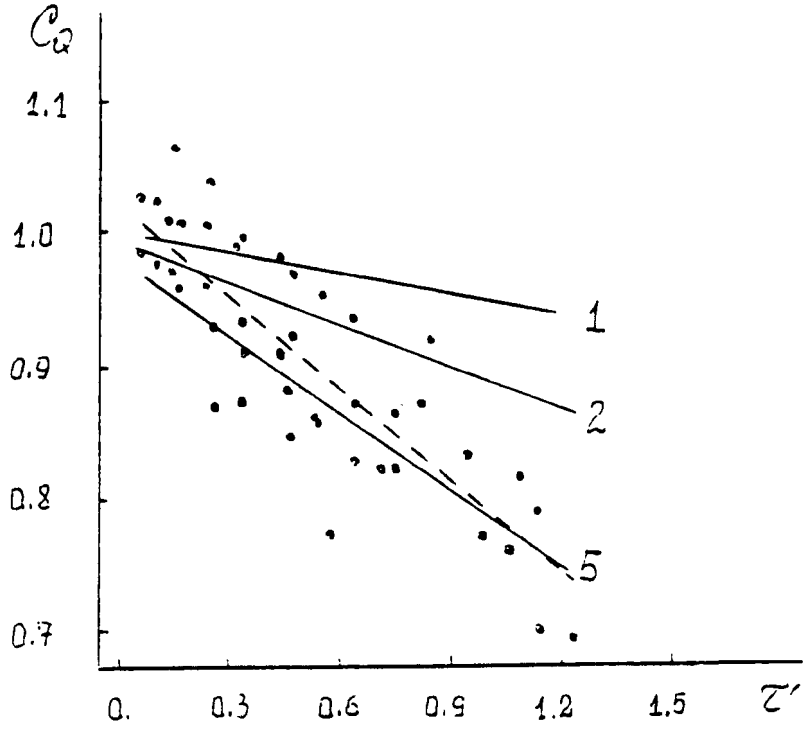

Figure 9.2b - INTR

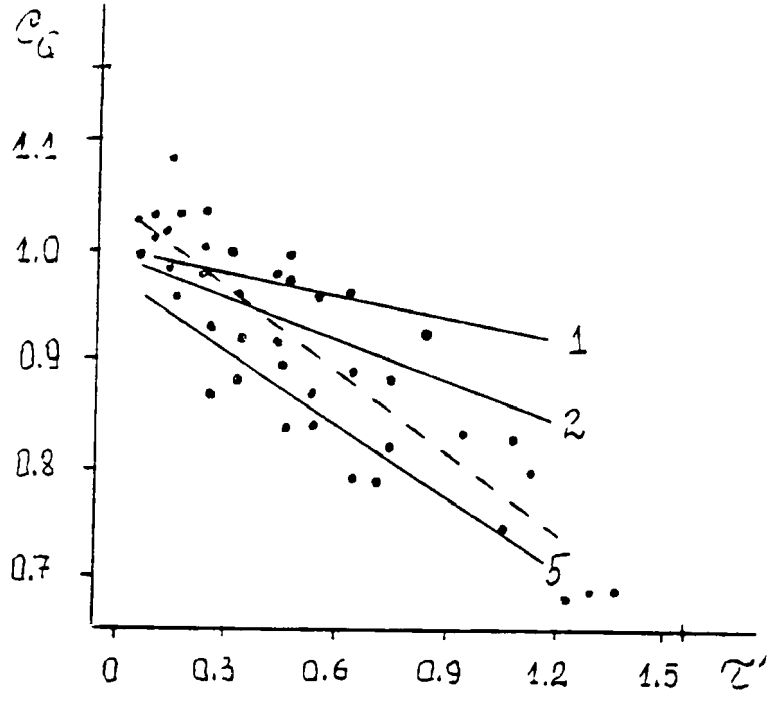

Figure 9.2c - NIRR

Figure 9.2. Solid curves are the least square fits for parameter C_Q, which was calculated for three spectral intervals: fig. 9.2a - PAR, fig. 9.2b -INTR, fig. 9.2c - NIRR and three models: No. 1, No. 2 and No. 5 from the table 9.2. Dashed curves are least square fits of measured values of C_Q during May 1986, 87, 89. The points are the direct measurements of C_Q and τ'.

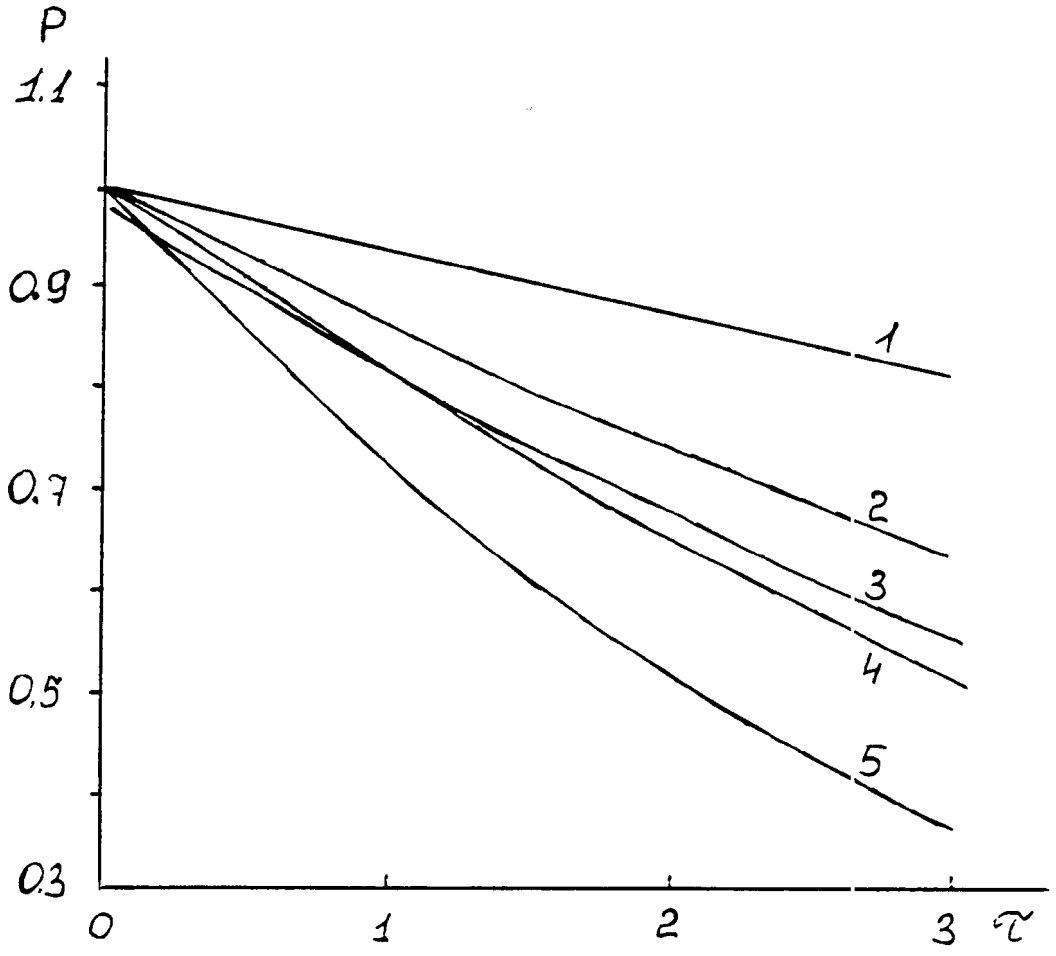

Figure 9.3. Dependence of the integral global solar transmission P through the cirrus cloud upon optical thickness, τ, when μ_0 = 0.8. Five optical models 1,2,3,4,5 were used in the calculations of P.

Table 9.3

The value of the parameters a and b of the linear regression $C = a + b\tau'$. "Calculation" parameters were obtained using the calculated values of C_Q and "Measurement" parameters were deduced from 1986-1989 observations.

g	ω	ω	a,b	INTR	PAR	NIRR	NIRR/PAR b
"Calculations"							
0.9	1.0	0.9	a b	1.00 -0.051	1.00 -0.036	0.99 -0.066	1.83
0.7	1.0	0.9	a b	0.994 -0.106	0.995 -0.091	0.993 -0.124	1.36
0.7	1.0	0.6	a b	0.989 -0.125	0.996 -0.191		1.77
0.7	0.95	0.9	a b	0.991 -0.142	0.993 -0.132	0.990 -0.154	1.17
0.7	0.9	0.6	a b	0.981 -0.194	0.989 -0.168	0.974 -0.222	1.32
"Measurement"			a b	1.023 -0.230	1.012 -0.213	1.036 -0.252	1.18

During two months of the experiment (May-June 1989) five one-half hour periods were observed when almost all the sky was covered by cirrus clouds, and there were no other cloud forms present.

During the whole experiment there were 14 such periods. The tables of the optical, meteorological and radiation parameters of the atmosphere for 1986 and 1987 data were given in Abakumova, G. M., et al., 1989, Chapter 4.

Table 4 presents the data collected in 1989. These data represent the following parameters, measured during the experiment: H is the height of the cloud base, ΔH is its

thickness, τ_{a,λ_o} is the aerosol optical thickness when λ_o = 0.55 μm, obtained from the measurements of the direct solar radiation in the PAR spectrum when the sun was unobscured by clouds; m_v (g/cm^2) is the water vapor content in the atmosphere, obtained from the aerological sounding; τ is the cloud optical thickness, obtained from the ground based measurements of the direct solar radiation; $Q^{meas.}$ is the downward flux of the integral global solar radiation, measured at the surface.

Table 4 gives the integral solar fluxes that were calculated using the optical and meteorological parameters obtained during the experiment. In these calculations we used the optical model No. 2 (g = 0.7, $\omega_{1,o}$ = 1.0, $\omega_{2,o}$ = 0.9). The linear regression C_Q on τ, obtained using this model, gives the best fit of the results to the 1989 measurements. Table 9.4 gives the calculated integral solar fluxes F, coming to the upward and downward hemispheres: on the surface (4), at cloud base (3) at cloud top (2) and at the top of the atmosphere (1). The radiative heating of the cloud layer by solar radiation $\delta T/\delta t$ was calculated for model 2 and for the rather peculiar model 5 which represents ice contaminated by aerosol.

9.3 Comparisons of calculated integral solar fluxes with aircraft observations.

The transmission P of the global integral solar radiation through the cirrus clouds is the ratio of the downward flux measured at the cloud base to that at cloud top. Values of P ranging from 0.98 to 0.7 were obtained using the pyranometer installed on board the aircraft on May 15, 1989. The sun's elevation corresponded to μ_o = 0.8.

Table 9.4

The data of the observations of cirrus clouds on May-June 1989 at ZSS and the results of calculations. The meanings of the symbols are in the text.

Date	15 May		18 May	31 May		7 June
Time Moscow	9-9:30	9:30-10	11-11:30	10-10:30	10:30-11	11-11:30
H,m	7000	6500	9000	8500	8400	10000
ΔH,m	1500	1500	1500	1700	1800	500
Cloud Amount	10	10	10	10	09	10
τ	0.25	0.47	0.47	0.15	0.27	0.15
$\tau_{a,\lambda o}$	0.1-0.2	0.1-0.2	0.1-0.2	0.3	0.3	0.2-0.3
μ_o	0.5	0.55	0.72	0.65	0.7	0.75
m_v,g/cm^2	1.0	1.0	1.7	1.7	1.7	2.5
Q^{meas},W/m^2	477	511	712	604	648	715
C_Q^{meas}	0.94	0.90	0.97	0.99	0.97	0.94
C_Q^{calc}	0.95	0.91	0.93	0.98	0.96	0.98
F↓ (1)	670	737	965	871	938	1005
(2)	659	727	956	861	929	996
W/m^2 (3)	606	637	876	833	881	970
(4)	486	520	720	653	700	775
F↑ (1)	189	220	248	214	234	227
(2)	179	210	240	205	226	219
W/m^2 (3)	136	140	180	183	190	200
(4)	97	104	144	131	140	155
∂T/∂t,K/Day model No. 2	1.1	2.0	3.3	0.74	1.3	2.9
∂T/∂t,K/Day model No. 5	6.7	12.1	20.1	4.7	7.8	18.3

Unfortunately, ground-based measurements of cirrus cloud optical thicknesses were not made under the aircraft.

In order to evaluate the observed optical thicknesses of cirrus clouds, the observed transmission values were compared with the detailed calculations carried out with the optical property models given in Table 9.2. A least square fit relating the transmittance, P, to τ' yielded the linear regression $\ln P = c + d\tau'$, when $\tau' = \tau/\mu_o$. Parameters c and d and the correlation coefficient r are given in Table 9.5.

Table 9.5

Parameters c and d of the linear regression lnP on $\tau' = \tau/\mu_o$ when μ_o = 0.5-0.8 for the five models of the cirrus cloud optical parameters.

Model No.	g	$\omega_{o,1}$	$\omega_{o,2}$	c	d	r
1	0.9	1.0	0.9	0.00243	-0.0617	-0.986
2	0.7	1.0	0.9	0.00802	-0.117	-0.993
3	0.7	1.0	0.6	-0.0329	-0.142	-0.989
4	0.7	0.95	0.9	-0.00634	-0.165	-0.997
5	0.7	0.9	0.6	-0.0255	-0.246	-0.994

If one considers all of the optical models No 1-5 as plausible alternatives for the calculations of the global radiation, it becomes very difficult to find τ using the observations of P. The problem becomes more tractable when we exclude from our calculations model No 1 for large spherical particles. Optical thicknesses, obtained from the linear regression using the values of P with given μ_o, are presented in Table 9.5. The minimum values of τ correspond to model No 5 of ice contaminated by aerosol, which

absorbs solar radiation in the visible spectrum. The maximum τ values correspond to model 2 of hexagonal prisms ($g = 0.7$, $\omega_{o,1} = 1.0$, $\omega_{o,2} = 0.9$).

Ground based measurements of τ were made on May 15, 1989, at ZSS and changed during the day from 0.1 to 2.5. These values are in general agreement with our theoretical calculations.

Table 9.6

The global radiation transmittance P and the cirrus cloud optical thickness τ for various optical models (2-5) when $\mu_o = 0.8$.

P	0.98	0.9	0.8	0.7
$\Delta\tau$	0.07-0.12	0.32-0.68	0.66-1.46	1.05-2.34

In summary, the ground-based and aircraft measurements of solar fluxes allow us to obtain the information about optical parameters of cirrus clouds, but the uncertainties in the values of these parameters are rather significant. The calculations of solar fluxes using model No. 1, which is characteristic of large spherical particles, do not agree with the experimental results. The heating of the cloud layer by solar radiation, calculated using the model 5, (aerosol contaminated ice) is six times larger than for model 2 (pure ice).

REFERENCES

Abakumova, G. M., et al., 1989: The geometrical, optical and radiative properties of cirrus clouds. Colorado State University, Atmospheric Science Report No. 456, 61 pp.

Liou, K. N., 1973: Transfer of solar irradiance through cirrus cloud layers. *J. Geophys. Res.*, 78, 1409-1418.

Liou, K. N., 1986: Influence of cirrus clouds on weather and climate processes: a global perspective. *Mon. Wea. Rev.*, 114, 1167-1199.

Rosinski, J., C. T. Nagamoto, G. Langer, 1970: Cirrus clouds as collectors of aerosol particles. *J. Geophys. Res.*, 75, 2961-2973.

Stackhouse, P. W., Jr., G. L. Stephens, 1990: A theoretical and observational study of the radiative properties of cirrus: results from FIRE 1986. Submitted to *J. Atmos. Sci.*.

Takano, Y., K.N. Liou, 1989: Solar radiative transfer in cirrus clouds. Part 1: single-scattering and optical properties of hexagonal ice crystals. *J. Atmos. Sci.*, 46, 3-19.

Van de Hulst, 1957: Light scattering by small particles. Willey, New York, 536 pp.

Volkovitsky, O. A., L. N. Pavlova, A. G. Petrusshin, 1984: Optical properties of crystalline clouds. Leningrad, Gidrometeoizdat Publishing House, 198 pp. (in Russian).

Warren, S. G., 1984: Optical constants of ice from ultraviolet to the microwave. *Appl. Optics*, 23, 8.

Chapter 10

The Use of Multi-channel Satellite Observations for the Identification of Cirrus Clouds

by E. A. Sterlyadkina, V. M. Sutovsky, and V. I. Yurov

This work develops multi-threshold methods for detecting ice crystal clouds above land and lower level cloudiness using multi spectral channel data of the AVHRR Satellite NOAA-11 radiometer. The work presents the method of analysis and compares results with the results of other investigations.

10.1 The Experiment and Initial Data

Satellite images were obtained during the Zvenigorod experiment in 5 channels of the AVHRR Satellite NOAA-11 (0.5-0.7; 0.9-1.1; 3.55-3.93; 10.5-11.5 and 11.5-12.5 μm) for 4 days: May 19 and 25, June 2 and 7, 1989. The satellite flew above the area under investigation at 2 p.m. - 3 p.m. (Moscow time). The initial satellite information was roughly processed, i.e. calibration was made, as well as space-locating, and distinguishing a part of the image (800 x 800 km^2 with its center at latitude 56° north and longitude 37.5° east). To make the comparison easier, the image was transformed into a longitude-latitude projection. A specialized combination of hardware and software for image processing (PERICOLOR-2000) was used for space locating and the analysis of the images.

10.2 Methods of Processing

To classify various types of underlying surfaces and clouds and, finally to identify and determine parameters of cirrus clouds, methods were developed to analyze the multi-channel images. For this purpose in each channel, histograms of received signals were constructed and analyzed. The following types of scenes were singled out for investigation: land, water, water clouds (solid and semitransparent cloudiness), cirrus clouds.

The most difficult task was the identification of semitransparent, thin ice crystal clouds. Such clouds can be detected through the analysis of ice cloud images in all the channels by using characteristic differences from both underlying surface and water drop clouds.

When ice crystal clouds are located above solid water clouds, the 3.7 μm channel (the albedo part) is most useful to detect cirrus clouds. It is known that within this range a signal from clouds contains both the reflected component and the component from its own heat radiation. Probhakara, et al., 1988 suggested these contributions be separated in accordance with the logic described below. Because of the low temperatures of cirrus clouds, the emitted radiation in the 3.7μm and 12 μm channels are close to each other, and in 12 μm channel the reflected signal is absent; therefore, it is straight forward to calculate the emitted radiation in the 3.7 μm channel. When we exclude the emitted contribution of the radiation from the whole signal received in this channel, we can then determine the clouds' reflectance. Proceeding from the fact that the reflectance of ice crystals is

significantly greater, we can divide crystal and water cloudiness. The absorption coefficient of the crystalline phase in this part of the spectrum is significantly higher than that of the liquid phase. Therefore, crystal clouds will look 'dark' on a background of bright water clouds.

10.3 The Results

As an example of the methods developed, let us consider the synoptic situation of June 7, 1989. Figure 10.1 shows the images made in channels 1, 2 and 5, as well as the result of dividing into classes (clusterization). We have chosen this case because of presence of cirrus clouds both above the Zvenigorod station, where surface measurements were made, and above other locations within 800 x 800 km area. Let us note that besides cirrus, there were clouds of the following types: cumuli-pluvial, (Cs) and cumuli, (Cu).

Histograms were constructed of reflectance and brightness temperatures (Figure 10.2). Channel 1 (λ = 0.63 μm) was used to separate clouds from clear scenes. On the histogram of channel 1 the clear scenes have narrow dispersion distributions, clustered around small values of reflectance. Any dense cloudiness has higher reflection coefficients and, on the histogram falls off to lower values to join the narrow maximum associated with the cloud free scenes, (Figure 10.2). It is difficult to find a reliable criterion which differentiates between the clear and cloudy scenes. This is because of the large variability of the scenes' parameters and the possibility of partially filled pixels. The experimental experience shows that a good criterion, A^1_{kp}, for such separation is the location of the first clearly seen local

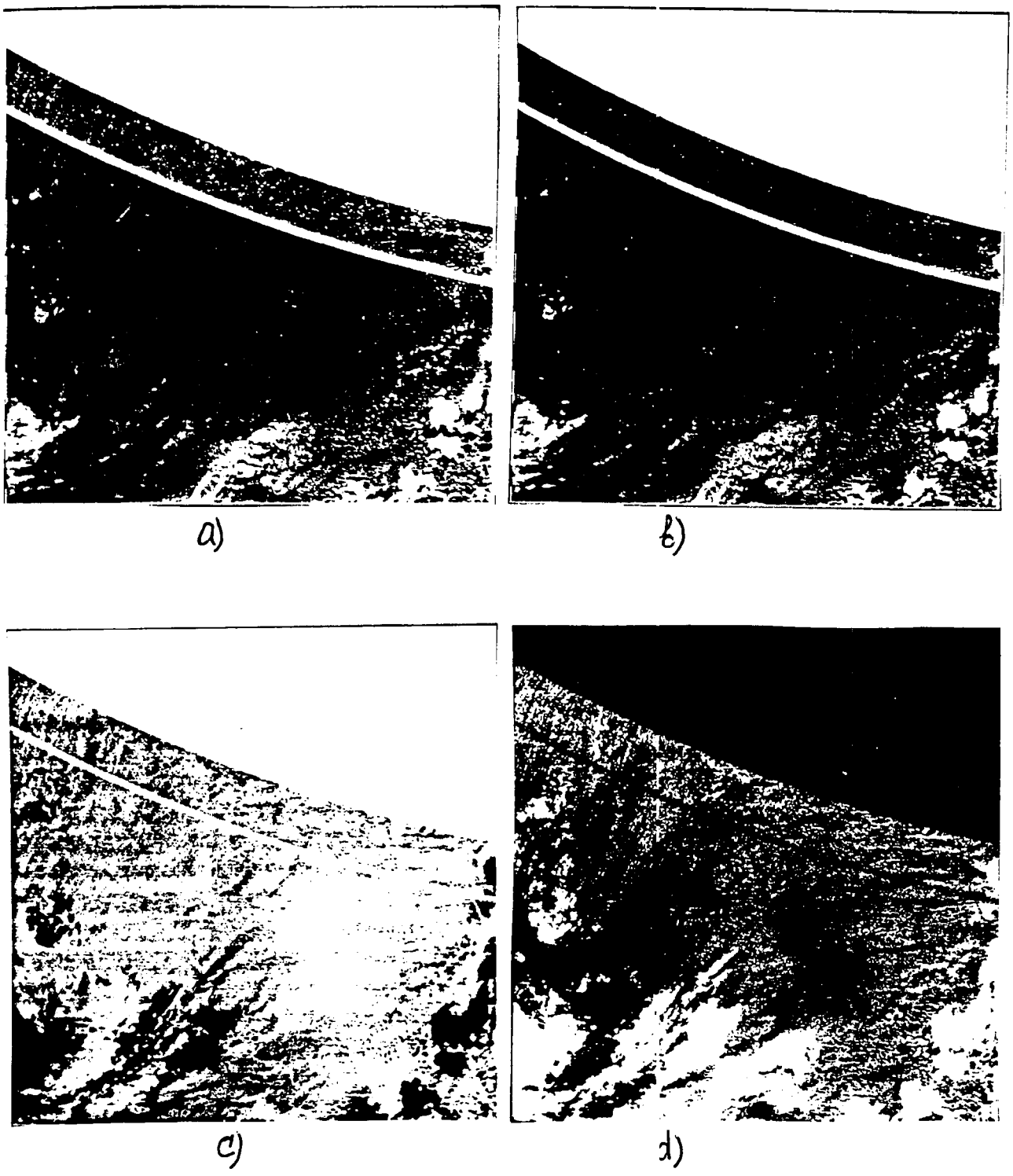

Figure 10.1 Cloud images in different channels of AVHRR over the area 800 x 800 km with the center 56 N, 37.5 E: a) λ = 0.63 μm; b) λ = 0.93 μm; c) λ = 12 μm; d) the result of clusterization (dividing into classes): black tone - water; dark grey - land surface; grayish - crystalline clouds; white - dense water clouds.

'small peak' at the right slope of the histogram (Figure 10.2 shows it with an arrow). The number of pixels which are in the area with $A^1 > A^1_{kp}$ - prove to represent cloudiness, while pixels with values $A^1 < A^1_{kp}$ can be related to cloud free scenes and semitransparent cirrus which increase the albedo by 20-40%.

To examine this criterion further, we used another approach to determine cloudiness. The following procedures were applied for each pixel. The albedo obtained on one of the preceding cloud free days (with the same conditions of observation) were subtracted from the value of the albedo obtained for a cloudy day. As a result, the open plots of land had the difference of albedo close to zero, while the cloudy scenes had a difference in albedo of more than 20%. The above procedure of selecting cloudiness was compared with the first way of obtaining cloudiness in accordance with the shape of the histogram. The correlation was 82% which witnesses a good correspondence of the methods.

As discussed above, two situations were considered for selecting ice clouds: 1) semitransparent ice crystal clouds over the land or water, and 2) crystal clouds over water clouds. It is impossible to determine the situation of the first type using only the first three channels of the AVHRR, because such pixels satisfy the condition $A < A^1_{kp}$ and are related to the land in accordance with this index. To find the semitransparent crystal cloudiness, we use the fifth channel (λ = 12 μm). The histogram of radiation temperatures is constructed in the fifth channel data for the subset of first channel pixels which are related to the cloud free land scenes. In this histogram the cloud free scenes have the shape of a narrow-dispersion distribution,

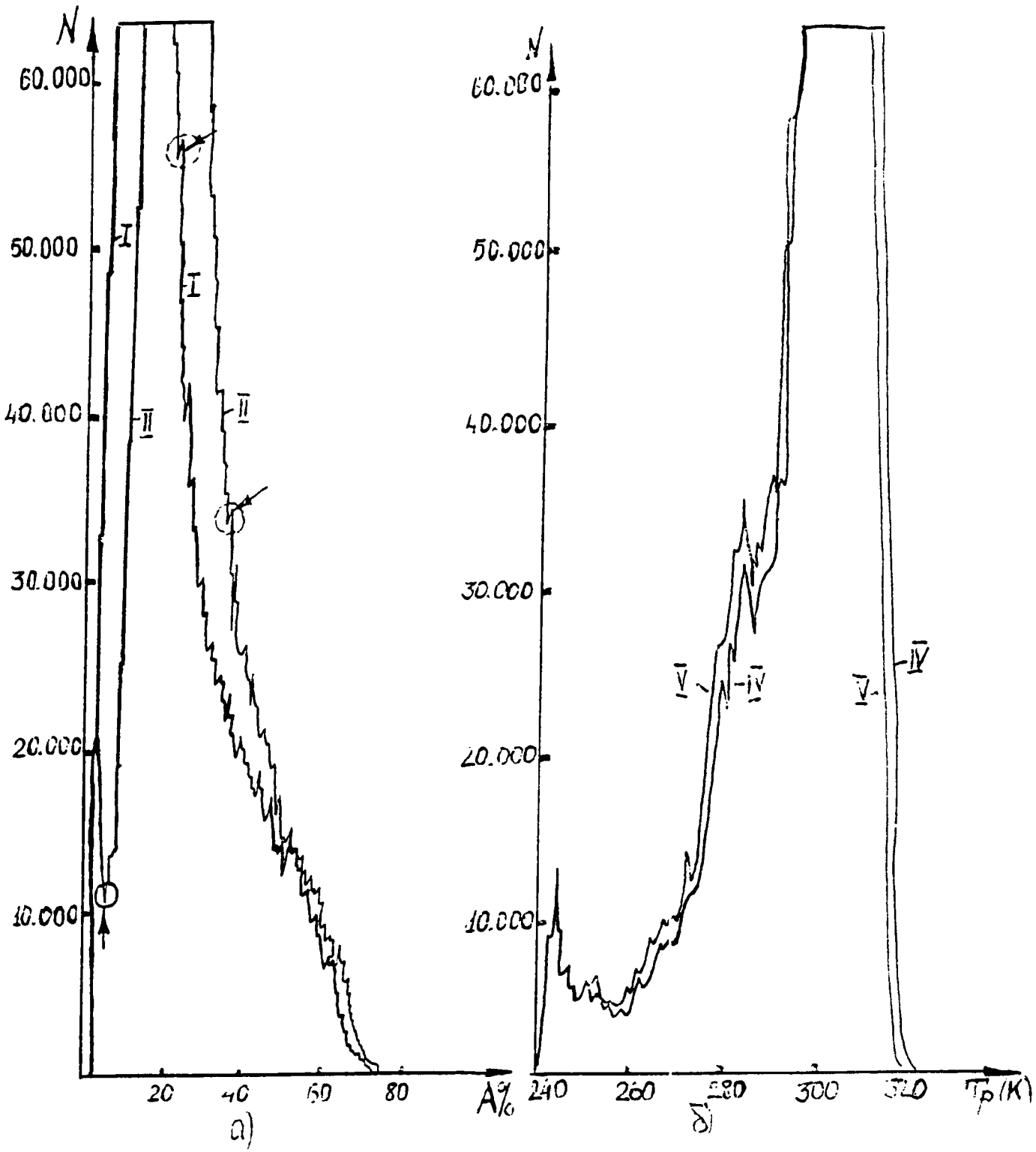

Figure 10.2 Histograms for 4 channels of AVHRR over image 512 x 512 pixels 7/06/89.

while the plots with semitransparent cloudiness (which are much colder than the Earth's surface) are located to the left of this narrow distribution. When we use the analogous approach, the first local maximum on the left slope of the histogram (shown by an arrow in Figure 10.3) can serve as criterion T^5_{kp}, dividing the cloud free scenes from crystal semitransparent cloudiness. Using this procedure, we can single out the semitransparent crystal cloudiness located on a background of land.

Using the following procedure we single out the total cloud amount (determined from the analysis of records in the first channel $A^1_1 > A^1_{kp}$), which includes clouds which have crystalline phase and are located over the water clouds. With this aim, a difference of signals between channels 3 and 5 corresponds to the reflected component of the signal at 3.7 μm. When we have clouds representing to the two phase states, the histogram has a bimodal shape because the reflective ability of crystalline and water-drop clouds differs significantly. Figure 10.4 displays the difference of channels 3 and 5 and shows crystal clouds as dark spots on a brighter background of liquid water clouds. Therefore having united the two amounts singled out at the first and second stages, we obtain the cluster of crystalline clouds (Figure 10.1d).

Since our main goal was the selection of cirrus clouds, the comparison of our results with the known methods is of interest. Figure 10.5, presents a representation of cirrus clouds for June 7 obtained using our methods. For comparison, Figure 10.5b presents the results of selecting cirrus clouds in accordance with methods of Prangsms (1986), where the difference between

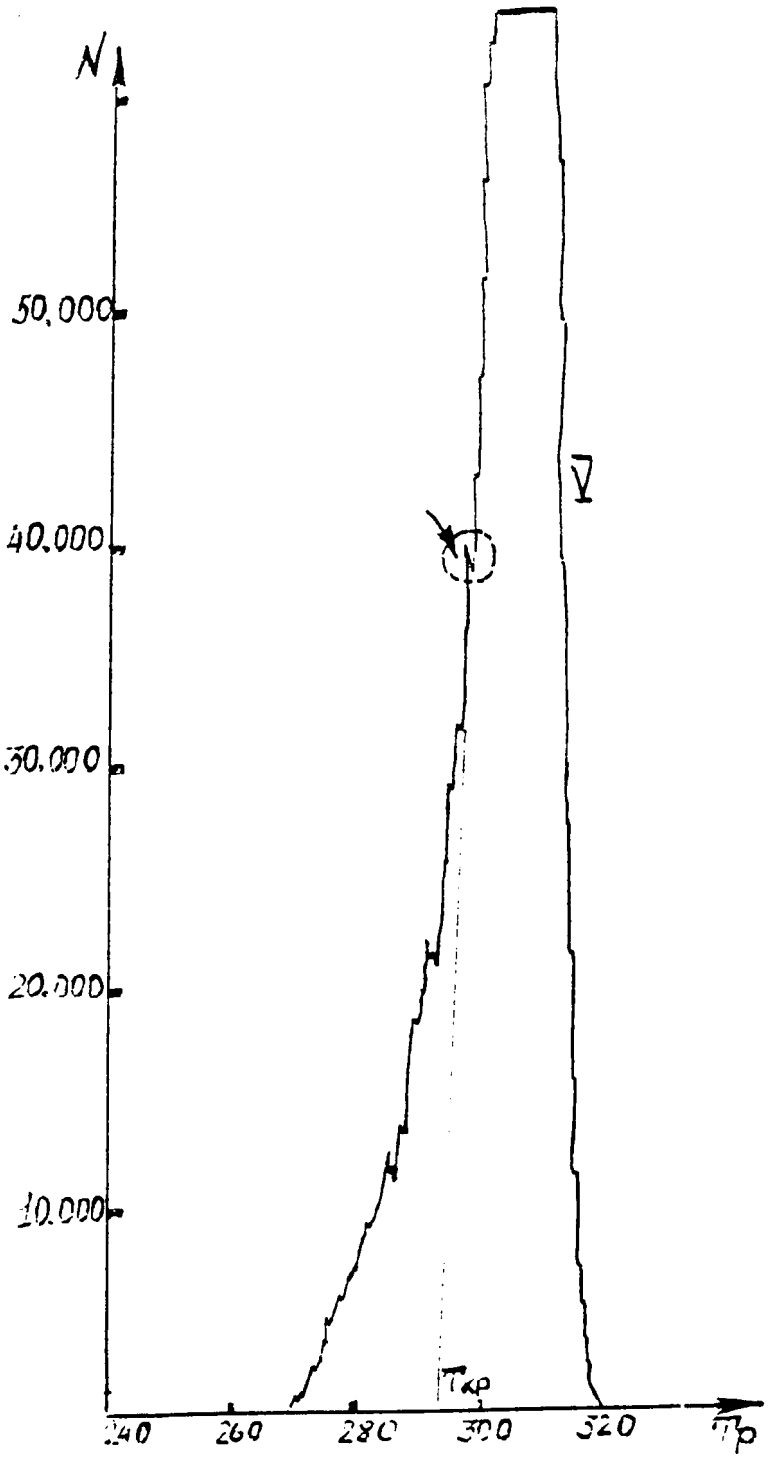

Figure 10.3 Histogram for land surface in channel 5 without cloudiness divided by channel 1 (the threshold for crystalline cloudiness over land surface is shown by an arrow).

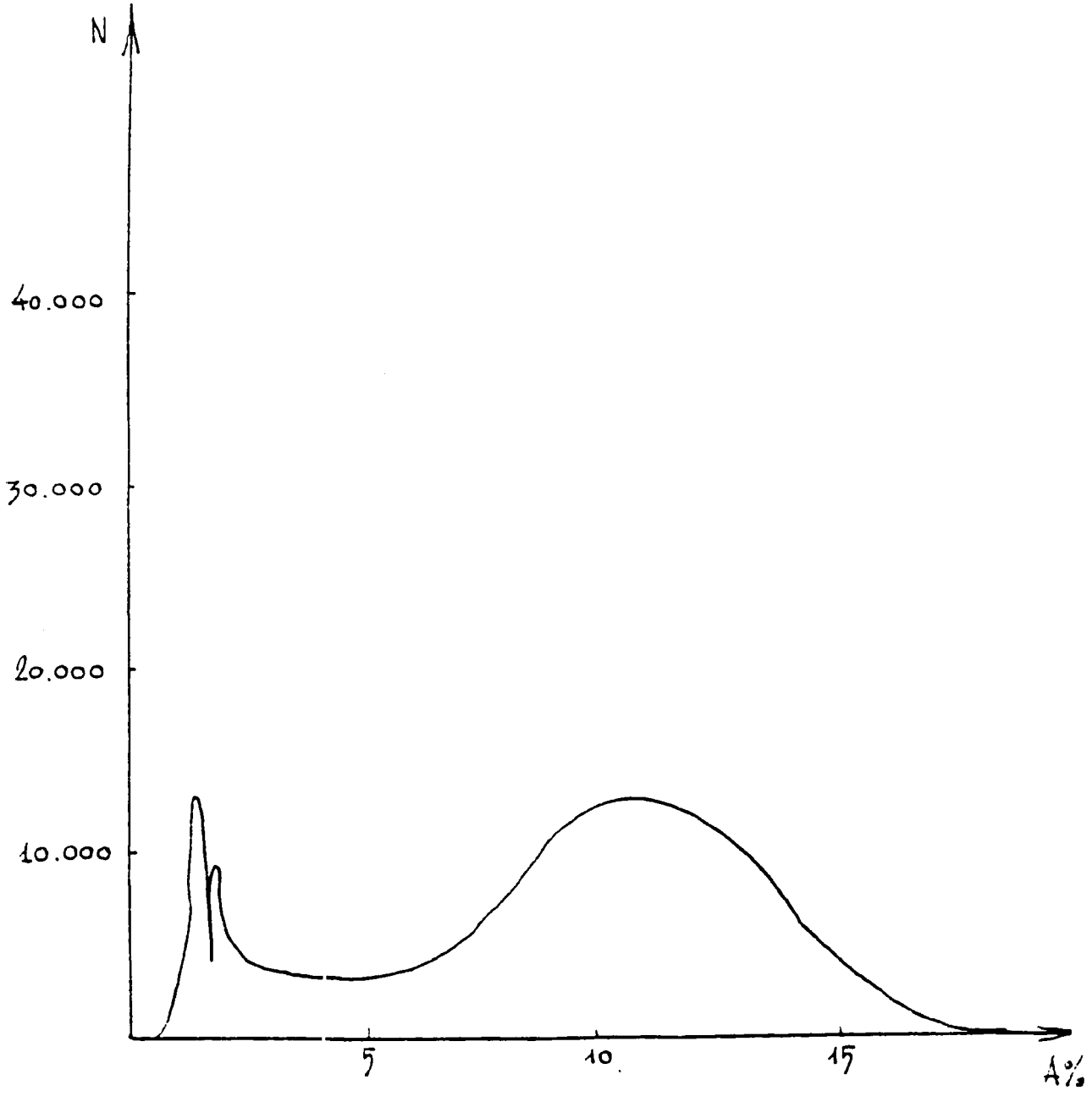

Figure 10.4 Histogram for reflected fluxes from the cloud system in channels 3-5 (λ = 3, 7 μm) 7/06/89.

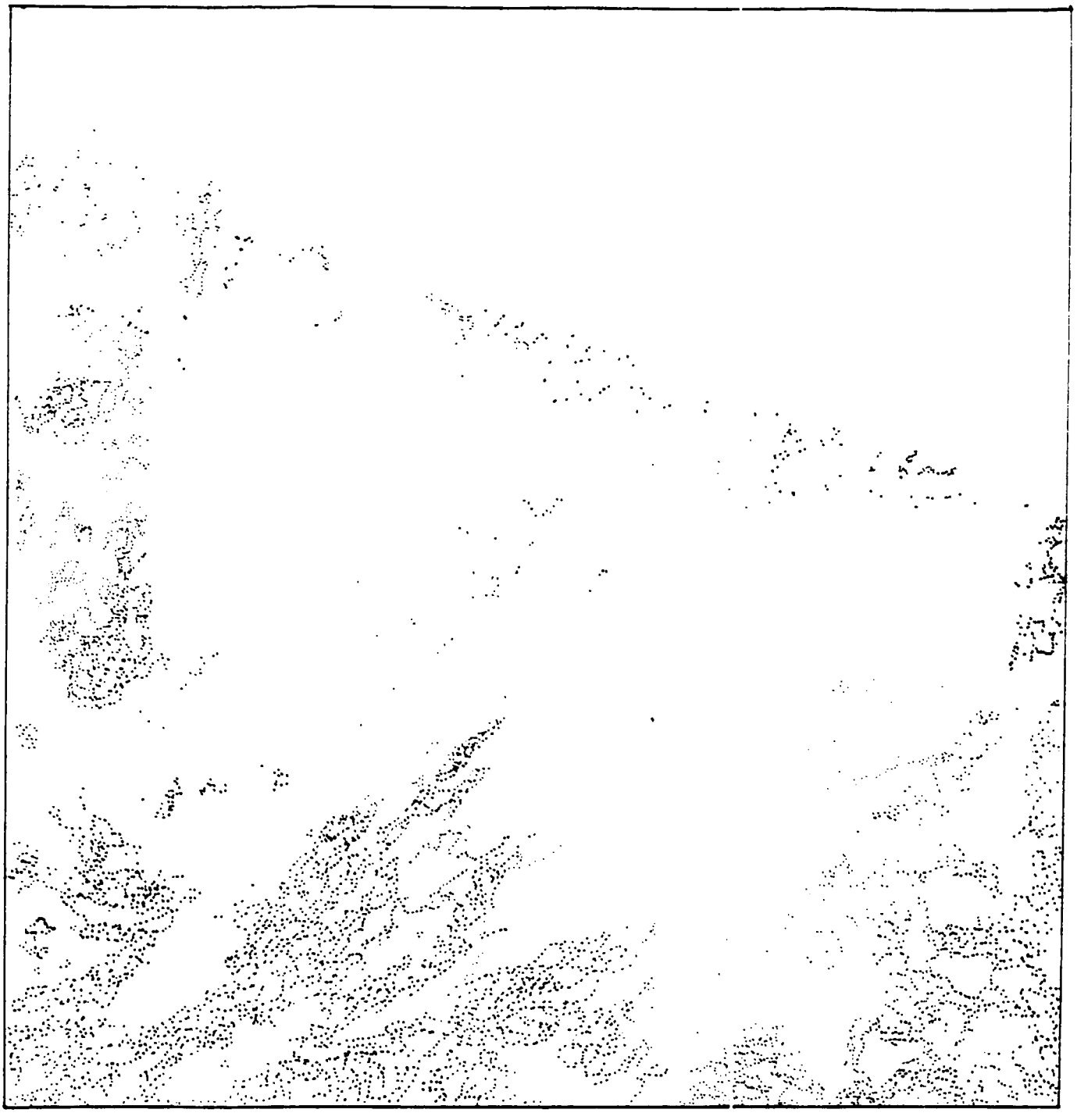

Figure 10.5 a) The image of cirrus cloudiness produced by our method.

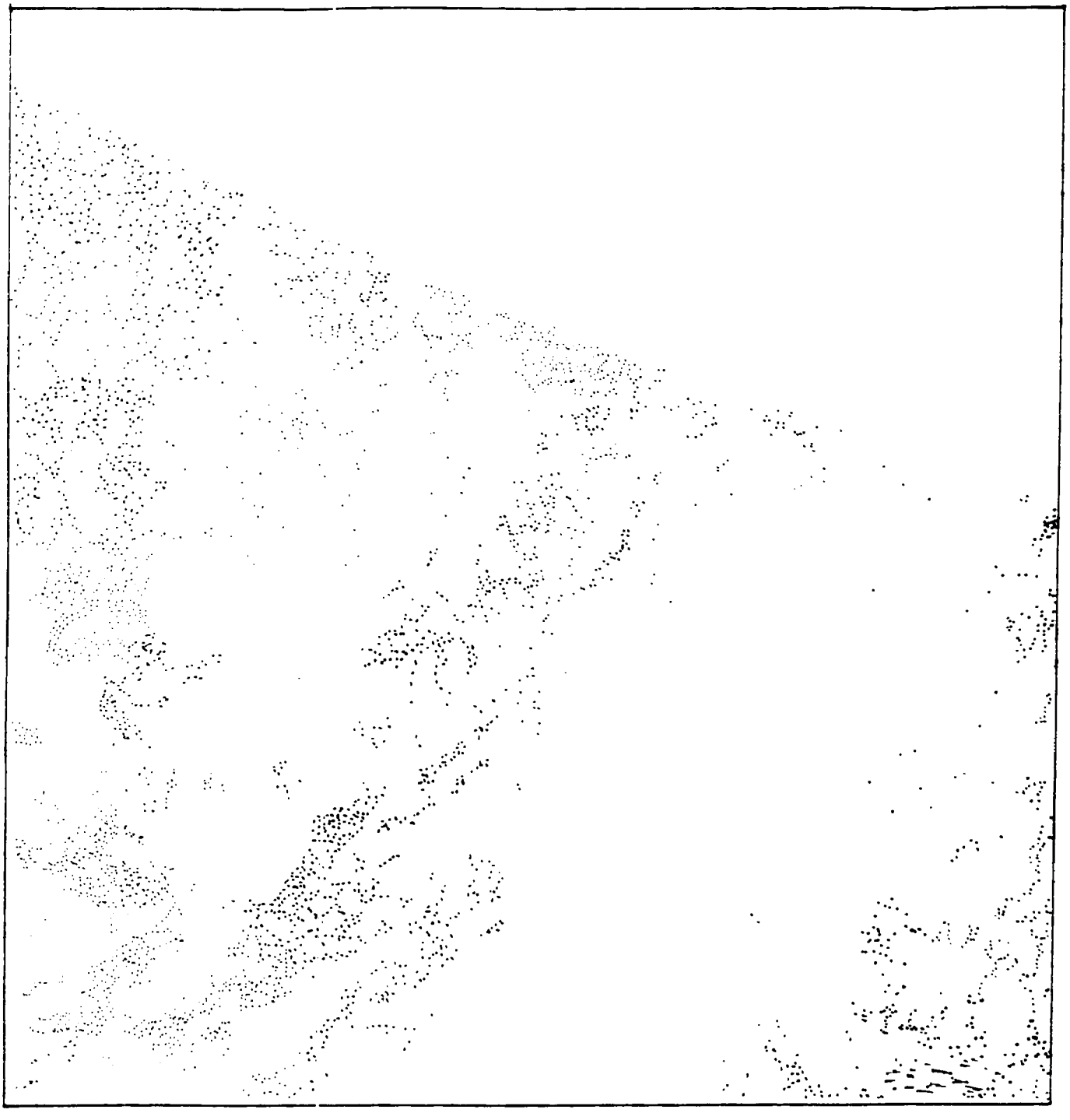

Figure 10.5 b) The image of cirrus cloudiness produced by the method of Prangsma et al. (1986).

radiation temperatures of channels 4 and 5 was the criterion. When the difference between the temperatures in these channels is within the limits of 4-6°C, the case is considered to be cirrus. Along with a good spatial correlation between the two method results, our approach gives a greater number of pixels which correspond to crystal cloudiness. This is because our approach is more sensitive for the determination of crystal clouds over a land surface. It is difficult to make final conclusions about the accuracy of the two methods. For this purpose, one needs to obtain independent measurements and make a cartographic picture of clouds from the earth. This stage of work is planned in the future.

REFERENCES

Prabhakara, et al., 1988: Thin cirrus clouds: seasonal distribution over oceans deduced from Nimbus-4 IRIS. *J. of Appl. Meteor.*, 27, pg. 379.

Prangsma, G. J. and J. N. Roozenkrans, 1986: Processing of row digital NOAA AVHRR data sea and land applications. Proc. from the 7th Int. Symp. on Remote Sensing Develop. and Environ. Manag. Enschede, 1, 63-66.

Chapter 11

Some Considerations and Conclusions

by E. M. Feigelson

The data obtained from five years of investigating cirrus clouds as well as FIRE I and other data, need thoughtful consideration. First of all, it is incorrect to say (following the WCRP) that the major cirrus influence lay in strengthening the greenhouse effect. Our calculations (see Abakumova, G.M., et al., 1989, Chapter 6) show that cooling induced by the albedo effect prevails in some cases. In the presence of cirrus the net radiation may be negative at the upper atmospheric boundary (relative to cloudless atmosphere) ranging between -1 and -18 W/m^2. These cases correspond to the situation of a low albedo underlying surface and the optical thickness of the cloud, τ, approximately 0.5. Cirrus particles are considered to be large hexagonal prisms distributed randomly in space. One can certainly not assume that as τ becomes larger the sign of the effect will change, since the greenhouse effect is saturated quickly: emissivity $\epsilon \sim 1$ when $\tau \sim 2$, while the albedo continues to grow, at least, up to $\tau = 20$. So it is certainly possible for cirrus clouds to induce cooling, rather than heating, of the earth. Of major importance here are non-spherical ice crystals which reflect solar radiation to a much larger degree than spheres (see Abakumova, G.M., et al., 1989, Chapter 6). Apparently, from the Zvenigorod observations the prevalence of the albedo effect over the greenhouse effect is more characteristic for summer than for winter.

On the basis of a detailed model of microphysics and radiation transfer, Stephens and Tsay et al. (1990) made the following assertion: "The forecast of even the sign of the feedback between cirrus and climate is premature."

To reach the solution of this problem, one must, first of all, consider the question of the shape and size of cloud particles and the validity of the assumption that they are randomly oriented in space. Apparently, large ice particles have a preferential horizontal orientation. This preferred orientation complicates the theory of radiation transfer. At the same time, Stephens (1980) shows that numerical results for large columns are similar in both cases.

Calculations done in Takano and Liou (1989) for plates demonstrate also that the reflection of light from clouds depends weakly on particle orientation for cloud optical thickness < 1; this is characteristic of our conditions (see Chapters 1, 2 and 5). On the basis of the well known diagram of Mahono and Lee we may assume that at temperatures below -25 °C columns and thick plates prevail. Therefore, the assumptions about the shape of large particles and their random distribution in space used in all our calculations of radiation fluxes are acceptable ones.

The problem associated with particle sizes is more complicated; no one doubts that small particles are possibly present with $r < 20\text{-}30\ \mu m$, where r is the radius of a sphere, equivalent in its area or volume (various sizes are called small in different works, sometimes with $r < 70\ \mu m$). Unfortunately no one has been able to determine their numbers and sizes surely and simply. Instances of observing small particles are described in different papers and attempts have been made to evaluate their optical characteristics. Platt and Spinhirne's

et al. 1989 microphysical aircraft measurements report concentrations of small particles ($r < 70\ \mu m$) in the upper part of a cloud at -63°C and an absence of large ones. Yet, this microphysical structure does not satisfactorily explain the optical measurements which were made from aircraft flying over the clouds at the same time.

The satellite and aircraft measurements, reported by Sassen, Heymsfield et al. 1990 suggest that $\zeta = Q_s/Q_a > 2$, which is possible, according to Mie theory, only when $r < 30\ \mu m$. Here Q_s is the scattering cross-section at $\lambda = 0.65\ \mu m$; Q_a is an absorption cross-section for $\lambda = 10\ \mu m$.

An interesting numerical experiment was reported by Stackhouse and Stephens (1990). They showed how the radiation heat exchange would be affected by the addition of small particles to a measured spectrum of $r > 30\ \mu m$, equivalent to an ice water amount $w = 0.0114\ g/m^3$. The concentration of small particles is considered to be nearly $10^{-3} cm^{-3} \mu m^{-1}$ in the range of $0 \leq r \leq 30\ \mu m$, which gives an addition to the water amount of nearly 0.0012 g/m^3. This small droplet population provoked growth of radiative heating by nearly 3 K/day from long wave radiation with an insignificant influence on solar radiation in the lower part of a homogeneous cloud with thickness of 2 km. Near the upper boundary, long-wave cooling grew by more than by 3 K/day, while solar heating increased by nearly 0.5 K/day. The most interesting effects of the addition of small particles, according to this article, is the increase of albedo by 50 per cent in the range of $0.8 \leq \lambda \leq 2.5\ \mu m$ (albedo is not presented for $\lambda < 0.8\ \mu m$). Using Mie theory (i.e. spherically shaped particles), the authors use a coefficient of asymmetry μ equal to 0.87 for all sizes of particles. This has three ramifications:

1. Too small (0.1) of an albedo, resulting from large non-spherical particles which undoubtedly have smaller value of μ (Abakumova, G.M., et al., 1989, Chapters 6 and 9 of this issue) and therefore a greater albedo.

2. Initial sharp disagreement between measured and calculated albedos turned into agreement when the authors have taken $\mu = 0.7$ for small and large particles.

3. However if $\mu = 0.7$, the contribution to the albedo of small particles is too large. These particles are more similar to spheres and should have a correspondingly greater value of μ and smaller albedo.

Therefore, small particles can exist in cirrus clouds and more numerous at low temperatures. The question arises - what are the relative concentrations of both small and large particles? This question is of a great interest for us, because all of our previous calculations of heat and solar radiation have used values of optical thicknesses τ_λ with $\lambda = 10.3$ μm or 2.1 μm (inferred from surface radiation measurements (see Chapter 3). We have assumed that these values of τ_λ depend weakly on the wave length if the particles are large. The correctness of this assumption is shown, for a rather wide range of τ_λ, (Abakumova, G.M., et al., 1989, Chapters 1 and 3) by comparing detailed calculations of extinction coefficients and observations. Further evidence of the validity of this assumption is the experimental result: (Abakumova, G.M., et al., 1989, Chapters 1 and 5):

$$\tau_{10.2} \approx \tau_{2.1} \approx 2\,\tau_A.$$

Here $\tau_{10.2}$, $\tau_{2.1}$ are optical thicknesses for $\lambda = 10.2$, 2.1 μm respectively, which are determined from the transmission of direct solar radiation measured with a field of view of

the receiver α = 15 min; τ_A was calculated from transmission measured simultaneously using thermoelectric actinometer (α = 10°).

Spectral transmission measurements show, on the bases of theoretical calculations (Abakumova, G.M., et al., 1989, Chapters 1 and 3), that the particles may be called small when $r_{ef} \leq 10\ \mu m$. Such particles, in accordance with the data of 1986, 1987, 1989 were seen in 15 per cent of cases, mainly in Cc clouds. Note that according to Kosarev and Mazin (1989) from multi-year data of microphysical measurements particles with $r < 20\ \mu m$ are seen in 20-30 per cent of cases. Therefore, the suggestion $\tau_\lambda = \tau_{10.2\,\mu m} \approx \tau_{2.1\,\mu m}$ which was considered by us to be basic for calculations of fluxes, seems to be mainly correct; this is also confirmed by the agreement of calculations and measurements presented in Abakumova, G.M., et al., 1989, and Chapters 4, 6 and 9.

The following major question remains: what are the relationships among the number density quantity - n(r) and, ice (or water) content - w and coefficient of extinction of visible light - β, obtained with the help of in situ aircraft measurements?

For water clouds, when n(r) is known, we can find β, and w; for ice clouds it is more complicated. Comprehensive determination of w and n(r) is extremely difficult using even the most sophisticated instruments, because of two reasons: a) the shape and actual volume of particles, and number of small particles are unknown, and b) large crystals may be porous. The first reason complicates the determination of β = f(n(r)), since the actual effective cross-section of extinction is impossible to determine. Most frequently the measured size distribution of particles, is transformed to a distribution for spheres of equivalent radius, which is indeterminate in itself. Sometimes all three parameters, n(r), w

and β, are measured separately. The authors of Chapter 7 have done so during the first series of experiments with aircraft measurements - microphysical, optical and radiative (Chapter 8), however the device used for measurement of β could work with sufficient accuracy only when $\beta \geq 2.5$ km^{-1}. Therefore, only episodic values of this parameter, apparently corresponding to local thickening of a cloud, were obtained (see Figure 7.4 in Chapter 7).

Simultaneous with aircraft measurements (May 15, 1989, from 1 p.m. to 3 p.m.) surface measurements were made of the optical thicknesses of clouds τ; in this case $\tau \approx 1.0$ during the flight. Knowing τ and the ice path $m = \int^{H}_{0} w(z)\, dz$ (H is the thickness of the cloud), we can determine the mass absorption coefficient $K = \tau/m$ which was equal to 0.050 m^2/g and agrees with the data of Kinnes and Ackerman et al. (1990). Here according to three days of measuring n(r) and w and calculating β in the FIRE experiment, it was possible to calculate values of a height averaged K:

$$K = \beta/w = 0.046;\ 0.049;\ 0.063\ m^2/g$$

We may note that in accordance with the earlier aircraft measurement values of m and of emissivity $\epsilon = I - e^{-\tau}$, K ranged from 0.05 - 0.1 (Feigelson 1989). One may suggest that the parameter K, which we consider as more accurate and objective than β since it is determined from both number and sizes of particles for cirrus cloud layers within the range of values 0.01-0.1 m^2/g.

The question arises: Is it necessary to know K or β when τ is measured? It <u>is</u> essential in order to determine the albedo of single scattering - ω, equal to $\tau_{SC}/\tau = \beta_{SC}/\beta = K_{SC}/K$.

Is it important to consider such a complicated problem as the ice nature of cirrus particles in forecasting and climatic models? Perhaps one can simplify the calculations, by considering cirrus to be liquid clouds and bearing in mind only their height and water content.

One suggested solution of this problem is presented by Rockel, 1988. Using the European model of mean-range weather forecast (ECMWE). Table 11.1 presents results from this work showing some parameters of the 5th and 10th days of the forecast. A forecast was calculated for 5 and 10 days, taking into account ice nature of cirrus cloud particles (A) and considering them to be water ones (B).

Table 11.1

Value (A)-(B) / A	% A	% B	Value (A)-(B) / A	% A	% B
Temperature with z = 6 km	1.3	2.6	Lower cloud amount	-1.5	-1.7
Surface temperature	0.7	1.3	Convective clouds	-2.3	-1.9
Precipitation	-4.5	-3.1	Radiative balance at the upper atmospheric boundary	56	64
Upper clouds amount	-0.7	-3,5	Radiative balance at surface	3.0	3.6

Keeping in mind the averaging of the parameters, the differences in the forecasts when the cirrus clouds are assumed to have ice properties and when they are assigned liquid properties are significant and become larger as the period of forecast is longer.

Next let us examine the results of work which was done in 1986-90 by the group of authors from the institutes mentioned in the introduction. Let us first summarize the results of this work.

1. Systematic comparison of calculations and measurements of solar heat radiation fluxes, (Chapters 4, 5, 6 and 9). Comparisons of fluxes of solar radiation

measured with aircraft and with calculations are given in Chapters 8 and 9. Possible reasons for the differences between calculations and measurements were analyzed. Recalling that C_Q is the ratio of the total solar radiation with cirrus to that with clear sky, the most systematic of the differences is the excess of the calculated values of the parameter C_Q over measured values deduced from the data of 1986-87 (according to 1989 results, the agreement is more satisfactory). The author of Chapter 9 obtains agreement between calculations and measurements (for 1986, 1987 data) by assuming the single scattering albedo, $\omega = 0.9$ in spectral range $0.3 \leq \lambda \leq 1.2$ μm. This suggests that the ice particles are polluted by soot or other substances. Possible other reasons for the differences are also mentioned. The extreme variability of the optical thickness τ of cirrus induces a large variability in solar radiation fluxes (Chapters 3 and 5). The dependency of C_Q on τ are presented in Chapters 5 and 9 where the half hour average data tend to smooth much of this variability.

2. The measurements of spectral transmission of the direct solar radiation and spectral optical thicknesses, τ_λ, calculated from them. The transmission was measured using a standard actinometer and the corresponding optical thicknesses τ_A were calculated. Calculations of extinction coefficients, are dependent upon sizes of the particles and of receiver's field of view. Two conclusions of practical importance come from these comparisons:

   a) The optical thickness of cirrus, τ, can be determined from measurements of transmission with the use of a standard actinometer: $\tau_A \approx 2\,\tau_\lambda$ where $\lambda = 10.2$ or 2.1 μm.

b) It is possible to detect the presence of small particles in clouds (Chapter 3).

3. Solution of some inverse problems (Chapter 2). The determination, of the vertical profiles of extinction coefficients of visible light inside a cloud allow one to calculate the heat radiation fluxes ("continual approach"); Abakumova, G.M., et al., 1989, Chapters 2, 4 and 5.

. Regression equations between optical thicknesses and solar and heat radiation fluxes (Chapters 4 and 9). Similar equations are obtained between the extinction coefficient of the visual spectral range (averaged over the cloud's thickness), thickness of a cloud and temperature (Chapter 2). Correlations are established between geometric and optical thicknesses of a cloud, and between the latter and temperature (Chapter 2). These correlations are important for the parameterization of radiation fluxes in climate models and for estimating the latter's sensitivity to the effect of cirrus clouds.

5. Spectral and integral fluxes of direct, diffuse and total solar radiation coming to the Earth's surface. This analysis is based upon the data of systematic (continuous in some cases) measurements which were conducted during the three years of the experiment (1986, 1978, 1989) (Chapters 5 and 6).

It is reasonable to assume that this multi-year data set depicts solar radiation coming to the surface in spring in the south-west of the Moscow Region in the presence of cirrus clouds. In addition, these data agree with multi-year measurements at the meteorological observatory of Moscow State University. The

latter, in turn, agree (winter excluding) with mean seasonal global data on occurrence of cirrus given by Hahn and Warren et al. 1984.

6. Synoptic analysis, Chapter 1. An analysis of cirrus cloudiness must systemically include aerological and surface meteorological information and constant visual observations of cloudiness.

When we design future programs to investigate cirrus clouds, we must consider the following topics. In future projects, the efforts of combining surface measurements with satellite and aircraft.

Equations relating the various parameters to one another may certainly be improved through the accumulation of more extensive data. Of course, the development of optical and microphysics models and their parameterization depending on thermodynamic values, level and thickness of clouds should be continued.

It is necessary to better understand, in which geographical areas and under which meteorological conditions the regression results can be applied.

And lastly, we must determine under which conditions cirrus clouds cool the earth and under which conditions they heat it.

REFERENCES

Abakumova, G. M., et al., 1989: The Geometrical, Optical and Radiative Properties of Cirrus Clouds. Colorado State University, Atmospheric Science Report No. 456, 61 pp.

Feigelson, E. M., 1989. The fluxes of thermal radiation by cirrus clouds. Collection of papers "Radiative Properties of Ci clouds," Moscow, "Nauka," 224 pages (in Russian).

Hann, C. Y., S. G. Warren, Y. London, R. M. Chervin, R. Yenne, 1984. Atlas of simultaneous occurrence of different cloud types over land. NCAR Boulder, CO.

Kinne, S, T. Ackerman, et al. 1990. Radiative transfer in cirrus clouds from airborne flux and microphysical measurements. Preprints of the Seventh Conference on Atmospheric Radiation

Kosarev, A. L., and Mazin I. P., 1989. Empirical model of physical structure of the upper-level clouds of the middle latitudes. Collection of papers, "Radiative properties of cirrus clouds," Moscow, "Nauka" 224 pages (in Russian).

Platt, C. M. R., and Y. D. Spinhirne, et al. 1989. Optical and microphysical properties of cold cirrus clouds, evidence for regions of small ice particles. *J. Geophys. Res.,* 94, 11151-11165.

Rockel, B., 1988. Parametrisierung von Eis-und wasser wolken und ihre stralungstransporteigenschaften fur grossraumige Atmospharenmodell. Mittelungen aus dem Institut fur Geophysik und Meteorologie der Unuversitat zu Kohln. Heft 58.

Sassen, K., A. Y. Heymsfield, et al. 1990. Is there a cirrus small particle radiative anomaly? Preprints of the Seventh Conference on Atmospheric Radiation, page 91.

Stackhouse, P. W., and G. L. Stephens, 1990. A theoretical and observational study of the radiative properties of cirrus. Submitted to *J. Atmos. Sci.*

Stephens, G. L., Si-Chee Tsay, et al. 1990. The relevance of the microphysical and radiative properties of cirrus clouds. *J. Atmos. Sci.*, 47, 1742-1753.

Stephens, G. L. 1980. Radiative transfer on a linear lattice: application to anisotropic ice crystal clouds. *J. Atmos. Sci.*, 37, 2095-2104.

Takano, Y. and K-N. Liou, 1989. Solar radiative transfer in cirrus clouds. *J. Atmos. Sci.,* 46, 20-36.

APPENDIX I

On the Climatology of Upper Layer Clouds

by I. P. Mazin, S. N. Burrovskaya and E. T. Ivanova

1.0 Introduction

It is well known that upper layer clouds (ULC)[1] influence the radiative energy budget of the earth. This is one of the reasons that cirrus cloud research has a high priority in most climate programs. The subject of this paper is cirrus cloud cover climatology. To be short, we shall refer to it as Cirrus-C^3 problem.

Today we know only one reliable way to solve this problem. It is based on routine surface-based weather observations. They are summarized according to the WMO synoptic code and include the data on the total amount of clouds, N, and the amount of lower layer clouds N_ℓ, however very often the knowledge of N and N_ℓ is insufficient to estimate the amount of upper layer clouds. A large set of data has been collected all over the world and it is widely used by scientists (Berlyand and Strokina, 1980; Warren et al., 1986 and 1988; Makhover and Nudelman, 1987).

If we base our research only on synoptic data, uncertainties arise in all the cases when more than 70% of the sky are screened by lower and middle layer clouds. The situations when lower, middle and upper layer clouds exist simultaneously, also lead to uncertainties if we speak about the ULC amounts. Indeed, in synoptic data one can find only the values of the total amount of clouds

[1]Sometimes we refer to them as Ci clouds.

N and the amount of lower layer clouds N_ℓ. Thus, if we designate the amount of middle and upper layer clouds together as N_s and suppose that ULC is dispersed in the sky randomly and independently from underlying clouds, we may easily find N_s from equation

$$N_s = (N - N_\ell)/(1 - N_\ell), \tag{1}$$

i.e.,
$$(1 - N) = (1 - N_s)\,(1 - N_\ell). \tag{2}$$

Here N_ℓ, N_s and N are given as fractions of a unity. The errors in estimating N_s values become too large when $1 - N_\ell << 1$, practically when $N_\ell > 0.7$. We shall classify these cases as uncertain situations.

If there are no middle clouds ($N_m = 0$), then $N_u = N_s$, where N_m and N_u are the amounts of middle and upper layer clouds, respectively. If there are no lower layer clouds ($N_1 = 0$), then $N_\ell = N_m$ and equation (2) is true if we replace N_s by N_u. In the cases when all three (lower, middle and upper) layers are present, it is impossible to define the amount of ULC and these cases are also classified as indeterminate.

A climatology of ULC (amounts) based on the technique of data processing described by (Warren, et al. 1986 and 1988), of course, differs from the real one. So the question is: To what degree may we generalize based upon the statistics derived from the observations of certain situations to all cases? An attempt to answer this question is one of the main goals of this paper. For this purpose, we have applied the unique data set obtained from regular aircraft network which

operated in the Soviet Union during six years (1958-1963). This network is shown in Figure I-1. It includes 31 stations in the whole territory of the USSR.

Aircraft observations allowed us to estimate the amount M of underlying clouds which had screened Ci clouds from the observers at ground stations, and thus to estimate its effect on Ci-C[3].

2.0 Climatology of Upper Layer Cloud Cover Based on Aircraft Observations

In 1958-1963, regular aircraft soundings of the atmosphere were performed at 31 aircraft sounding stations (ASS) of the USSR. The data obtained in this 6-year period provided the basis for calculating frequencies of occurrences and amounts of Ci clouds in different regions of the USSR, despite the presence of underlying clouds. This gives us the means to examine the effect of underlying clouds on the amount of ULC and thus to estimate the accuracy of ULC climatology based on ground observations.

The ASS's operated for only six years and the observational series were not very long; therefore to enlarge the statistics, the Soviet territory was divided into eight parts and united the data set of ASS's in a separate series for each region. The aircraft stations and selected regions are shown in Figure I-1 and listed in Table I-1.

The technique of data processing was described by Burkovskaya et al., 1990, and is summarized below.

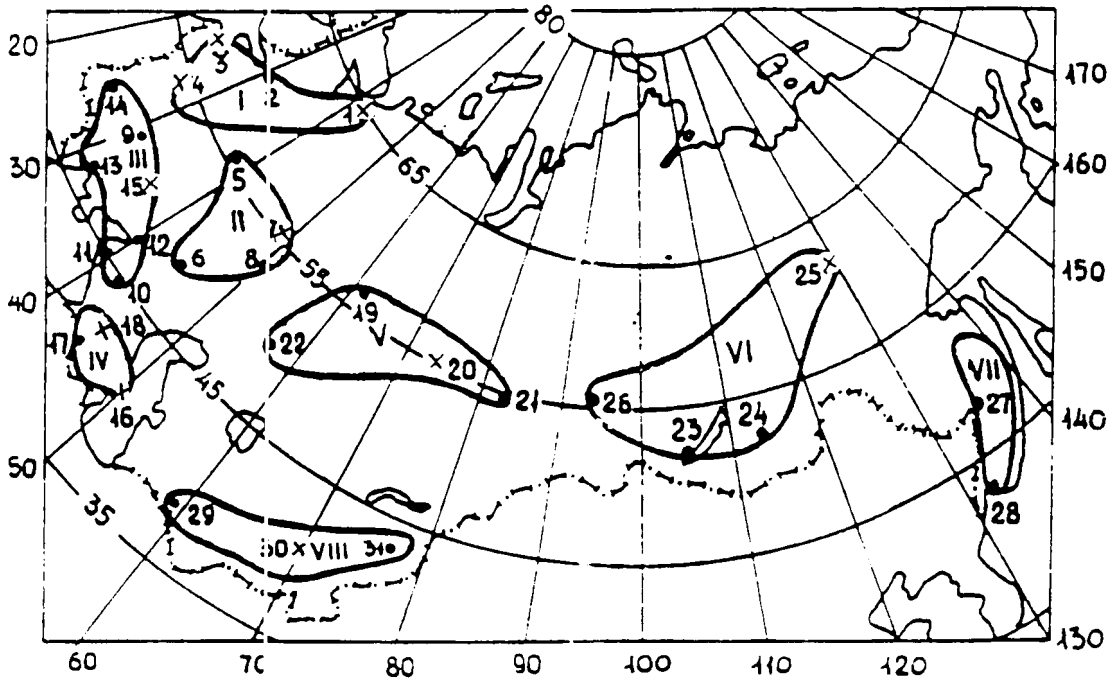

Figure I-1 Aircraft sounding stations in different regions (Roman numerals). Stations are indicated by Arabic numerals (see Table I-1). Stations chosen for comparison are designated by crosses.

Table I-1

Aircraft Sounding Stations

1	2	3	4	5	6	7	8
1. Arkhangelsk 2. Leningrad 3. Riga 4. Minsk	5. Moscow 6. Volgograd 7. Kasan 8. Samara (Kuybyshev)	9. Kiev 10. Min.Wody 11. Krasnodar 12. Rostov na Donu 13. Odessa 14. Lvov 15. Kharkov	16. Baku 17. Erevan 18. Tbilisi	19. Sverdlovsk 20. Omsk 21. Novosibirsk 22. Aktubinsk	23. Irkutsk 24. Chita 25. Yakutsk	26. Khabarovks 27. Vladivostok	28. Ashkhabad 29. Tashkent 30. Alma-Ata

Let n be the number of cloud layers. M is the portion of the sky covered by i-th layer. We assume that the spreading of clouds in each layer does not depend on clouds in other layers. Thus, M_1 is the part of the sky covered by the first cloud layer and $(1-M_1)$ is the part of it free from these clouds, i.e., the total part occupied by gaps in this cloudy layer. If M_2 is the amount of clouds in the second layer, and K_2 is the part occupied by the second layer clouds in the gaps of the first layer, then

$$K_2 = M_2 (1 - M_1) = M_2 (1 - K_1). \quad (3)$$

Thus, the total part of the sky covered by two first layers of clouds is $(K_1 + K_2)$. Repeating this procedure for the third layer and so on, we obtain for the n-th layer:

$$K_n = M_n [1 - K_1 + K_2 + \ldots + K_{n-1})] \quad (4)$$

and for the total amount of clouds M_t, if n layers are present, we find

$$K_t = K_1 + K_2 + \ldots + K_n - \sum_{i} M_i - \sum_{i \neq j} M_i M_j + \sum_{i \neq j \neq k} M_i M_j M_k - \ldots (-1)^{n-1} M_1 M_2 \ldots M_n \quad (5)$$

Following the above procedure, we calculate amounts, M, of clouds in lower and middle layers together and amounts, N, of Ci clouds. The results are demonstrated in Figures I-2 and I-3. Here, in circle diagrams, M is the frequency of occurrence of different cloudiness in lower and middle layer clouds together (Figure I-1) and values of N for Ci clouds (Figure I-3) are shown.

We can see from Figure I-2 that, for all the seasons, the situations which we classify as uncertain ($M > 0.7$) are found very often. For example, in the first region we find these situations in 81% of the cases for winter, and in 68% for the

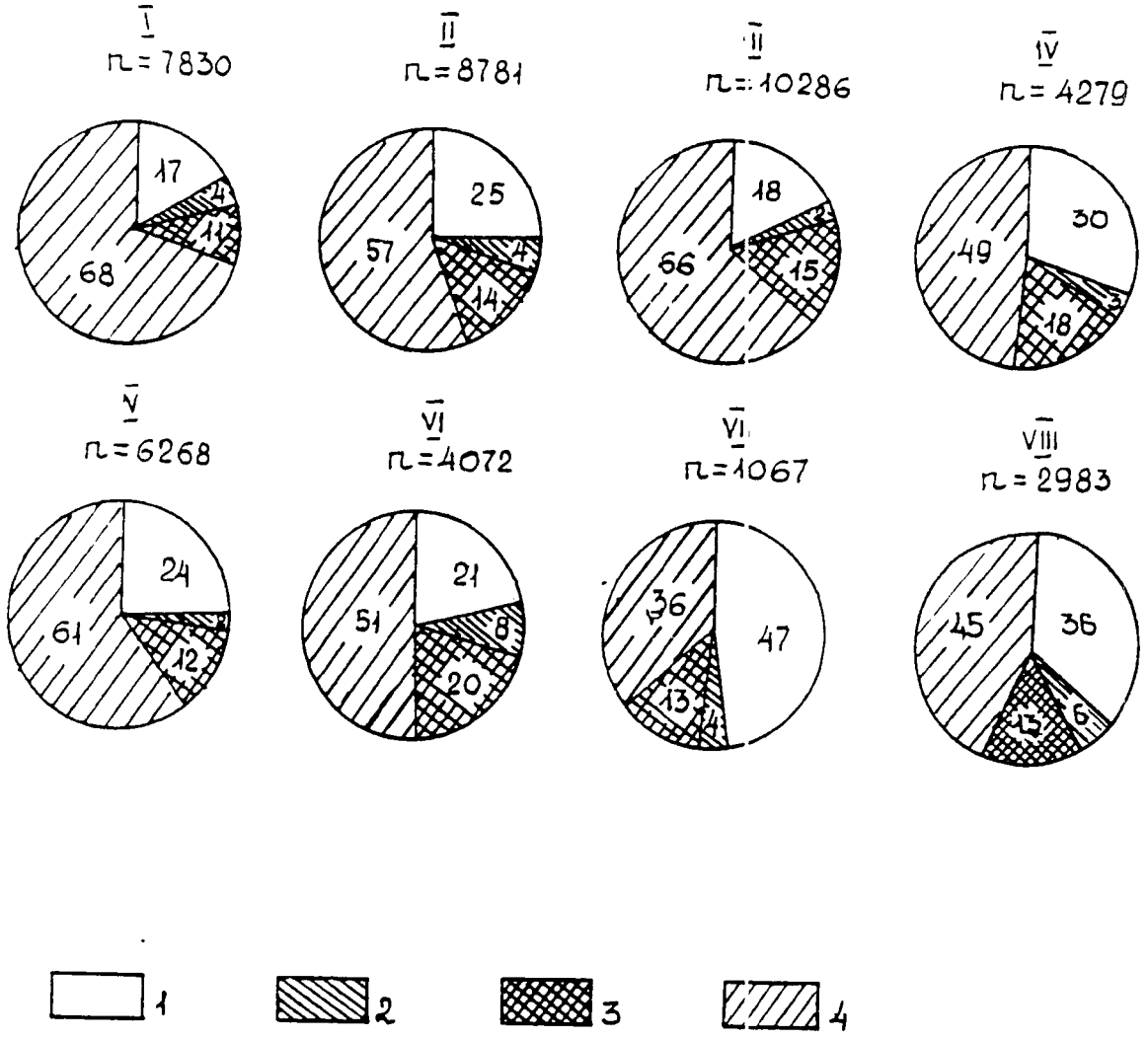

Figure I-2 Frequencies of occurrences of the total amount of clouds of lower 2 layers M (in parts of a unity) for different regions and seasons. n is the number of observations. Numbers inside the circle - frequency of occurrence percentage, a, year; b, winter; c, spring; d, summer; e, autumn. 1: M = 0; 2: 0.0 < M ≤ 0.3; 3: 0.3 < M ≤ 0.7; 4: M > 0.7.

b

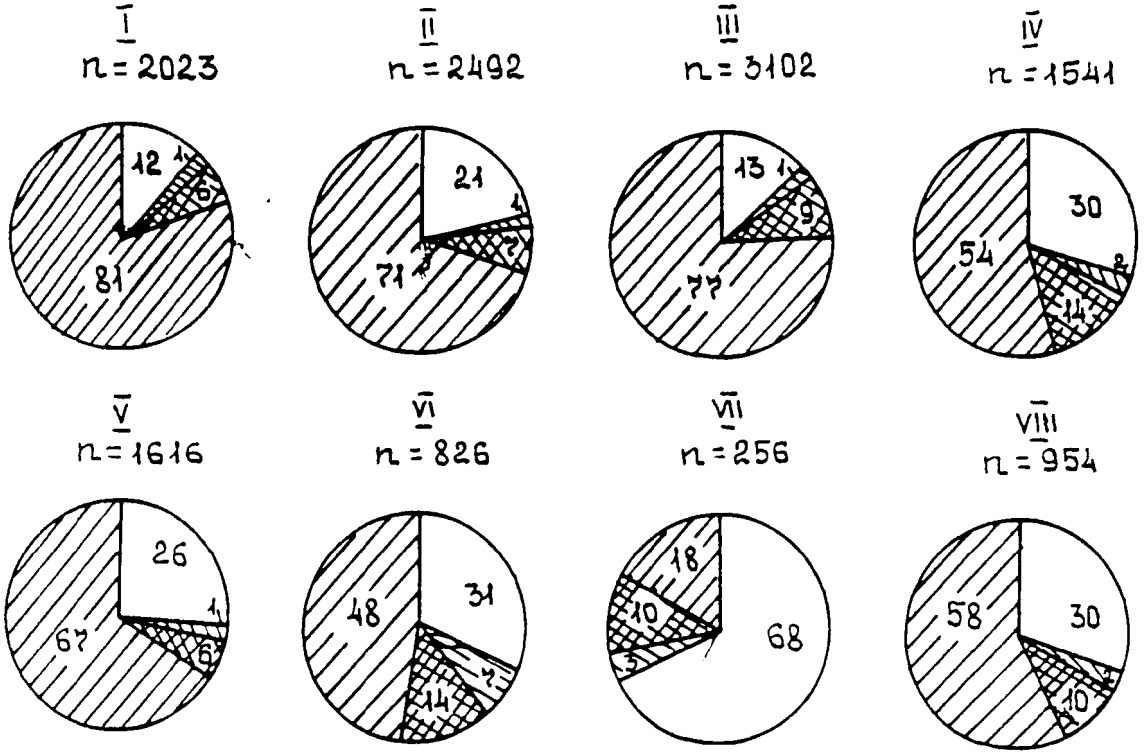

c

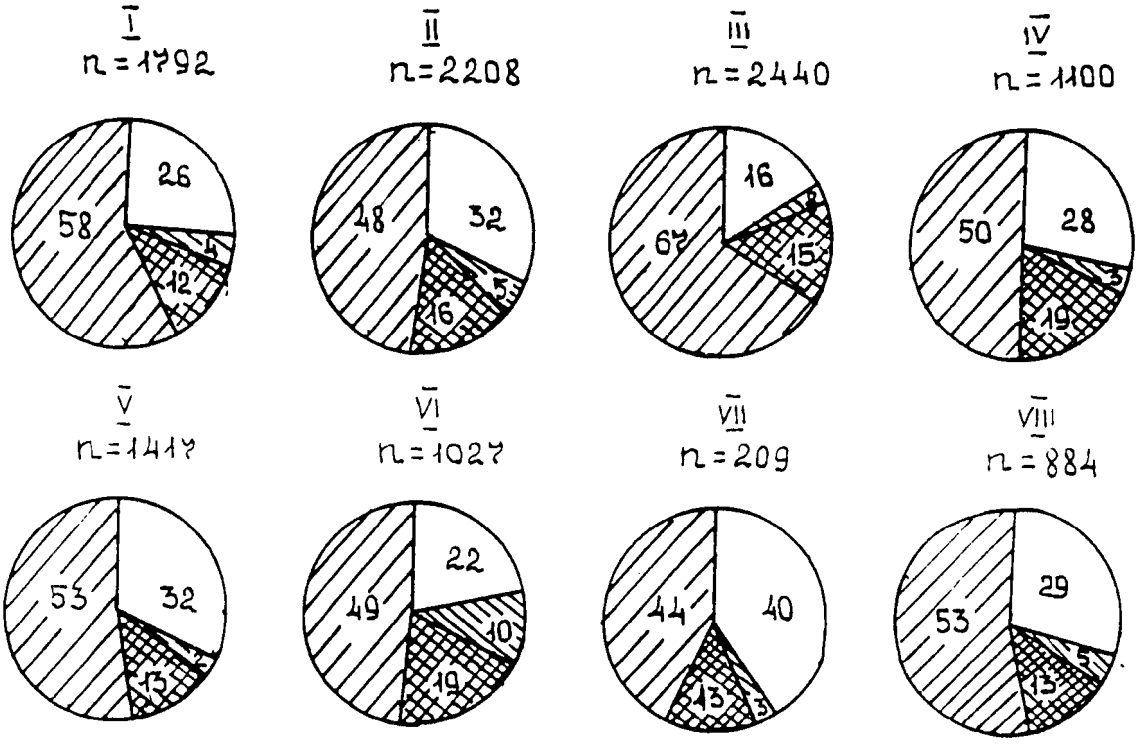

Figure I-2, Continued

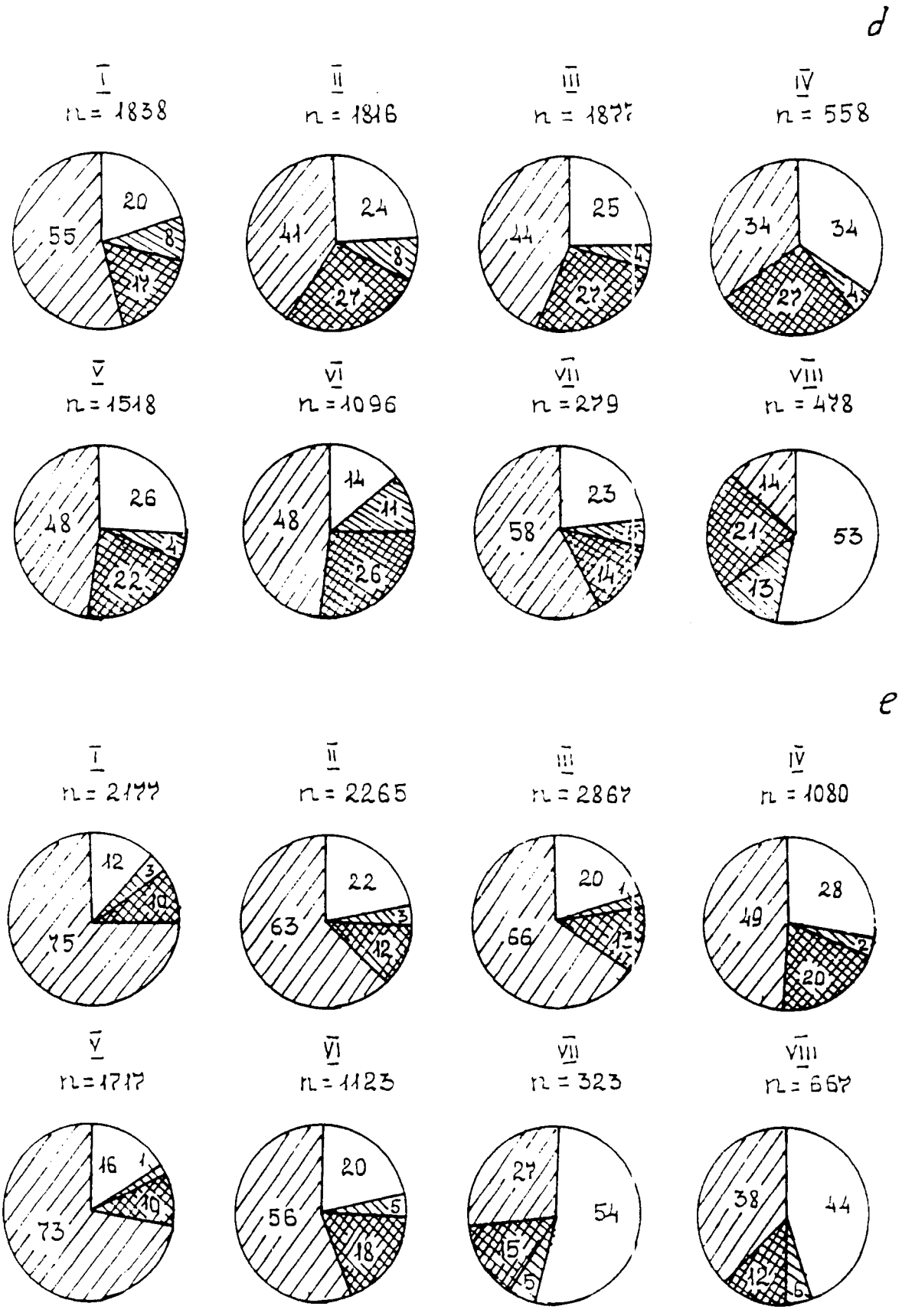

Figure I-2, Continued

a

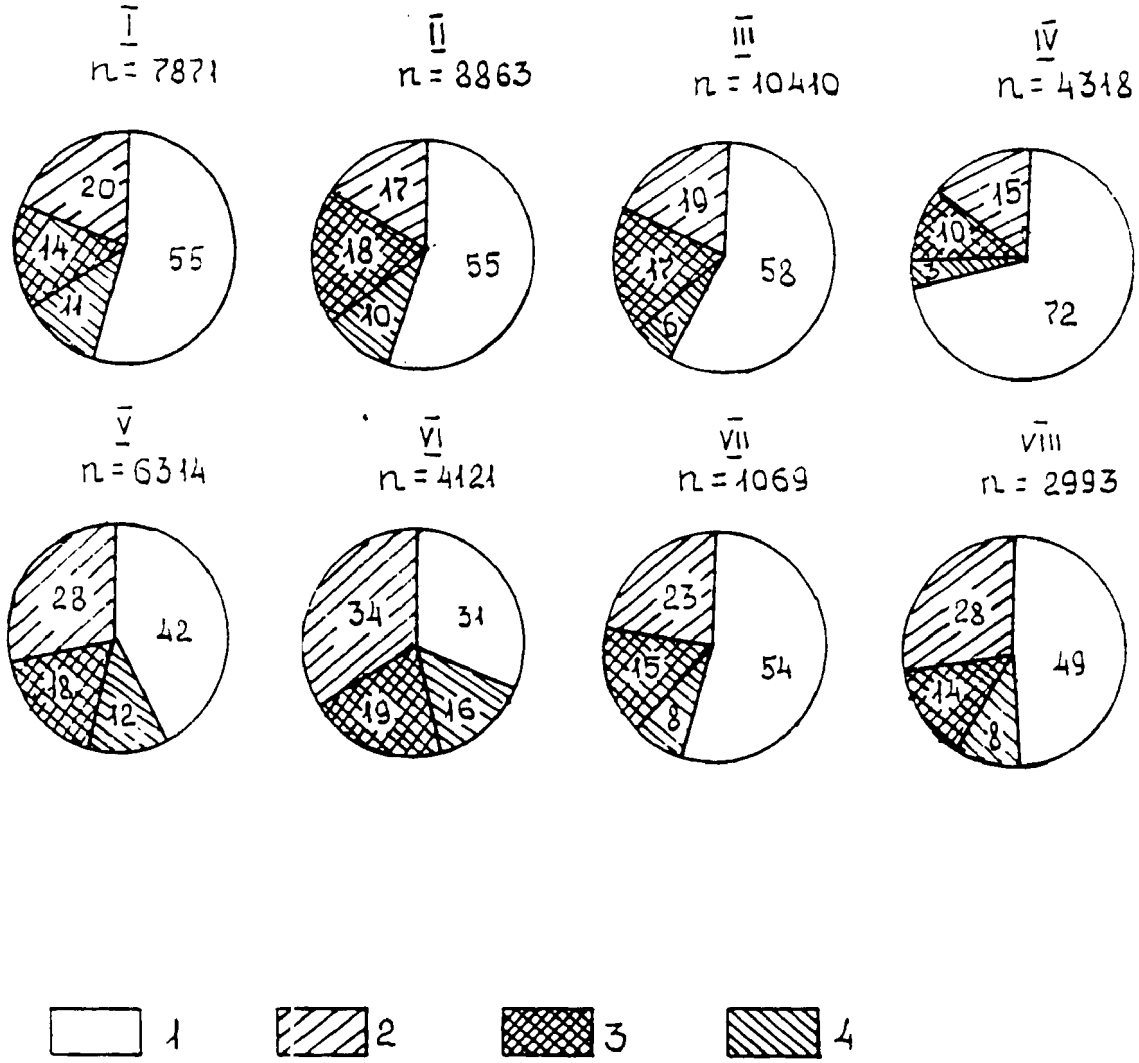

Figure I-3 Frequency of occurrence of the total amount N (in parts of a unity) of upper layer clouds for different regions and seasons. n - number of observations. Numbers inside the circle - frequency of occurrence percentage, a, year; b, winter; c, spring; d, summer; e, autumn. 1: $N = 0$; 2: $0.0 < N \leq 0.3$; 3: $0.3 < N \leq 0.7$; 4: $N > 0.7$.

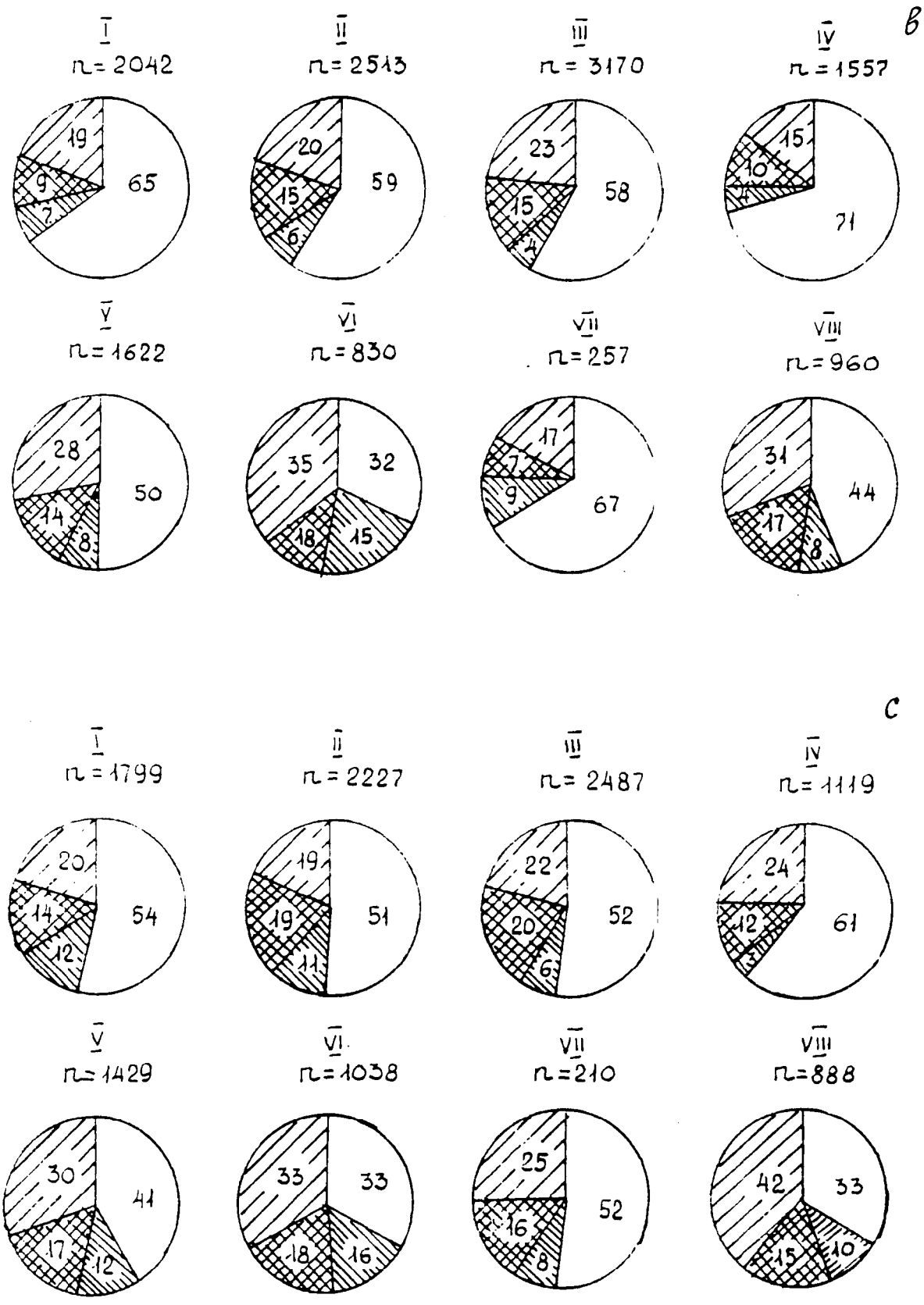

Figure I-3, Continued

d

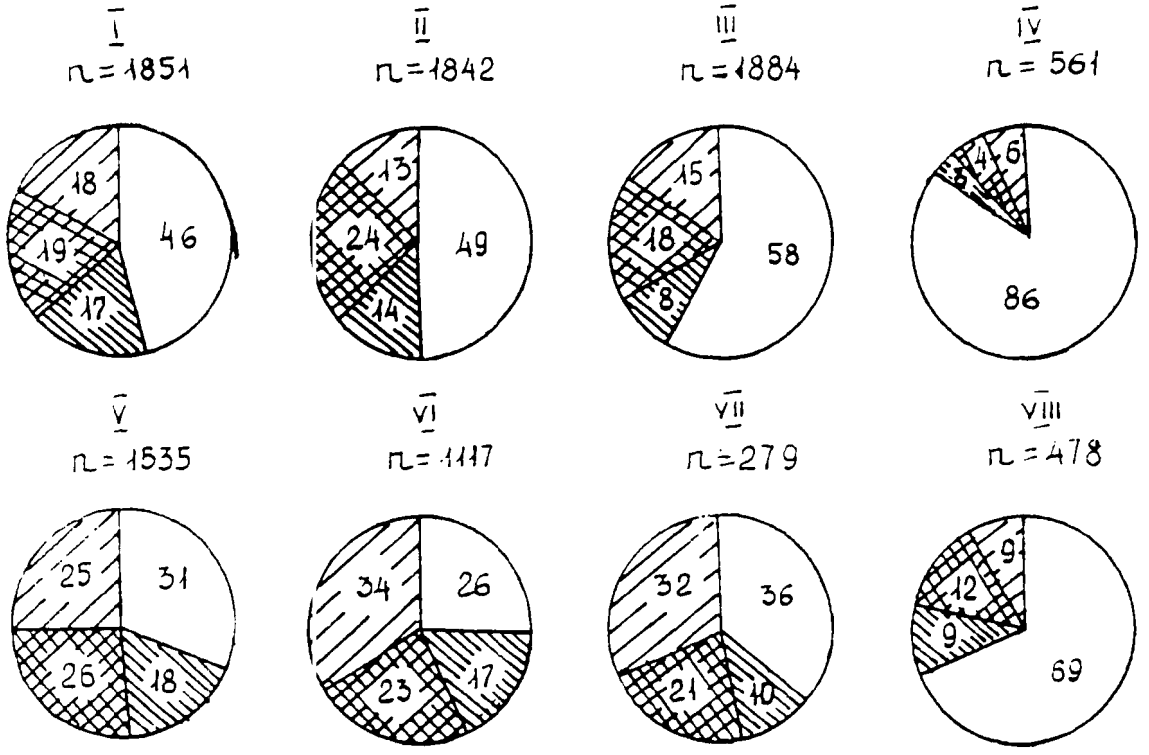

e

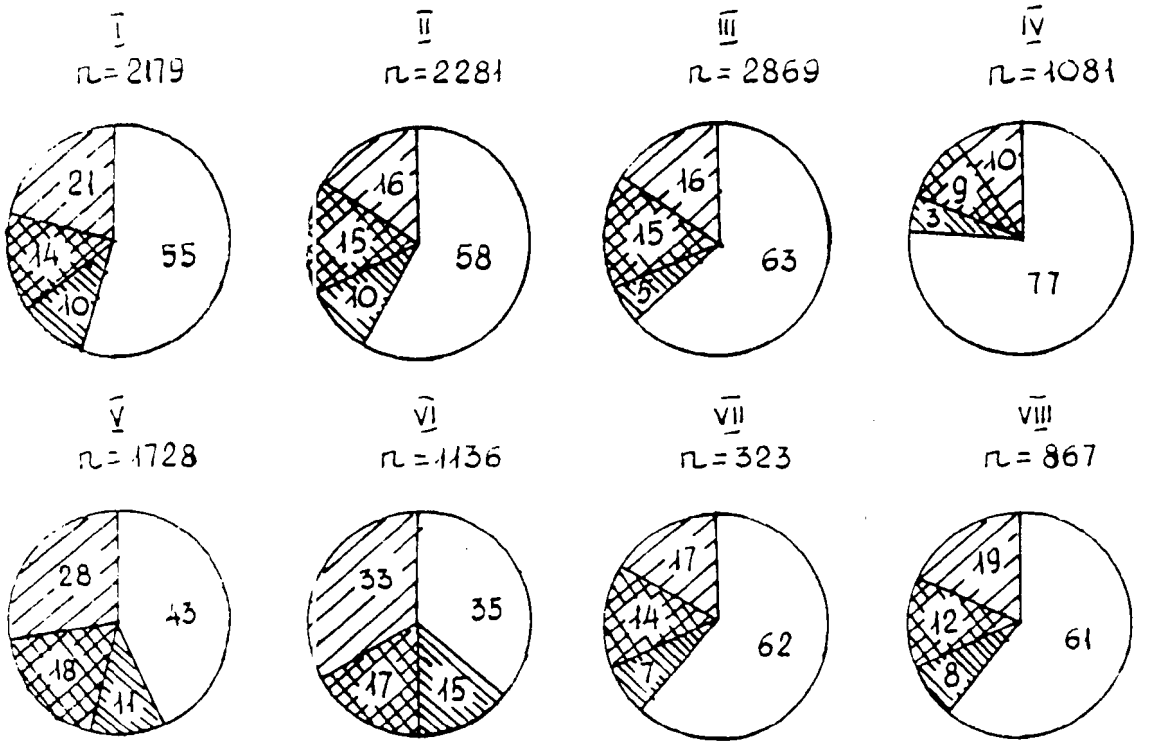

Figure I-3, Continued

whole year. In some regions such situations are less frequent. Figure I-2 shows that approximately in 50% of the cases, there are no Ci clouds at all, and in 15-30% of the cases $N > 0.7$.

To determine the effect of underlying clouds on the value of N, we divided all the observations into four series, when $M = 0$, $0 < M \leq 0.3$; $0.3 < M \leq 0.7$; and $0.7 < M \leq 1.0$. For each series of observations we calculate the distribution F(N), where F(N) is the cumulative frequency (in %) of situations when the amount of Ci clouds was not larger than N. In Figure I-4 we see variation of F(N) with M for $N = 0$; 0.3 and 0.7. If the amount N of Ci clouds was not dependent on the amount of underlying clouds M, then all the lines on the plot of Figure I-4 would be horizontal. The deviations from the horizontal lines show the degree of variability in N when M changes. In some regions, the variability, on the average, is rather small, the deviation from the horizontal line does not exceed 5%, but in some regions (especially if we speak about a period shorter than a year, i.e., seasons or months), the difference may reach 10% and sometimes even more.

Next, let us examine how the cumulative distribution F(N) may depend on the used technique of observations and data processing. For this purpose we identified distributions F(N) for the cases when $0 < M \leq 0.7$; $0.7 < M \leq 1.0$ and for all the cases ($0 \leq M \leq 1.0$). The difference between the curves marked 0-7 and 0-10 in Figure I-5 shows the possible differences in the results based on ground observations and actual ones, at least for the USSR territory. For most regions in

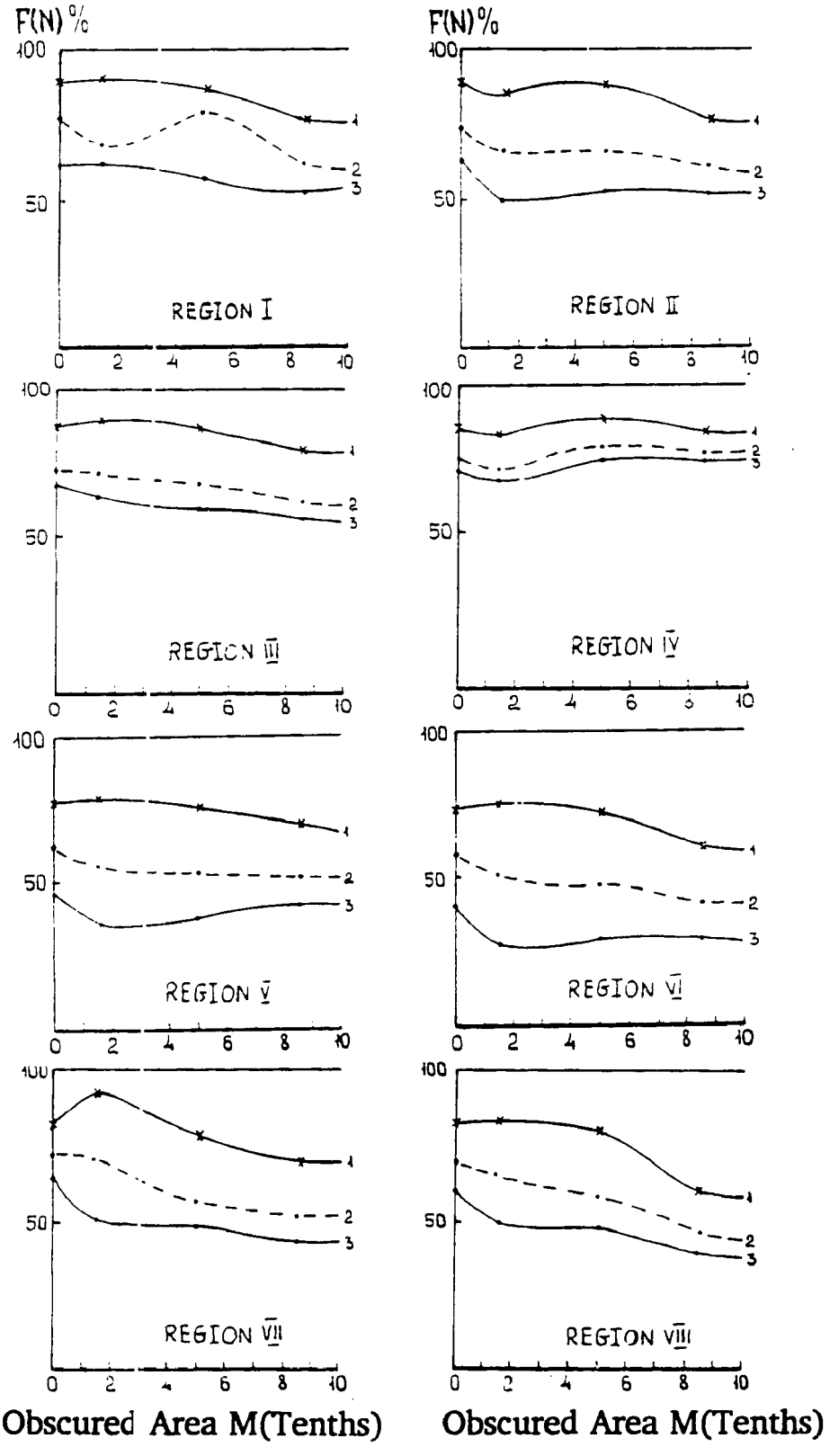

Figure I-4 Frequency of occurrence (%) in situations when cirrus clouds are absent (curve 3), their occurrence in amounts not greater than 0.3 (curve 2) and greater than 0.7 (curve 1) with different amounts of underlying clouds M.

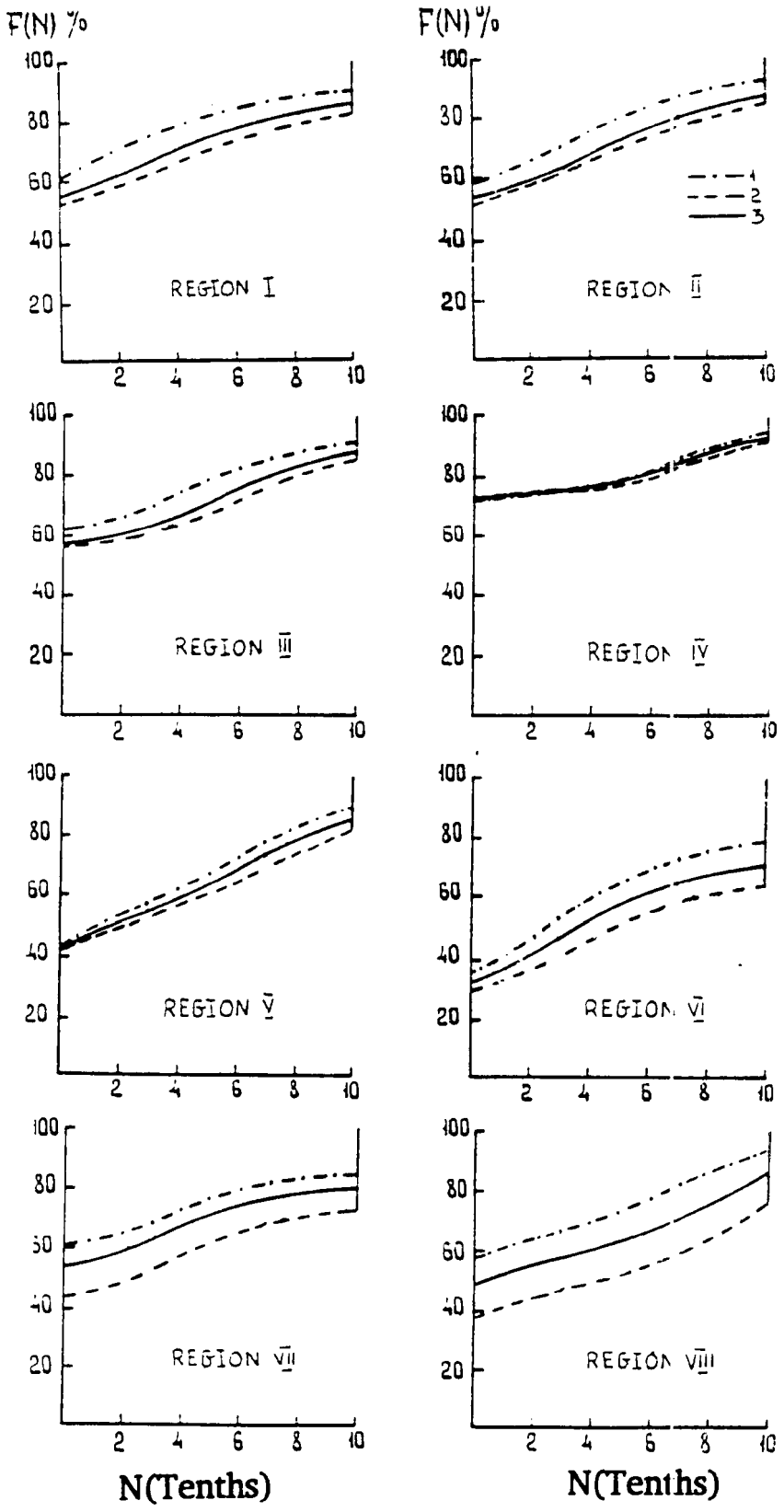

Figure I-5 Accumulated frequency F(N)% of cirrus cloud amount with different amounts of underlying clouds M (in parts of a unity). 1: $0.0 \leq M \leq <0.7$; 2: $0.7 < M \leq 1.0$; 3: $0.0 \leq M \leq 1.0$.

the USSR, the difference does not exceed 5-7%, for year-averaged values. In some regions (Central Asia, for example) the difference is 10%.

The discussed difference becomes especially noticeable, if one is interested in quantile values of N_F for $60 < F < 80\%$. As we can see from Table I-2, the difference ΔN_F for $F = 75\%$ may reach 20% even more (see the values for regions 7 and 8).

3.0 Conclusion

World meteorological centers archive data obtained at ground and ship stations all over the world for many years. Approximately only 50% of these data were used in attempts to compile a climatology of Ci clouds. The part of the data does not allow us to find the amount of Ci clouds because of uncertain situations. Nevertheless, it is of great importance that the climatology of ULC being compiled as described above, differs only slightly from the actual climatology, despite the fact that the selection of observational data was not random. This is the case for most of the USSR territory.

Thus, if we speak about F(N) - the cumulative frequency of occurrence of ULC - the value obtained from the restricted selections, Warren et al., 1986 and 1988, may deviate from an actual value by no more than 10%.

The small data set of aircraft observations does not allow us to judge this compatibility for shorter periods. If we speak about the values averaged over many years, we would not expect deviations exceeding those mentioned above. The analysis of the aircraft sounding data allows to conclude that:

For middle latitudes, at least for the Soviet territory, surface observations provide data for making statistical relations F(N) in Ci-C^3 problem with an accuracy of 10%.

The function F(N) calculated from the surface-based data, may be corrected by lowering curve F(N) by 5 to 7%.

TABLE I-2

50%, 75%, and 90% of Ci cloud frequencies of occurrences when they are incompletely screened by lower lying clouds (N_ℓ^7) irrespective of lower laying clouds (N_ℓ^{10}) and difference $\Delta N = N_\ell^{10} - N_\ell^7$.

F (%)	winter			spring			summer			autumn			year		
	N_ℓ^7	N_ℓ^{10}	ΔN	N_ℓ^7	N_ℓ^{10}	ΔN	N_ℓ^7	N_ℓ^{10}	ΔN	N_ℓ^7	N_ℓ^{10}	ΔN	N_ℓ^7	N_ℓ^{10}	ΔN
1	2	3	4	5	6	7	8	9	10	11	12	13	14	15	16
								REGION I							
50	0.0	0.0	0.0	0.0	0.0	0.0	0.0	0.0	0.0	0.0	0.0	0.0	0.0	0.0	0.0
75	2.0	4.2	2.2	3.0	5.4	2.4	3.2	5.2	2.0	3.2	6.0	2.8	3.0	5.1	2.1
90	9.4	10.0	0.6	10.0	10.0	0.0	7.6	10.0	2.4	8.2	10.0	1.8	9.0	10.0	1.0
								REGION II							
50	0.0	0.0	0.0	0.0	0.0	0.0	0.0	0.5	0.5	0.0	0.0	0.0	0.0	0.0	0.0
75	4.3	6.0	1.7	4.3	5.4	1.1	4.0	5.0	1.0	3.5	4.5	1.0	3.9	5.6	1.5
90	8.3	10.0	1.7	9.0	10.0	1.0	7.0	8.2	1.2	8.0	10.0	2.0	8.0	10.0	2.0
								REGION III							
50	0.0	0.0	0.0	0.0	0.0	0.0	0.0	0.0	0.0	0.0	0.0	0.0	0.0	0.0	0.0
75	5.1	6.2	1.1	5.0	6.1	1.1	3.3	4.6	1.3	3.6	4.5	0.9	4.0	5.7	1.7
90	10.0	10.0	0.0	10.0	10.0	0.0	7.5	10.0	2.5	8.8	10.0	1.2	9.4	10.0	0.6
								REGION IV							
50	0.0	0.0	0.0	0.0	0.0	0.0	0.0	0.0	0.0	0.0	0.0	0.0	0.0	0.0	0.0
75	3.0	3.0	0.0	7.0	7.0	0.0	0.0	0.0	0.0	0.0	0.0	0.0	3.0	3.0	0.0
90	8.3	10.0	1.7	10.0	10.0	0.0	3.0	3.8	0.8	6.6	7.4	0.8	8.6	9.1	0.5
								REGION V							
50	0.0	0.0	0.0	2.0	2.8	0.8	2.7	3.1	0.4	2.2	2.2	0.0	1.4	1.9	0.5
75	5.4	8.0	2.6	8.2	10.0	1.8	6.1	7.0	0.9	7.0	8.3	1.3	6.7	7.4	0.7
90	10.0	10.0	0.0	10.0	10.0	0.0	10.0	10.0	0.0	10.0	10.0	0.0	10.0	10.0	0.0

TABLE I-2, Continued

F (%)	winter N_ℓ^7	winter N_ℓ^{10}	winter ΔN	spring N_ℓ^7	spring N_ℓ^{10}	spring ΔN	summer N_ℓ^7	summer N_ℓ^{10}	summer ΔN	autumn N_ℓ^7	autumn N_ℓ^{10}	autumn ΔN	year N_ℓ^7	year N_ℓ^{10}	year ΔN
1	2	3	4	5	6	7	8	9	10	11	12	13	14	15	16
								REGION VI							
50	0.0	0.0	0.0	2.4	3.3	0.9	3.3	4.3	1.0	2.2	3.1	0.9	2.7	3.7	1.0
75	7.5	9.4	1.9	7.0	10.0	3.0	8.0	10.0	2.0	7.0	10.0	3.0	7.6	10.0	2.4
90	10.0	10.0	0.0	10.0	10.0	0.0	10.0	10.0	0.0	10.0	10.0	0.0	10.0	10.0	0.0
								REGION VII							
50	0.0	0.0	0.0	0.0	0.0	0.0	3.3	3.5	0.2	0.0	0.0	0.0	0.0	0.0	0.0
75	0.0	6.1	6.1	6.6	7.3	0.7	10.0	10.0	0.0	3.0	4.6	1.6	4.6	6.3	1.7
90	3.0	9.2	6.2	10.0	10.0	0.0	10.0	10.0	0.0	8.2	10.0	0.8	10.0	10.0	0.0
								REGION VIII							
50	1.6	2.8	1.2	2.8	5.0	2.2	0.0	0.0	0.0	0.0	0.0	0.0	0.0	0.4	0.4
75	6.5	9.0	2.5	8.2	10.0	1.8	1.8	2.4	0.6	2.9	3.9	1.0	5.6	8.1	2.5
90	10.0	10.0	0.0	10.0	10.0	0.0	6.2	7.0	0.8	10.0	10.0	0.0	9.1	10.0	0.9

4.0 Representativeness of aircraft observations

The conclusions made above are based on aircraft observations performed at the aircraft sounding stations, but aircraft soundings were not as regular as routine weather observations. The representativity of the aircraft sample is not known, a priori. In other words, we have to understand how much the cloud climatology based on ASS data may deviate from the actual one. To do this, we compare the ASS and weather observational data included in the synoptic reports. For this purpose, we chose 10 arbitrary stations in different regions, marked with crosses in Figure I-1. The numbers of aircraft and routine weather observations for each station in each season are indicated in Table I-3. Aircraft soundings were missing in approximately 20 to 40% of the cases. In Yakutsk the absence of aircraft soundings is very evident; therefore this station was not used in the analysis. To estimate the degree of randomness of missing cases, we compare the clear sky situations in both aircraft and ground observations. It is evident that clear sky situations may be distinguished with a high degree of confidence in any (aircraft or ground) observations.

In Figure I-6 the diurnal course of the clear sky situations δ_g(%) at the chosen stations in all the seasons, year-averaged, are presented. Worthy of note is the fact that in daytime (13.00) the frequency of clear sky occurrence is the least. This may be explained by the more frequent occurrence of convection at that time and, also, by the fact that it is difficult to observe the small amount of Ci clouds at night time.

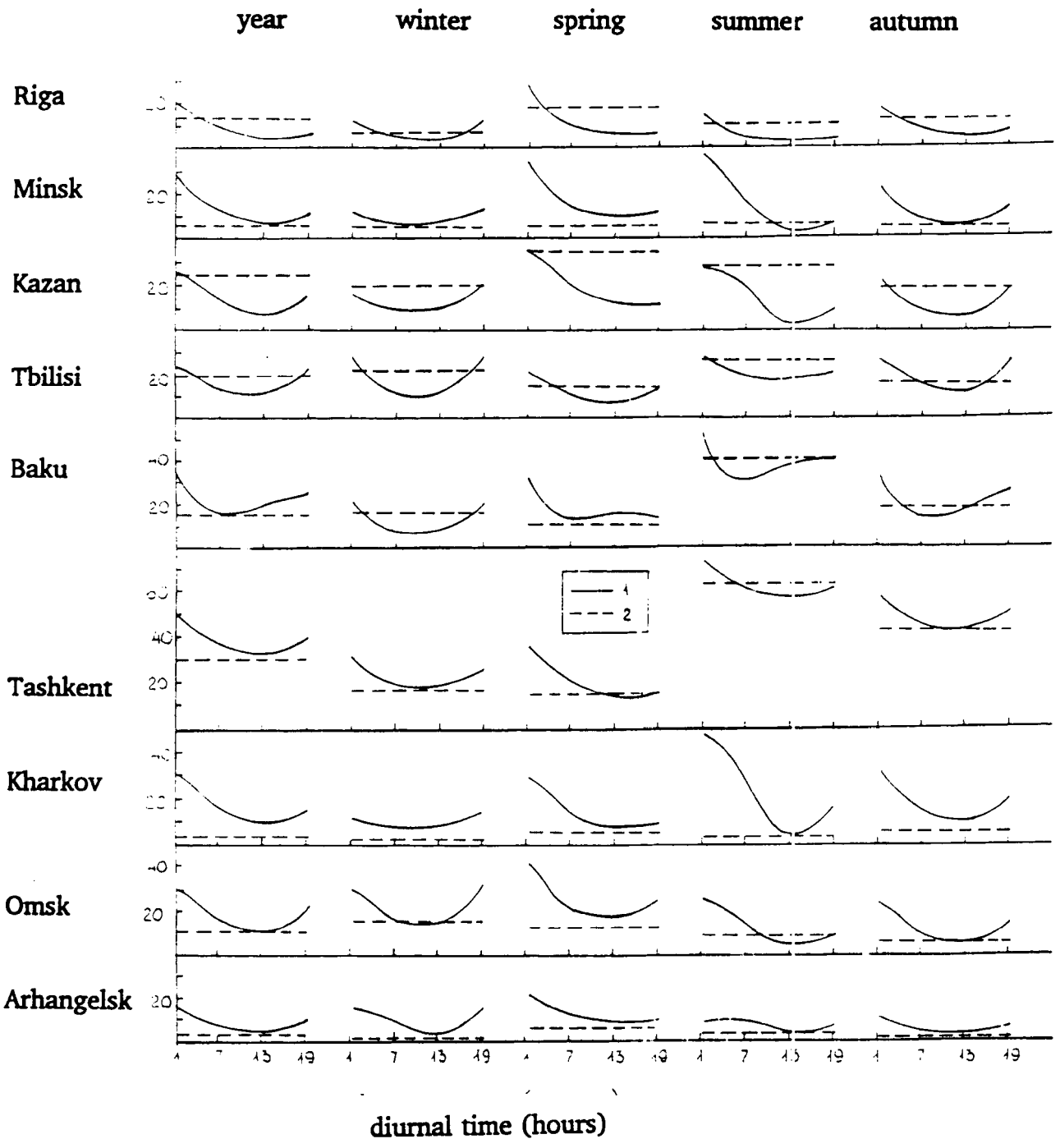

Figure I-6 Frequency of cloudless situations δ(%) for different stations averaged over a year and seasons. 1 δ_g - daily course according to surface observations, 2 δ_a - data from aircraft sounding.

Table I-3

Number of aircraft soundings and surface-based (one-term) observations in 1958-1963 included into the statistics for intercomparison.

Season	Arkhan gelsk	Riga	Minsk	Kharkov	Kazan	Tbilisi	Baku	Omsk	Tashkent	Yakutsk
Winter	459/539	436/537	419/540	390/540	503/540	591/494	608/455	337/539	466/532	69/540
Spring	357/545	439/531	284/546	303/541	328/546	490/482	362/499	345/540	399/519	66/540
Summer	432/517	359/518	320/539	279/529	251/531	451/486	41/498	433/513	226/528	75/515
Autumn	542/538	447/530	428/542	366/542	359/540	539/504	336/479	383/538	348/531	123/537
Year	1790 2139	1681 2116	1451 2166	1338 2151	1441 2158	2071 1965	1347 1932	1498 2130	1439 2111	333 2131

In the same figure, values δ_a representing the clear sky situations of aircraft observations are marked by straight dotted lines. In four of the nine cases (Kharkov, Omsk, Arkhangelsk, Minsk) $\delta_a < \delta_{g,min}$, for all seasons while in Baku and Tashkent $\delta_a \approx \delta_{g,min}$, in Tbilisi and Riga $\delta_a > \delta_{g,av}$. We believe that the largest number of missed aircraft soundings were for clear cloudless situations. Basically, the frequencies of occurrences of cloudless situations obtained with aircraft and ground observations is 10% of the total number of observations. Let us note this estimate and move on to the comparison of accumulated frequencies of occurrences of Ci amount, F(N), according to the aircraft and ground observations.

Shown in Figure I-7 are the year- and season averaged values of Fg(H) for all 10 stations. As a rule, the amount of Ci clouds is higher in the daytime (1300 hrs) and less at night time (0100 hrs). This is not surprising since at night, it is more difficult to observe Ci clouds visually.

In Riga, Minsk, Arkhangelsk and Kazan, the frequency of Ci clouds observed at night is noticeably less 15....20% . On the whole for all the chosen stations, the frequency of occurrence $F_g(N)$ varied in the range of 10-30% depending on time of observations.

The different signs in Figure I-7 refer to different terms of observations and to the situations when N could be determined, i.e., when the amount of underlying

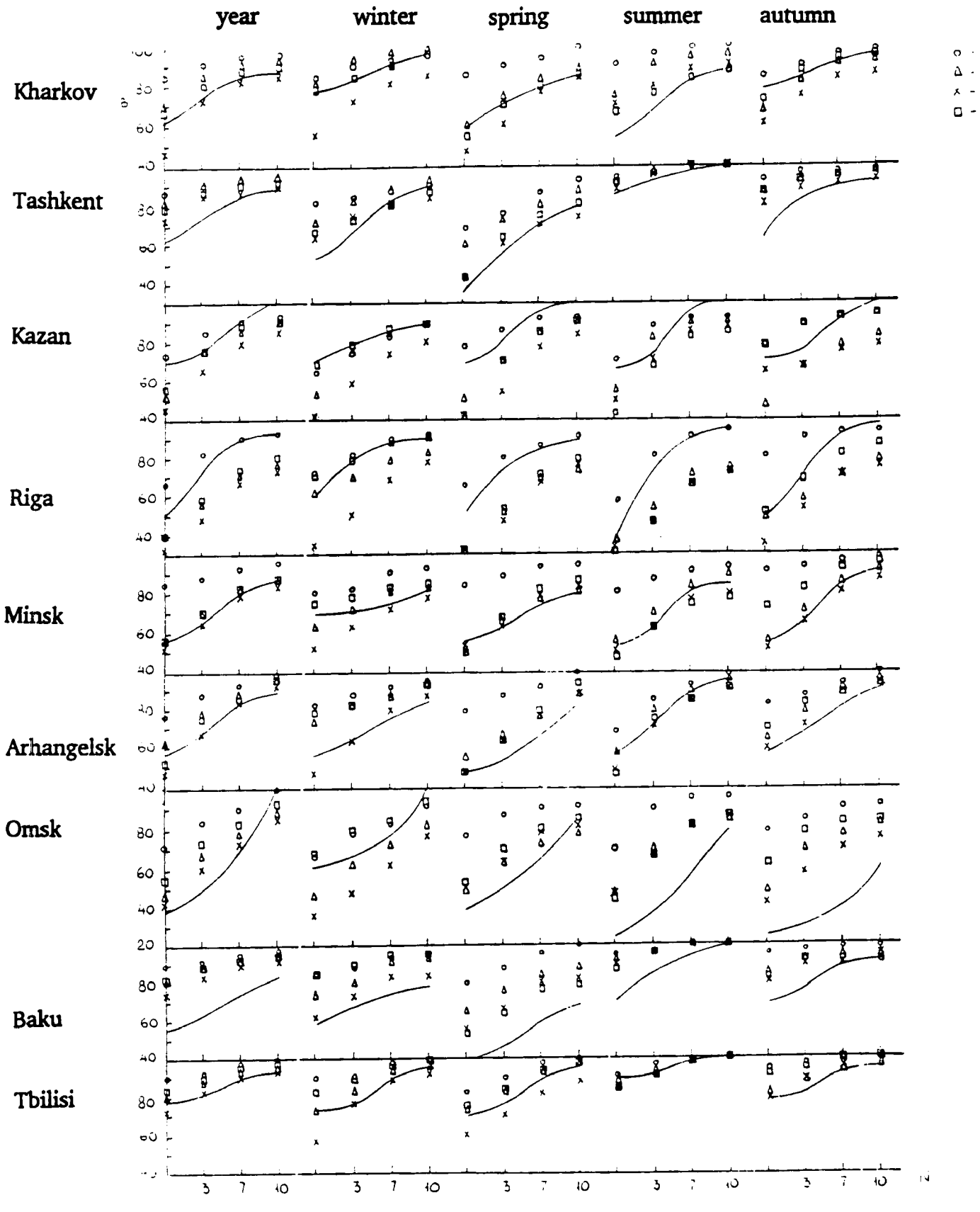

Figure I-7 Accumulated frequency F(N) (%) of Ci clouds amount (N - in tenths) for 4 series of surface observations (1: 0.1 hrs; 2: 0.7 hrs; 3: 13 hrs; 4: 19 hrs) and for aircraft sounding data (solid lines) for different stations averaged over a year and seasons.

clouds M did not exceed 0.7, and at the same time, when clouds were present in the sky in no more than two layers. Curve Fa(N) corresponds to aircraft data for the cases, when $M \leq 0.7$.

The comparison of $F_g(N)$ with $F_a(N)$ shows that differences $\Delta F = F_a(N)-F_g(N)$ between aircraft and ground observations for all stations and seasons mainly do not exceed the limits of the diurnal course. In Baku the frequency of presence of Ci clouds according to aircraft observations was 10-15% less compared to daytime ground observations, and in Omsk this difference was even more. It reached 20% in summer and autumn.

The comparison of the frequency of occurrence of different amounts, N, of Ci clouds obtained with aircraft $F_a(N)$ and ground $F_g(N)$ observations with the amount of underlying clouds $M < 0.7$, leads us to conclude that aircraft data define the values of F(N) within 10...15% of the ground values. Most of the missed aircraft soundings fall on cloud free situations; therefore, appropriate corrections may be made and biases may be diminished and become half as much.

Within the limits of these deviations we may consider the aircraft data to be representative of the statistics of Ci amounts for different seasons and annual averages. Within these limits the conclusions from Section 3 of the present paper should be considered reliable. One may overlay the ground observational data on the amount of Ci clouds obtained in the cases when $M \leq 0.7$ for all possible cases, i.e., for an arbitrary value of M keeping in mind possible biases mentioned above.

In summary, we conclude, that Ci-C^3 problem may be solved on the basis of routine weather observations with the accuracy satisfying the present needs.

REFERENCES

Berlyand, T. G. and P. A. Strokina, 1980: Global distribution of total amount of clouds (in Russian). Leningrad, Gidrometeoizdat, 71 pages.

Burkovskaya, S. N., E. T. Ivanova and I. P. Mazin, 1990: On overlapping of cirrus clouds with lower clouds over the USSR (in Russian). Meteorologia i Gidrologia, N3, 11-17.

Makhover, Z. M. and L. A. Nudelman, 1987: Aviation and climatic characteristics of the Northern Hemisphere. V.1. Cloudiness (in Russian). Hydrometeorological Research Center of the USSR. Moscow, Gidrometeoizdat, 3-10, 218 maps.

Warren, S. G., C. Y. Hahn, J. London, R. M. Chervin and R. L. Jenne, 1986: Global distribution of total cloud cover and cloud type amounts over land. NCAR/TN-273 STR, Boulder, Colorado, 29 pages and 199 maps.

Warren, S. G., C. J. Hahn, J. London, R. M. Chervin, R. L. Jenne, 1988: Global distribution of total cloud cover and cloud type amounts over the ocean. NCAR/TN-317+STR, Boulder, Colorado, 42 pages and 170 maps.

APPENDIX II

Scattering of Light by Crystal Clouds

by L. N. Pavlova and A. G. Petrushin

The present paper presents some results of the theoretical and experimental studies of optical characteristics of crystal and mixed ice/water clouds.

The experimental works were carried out in the cooling chamber (100 m^3 in volume) at the Institute of Experimental Meteorology (Obninsk, Kaluga region). The cloud medium created in the chamber contained crystals with habits and size ranges corresponding to those observed in high clouds and crystal fogs. This medium was formed by introducing Ag I nuclei into a super cooled droplet fog.

A system of various instruments for the measurement of the cloud medium's optical and microstructure characteristics was used in the experiments. First, to determine the phase condition of the cooling chamber medium, a measurement of the depolarization relation $D(\pi)$ in the back scattered direction measurement was used. Second, to study the microstructure characteristics in addition to the commonly applied replicator method, video imaging techniques were used. The minimum particle size (diameter) detected by the device was 5-7 μm. Third, to measure the scattering phase functions ($P(\theta)/4\pi$) an instrument was used with the angular aperture of the receiver 0.015°. It provided measurements in the scattering angle range $\theta \sim 10°$ to 170° for 10 sec time intervals. This allowed us to observe the scattering phase function for relatively small ice crystals ($<70\mu$m).

The results of an experiment with an initial drop medium which gradually crystallized are given in Figure II-1. Experimental values obtained for the drop medium correlate well with estimated values for the model C.1 [Deirmendjan, 1969]. In the experiment with a crystallized fog, crystals with the plate form 4-50 μm in size were formed with 30% aggregates consisting of 2-3 particles. As crystal generation increases, the maximum in the phase scattering functions at scattering angle $\theta \approx 22°$ corresponding to the minor halo circle appears and a relative part of the intensity of radiation scattered in the side directions increases. The variation of the scattering radiation angle distribution in the medium obtaining columnar crystals is similar to the one given in Figure II-1 at the corresponding $D(\pi)$ values.

Figure II-2 shows the mean, normalized phase scattering function for crystals of different shape and size (crystals - columns 20-25 μm diameter, plates with the modal diameter 50 μm and a combination of plates and combination of plates and columns (curve 2), as well as the phase scattering function of the drop cloud (curve 1). The data show that the influence of crystal shape and size on the phase scattering function results in the mean spread within limits of ± 30%. Thus the crystals have a greater effect on the radiation scattering than the drops for angles 60-140° compensating for the decrease of scattering at $\theta \sim 2° - 40°$. The experimental phase scattering function is in satisfactory agreement with the estimated phase scattering function for a crystal medium within the scattering angle range $\theta \sim 20° - 170°$.

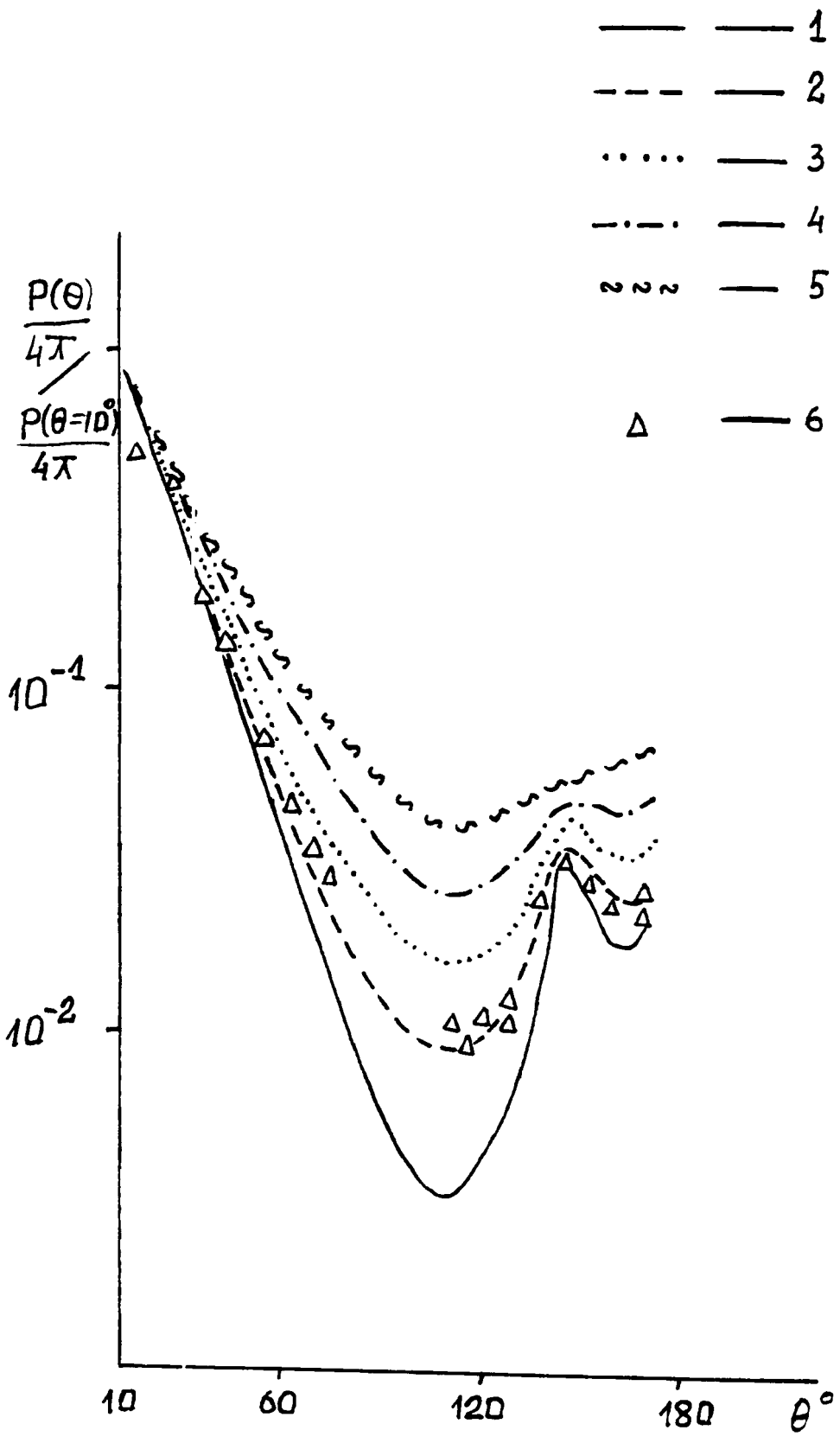

Figure II-1 The variation of the normalized phase scattering functions ($P(\theta)/4\pi$: $P(\vartheta = 10^{\circ})/4\pi$) with the increasing $D(\pi)$. 1: drops, the estimated values; 2: drops, the experimental values; 3: $D(\pi) = 0.08$; 4: $D(\pi) = 0.15$; 5: $D(\pi) = 0.25$; 6: $D(\pi) = 0.40$.

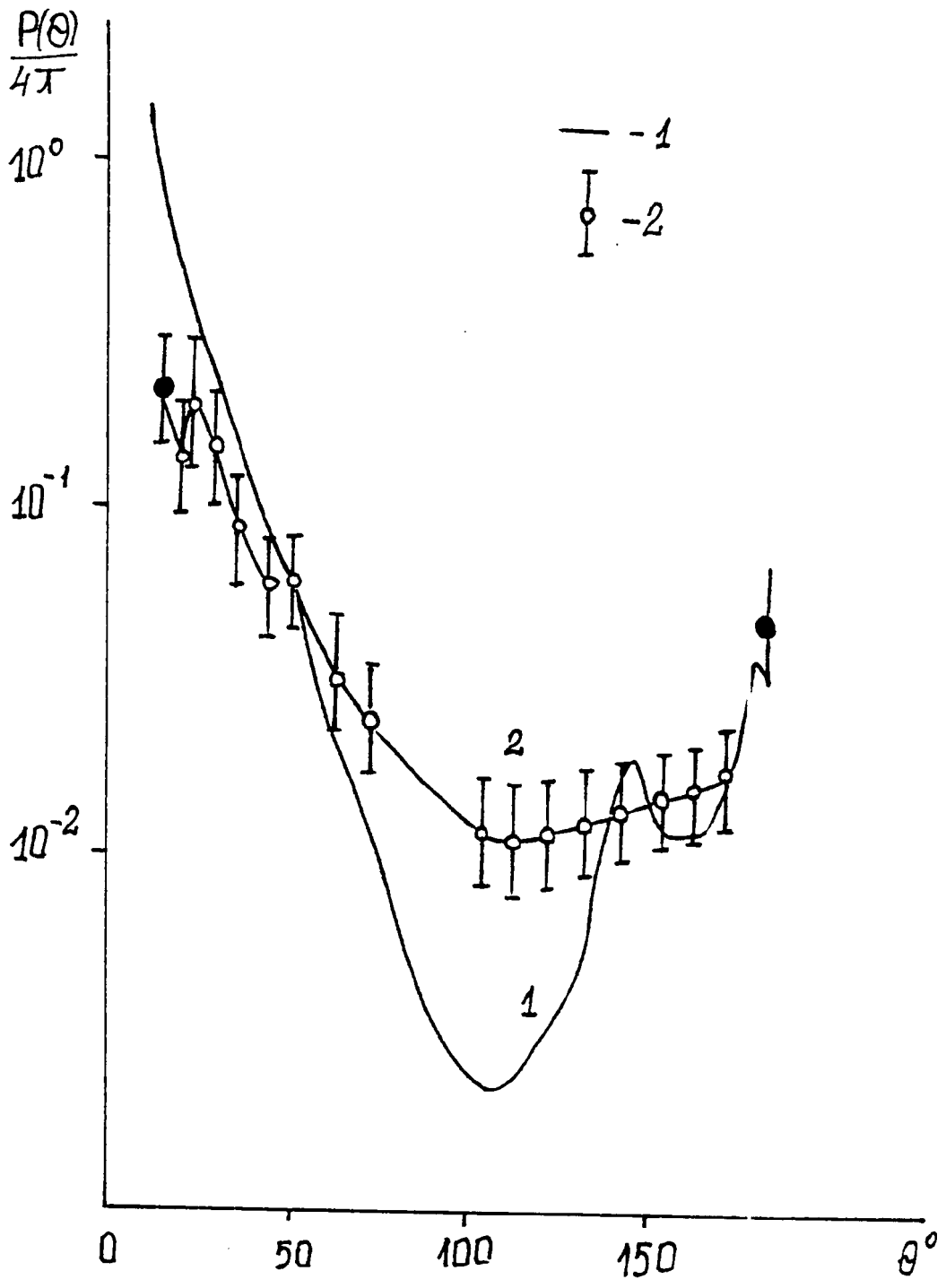

Figure II-2 The phase scattering functions of the drop and crystal cloud media. 1: drops, 2: crystals of different shape and size.

$$\frac{P(\theta)}{4\tau} - \frac{1}{2}T\left(\frac{\tau}{2}-\frac{\theta}{2}\right)\left[\frac{3}{4}+\frac{1}{4}T_o\left(\frac{\tau}{2}-\frac{\theta}{2}\right)\right]$$

here

$$T\left(\frac{\tau}{2}-\frac{\theta}{2}\right) - \frac{2T_o\left(\frac{\tau}{2}-\frac{\theta}{2}\right)}{1+T_o\left(\frac{\tau}{2}-\frac{\theta}{2}\right)}$$

T_o $(\tau/2 - \theta/2)$ is the Fresnel reflection coefficient.

In the case of random orientation of particles in space, the scattering phase function for unpolarized light depends only upon the scattering angle, therefore an asymmetry of the optical properties of this medium should not be observed. However in the real crystal medium where only a portion of the crystals may have a predominant orientation, the experimentally observed and calculated ratios of phase scattering function in the horizontal (h) and vertical (v) planes of observation for $\theta = \pi/2$ shows that $P(\theta)/4\pi \mid_h / P(\theta)/4\pi \mid_v$ < 2 can be expected.

The experimentally observed and calculated difference of the scattering functions for different planes do not exceed the divergence between the maximum and minimum values $P(\theta)/4\pi$ measured in one plane. Therefore, when the averaged phase scattering function of the crystal cloud is presented in the first approximation, the asymmetry of the scattering phase function may be neglected.

APPENDIX III

Occurrence and Radiative Properties of Upper Level Clouds under Various Climatic Conditions

This paper reports results of investigations of cirrus clouds' effects upon direct, diffuse and global radiation, deduced from long-term actinometric observations in regions with various climatic conditions.

3.1 Occurrence of upper level clouds and their effects on solar radiation deduced from ground-based observations in Moscow

by G. M. Abakummova, T. V. Evnevich, O. M. Izakova,

E. I. Nezval' N. E. Chubarova and O. A. Shilovtseva

3.1.1 Cirrus cloud occurrence

In order to study the frequency of cirrus cloud occurrence, hourly cloud amount observations performed by the Moscow State University meteorological observatory within the period of 1968 to 1985 (number observations - 131490) have been used.

Total sky cover (P 10/10) for high level clouds comprises 3.9 per cent of the time interval. P 10/10 is at a maximum during the spring period (40.8 per cent - March to May) and it is a minimum in summer (14.8 per cent) (see Table III-1). Diurnal changes in P are slight: coefficient of variation is equal to 8%. The P maximum takes place in morning hours, while it is minimum in daytime and evening hours. There is no obvious tendency for P to change from year to year.

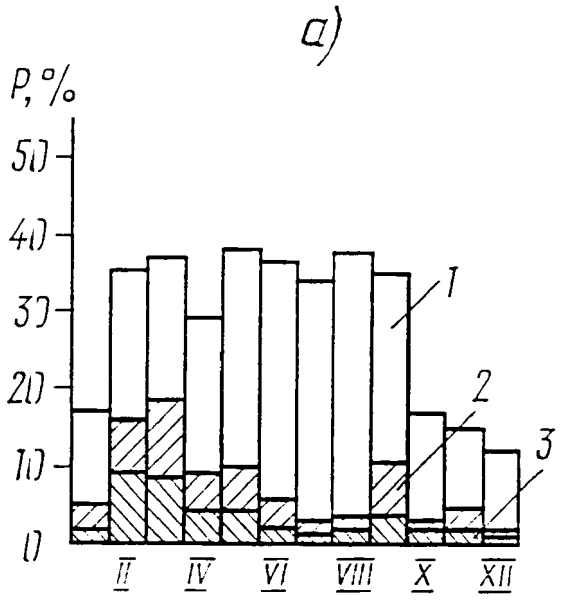

a) all observations:
1: Ci and other types of clouds;
2: only Ci;
3: continuous cover of Ci

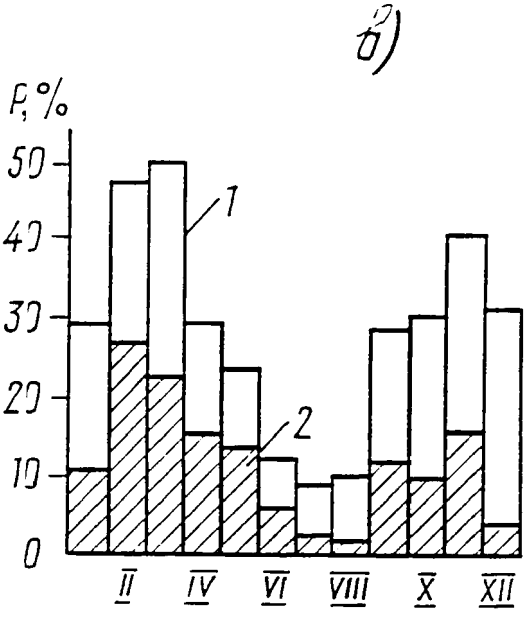

b) all observations with high level clouds:
1: only Ci;
2: continuous cover of high level clouds.

Figure III-1 Frequency of high level clouds.

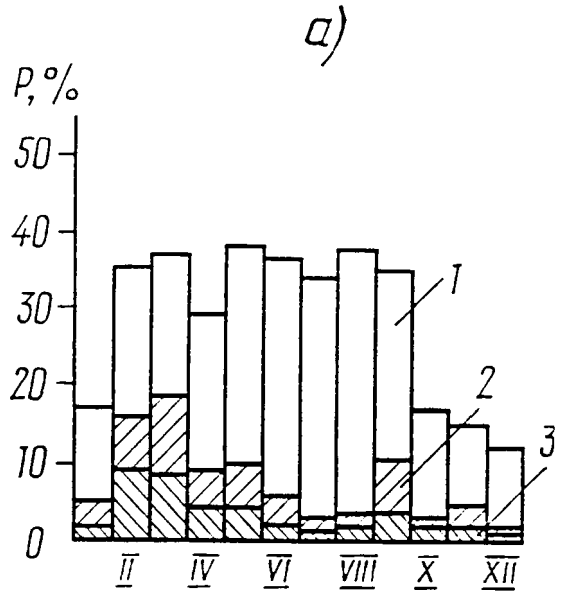

a) all observations:
1: Ci and other types of clouds;
2: only Ci;
3: continuous cover of Ci

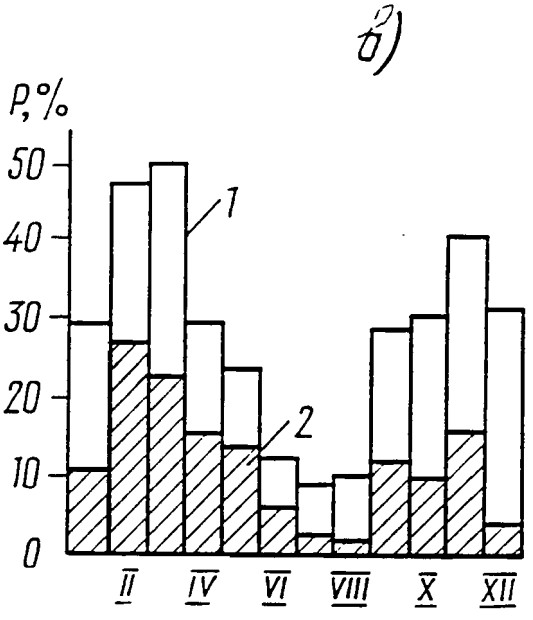

b) all observations with high level clouds:
1: only Ci;
2: continuous cover of high level clouds.

Figure III-1 Frequency of high level clouds.

TABLE III-1

Frequency (P) of continuous cover of high level clouds in %

Months	Jan.	Feb.	March	April	May	June	July	August	Sept.	Oct.	Nov.	Dec.
p	9.6	13.9	17.1	12.4	11.3	5.6	3.6	5.6	6.4	6.2	4.3	4.0

The analysis of synoptic situations in the 1971-1985 data set (January, May, July and October) revealed that a continuous cirrus cover without lower layers of clouds is most likely to be observed at the peripheries of anticyclones (15 to 30 per cent). As a whole, in an anticyclonic field, high level clouds are noted in from 52 to 55 per cent of the events in May, July, October and in 69 per cent of the events in January. In a low gradient field Ci are present 20 to 26 per cent of the time, in autumn (October) it is noticeably greater (40 per cent) (see Table III-2). In cyclones, notably due to observation by low and middle clouds, a continuous cirrus cover is observed only in 10 to 15 per cent of the events.

Using upper air maps in the analysis of the 1983 to 1985 data for cold (months: December-March) and warm (months: May-September) periods, continuous cover of high level clouds appeared just ahead of the ridge in northwesterly flow 49 per cent of the time. During the warm period in 39 per cent of the events, Moscow found itself right at an anticyclonic ridge which benefited the formation of clouds at great heights and prevented development of convective cloudiness as well.

To study in more detail the occurrence of high level clouds use has also been made of hourly observations from 0900 to 1800 local time during 1980 to 1985. Separately for each day of each month the following data sets were assembled: when Ci clouds were observed in combination with other forms of clouds (Ci + others); observations only with Ci (i.e. with

other level clouds being absent); continuous sky cover by high level clouds (Ci_{10}). The data comprised 21920 events.

Frequency of occurrence was calculated for each month of a year as the ratio of a total number of Ci events to the entire number of observations during a month and was expressed in per cent. For each month a six-year average occurrence was calculated. An average seasonal quantity

TABLE III-2

Frequency of continuous cover of high level clouds in the presence of different synoptic situations according to the ground measurements in Moscow (1971-1985); n - number of cases

Month		Anti-cyclone	Cyclone	Low gradient field	Saddle	All
January	n,%	57 68.7	9 10.8	17 20.5	- -	83 100
May	n,%	62 54.8	15 13.4	30 26.5	6 5.3	113 100
July	n,%	30 51.7	10 17.2	15 25.9	3 5.2	58 100
October	n,%	35 51.5	6 8.8	27 39.7	- -	68 100

was also obtained for each year individually as a whole for the total period and for an average annual period.

The results obtained are tabulated in Table III-3 where it is shown that the greatest frequency of occurrence is related to Ci observed with other cloud forms; a continuous sky cover by Ci alone is a rarer occurrence. Represented also in the table are the Ci statistics from the twenty-year data set from 1966-1985. Comparing these quantities demonstrates that occurrences of Ci_{10} over both time periods are comparable.

The annual cycle of cirrus occurrence is illustrated in Figure III-1. The peculiarities of the Ci annual cycle are explained by a greater cyclone activity in winter and by a prevalence of low level cloud and development of convection in the second half of summer.

TABLE III-3

Frequency of high level clouds (Ci), MSU, 1980-85

	Ci and other types of clouds	Ci (only)	Continuous cover of Ci	Ci^*_{10} 1966-1985
P, %	28,0	8,2	3,5	3,9
$\pm\sigma$	2,4	1,4	0,5	0,8
V,%	9	17	14	20

It is of interest to consider the share of $Ci_{0,}$ continuous sky cover of Ci, in the absence of the clouds. As is shown in Table III-4, a maximum occurs from February to April-May, while a minimum is found in December. The annual cycle of the ratio of high level cloud occurrence for each month and occurrence in general for a year is listed in Table III-5. Comparing the Ci_{10} results with the 1966-1985 data demonstrates that for the annual cycle

of continuous sky cover are consistent. As a whole, the variability of the six year sample is somewhat greater than that for a 20-year period. The annual cycle of Ci occurrence for each individual year repeats reasonably the average cycle for whole period, however, in some years there are significant differences. Thus, for instance, in 1983 the minimum of the Ci occurrence alone is observed in February, while in other years the maximum is usually observed in February. This fact may be explained by powerful cyclonic activity. In August 1985 Ci occurrence was relatively high; this is probably associated with the frequent passage of fronts.

Tabulated in Table III-6 are the data of Ci occurrence averaged for the seasons. Spring and summer values differ only slightly (35 and 36 per cent); in winter and in autumn the frequency of occurrence are virtually the same (21.2 and 22.4 per cent). These data are compared with those given by Hahn, C. J. and S. G. Warren et al., 1986. It is possible that the factor of two differences between our data are explained by the fact that we used data from only one station, while in the atlas the average values of P for all ground-based stations within a cell of 5° x 10° were listed, and then were averaged for a zone of 50 to 70° of northern latitude.

TABLE III-4

Portions of continuous cover of high level clouds (Ci_{10}) among all observations with high level clouds (Ci only)

Month	Jan.	Feb.	March	April	May	June	July	August	Sept.	Oct.	Nov.	Dec.
Ci_{10}/Ci_{only},%	37.2	55.4	45.5	49.7	49.7	40.4	27.0	23.9	40.7	33.0	37.6	12.6

TABLE III-5

Annual cycle of frequency of high level clouds in relation to the mean value for the year as a whole

Month	Jan.	Feb.	March	April	May	June	July	August	Sept.	Oct.	Nov.	Dec.
Ci and other cloud types %	5.2	9.2	11.3	8.2	11.2	10.5	10.1	11.2	10.1	5.0	4.4	3.6
Ci only %	5.7	16.0	20.2	8.9	9.7	5.3	3.6	4.0	10.6	5.4	7.6	4.0
Ci_{10} %	5.0	20.8	21.6	10.4	11.3	5.0	2.2	2.2	10.1	4.2	5.9	1.3
Ci^{*}_{10} % 1966-1985	9.6	13.9	17.1	12.4	11.3	5.6	3.6	5.6	6.4	6.2	4.3	4.0

Therefore, upper layer clouds play a considerable role in the formation of Moscow cloud cover, especially in transitional seasons.

3.1.2 Radiative transmission of cirrus clouds

To estimate the effects of Ci on integral solar radiation (INTR) and ultra-violet radiation (UVR) the quantities C_Q and C_D derived according to the procedure specified in Chapter 8 were used.

For solar elevation angles greater than 10°, as in the case of Zvenigorod experiment, dependencies of quantities C_D and C_Q upon h_o have not been detected. This made it possible to derive average values of C_Q, C_D

TABLE III-6

Average of frequency of high level clouds for different seasons, in %

Season		Winter	Spring	Summer	Autumn
Ci and other cloud types	MSU	21. 2	35.0	36.3	22.4
	Global Distribution.., 1986	44	46	42	44
Ci_{only}/Ci + others	MSU	29.1	35.3	11.4	34.4
	Global Distribution.., 1986	61	56	37	45

Ci_{only} - Only Ci
Ci + others - Ci and other cloud types

and their coefficients of variation V% (see Table III-7), for warm and cold periods, for all the forms of upper layer clouds, as well as for the most frequently occurring

forms and their combinations: Ci; Ci+Cs; Ci+Cc. When processing the different cases, those characterized by values of $C_{D,INTR} < 1.0$ and less than $C_{D,UVR}$, were excluded. The presence of such data may be connected with an inexact determination of $D_{O,INTR}$ which is very sensitive to atmosphere transparency. Let us remember, that when measuring diffuse radiation, the near-solar zone of radius of 5° was being screened.

As a whole, C_Q for global radiation is higher in summer than in winter for all types of clouds, including Ci. In the presence of upper layer clouds, the diffuse INTR increases on the average by 30 to 60 per cent, while the diffuse UVR remains practically unchanged. Illustrated in Figure III-2 are the curves of $C_{D,INTR}$ and $C_{D,UVR}$ distributions for warm and cold periods. The curves of $C_{D,INTR}$ distribution have a distinctly visible positive asymmetry. The combinations Ci+Cs and Ci+Cc have more complicated forms as a result of the greater variability of cloud optical thicknesses. Diffuse UVR not only increases (up to 50 per cent) in the presence of high level clouds, but also decrease (up to 40 per cent), since the $C_{D,UVR}$ distribution is close to normal. It should be pointed out that the increase of diffuse UVR is considerably less than for INTR. Due to the influences of Rayleigh and multiple scattering, scattered UVR losses are considerably greater than in the case of INTR. In the presence of clouds with relatively small optical thicknesses, the flux into

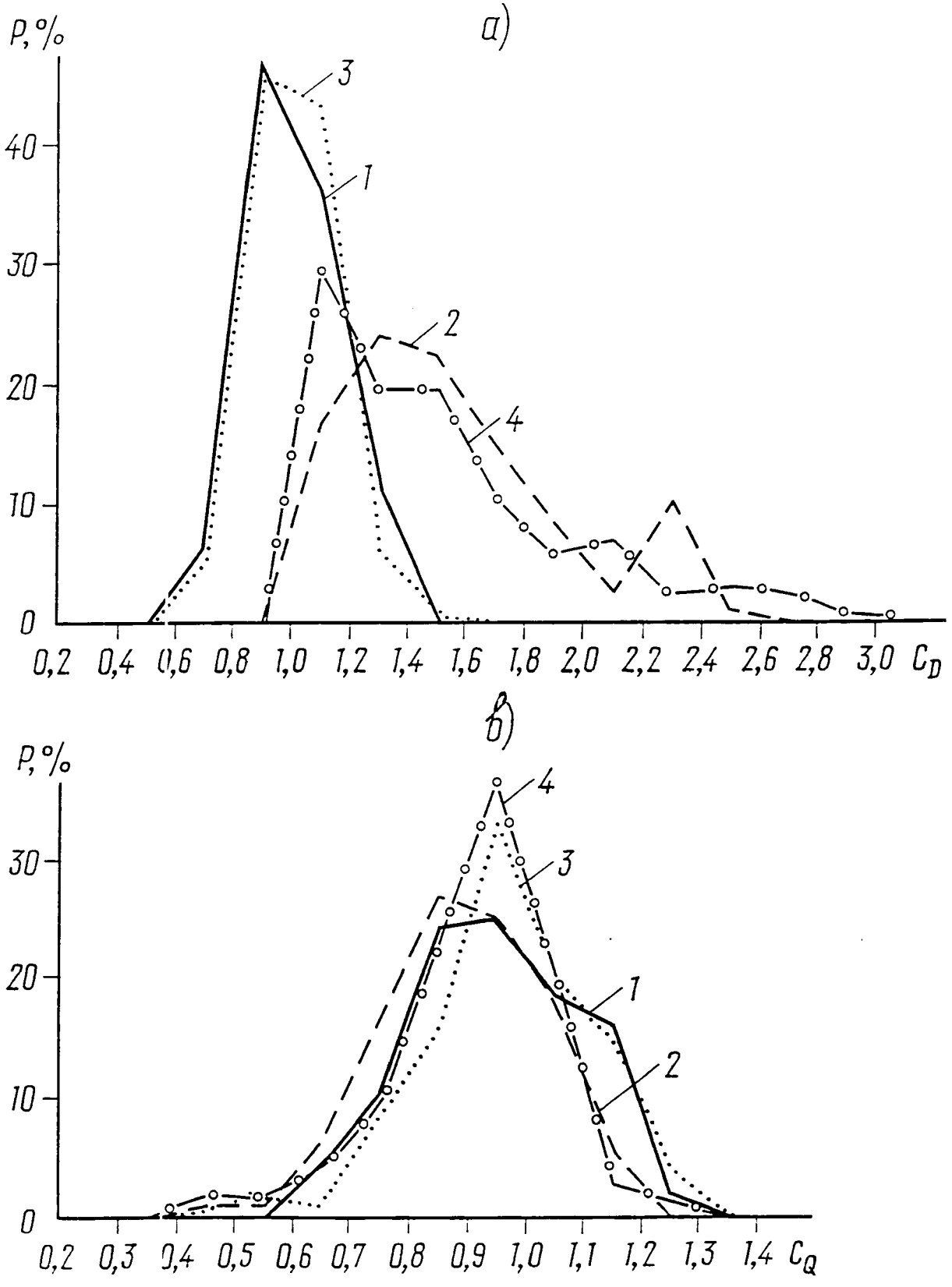

Probabilities of C_D (Panel (a)) and C_Q (Panel (b))

Figure III-2 In the ultraviolet portion of the spectrum (1: cold period, 3: warm period) and in integral spectrum (2: cold period, 4: warm period).

TABLE III-7

Average values of C_Q and C_D for integral and ultraviolet

radiation in the presence of different types of high level clouds and their coefficients of variation (V,%)

Types of clouds	Portion of spectrum	Number of observations	C_Q	V,%	C_D	V,%
Warm period (grass)						
Ci,Cs,Cc	INTR	170	0.91	15	1.34	34
	UFR		0.96	18	1.01	14
Ci	INTR	110	0.94	13	1.43	31
	UFR		0.99	14	1.00	13
Ci + Cs	INTR	36	0.87	18	1.18	29
	UFR		0.90	21	1.04	11
Ci + Cc	INTR	24	0.86	16	1.15	20
	UFR		0.94	13	0.99	11
Cold period (snow)						
Ci,Cs,Cc	INTR	108	0.88	16	1.58	25
	UFR		0.95	11	1.01	12
Ci	INTR	108	0.88	16	1.58	25
	UFR		0.95	11	1.01	12
Ci + Cs	INTR	46	0.83	18	1.78	26
	UFR		0.97	16	1.06	12
Ci + Cc	INTR	16	0.93	15	1.45	26
	UFR		0.90	13	0.91	12

the upper hemisphere may be greater than the flux towards the Earth's surface. Colder periods are characterized by increases in occurrence of large values of $C_{D,INTR}$ in comparison with a warmer periods. As a whole, the global INTR reduction is greater than for UVR and can reach 60 per cent, while the decrease in ultra-violet radiation reaches only 40 per cent. This arises as a result of the fact that the quantity C_Q depends both upon cloud density and upon the partitioning of direct and diffuse radiation for clear skies.

$$C_Q = C_{S'} \cdot S'_o/Q_o + C_D \cdot D_o/Q_o; \qquad (1)$$

where S' is a direct radiation upon a horizontal surface. In spite of the fact that, with dense high level clouds, diffuse INTR increases noticeably, its contributions to the total radiation is small for clear skies; this is substantially different from the UV region of a spectrum.

As indicated in Chapter 5, the influence of high level clouds upon solar radiation is comparable with the effects of aerosol. Thus, when determining values C_Q and C_D, correct consideration of atmospheric transparency is of great importance when (Q_o, D_o) are calculated for cloudless sky radiation. As a rule, multiple year average values of Q_o and D_o are used. In the context of this comparison, different methods of considering atmospheric transparency have been carried out when the Ci influence upon INTR and UVR is being estimated. For the 1968-1985 May case, example values of C_Q and C_D were derived by considering atmospheric transparency for the day with Ci or in adjacent neighboring days in cases of stable synoptic situations. These results were compared with two other methods, where

transparency conditions are approximately taken into account. With the second method, values of Q_o and D_o, corresponding to the average transparency coefficient for each year in May were chosen as a denominator in Eq. 1. The third method used a Q_o and D_o from a multiple year average transparency coefficient for the given month.

Comparing results obtained by the three methods revealed that average, minimum, maximum values of C_Q and C_D as well as values of their variation coefficients turned out to be close, except for $C_{D,INTR}$ (see Table III-8, Figure III-3). In a number of cases, when using the second and third methods, values of $C_{D,INTR}$ turned out to be less than one, despite the fact that such values were excluded during the original processing of data, when the first method was employed. At the same time, maximum values $C_{D,INTR}$ exceed values of $C_{D,INTR}$ obtained using the first method. Therefore, in order to estimate properly the variability of solar radiation, especially for the diffuse integral component in the presence of Ci, correct consideration of atmosphere transparency conditions are essential.

The effects of Ci clouds upon the 1980-1985 global and diffuse integral ultra violet (UVR), the photosynthetically active (PAR) and the near infrared radiation (NIRR) were estimated with the aid of the third method.

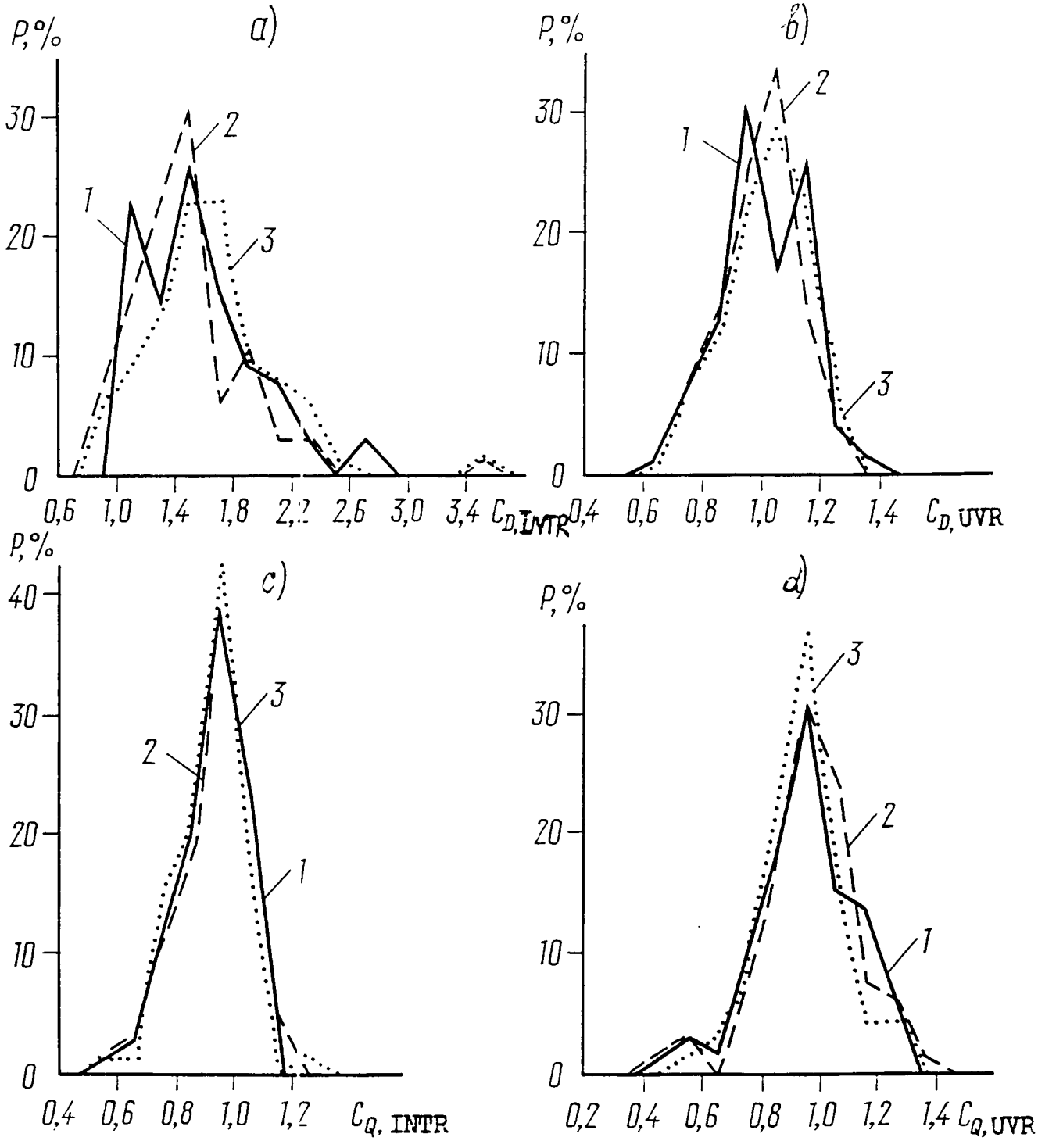

Figure III-3 Probabilities of $C_{D,INTR}$ (a) $C_{D,UVR}$ (b) $C_{Q,INTR}$ (c) and $C_{Q,UVR}$ (d) received by various methods of determination of atmospheric transparency.

TABLE III-8

Values C_D and C_Q received by various methods (May, 1968-85, number of observations - 66)

$C_{Q,INTR}$					$C_{Q,IIVR}$			
Method	Mean	Max	Min	V,%	Mean	Max	Min	V,%
1	0.92	1.21	0.50	14	0.95	1.29	0.45	18
2	0.93	1.18	0.52	13	0.96	1.29	0.46	17
3	0.91	1.25	0.53	13	0.94	1.27	0.46	17

$C_{D,INTR}$					$C_{D,IIVR}$			
Method	Mean	Max	Min	V,%	Mean	Max	Min	V,%
1	1.54	2.68	1.00	26	0.99	1.32	0.66	17
2	1.47	3.52	0.92	28	1.00	1.28	0.66	13
3	1.62	3.61	0.85	28	1.01	1.28	0.64	14

Taking into account the influences of atmosphere transparency and underlying surface albedo, the whole data set was divided into two periods: from December to March (stable snow cover) and from April to October (grass).

It is seen from Figure III-4 that Ci increases mainly the diffuse radiation within the whole range of a spectrum all year round. Given in the tables are

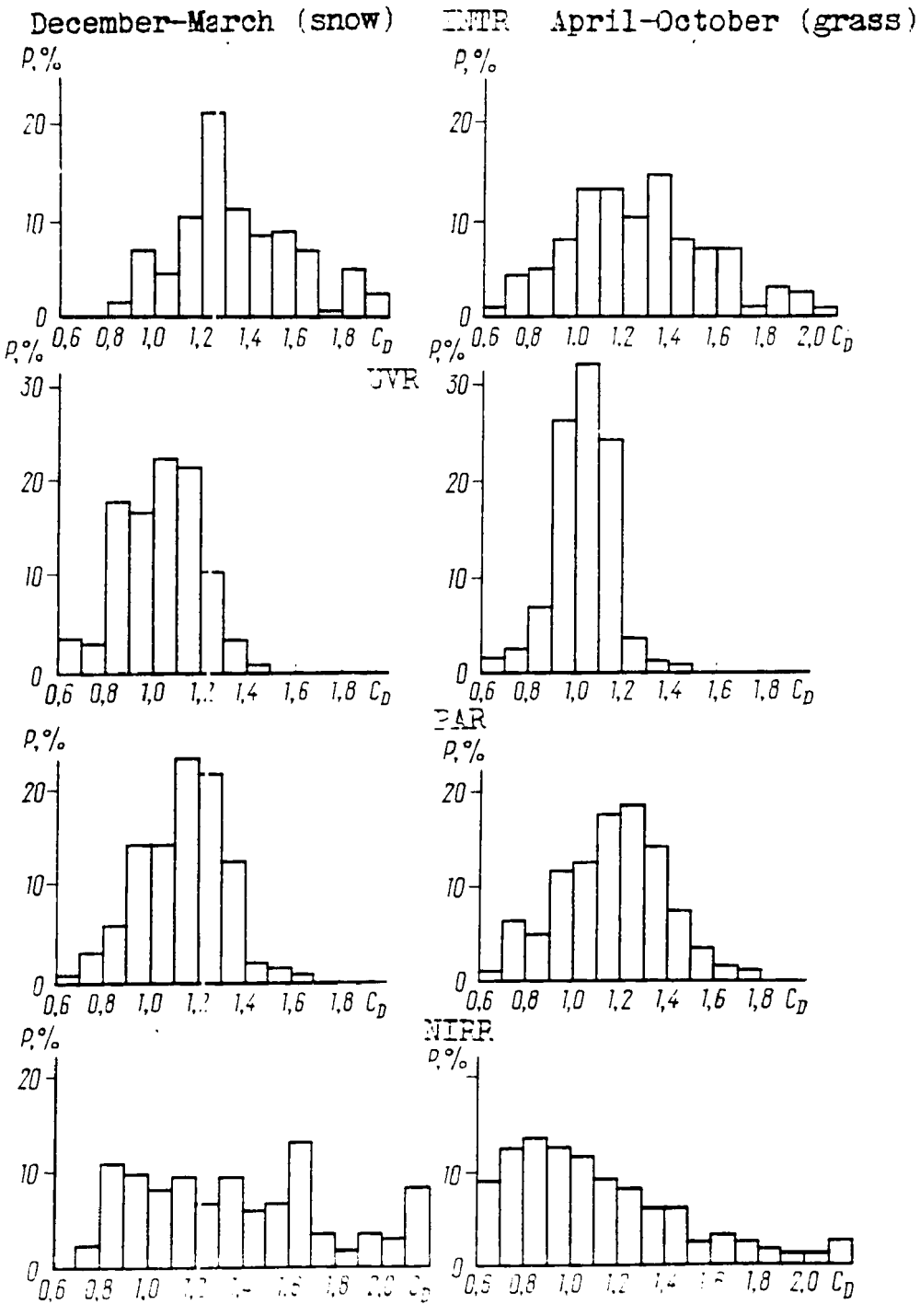

Figure III-4 The transmission of diffuse radiation under conditions of continuous cover of high level clouds in different portions of spectrum.

average quantities C_D and C_Q, modal values - M_o, standard deviation - σ and the coefficient of variation - V. For both periods, the mean value of C_D for UVR is 1.03; the mode is close to one, while the value of V, the smallest in comparison with other spectral regions, is between 11 and 16 per cent. However, in some cases diffuse UVR can increase or decrease depending upon cloud density by 30 to 40 per cent. Under the influence of high level clouds the diffuse NIRR changes most of all. It, more often than not, increases and on occasion may increase by a factor of four. Differences in the quantity C_D for UVR and NIRR are explained by the dissimilar interaction of high level clouds and diffuse radiation in these spectral regions.

The PAR distribution of transmission is close to that for an integral flux with average and modal values of $C_{D,PAR}$ being close in warm and cold periods and between 1.15 and 1.20, respectively. Diffuse radiation may increase to a maximum by 60 to 70 per cent.

A high level cloud influence upon global radiation is more monotonic for all the spectrum parts and is less than in case of the diffuse component. The quantity C_Q varies from 0.5 to 1.3 (see Figure III-5).

Thus, in the presence of high level clouds direct solar radiation decreases in all spectral regions and the global radiation decreases also, but by less than 10 per cent. A greatly increasing diffuse radiation partially compensates for the losses in the direct component.

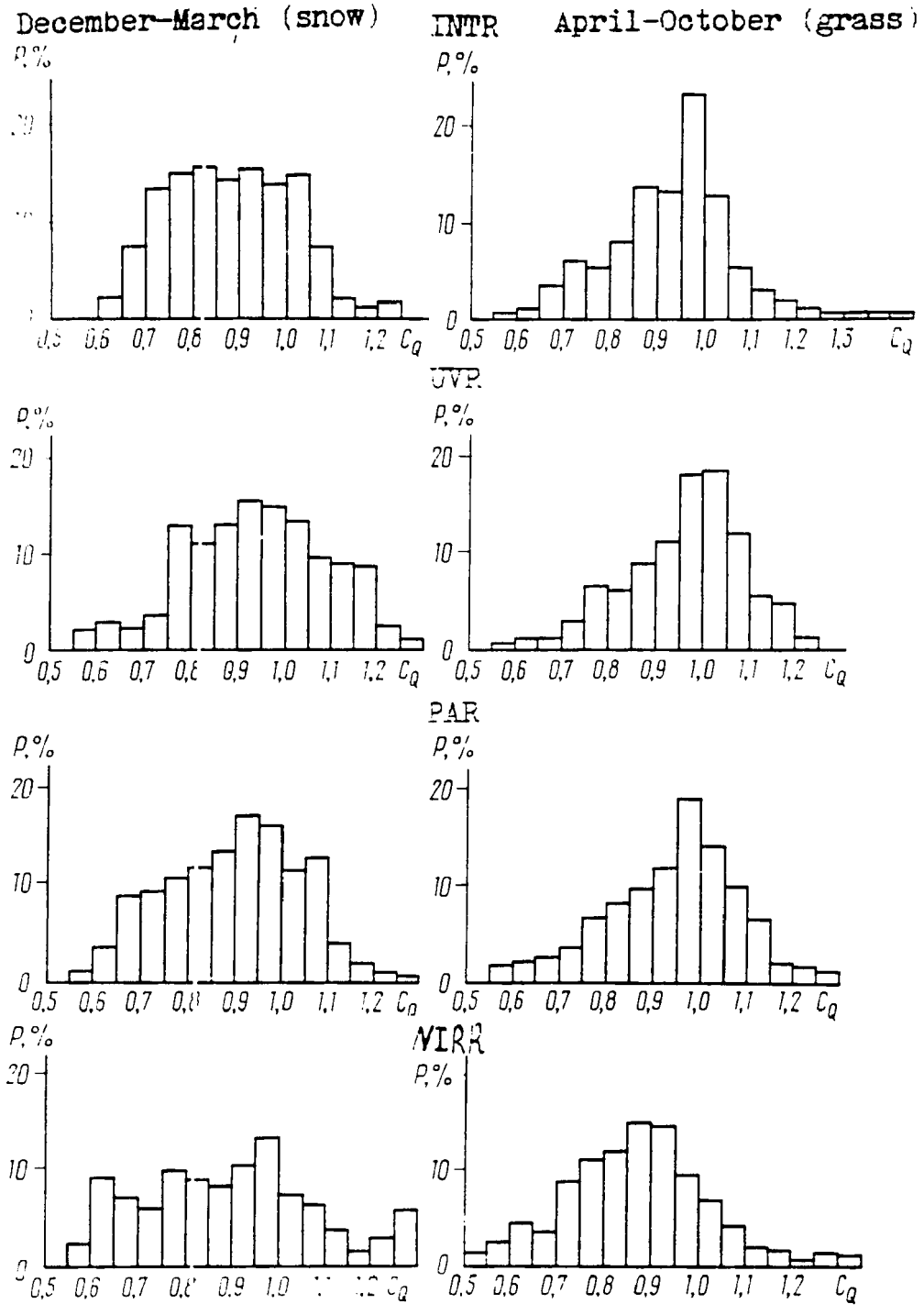

Figure III-5 The transmission of global radiation under conditions of continuous cover of high level clouds in different portions of spectrum.

TABLE III-9

The transmission of radiation of continuous cover of high level clouds, per cent, 1980-85, MSU

		Grass						Snow					
		Mode	Mean	σ	V,%	Max	Min	Mode	Mean	σ	V,%	Max	Min
C_D	INTR	1.34	1.26	0.29	23	2.28	0.65	1.25	1.37	0.29	21	2.00	0.81
	UVR	1.04	1.03	0.12	12	1.41	0.66	1.08	1.03	0.17	16	1.50	0.63
	PAR	1.22	1.16	0.22	19	1.72	0.59	1.18	1.14	0.18	16	1.61	0.72
	NIRR	1.05	1.61	0.64	40	4.34	0.47	2.64	2.64	0.82	37	4.11	0.91
C_Q	INTR	0.98	0.93	0.13	14	1.36	0.61	0.81	0.81	0.13	15	1.25	0.63
	UVR	1.00	0.97	0.13	13	1.33	0.60	0.94	0.94	0.16	17	1.33	0.57
	PAR	0.98	0.94	0.16	17	1.38	0.56	0.94	0.94	0.14	16	1.57	0.61
	NIRR	0.89	0.89	0.15	17	1.41	0.52	0.97	0.97	0.17	19	1.54	0.55

REFERENCES

Hahn, C. J., S. G. Warren, Y. London, R. M. Chervin, R. Yenne, 1986: Global distribution of total cloud cover and cloud type amount over land. United States Department of Energy and NCAR, Boulder, CO.

3.2 Ultra-violet radiation measurements made in Kislovodsk

by Yu. V. Glushchenko

Beginning in 1984 and continuing to the present, systematic observations of ultra-violet radiation within the wave length of 315 to 400 nm and 280 to 315 nm in units of biological efficiency $(mW/m^2)_e$[1] were made using a biological photometer (angle of view 2.3°) in Kislovodsk (the Caucasus, height above sea level is about 900 m). The absolute accuracy of measurements is approximately equal to 30%, with a relative accuracy of 8%. Observations are conducted at 9, 12, 15 o'clock local time.

In a study of the variations of ultra-violet radiation fluxes arising from Ci cloud variability, two contrasting situations may be outlined: events consisting of a clear sky and a dense cloud covering either the whole sky, or only covering the sun. In the case of a dense cloud the value of S relative to D is so small that its contribution to Q may be neglected. The case represented in Figure III-6 corresponds to the direct line passing through the origin of coordinates on plane {Q,D}, where clear sky values are shown as points. When drawing the direct line, use was made of the data obtained in Kislovodsk at local noon, for the 1984-87 data when snow cover was absent.

In the ultra-violet part of spectrum the optical thickness of Rayleigh scattering is larger than the optical thickness of aerosol. That is why aerosol variability contributes a relatively small spread to the data provided in Figure III-6 for the clear sky case. When Ci are present, variations in Q and D change with cloud optical thickness, τ, and are of

[1] mW/m^2 - erythema-effective

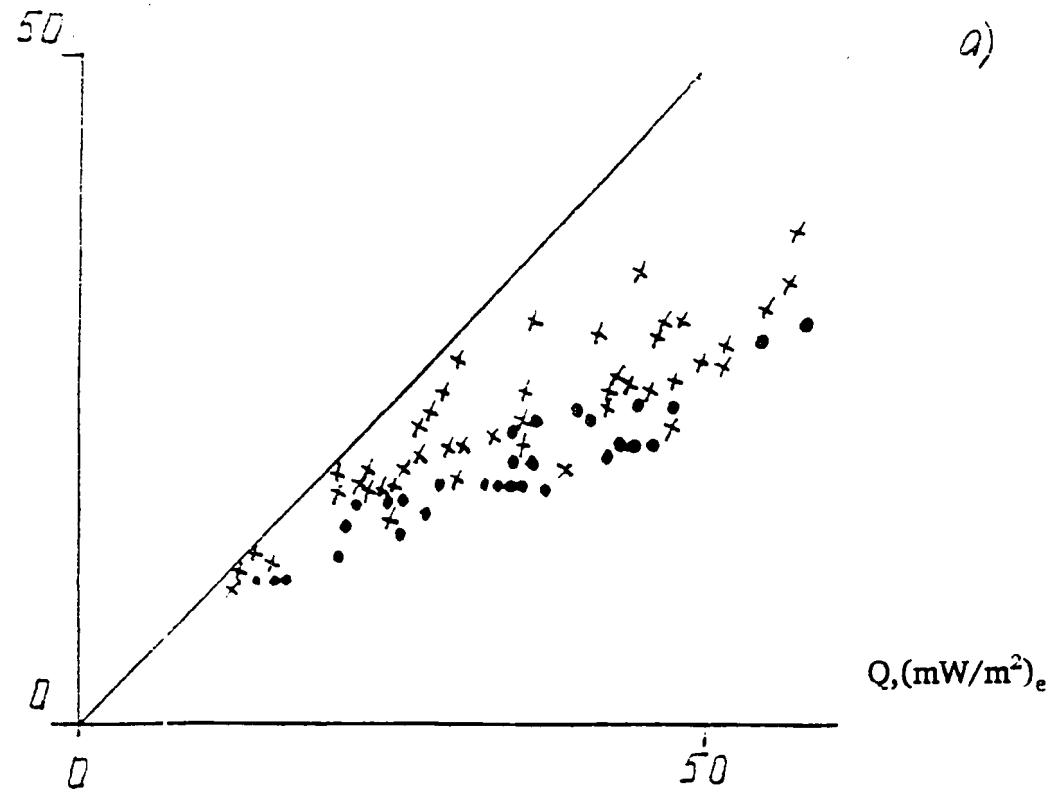

a) $\Delta\lambda$ = 0.280-0.315 μm;

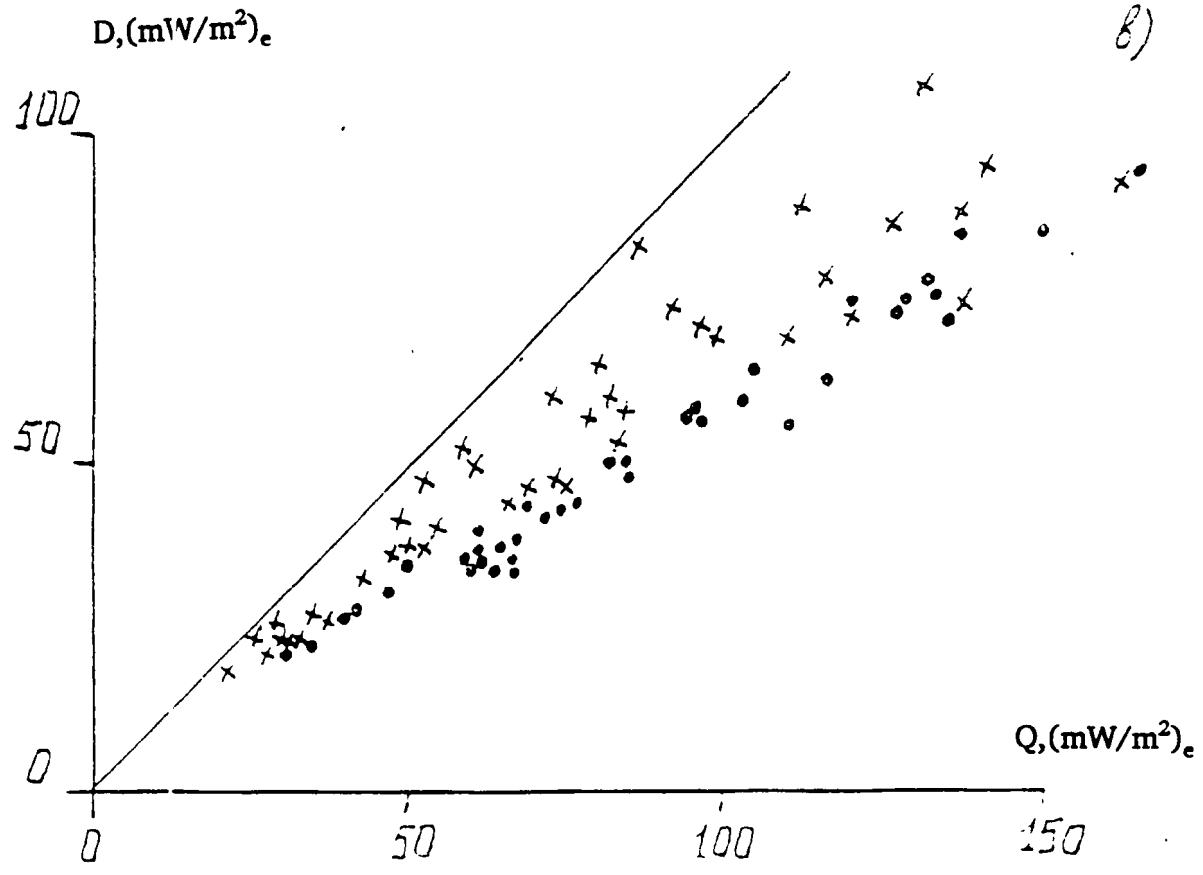

b) $\Delta\lambda$ = 0.315-0.400 μm;
• - under clear sky; x - under Ci.

Figure III-6 The correlation between D and Q in Kislovodsk, 1984-87.

opposite sign, i.e. the contribution of D to Q with growth of τ increases, and will be the greatest for the case when Q = D, and the smallest for clear sky conditions. This is precisely what we observe in Figure III-6, where crosses are values of pairs {Q,D}, with Ci present. A quantitative estimate of the change of the contribution of D to Q with Ci present is listed in Table III-10, where a coupling has been determined for the cases of a clear sky and three categories of amounts Ci clouds using a linear relationship:

$$D = K \cdot Q + B,$$

where K is the coefficient which may be considered as a linear approximation to the Sun's zenith angle for $\theta < 75°$ (i.e. atmosphere mass $m \leq 4.0$). The Table III-10 calculations are based on the observed fact that the average optical thickness of Ci clouds increases as the amount of Ci clouds increase.

TABLE III-10

$\Delta\lambda$ = 0.315 - 0.400 μm				$\lambda \leq$ 0.315 μm			
Cloud amount	K	B	N	Cloud amount	K	B	N
0	0.382	0.11	67	0	0.564	0.03	67
1-4	0.383	0.05	30	1-4	0.576	0.06	30
5-9	0.495	0.11	20	5-9	0.723	0.03	20
10	0.613	0.29	47	10	0.742	0.30	47

3.3 The Influence of High Level Cloudiness upon Solar Radiation

by V. K. Russak

The goal of this report is to estimate the influence of high level clouds on solar radiation transfer using data supplied by the Tyravere actinometric station. The data were hourly sums of direct (S) and diffuse radiation (D), recorded with electronic integrators and hourly visual observations of cloud forms and amounts.

In summer, when the amount of low level, dense cloudiness decreases, the upper layer cloud role increases. Between May and August in Tyravere, cirrus (Ci) clouds are most frequently observed (in 21 to 26 per cent of observations). Data from May, June and July, 1958-1987 were chosen to be processed, when continuous cloud layers of cirrus - Ci (277 hours total) or cirrostratus - Cs (104 hours) were observed. Only dimensionless quantities C_S and C_D characterizing transmission and scattering of direct radiation by high level clouds were analyzed.

Values of C_S were calculated from the formula $C_S = S/S_o$. In this case S is the hourly sum of direct radiation measured under the conditions of Ci or Cs, S_o is the hourly sum of direct radiation, with the sky being clear, calculated using Buger's formula. To obtain the coefficient of atmospheric transparency with mass m - P_m the average monthly value of P_2 calculated from 30 years of Tyravere data for the given month was used. Transformation to a P_m value was carried out using a Miirk monogram [Miirk, Kh., 1959]. The air mass was calculated according to the sun's average height for the given hour.

The quantity C_D was calculated from the formula $C_D = D/D_o$, where D is the measured hourly sum of diffuse radiation in the presence of Ci or Cs, and D_o is an hourly sum of diffuse cloudless sky radiation. The latter, in connection with the atmospheric transparency and the sun's height - h_o, was determined based on fixed actinometric observations taken in Tyravere from 1955 to 1960.

C_S and C_D value variations were caused mainly by the variability of optical cloud density as well as by the sun's height change. Average values of C_S and C_D and their standard deviations were determined for the five step intervals of the sun's height $10° \leq h_o \leq 55°$.

Cirrus clouds, on the average, are optically less dense compared to cirro-stratus (Figure III-7). Within the range of the solar heights considered, $10° \leq h_o \leq 55°$, transmission of the sun's direct radiation by Ci clouds varies, on the average, from 0.25 to 0.65, while for Cs from 0.2 to 0.45, growing as the sun's height increases. Variation of values of C_S for Ci clouds is greater than for Cs clouds. In the first case the variation coefficient V = 0.42 to 1.13, in the second, V = 0.31 to 0.73.

Diffuse radiation for the available high level cloud data noticeably exceeds clear sky values. C_D grows as the sun's height increases, this growth being more rapid with cirro-stratus clouds than for cirrus.

For Ci, the variation coefficient is between 0.17 to 0.33 and for Cs, between 0.10 to 0.27.

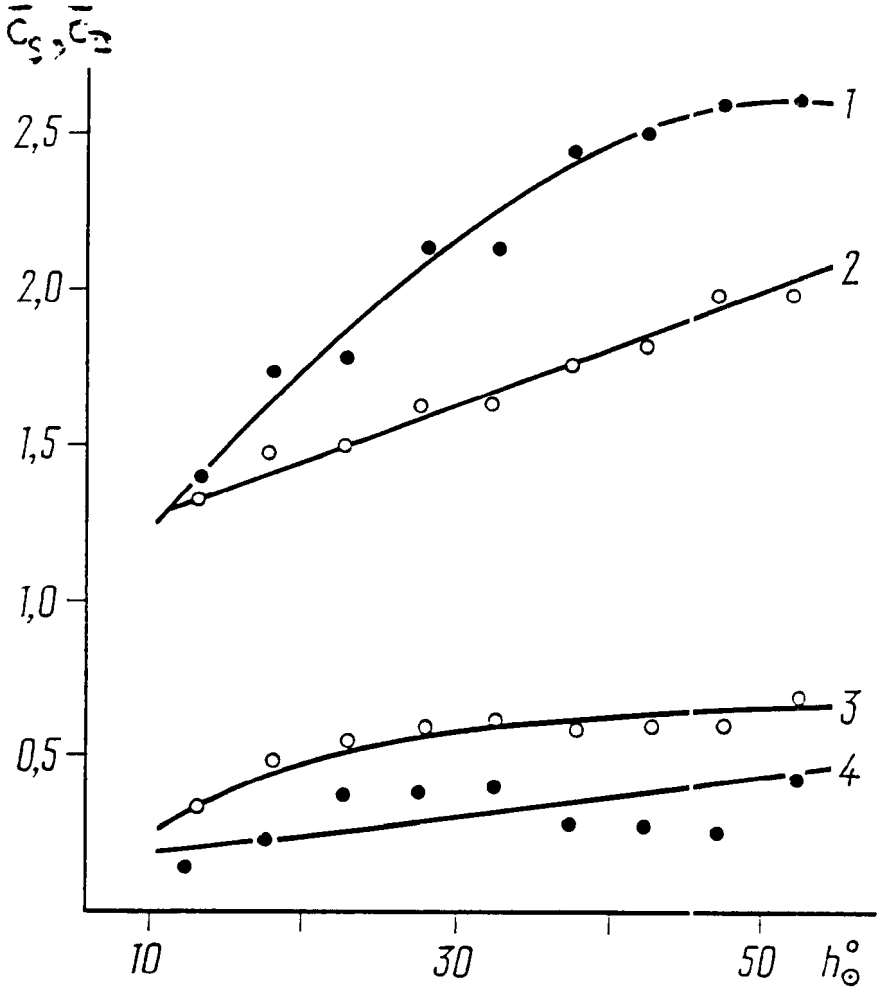

Figure III-7 The average dependence of C_S and C_D upon the height of the Sun with upper layer clouds present (1,4 - Cs, 2,3 - Ci).

The curves shown in Figure III-7 have been smoothed. They are within the limits of 95% significance of the average value of a corresponding quantity,

i.e. within the limits of $\pm 1.96 \frac{\sigma}{\sqrt{n}}$ (n is the number of observations of C_S or C_D within a five step interval h_o, σ is their standard deviation).

Distributions of C_S and C_D values are different under conditions of cirrus clouds and cirro-stratus (see Figures III-8a and b). According to our observations in only in 50% of the events does cirrus reduce the direct radiation less than by 40%, while when cirro-stratus clouds are present, such a reduction takes place, on the average, only in 14% of events. More often than not (63% of all the events observed), cirro-stratus clouds reduce solar radiation by 60% or more.

When considering scattered radiation by cirrus, small values of C_D are more common (in 50% of events they do not exceed 1.8, see Figure III-8b). Cirro-stratus are more favorable for scattering, where values of C_D = 1.8 to 2.6 are dominant.

To estimate the ratio of direct and diffuse radiation under conditions of high level cloudiness, we have taken into account the ratio of hourly sums of S' and D ($S' = S \sin h_o$) as a function of h_o. Similar to the C_S and C_D processed data quantities, S'/D values were distributed according to five step intervals of h_o and their average values and standard deviations were determined. The values of C_S in figures 8c and 9 suggest that the global radiation, $Q = S' + D$, is mainly determined by diffuse radiation. Only at $h_o \approx 50°$ does direct radiation become comparable with scattered contributions. Under cirrus conditions S' already reaches the value of D at $h_o \approx 20°$, while for $h_o \approx 50°$ it is 2/3 of the global. For

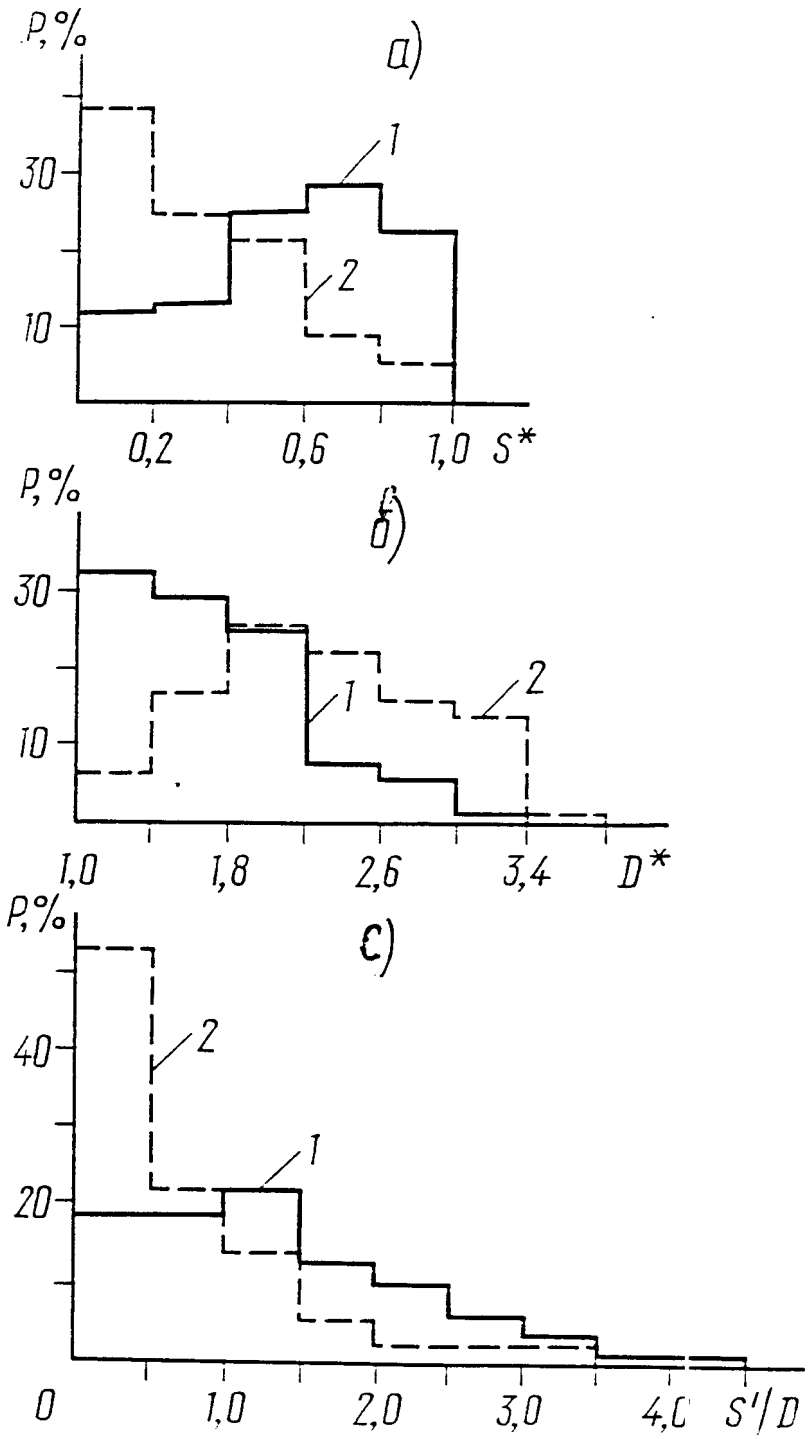

Figure III-8 The distribution of transmission of direct (a), diffuse (b) radiation, and the ratio of direct to diffuse radiation (c), per cent.—— Ci, ------ Cs.

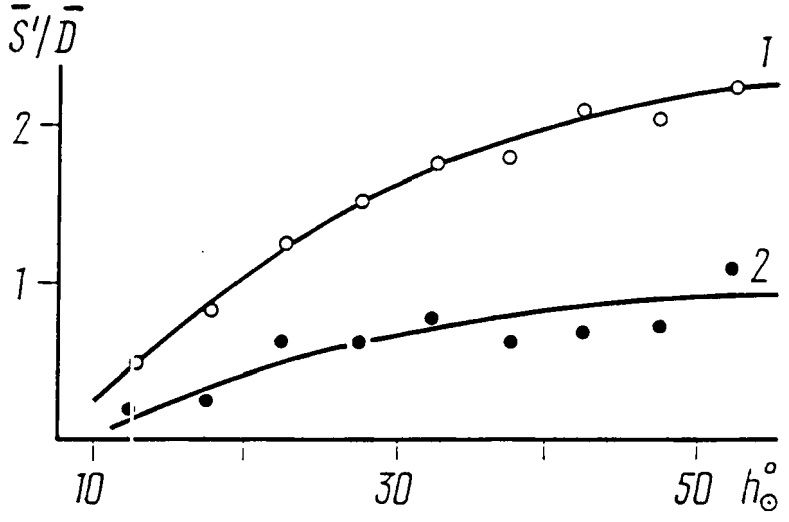

Figure III-9 The average dependence of the ratio of direct to diffuse radiation upon the Sun's height under Ci (1) and Cs (2) conditions.

the case of a cloudless sky in Tyravere in summer, the shares of direct and diffuse components in the global radiation become equal at $h_o \approx 10°$; and at $h_o = 55°$ the value S' exceeds the quantity D by approximately 6 times.

Variability of values of S'/D is greater under cirro-stratus conditions: variation coefficient V = 0.50 to 1.17; under cirrus, V = 0.52 to 0.79. In the majority of cases (53 per cent) of hourly sums analyzed when Cs clouds were present, $S' \leq 0.5D$ (see Figure III-8c). For Ci the distribution of S'/D has a more gentle shape and only in 38 per cent of the events is $S' \leq D$.

REFERENCES

Miirk, Kh., 1959: The monogram for calculation and reduction some characteristics of transparency of atmosphere. *Investigations of Atmospheric Physics*, N 1, c. 15-25 (ASE SSR).

3.4 Radiative properties of cirrus clouds in polar regions

by M. S. Marshunova

Institute of Arctic and Antarctic State Committee of Hydrometeorology

High level clouds over polar regions have received considerably less attention than those over other regions of the globe. Extensive explorations were carried out by the Flying Meteorological Observatory (FMO) in the Arctic during the period from 1949 to 1965 and by drifting stations "Severny polyus"; these efforts provided observations necessary for investigating high level cloudiness. Special investigations were performed from 1957 to 1960 and in 1976.

Altogether during the FMO period 1900 observation periods were conducted, with high level clouds being absent in 28% of cases and upper cloudiness being observed in 20% of the cases, while 51% of flights were carried out under conditions which did not allow determination of whether or not high level clouds were present. Since such conditions, more often than not, take place in the proximity of atmospheric fronts where high level clouds are likely to occur, one may assume that the frequency of occurrence of upper layer clouds is considerably greater than 20%. The data are rather close to those obtained for European Territory Soviet (ETS).

Observations reveal that Arctic cirrus clouds (Ci) comprise 64% from all the events of high cloudiness noted. Cirro-cumulus (Cc) frequency of occurrence is equal to 29%, while cirro-stratus (Cs) accounts for only 7% of the observations. These results are also similar to those obtained for ETS. Put another way, the

frequencies of occurrence of the basic forms of high level clouds over the Arctic and mid latitudes are about the same.

The results of processing data on high level cloud amount are listed in Table III-11. As seen from the table, continuous cloudiness or nearly continuous is common only for cirro-stratus.

The opportunities of probing upper layer clouds in the Arctic are few in number. In 1958-1959 the high cloud layers were probed 44 times and the heights of lower and upper boundaries were measured. From these data the author derived the annual course of a cloudiness boundaries (see Figure III-10a). During the coldest months, formation of high level cloudiness begins at lower heights and the annual course of upper boundary is determined by the tropopause height. When compared with temperate latitudes (see Figure III-10b), it is seen that the character of the annual course of cloud boundaries is the same. The data from Leningrad represent a large number of observations and they reflect a reliable cloud height distribution.

The height of lower and upper boundaries of high level cloudiness in the Arctic is 0.8 to 1.2 km lower in temperate latitudes. Thickness is, on the average, about 2 km, but it appears to vary greatly: from several hundreds of meters to 4 km (see Table III-12). 63.6% of the observed samples had thicknesses between 1.1 to 3.0 km.

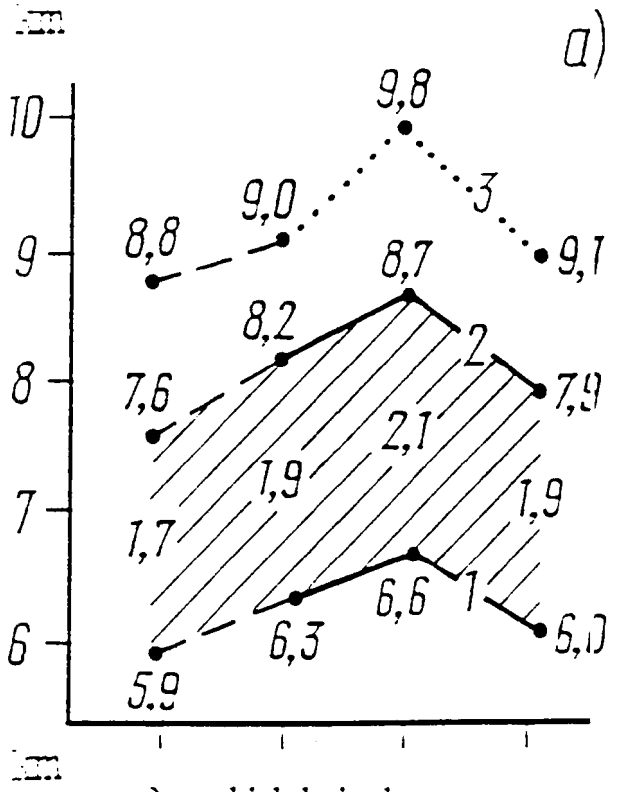

a) high latitude

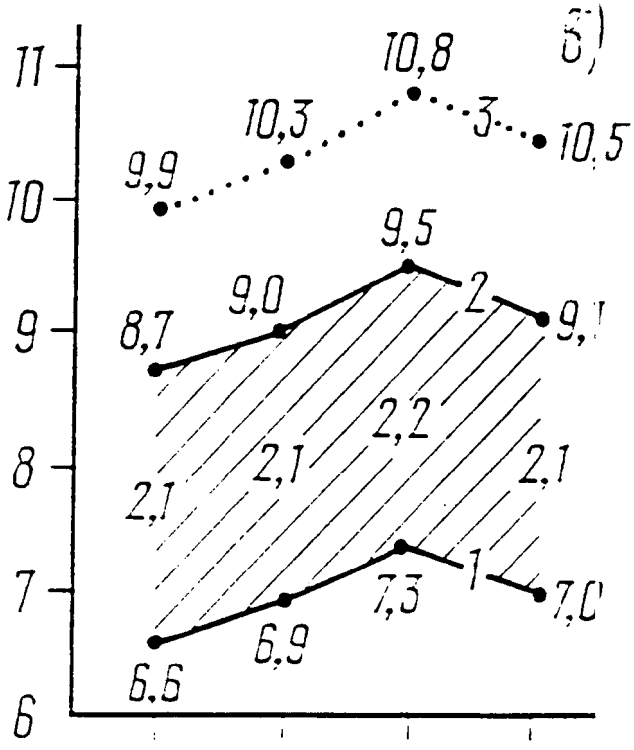

Winter Spring Summer Autumn

b) Leningrad region

Figure III-10 The annual course of lower (1) and upperer (2) mean neight borders of high level clouds and tropopause (3).

TABLE III-11

The frequency of upper layer clouds amount, per cent.

The kind of clouds	Cloud Amount									
	1	2	3	4	5	6	7	8	9	10
Ci	2	16	15	13	9	7	9	10	11	8
Cc	7	7	10	7	7	-	12	6	15	29
Cs	-	-	1	-	1	2	4	9	7	76

TABLE III-12

The frequency of vertical size of clouds in per cent

Period of time	ΔH (km)				
	0.0-0.5	0.6-1.0	1.1-2.0	2.1-3.0	3.1-4.0
April-September	10.0	13.3	46.7	23.3	6.7
October-March	14.3	21.5	21.4	28.5	14.3
Year	11.4	15.9	38.6	25.0	9.1

In the Antarctic the vertical boundaries of clouds were determined with the help of a Meteorological Radar Installation (MRI) operating on the Antarctic continent coast at Molodezhnaya station. From July 1, 1980 to January 1, 1981 high and low cloud boundary analyses have been performed using MRI. Based on these data the lower boundary of high level clouds has been detected from 5.0 to 6.5 km, with the upper boundary, from 5.5 to 8.0 km.

Stationary actinometric observations taken at the Arctic and Antarctic polar stations, at the drifting stations in the Arctic basin and on board scientific ships in the North European Basin (NEB) served as sources of data for the investigation of solar radiation fluxes. Among the observations, a number of events with the presence of cirrus only cloudiness have been chosen for the investigation where direct solar radiation was obtained as the difference between global and diffuse radiation (see Figure III-11).

Analysis of data with high level cloudiness being present revealed that in all the regions of the Arctic with a homogeneous underlying surface, the flux of diffuse radiation is equal for the same solar zenith angle.

With virtually continuous high level cloudiness and snow cover, diffuse radiation is doubled compared to the radiation for a cloudless sky and comprises 40 to 50 per cent of global radiation even for the higher solar elevation angles (see Table III-13).

The large diffuse radiation contribution to the global radiation in the presence of clouds is related not only to the scattering by the clouds proper, but also to additional scattered radiation reflected by the high-albedo underlying surface.

Average quantities of global radiation (Q) in the presence of continuous high level cloudiness differ slightly from the radiation of a cloudless sky (Q_o). In separate cases, Q, may even exceed the radiation of a cloudless sky (Q_o). Only oceanic regions are an exception (see Tables III-13 and 14). The lowest values were observed on the eastern coast of the Antarctic peninsula (region of station

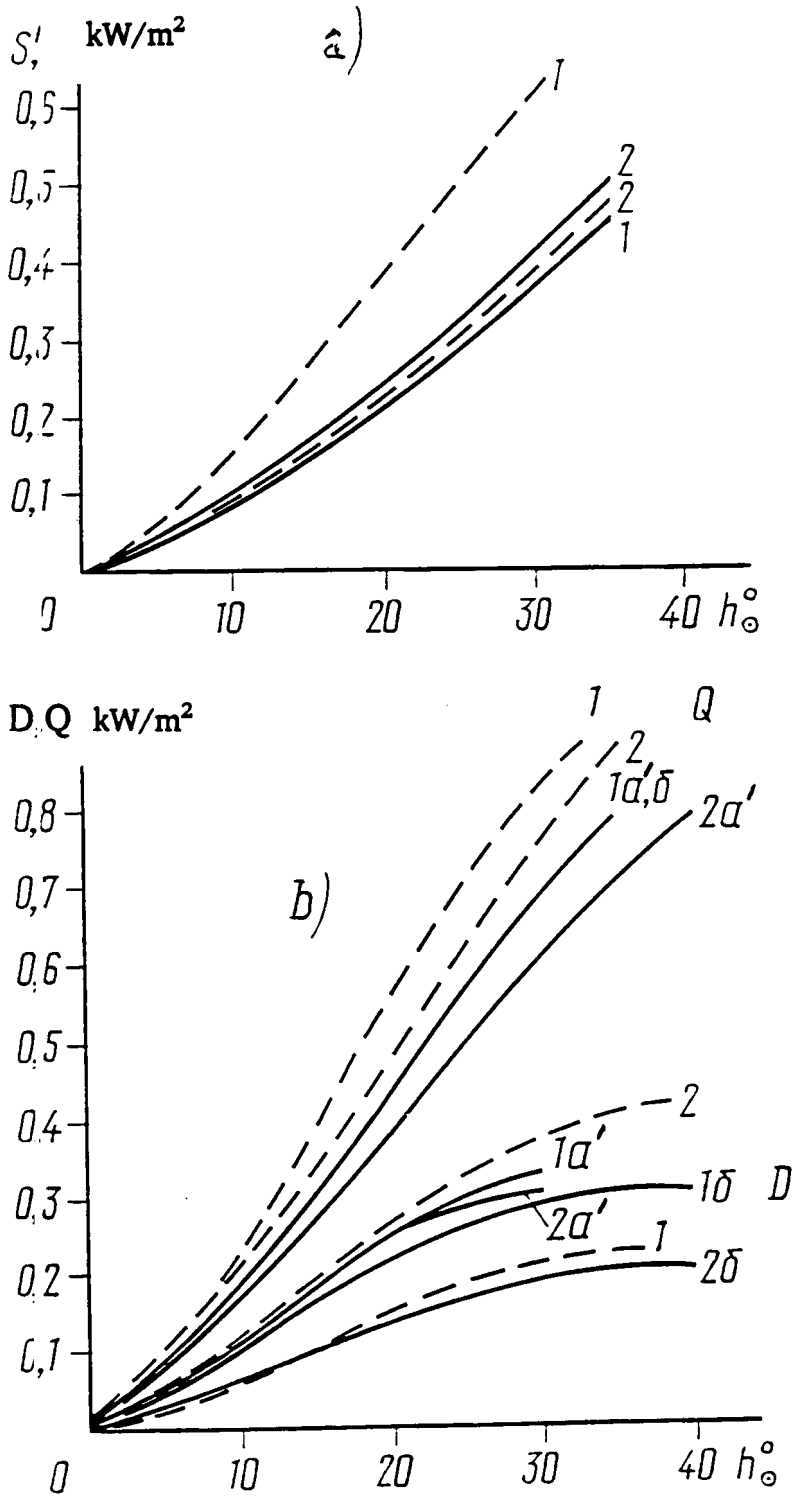

1 - Central region; 2 - Coast;

a' - Spring; δ - summer;

- - Arctic;

___ Antarctic

Figure III-11 Direct (a), diffuse and global (b) radiation under continuous upper layer clouds.

Bellinshousen), where the frequency of the occurrence of atmospheric fronts is great and high level, high density clouds are found the year round. That is why the decrease of global radiation by 30 to 50% takes place with respect to the sun's height and season. It is only 10 to 15% lower than for continuous middle layer cloudiness in the same region. In other regions similar differences comprise 20 to 25%.

Coefficients of variation tabulated in Table III-15 represent the change in radiation flux determined by variability of the microstructure of cloud cover and its thickness.

Table III-15 also contains data on the global radiation for middle and low level cloudiness. Upper layer clouds show less global radiation variability while in the Central Antarctic it is nearly the same as with the sky being clear.

TABLE III-13

The ratio of diffuse radiation to global radiation flux (D/Q)

Regions	10°		20°		30°	
	clear	10/0 Ci, Cs	clear	10/0 Ci, Cs	clear	10/0 Ci, Cs
Arctic coast spring	0.48	0.60	0.39	0.50	0.22	0.48
Arctic coast summer	0.30	0.50	0.20	0.40	0.15	0.35
Arctic basin	0.49	0.57	0.31	0.47	0.21	0.44
North European basin	0.26	0.56	0.51	0.43	0.12	0.38
Antarctic coast	0.30	0.68	0.18	0.56	0.15	0.52
Central Antarctic (3.5 km upper sea level)	0.25	0.45	0.12	0.32	0.10	0.26

TABLE III-14

Average value of C_S, C_D and C_Q under the continuous upper layer clouds (h_o = 30°)

Regions	Seasons	C_S	C_D	C_Q
Arctic coast	spring	0.66	1.8	0.97
	summer	0.66	1.6	0.92
Arctic basin	year	0.60	3.3	0.97
North European basin	year	0.65	1.6	0.72
Antarctic coast	year	0.58	3.0	0.95
Central Antarctic	year	0.79	1.8	0.99

TABLE III-15

Variation coefficients of global radiation fluxes under the continuous cloud layers of different levels, per cent

Cloudiness	Regions	Height of Sun		
		10°	30°	30°
Clear		22	11	7
10/0 Ci, Cs, Cc	Arctic	28	20	12
	Antarctic coast	25	18	8
	Central Antarctic	20	14	18
10/10 As, Ac	Arctic	33	25	18
	Antarctic coast	39	28	24
	Central Antarctic	22	18	13
10/10 St, Sc	Arctic	37	32	30
		43	32	28

APPENDIX IV

LIST OF ABBREVIATIONS

CAO - Central Aerological Observatory (Russian State Committee for Hydrometeorology

HMC - Hydrometeorological Central (Russian State Committee for Hydrometeorology)

IAAP - Institute of Astrophysica and Atmoshperic Physics (Estonia Academy of Sciences)

IAA - Institute of Arctic and Antarctic (Russian State Committee for Hydrometeorologg)

IAP - Institute of Atmospheric Physics (Academy of Sciences of the USSR)

IEM - Institute of Experimental Meteorology (Russian State Committee for Hydrometeorology)

M.O. - Meteorological Observatory of the MSU

MSU - Moscow State University

SCRCP - Soviet Cloud Radiation Climatology Programme

WCRP - World Climate Research Programme

Z.S.S. - Zvenigorod Scientific Station of IAP

APPENDIX V

LIST OF AUTHORS FROM THE DIFFERENT SOVIET INSTITUTIONS

IAP **Institute of Atmospheric Physics (Russian Academy of Sciences)**
109017 Moscow, Pyzhevsky, 3.

P. P. Anikin
E. M. Feigelson
I. A. Gorchakova
Yu. V. Glushenko
E. V. Romashova
I. N. Plachina
T. A. Tarasova
A. V. Tichonov

CAO **Central Aerological Observatory (Russian State Committee for Hydrometerology)**
141700 Dolgoprudny Moscow Region Pervomayskaya, 3.

S. N. Burkovskaya
E. T. Ivanova
A. L. Kosarev
G. N. Kostyanoy
L. V. Kravetz
I. P. Mazin
A. Ya Naumov
Yu. F. Stanevskaya
N. A. Zaytseva

MSU **Moscow State University**
119899 Moscow GSP-3 Leninskiye Gory Geographical Department, Chair of Meteorology and Climatology, Meteorological Observatory.

G. M. Abakumova
N. E. Chubarova
E. I. Nezval
O. A. Shilovseva
E. V. Yarcho

HMC Hydrometeorological Centre (State Committee for Hydrometeorology)

E. A. Sterlyadkina
V. M. Sutovsky
V. I. Yurov

IEM Institute of Experimental Meteorology (State Committee for Hydrometeorology)
249020 Obninsk Kaluga Region Lenin Street, 82.

L. N. Pavlova
A. G. Petrushin

IAA Institute of Arctic and Antarctic (USSR State Committee for Hydrometeorology)
199226 Sankt-Peterburg Bering Street, 38.

M. S. Marshunova

IAAP Institute of Astrophysics and Atmospheric Physics (Estonia Academy of Sciences)
202444 Estonia Tyravere Observatorium Street, 3 Flat 4

V. K. Russak